REPORT NO. NADC-89042-60

RHEOENCEPHALOGRAPHY IN SIMULATED AVIATION ENVIRONMENTAL STRESS

Barry S. Shender, Ph.D.
Air Vehicle and Crew Systems Technology Department (Code 6023)
NAVAL AIR DEVELOPMENT CENTER
Warminster, PA 18974-5000

1 JUNE 1989

INTERIM REPORT
Program Element No. 62233N
Project No. MM133-130

Approved for Public Release; Distribution is Unlimited

Prepared for
OFFICE OF NAVAL TECHNOLOGY (ONT-20)
Washington, DC 20390
and
NAVAL MEDICAL RESEARCH & DEVELOPMENT COMMAND (NMR&DC-40)
Naval Medical Command National Captial Region
Bethesda, MD 20814

NOTICES

REPORT NUMBERING SYSTEM — The numbering of technical project reports issued by the Naval Air Development Center is arranged for specific identification purposes. Each number consists of the Center acronym, the calendar year in which the number was assigned, the sequence number of the report within the specific calendar year, and the official 2-digit correspondence code of the Command Officer or the Functional Department responsible for the report. For example: Report No. NADC-88020-60 indicates the twentieth Center report for the year 1988 and prepared by the Air Vehicle and Crew Systems Technology Deartment. The numerical codes are as follows:

CODE	OFFICE OR DEPARTMENT
00	Commander, Naval Air Development Center
01	Technical Director, Naval Air Development Center
05	Computer Department
10	AntiSubmarine Warfare Systems Department
20	Tactical Air Systems Department
30	Warfare Systems Analysis Department
40	Communication Navigation Technology Department
50	Mission Avionics Technology Department
60	Air Vehicle & Crew Systems Technology Department
70	Systems & Software Technology Department
80	Engineering Support Group
90	Test & Evaluation Group

PRODUCT ENDORSEMENT — The discussion or instructions concerning commercial products herein do not constitute an endorsement by the Government nor do they convey or imply the license or right to use such products.

Reviewed By: Phillip E. Whitley Date: 2/15/90
Branch Head

Reviewed By: [signature] Date: 5 Mar 90
Division Head

Approved By: W. H. Mooney Date: 6 March 90
Director/Deputy Director

UNCLASSIFIED

SECURITY CLASSIFICATION OF THIS PAGE

REPORT DOCUMENTATION PAGE

Form Approved OMB No. 0704-0188

1a. REPORT SECURITY CLASSIFICATION: Unclassified	1b. RESTRICTIVE MARKINGS
2a. SECURITY CLASSIFICATION AUTHORITY	3. DISTRIBUTION / AVAILABILITY OF REPORT: Approved for Public Release; Distribution is Unlimited
2b. DECLASSIFICATION / DOWNGRADING SCHEDULE	
4. PERFORMING ORGANIZATION REPORT NUMBER(S): NADC-89042-60	5. MONITORING ORGANIZATION REPORT NUMBER(S)
6a. NAME OF PERFORMING ORGANIZATION: Air Vehicle and Crew Systems Technology Department; 6b. OFFICE SYMBOL (If applicable): 6023	7a. NAME OF MONITORING ORGANIZATION
6c. ADDRESS (City, State, and ZIP Code): NAVAL AIR DEVELOPMENT CENTER Warminster, PA 18974-5000	7b. ADDRESS (City, State, and ZIP Code)
8a. NAME OF FUNDING / SPONSORING ORGANIZATION: ONT/NMR&DC; 8b. OFFICE SYMBOL (If applicable): ONT 20 NMR&DC 40	9. PROCUREMENT INSTRUMENT IDENTIFICATION NUMBER
8c. ADDRESS (City, State, and ZIP Code): WASHINGTON, DC 20361	10. SOURCE OF FUNDING NUMBERS: PROGRAM ELEMENT NO. 62233N; PROJECT NO. MM33-130; TASK NO.; WORK UNIT ACCESSION NO.

11. TITLE (Include Security Classification)

(U) Rheoencephalography in Simulated Aviation Environmental Stress

12. PERSONAL AUTHOR(S)

Barry Scott Shender, Ph.D.

13a. TYPE OF REPORT	13b. TIME COVERED	14. DATE OF REPORT (Year, Month, Day)	15. PAGE COUNT
INTERIM	FROM _____ TO _____	1989 June 1	240

16. SUPPLEMENTARY NOTATION

Ph.D. Thesis Biomedical Engineering, Drexel University Philadelphia, PA.

17. COSATI CODES			18. SUBJECT TERMS (Continue on reverse if necessary and identify by block number)
FIELD	GROUP	SUB-GROUP	Non-Invasive Cephalic Fluid Monitoring, Acceleration Stress, Impedance Measurements, Rheoencephalography
06	10	10	

19. ABSTRACT (Continue on reverse if necessary and identify by block number)

The use of electrical impedance plethysmography of the head, or Rheoencephalography (REG), has been demonstrated in a high acceleration stress environment on human volunteer subjects. Acceleration stress was applied in the head-to-foot direction and is referred to as +Gz. The REG instrument divides the cephalic impedance waveform into two components: 1) a baseline impedance signal, Zb, that is referable to the bulk movement of blood in and out of the head, and 2) a pulsatile impedance waveform that is heart beat coincident. The REG waveform also contains information about cerebrospinal fluid (CSF) volume changes and shifts resulting from the application of acceleration stress. Blood and CSF shifts in and out of the cranial and spinal compartments impinge directly upon the overall function of the central nervous system. The high acceleration environment provides an ideal arena in which to alter cephalic

(Continued)

20. DISTRIBUTION / AVAILABILITY OF ABSTRACT	21. ABSTRACT SECURITY CLASSIFICATION
☒ UNCLASSIFIED / UNLIMITED ☐ SAME AS RPT. ☐ DTIC USERS	Unclassified

22a. NAME OF RESPONSIBLE INDIVIDUAL	22b. TELEPHONE (Include Area Code)	22c. OFFICE SYMBOL
Barry S. Shender	(215) 441-3520	6023

DD Form 1473, JUN 86 *Previous editions are obsolete.* SECURITY CLASSIFICATION OF THIS PAGE

S/N 0102-LF-014-6603 UNCLASSIFIED

BLOCK 19 (Continued)

fluid volumes noninvasively in order to obtain basic physiologic knowledge of importance to both aviation and clinical medicine.

This information has been obtained in a noninvasive, safe, convenient, and unobtrusive manner on the Naval Air Development Center (NAVAIRDEVCEN) human centrifuge. Using data derived from three different sets of human centrifuge. Using data derived from three different sets of human experiments conducted in a high +Gz environment have led to the characterization of the changes in the REG waveform that occur with increasing acceleration load. Alterations in the Zb waveform indicate its utility as an aid in determining the effectiveness of anti-G protective devices, such as reclining aircraft seats, and anti-G techniques, such as anti-G straining maneuvers. Use of the Zb waveform provides the first indirect (or direct) estimate of the bulk movement of blood under a +Gz load as predicted by the hydrostatic column theory of the physiological response to increasing acceleration load.

An outline for animal and human experimentation necessary to develop a mathematical model to describe the changes in both vascular and CSF compartments is presented.

CONTENTS

CONTENTS (continued)

FIGURES

FIGURES (continued)

TABLES

TABLES (continued)

INTRODUCTION

MOTIVATION

Advanced aerospace vehicles are capable of rapidly generating and sustaining acceleration forces at magnitudes and durations that exceed the unprotected tolerance limits of their human operators. The primary effect of acceleration stress directed in the head-to-foot direction (+Gz), caused by acceleration forces applied in the foot-to-head direction, is such that the downward loading of the blood in the heart-brain hemodynamic column decreases the ability of the heart to pump blood to the level of the brain. The net result of sustaining high acceleration maneuvers is that blood is pooled in the extremities and abdomen while the head is deprived of blood flow. During increased +Gz load the reduction of blood pressure at head level is manifested by a diminution of visual function progressing through loss of visual acuity, peripheral light loss (PLL), loss of central vision, complete "blackout," and finally loss of consciousness (LOC).[85]

Current aircraft designs enable aircrew to fly faster with more maneuverability than ever before. Unfortunately, the increases in aircraft ability have not been matched by a fundamental increase in human capability to withstand high levels and onset rates of acceleration stress. Future aircraft designs will place even greater physiological demands upon their aircrew. Therefore, the problem of acceleration stress-induced loss of consciousness (termed "GLOC") is of increasing concern in the aerospace community because it places in dire jeopardy both aircrew and aircraft.

To express the underlying need for research about this phenomenon, the following is a quote from J. A. Gillies, editor of "A Textbook of Aviation Physiology:"

"... It is clear that some confusion exists as to the behavior of the cerebral circulation during exposure to positive g (a + Gz load). The importance, and in some cases even the existence, of the various mechanisms which have been postulated, cannot be assessed until it is possible to measure cerebral blood flow accurately and continuously on a centrifuge." (19,page 599)

Presently, the major emphasis in dealing with the problem of PLL and LOC under +Gz is the concern for maintaining blood flow in the cerebral circulation. It is vital that such blood flow be maintained in order to preserve the long term homeostasis of the central nervous system (CNS). However, over the relatively short periods of interest in preventing PLL and LOC, consideration of cephalic blood volume may also be significant. Hemoglobin in the blood is the major oxygen buffer in cephalic neural tissues[37] and PLL and LOC under a +Gz load are caused not only by the critical reduction of blood flow to the head, but also by reduction of the primary reservoir of available oxygen.[3,65] The effects of +Gz on the oxygen availability to neural tissues, as well as benefits of +Gz protective straining/respiratory maneuvers (M1 or L1), may well be reflected in cephalic blood volume changes.

Rheoencephalography (REG), also known as electrical impedance encephalography, is a subset of electrical impedance plethysmography (EIP). EIP methods have been applied successfully in the aerospace environment to the evaluation of respiration,[4] cardiac output,[40] and limb engorgement.[44] In general, EIP relates changes in physiologic events to changes in electrical impedance. The method depends upon changes of volume and/or conductivity of a body segment subtended by an array of electrodes. Although the exact mechanism of the impedance variations in REG is subject to some controversy, there is little doubt as to the occurrence of pulsatile variations that are synchronous with the heartbeat.[61] It has been shown that these pulsations depend upon integrity of cephalic blood flow.[23]

Blood and cerebrospinal fluid (CSF) volume shifts impinge directly upon the function of the CNS.

The high acceleration environment of a human centrifuge provides a means to conveniently induce these shifts in order to investigate the physiologic response of the CNS to these changes. Therefore, the objective of this thesis is to provide a means for noninvasive monitoring of cephalic fluid volume changes under acceleration stress via the use of rheoencephalography. Relative changes in cephalic fluid volume due to pulsatile flow and bulk shifts of blood will be measured. From these measurements it will be possible to monitor the physiological changes in fluid volume predicted by the hydrostatic column theory of the physiological response to acceleration stress. It will be shown that results from the latter measurement are useful in determining the effectiveness of anti-G protective devices and maneuvers designed to ameliorate the effect of acceleration stress. Finally, the utility of this technique will be discussed in terms of the formulation of a model describing the state of the blood and CSF compartments of the CNS under acceleration stress.

EFFECTS OF ACCELERATION STRESS

The importance of maintaining adequate blood circulation in the head has been demonstrated in both clinical and aviation environments.[19] This is particularly true when flying high onset +Gz aircraft because of the physiological reaction to the acceleration forces involved. In this manuscript "g" refers to acceleration due to gravity, *i.e.* 9.8 m/sec^2. Values associated with +Gz are expressed in units of g in the head-to-foot direction.

When acceleration forces are imposed on a person the physiological reaction to that force is in the opposite direction. Of particular interest in maintaining circulation to the head is acceleration in the head-to-foot direction. Forces resulting from +Gz acceleration act to drain blood from the head to the large capacitance veins of the extremities and abdomen. When these veins are filled to capacity and pressure throughout the cardiovascular (CV) system has stabilized as much as possible under stress, the space comprising the interstitial tissues becomes involved. These tissues which surround the vessels are not subjected to the increase in hydrostatic pressure and remain at a pressure which is low relative to that within the blood vessels. Therefore, the transmural pressure is increased and the resulting gradient leads to filtration of fluid through the vessel walls.[19,page558]

For a normal man at 1 g, the heart must overcome an approximately 30 cm hydrostatic column for blood to reach the CNS. This corresponds to a hydrostatic pressure of approximately 22 mmHg (*i.e.* 300 mm × 1.055 gm/cm^3 {density of blood}/13.6 gm/cm^3 {density of mercury}). Therefore in an average man, assuming a systolic arterial pressure of 120 mmHg at heart level (at the third intercostal space), arterial pressures at head and foot levels are 98 and 170 mmHg, respectively. With each 1 g increase in +Gz load, the hydrostatic column effectively increases by another 30 cm until a point is reached in which pressure in the head is critically decreased and blood supply is arrested. Theoretically, arterial pressure at eye level in the average human reaches zero at approximately +5.5 Gz. At this point, assuming that the arterial pressure at heart level had been 120 mmHg at 1 g, the arterial pressure at the base of the brain would become zero and pressure at the feet would be 370 mmHg. Therefore, a differential pressure of 250 mmHg would be necessary to return blood from the feet to the heart. This description of changes in blood pressure and redirection of blood flow forms the basis of the hydrostatic column theory of the human physiological response to applied acceleration stress.

The physiologic symptoms accompanying increasing levels of acceleration stress are particularly detrimental because they can be rapid in onset, their occurrence is somewhat unpredictable, and they limit the most important sensory central nervous inputs to the crew-member. Human physiologic response to a +Gz load depends upon the level and rate of onset of the acceleration. When acceleration is gradually applied (+0.067 to +0.02 Gz/sec), visual function decreases in stages from grey-out to blackout. However, under very high onset rates (*e.g.* >+6 Gz/sec) an individual can lose conscious-

ness without recognizable loss of peripheral vision.[75] On the other hand, at lower onset rates an individual can experience blackout and still retain normal cortical function.[19] Lambert[42] demonstrated that this effect is of retinal origin in an experiment in which vision in one eye was maintained by application of 30–40 mmHg suction to the eyeball while the other unprotected eye "blacked-out." Since the blood pressure at eye level must be less than 20 mmHg for blackout to occur, the arterial pressure in the cerebral cortex must be lower than this during the period prior to LOC. Therefore, such symptoms jeopardize not only the life of the crew, but also the successful completion of a vital mission and an extremely costly aircraft.

Among the many tantalizing observations related to +Gz-tolerance may be found in the following: (a) straining/respiratory/maneuvers helpful in delaying the onset of PLL and LOC in the short term are of a general nature that is detrimental to circulation in the long term. (b) The onset of PLL and LOC (in common with syncope at 1 g) seems rather sudden to be explained by loss of flow alone. (c) Net negative blood velocities, when measured by the doppler ultrasound technique, have been observed in the superior temporal artery for extended periods of time under a +Gz load without significant decrease in pilot performance.[38]

Insight into these observations is aided by consideration of some basic physiologic features of neural tissues. These tissues, including the retina and brain, have closely regulated but barely adequate blood circulation to supply nutrients (oxygen, glucose, *etc.*) and remove metabolites — in contrast with most other organs whose abundant blood supplies reflect their circulatory interface function. Neural tissue comprises only three percent of body weight while it receives about 15% of the cardiac output and consumes about 25% of the oxygen.[30] In the retina and in neural grey matter, oxygen consumption can be as high as 12 ml/100 gm/min.[30] In comparison with cardiac and skeletal muscles (having a similarly high oxygen extraction fraction), neural tissues lack an intrinsic oxygen buffer such as myoglobin. In the brain, oxygen is used only in the "terminal respiratory chain" of enzymes for oxidative phosphorylation in the mitochondria, *i.e.* ATP synthesis. This process is usually limited by the supply of ADP and inorganic phosphate rather than oxygen tension. Oxygen uptake by mitochondrial suspensions continues until the local partial pressure of oxygen falls to 0.1 mmHg.[30] Therefore, when oxygen supply becomes limiting, it is because the volume of oxygen has been exhausted.

Oxygen consumption in the brain is 40–50 ml/min,[76] or approximately 3 ml O_2/100 gm/min. There is about 2.8 ml of oxygen dissolved in the tissue, or 0.19 ml O_2/100 gm (see Appendix A). The 75 ml of blood in the cerebral circulation contains about 15 ml of oxygen (at 100% saturation), mostly combined with hemoglobin.[37] (Approximately 1.5% of the oxygen in blood is dissolved). Therefore the hemoglobin in blood is the major oxygen buffer for the neural tissues. Using these figures, if blood flow to the brain was stopped or reversed at neck level, the 17.8 ml of cephalic blood would be consumed in approximately 21–27 seconds. This assumes that once arrested, oxygen is consumed at the normal rate and that all of the blood is available for consumption. However, blood in the dural sinuses of the head and arterial and venous blood trapped in the neck is unavailable to neural tissues. Therefore, this rate is not inconsistent with neck occlusion studies reported by Rossen *et al*[65] in which blood flow to the head was occluded with a cervical cuff. This produced unconsciousness in an average of 5.5 seconds.

In an experiment in which 40 high +Gz runs were performed,[75] a strength-duration-tolerance curve was calculated. It was found that brain function and vision could be sustained at any +Gz level for 3 seconds due to the oxygen stored in brain tissue even if blood flow was cut off completely. +Gz-tolerance decreases rapidly with increasing duration and reaches a minimum of about +3 Gz at about 8–10 seconds. Then CV compensation (see below) becomes a factor and at complete compensation adds an additional +2 Gz-tolerance.[75]

Therefore, PLL and LOC during +Gz are caused not only by interruption of blood flow to the head, but also by subsequent removal of the major proportion of available oxygen. This view is consistent with observations of the retinal vessels noted during acceleration stress under direct ophthalmoscopic observation using fluorescein as an indicator. During a +Gz load not only is there a total cessation of pulsatile flow but an apparent backward flow of fluoroscein dyed arterial blood from distal ophthalmic artery towards the carotid system. At offset of +Gz acceleration, the dye then returns to the ophthalmic artery and then is cleared from the arterial system.[43]

In centrifuge studies in which direct opthalmoscopic observation of the retina was performed, it was observed that blackout was accompanied by an emptying and collapse of the arterioles although the veins remained normal in appearance. There is no direct arterial supply to the fovea and visual acuity degenerates and disappears prior to true blackout. There was a 'clear period' of at least six seconds before signs of visual impairment.[13] In another study in which blood velocity under acceleration stress was measured with a doppler ultrasound technique, at the point in which velocity reached zero, an unexpected five second delay prior to LOC occurred.[38] It can be argued that even with the critical reduction of retinal blood flow is produced under high acceleration stress there remains a reserve of oxygen necessary for maintenance of cortical function.

The CV system exhibits a series of reflex responses when exposed to changes in blood pressure. High pressure stretch receptors are located in the carotid sinus and aorta. As pressure drops, the inhibitory action of these receptors is reduced which then causes the brain stem reticular formation to induce vasoconstriction, increased heart rate, and force of contraction. Since arterial pressure changes are most dramatic above the heart, the carotid sinus is the primary sensor for responding to low pressure during +Gz.[20]

The atrial stretch receptors perform a similar function on the low pressure portion of the CV system under +Gz acceleration. Small reductions in filling volume decrease the rate of inhibitory discharge of these receptors. These work synergistically with the high pressure receptors under stress to increase heart rate and maintain cardiac output.[20]

Gauer and Zuidema[15] describe the human physiological response to varying periods of acceleration as follows:

1) Abrupt acceleration [0–2 s]: Mechanical injury to the tissues may be produced, while the inherent oxygen store of the cells prevents symptoms due to blood stasis.

2) Brief acceleration [2.1–10 s]: This is the most vulnerable period of the oxygen supply to the brain. Oxygen stores are exhausted and the CV compensation mechanisms have not yet become effective. Stagnant hypoxia results.

3) Long term acceleration [10.1–60 s]: Protective CV mechanisms are now in force and adverse symptoms that arose with high +Gz onset disappear.

4) Prolonged acceleration [>1 min]: The protective mechanisms that depend on increasing smooth muscle tone do not seem to fatigue and the extravasation of plasma fluid is comparatively slow. +Gz-tolerance is high for long periods of time.

It has been shown that cerebral blood flow is maintained during acceleration and is not reduced in accordance with simple hydrostatic principles.[19,page597] The stability of the vascular system under acceleration is largely due to the strength of the vessel walls. These walls are relatively thin and have

no collagen fibers, except for the capillaries which have a delicate but strong elastic framework. According to Dhenin[12] and Henry *et al*,[29] some of the mechanisms responsible for maintaining blood flow to the brain are:

1) The cerebral vessels and brain are enclosed in the skull and are surrounded by cerebrospinal fluid (CSF). CSF pressure (CSFP) falls due to hydrostatic effects during +Gz in parallel to reductions in arterial pressure so that the pressure differences across the walls of the cerebral vessels remain close to normal.[12] Henry *et al*[29] have shown that the internal and external vertebral venous plexes are protected from collapse by subatmospheric (20–60 mmHg below ambient) CSFP. Periosteal adhesions of intracranial veins also aid in keeping these vessels patent.[5] Therefore, a pathway is provided for return of blood from the brain to the heart.

2) There is active vasodilation of the cerebral arterioles so that resistance to flow is reduced.

3) The column of blood in the upper part of the jugular veins create a "siphon effect" that can maintain cerebral circulation as long as the column remains patent. This effect can be maintained up to about +4–5 Gz.

Henry *et al*[29] have commented on the mechanisms underlying this effect in the following manner. They propose that the drop in venous pressure is accompanied by a decrease in cerebral vascular resistance. As pressure in the venous plexus about the spinal cord drops during acceleration, blood is drained into the lower abdomen. This now empty space is filled by CSF originating from the cranium. Then a passive distention of the cerebral vessels would then occur to replace the space evacuated by the CSF. A small amount of blood would then be aspirated from the arterial tree during this distention, aiding an individual to maintain consciousness during brief acceleration exposures.

ASPECTS OF THE CEREBRAL CIRCULATION

(Note: Unless otherwise indicated, the primary source of information for this section is based upon Heistad *et al*.)[28]

The cerebral circulation is highly specialized. The brain-blood barrier provides isolation and protection from ionic changes and humoral stimuli. As compared to other vascular beds, large arteries account for a greater percentage of vascular resistance in the brain. Autoregulation in the brain is normally very effective and is responsive to changes in arterial pressure and chemical stimuli.

The brain is supplied primarily by two carotid and two vertebral arteries. It has a high capillary density. It is drained by two systems of veins. Blood to the cerebral and cerebellar corticies flows through vessels on the surface of the brain. Blood emanating from the basal areas flows into the deep venous system, including the straight sinus. Blood exits the skull via the internal jugular and other veins.

The main input variables which determine cerebral blood flow (CBF) are the arterial blood pressure at the base of the skull, jugular venous blood pressure, local autoregulation, and the state of the cranial and caudal veins of the skull. Blood flow rate to the cranial vessels is dependent upon the total hydraulic resistance and is determined by the difference between cephalic arterial and venous pressures. In the closed cranium, CSF and venous pressures balance and the rate of blood outflow is determined by the difference in cranial venous and jugular pressures and upon the vascular resistance of the cerebral venous system.[27]

In dogs and cats, the brain is primarily supplied via the external carotid artery while the contribution by the internal carotid artery is relatively minor. The external carotid branches into a complex network of anastomoses, the 'rete mirabile,' prior to its junction with the circle of Willis (COW). The outflow of blood in dogs and cats has both extra- and intra- cerebral components and therefore communications between the two must be severed for measurements of venous outflow to accurately represent CBF. In primates and rabbits, the major source of CBF is the internal carotid artery and there is no rete-like structure prior to joining the COW. The jugular veins of the primate, in contrast to the canine and feline, represent cerebral venous outflow without significant extracerebral contribution. This assumption is valid if measurements are performed at the jugular bulb.

The circle of Willis is formed by anastomoses of the major arteries supplying blood to the brain in man. The COW can provide important collateral circulation when a proximal vessel is occluded. Emanating from the COW are the anterior, middle, and posterior cerebral arteries. These then traverse the convex surface of the cerebrum. The basilar artery system supplies the brain stem and the cerebellum. Regions bordering the areas supplied by the anterior, middle, and posterior cerebral arteries are the "boundary zones." These areas are particularly vulnerable to reductions in cerebral blood flow. Prolonged hypotension may produce ischemic necrosis that is most pronounced in these boundary zones.

In addition to the COW, the pial vessels also have a rather extensive network. This network may compensate for occlusion of arteries distal to the COW and attenuate the reduction in flow. These vessels account for a large portion of the total cerebral vascular resistance (CVR) and their responses are generally representative of the entire cerebral circulation.

According to Gregg and Huvos,[24] total CVR is influenced by intracranial pressure, blood viscosity, and vascular diameter as opposed to direct neural control. The sympathetic fibers innervating the cerebral vessels are apparently physiologically inactive. While CVR becomes elevated in a direct and linear fashion by increased intracranial pressure, CBF remains relatively constant until pressure reaches a very high level (approximately 45 cm of water). CBF increases proportionately to decreased red blood cell concentration. The most important factor affecting CVR, vascular diameter, is determined by structural changes, neurogenic factors, and metabolite concentrations.

The most important factors affecting chemical regulation include O_2, CO_2, and pH. CO_2 and hydrogen ion (H^+) concentration have a pronounced vasodilatory effect on vascular tone. Therefore, changes in CO_2 concentration or in pH strongly influence CBF and CVR. The action of CO_2 may be mediated by the direct effects of H^+ on cerebral arterioles. Hydrogen ion concentration close to the vascular muscle depends on HCO_3^- concentration and on partial pressure of CO_2 (P_{CO_2}) of the extracellular fluid in that location. The latter depends on arterial partial pressure of CO_2 ($PaCO_2$) and on CSF P_{CO_2}. When P_{aCO_2} is increased, molecular CO_2 diffuses across the brain-blood barrier, raises the local P_{CO_2} of the vascular muscle, and reduces extracellular pH. This produces vasodilation by relaxation of the vascular muscle. There is an indication that the major mechanism of action of CO_2 on cerebral circulation is mediated via changes in CSF pH.

Low O_2 tensions (20–30 mmHg) also causes vasodilatation. Similar responses occur with changes in CSF P_{O_2} in the vicinity of the pial vessels. Also during combined occurrences of arterial hypoxia and hypercapnia, cerebral vasodilator effects become additive.

ASPECTS OF THE CEREBROSPINAL FLUID (CSF) SYSTEM

The cranio-spinal system is basically a closed system, *i.e.* changes in blood volume entering into

the head will be accompanied by a shift of venous blood and/or CSF out of the head into the spinal cavity. CSF shifts from cranial to spinal space periodically with respiration and aperiodically with respect to slow blood volume changes in the skull. Cardiac synchronous volume shifts are compensated for by a redistribution of CSF and venous blood in the cranial space.[27] This compensation is produced by direct hydraulic contact of the blood vessels with the spaces containing CSF, extensive connections between cranial and spinal veins, and free communications between CSF cavities in the skull and spinal canal.[57]

Changes in CSFP have been used to make relative estimates of blood volume shifts. Since the product of pressure and volume is theoretically constant in an enclosed space, one may calculate from the pulsatile pressure the changes in fluid volume which are responsible for these pressure changes. Here, fluid volume consists of the sum of the average volume of intracranial space, intracranial blood, and intracranial "free space" (*i.e.* CSF).[27] CSFP is determined by the volume of arterial and venous blood, CSF, and brain tissue, and by the mechanical properties of membranes surrounding the brain and bones of the skull. Hydrostatic pressure accounts for one third of the total CSFP, 10% is attributed to the elasticity of the meninges, the balance depends upon blood pressure, particularly venous pressure, and on the secretion pressure. CSFP is always a few centimeters of water higher than venous pressure[51].

CSFP is affected in the following manner. Change in venous pressure causes a change in CSFP of a comparable magnitude and direction. In fact, venous volume is directly determined by the difference between venous and CSF pressures. Change in arterial pressure causes variable alterations in CSFP in magnitude and direction. The rise and fall of CSFP is due to variations in blood volume in the craniospinal cavity. Therefore, CSFP is dependent upon the tone of the cerebral vessels.[57]

CSFP may increase during such maneuvers as straining, coughing, and vomiting. CSFP may also vary during shifts in posture. These oscillations are balanced by an adaptation or by a reaction of the cerebral blood circulation. Alterations in rheoencephalographic recordings have been observed with various functional tests such as Queckenstadt's maneuver (compression of both jugular veins to block venous outflow), carotid compression, and after withdrawal of CSF.[57] As an example, Queckenstadt's maneuver results in an increase in CSFP and upon removal of the compression, CSFP declines relatively faster than the rate at which blood returns to the head. Reaction of CSFP to carotid compression varies depending upon the state of the circulatory system and may increase or decrease.[51] External agents which cause a decrease in tone (*e.g.* CO_2, amyl nitrite) cause an increase in CSFP. External agents causing an increase in tone (*e.g.* O_2) lead to a fall in CSFP.[57] A decrease in CSFP leads to a decline in blood volume as registered by REG.[27]

The mechanism of support provided by the CSF system is particularly important in the acceleration environment. The brain is protected from a reduction in systemic blood pressure by virtue of the fact that it is enclosed in a rigid container, is surrounded by CSF, and such a drop in pressure is often accompanied by a similar decline in CSFP. Therefore, the transmural pressure in cerebral vessels remains almost constant with no tendency for collapse. If, at the same time, venous pressure in the neck falls below atmospheric, blood is sucked through the brain by siphonic action. Cerebral circulation continues as long as the vessels remain patent and until some part of the system empties. Increasing the driving pressure through the siphon can restart the system.[19] Akesson[2] found that an increase in CSFP leads to vasodilatation of the pial arteries, which reduces the resistance to flow within them. This and the siphon effect may act to maintain circulation.

Rushmer *et al*[66] found that CSFP and venous pressure vary simultaneously (and almost equally) over a wide range of negative and positive acceleration loads in cats. They claimed that there is virtu-

ally complete protection for veins and small vessels. While the arteries are less fortunately placed, they too receive some compensation from CSF.

Another biophysical aspect of CSF aiding circulation under acceleration is the difference between the specific gravities of the brain and CSF; 1.048 and 1.008, respectively. A 1500 gm brain in such an environment exerts a force of approximately 35 gm on the base of the skull. As an analogy, consider spinning a water filled balloon. As it spins faster and faster, a point will be reached in which the pressure from the centrifugal force will burst the balloon. If, however, the balloon is surrounded by water, the external and internal pressures are balanced and the whirling balloon remains intact.

The level of protection afforded by CSF depends upon the level, rate, and duration of the acceleration stress applied. If the stress acts for less than one second, there is not enough time for compensation flows to occur. If the stress is prolonged (5–7 seconds), effective compensation begins.

ANTI-G PROTECTIVE DEVICES AND MANEUVERS

There are a number of methods that have been applied in the high-G environment to ameliorate the physiological consequences of a +Gz load. These include anti-G suits (AGS), acceleration sensitive AGS inflation valves, modified body position seats, and performance of anti-G straining maneuvers (AGSM).

An early AGS and pneumatic valve was described by Wood in a 1978 review article.[84] This combination was first used in World War II. The suit consisted of calf, thigh, and abdominal bladders that were simultaneously pressurized to a level proportional to the acceleration load.

The physiological response to the action of AGS is a combination of effects. Primarily, the AGS acts to increase systemic blood pressure. External pressure applied to the legs acts to increase arterial resistance to inflow, although this is achieved by a decrease in the arteriolar transmural pressure. At the same time compression of the veins forces blood from the capacitance vessels back into the general circulation and increases vasomotor tone, thereby reducing the available space for pooling. Additionally, externally applied abdominal pressure increases the intraabdominal pressure and prevents the descent of diaphragm. This reduces the hydrostatic column height between the heart and the brain. For longer periods of acceleration (>20 seconds), leg compression acts to prevent or reduce blood pooling in the capacitance vessels which acts to help maintain cardiac output.[19]

Similar suits as those described above by Wood[84] are in use today and are pressurized in direct proportion to the acceleration load, with maximum inflation of 11 psi lower bladder pressure. The inflation rate is approximately 1.5 psi per Gz. A variation of this suit design, the pulsating AGS (PANGS) has been developed by researchers at Drexel University in Philadelphia (35) in which inflation of the bladders is controlled by heart rate and acceleration load. PANGS can inflate its bladders sequentially in an attempt to "milk" the pooled blood in the lower legs up to the heart and head in concert with cardiac contraction.

There have been a number of anti-G valve (AGV) designs. These include the ALAR™ standard, the ALAR™ high-flow, and a rapid reponse electronically controlled servo valve (SCAG). The latter can be programmed to follow or to anticipate the onset of acceleration. A study on the effect of valve reaction speed on +Gz-tolerance was performed at the Naval Air Development Center (NADC) in 1986.[9] In this study, there was no statistically significant difference in +Gz-tolerance demonstrated among these different configurations. Another valve, the "Bang-Bang anti-G servo valve," was studied at Wright Patterson AFB, also in 1986.[1] In this study +Gz-tolerance was increased primarily due to the

increased levels of suit pressurization obtained (12–13 psi).

Since the mid-1930's, investigators have shown that aircrew can tolerate higher levels of acceleration stress if they ride in a supinated rather than an upright position. When an individual reclines, the effective heart-head distance is reduced, the hydrostatic load on the heart is reduced, and +Gz-tolerance is increased.

Harald von Beckh in the late 1970's[81] created the Pelvis and Legs Elevating, or PALE, seat in which the pelvis and legs are raised without changing the position of the head with respect to the vertical. This design was an attempt to not only increase anti-G protection but to avoid the problems of limited out-of-cockpit visibility and changing the angle of vision with respect to displays that occurred with other reclining seats. In a study with ten subjects, von Beckh noted that at seat-back-angles (SBA) of 13° and 30°, there was no increase in +Gz-tolerance as measured by a reduction of peripheral vision to a forward 60° cone. At a 45° SBA, some improvement occurred (approximately 0.5 Gz) and above a 60° SBA, the improvement became quite apparent (about 1.5 G). In 1985, Hrebien and Hendler[31] reported on a series of human centrifuge experiments in which a PALE seat was used. They found that subjects wearing an uninflated AGS demonstrated a mean increase in +Gz-tolerance of 1.67 G when they were reclined at a 60° SBA versus a 15° SBA.

Presently, the most effective method to combat the deleterious effects of +Gz is the performance of an AGSM, called an M1 or L1. Gillingham and Fosdick[21] have reported on high +Gz training conducted at USAFSAM at Brooks AFB, Texas, in which effective L-1 maneuvers are taught to pilots. They describe the L-1 as consisting of vigorous tensing of arm and leg muscles to decrease blood pooling and cyclically increasing intrathoracic pressure with the chest and abdominal muscles to increase blood pressure. Together, these act to raise cephalic blood pressure. The respiratory portion of the L-1 consists of a three second cycle, of which about 2.5 seconds is expiratory and 0.5 second is inspiratory. The former phase is a forced expiration performed against a closed glottis. At NADC, subjects are often told that saying the word "HOOK-KAH" aids in the performance of the L-1. Inspiration is accompanied by the phrase "HOOK" and the release is paired with "KAH." The M-1 differs from the L-1 in that the glottis is partially closed and the individual "grunts" during the strain. The rapid exhalation/inhalation phase of the strain should last no more than one second because during this period, there is no added +Gz protection.

RHEOENCEPHALOGRAPHY (REG)

BACKGROUND

Why should one study and employ the use of impedance measures?

An inherent property of matter is its exhibition of a resistance to passage of electrical current. This is defined by $\rho = E/J$; where ρ = resistivity of the material, E = electric field, and J = current density. In the case in which resistance of a body segment, subtended by measurement electrodes, is to be determined the following assumptions are made.[55,61] The segment has a uniform cross sectional area and is filled with a homogenous conducting material. There is a uniform current density between the electrodes. The length of the segment between the measuring electrodes and the area remain constant while blood enters (exits) the segment. The overall volume is constrained to be a constant. Also, ρ is unchanged during measurement. If, for example, a segment in a current field has a hole drilled through it and the external dimensions are fixed, the current lines will experience a high resistance path as they approach the hole (a high resistance area filled with a poor conductor, *i.e.* air). This will give rise to a non-uniform electrical field and a non-uniform current density distribution. The introduction of the hole does not effect ρ (a constant dependent upon the material and temperature). Therefore, this effect at the measuring terminals is seen as a change in resistance.[55,page13] Given the above assumptions, a body segment modeled as a perfect right cylinder exposed to an electric field (defined by $E = V/L$; where V = voltage and L = length of the segment) with a current density given by $J = I/A$ (where I = current and A = cross sectional area), one can solve for resistance, R, by using Ohm's Law ($R = V/I$). The measured impedance of the segment is then given by $R = \rho L/A$.

The resistance of biological material is a quantitative measure of the total number of conducting species in a current field. With systole, more conductors appear between electrodes so that total tissue resistance falls in an amount that is quantitatively related to net increase in blood volume.[67] Recall that volume (V) for a perfect right cylinder is given as $V = LA$. In cases in which the length of a body segment is fixed, *e.g.* the forearm, the change in resistance, ΔR, can be expressed as a small change in volume as

$$\Delta R = R_1 - R_0 = \frac{\rho L}{A_1} - \frac{\rho L}{A_0} \tag{1}$$

where R_0 and A_0 are the base resistance and cross sectional area values, respectively, and R_1 and A_1 are the new values of resistance and cross sectional area, respectively. Substituting for base volume, V_0, and new volume, V_1, gives

$$\Delta R = \rho L \left(\frac{L}{V_1} - \frac{L}{V_0} \right) \tag{2}$$

$$= \rho L^2 \left(\frac{V_0 - V_1}{V_0 V_1} \right) \tag{3}$$

$$= -\rho L^2 \left(\frac{V_1 - V_0}{V_0 V_1} \right) \tag{4}$$

If V_1 is not appreciably greater than V_0, then ΔR can be expressed as

$$\Delta R = -\left(\frac{\rho L^2}{V_0^2}\right)\Delta V, \tag{5}$$

where $\Delta V = V_1 - V_0$.

Electrical impedance plethysmography (EIP) is a noninvasive technique that is used to measure the change in resistance that arises from changes in volume of various biological tissues. Use of Equation 5 has been classically applied in EIP to investigate cardiac and respiratory function[63] and vascular changes in body segments, such as the extremities,[61] in which the assumption of cylindrical cross sectional area is valid. When investigating the state of cephalic circulation, EIP is called Rheoencephalography. However, this equation does not readily apply to analysis of resistance changes across the head.[46] (See also the section entitled "Classical Modeling of REG Waveform: R = ρL/A."). This is due to the shape of the head and the relative rigidity of the structure. Under normal conditions, each systole is accompanied by an influx of 6.5 ml of blood into the head corresponding to an expansion of 0.2 mm.[27] There is some dispute over the amount of this volume in that Moskalenko *et al*[57] report a influx of 12–15 ml of blood per systole into the head.

Since the expansion of this volume is relatively small, an absolute change in intracranial blood volume must be associated with a displacement of CSF. Since CSF is a better conductor than blood, one would expect to note an increase in overall cephalic resistance with systole rather than the observed decrease.[46] Therefore, simple volumetric considerations alone are not sufficient when applied to REG analysis.

Changes in cardiac output are reflected in cerebral hemodynamics and registered by the REG. Changes, particularly of a diffuse or generalized nature in cephalohemodynamics, will be INSTANTLY reflected in the REG. It is this temporal sensitivity that makes the REG so attractive.[67]

Contributing to the REG is the circulatory inflow from the internal carotid, vertebral, and external carotid arteries and the cerebrospinal fluid (CSF) (ρ for CSF is ≈ 65 Ω-cm (16)). The REG is a function of pulsatile flow. The pulse wave causes a drop in overall impedance with its influx of electrical carriers.[59] The blood contains about 45% highly resistive blood cells and about 55% highly conductive plasma (ρ for whole blood is ≈ 154 Ω-cm (16)). Note that in Equation 5, ρ is a constant throughout the cardiac cycle. Lifshitz[46] theorized that the blood entering the head with systole, which is distributed through the arterial network, would have an electrical shunting effect greater than the large mass of blood in the venous sinuses. The overall effect would be a transitory decrease in ρ with systole of approximately 0.1 percent. Other important resistivities are: ρ for brain is ≈ 250–300 Ω-cm, ρ for skin is ≈ 300 Ω-cm, and ρ for excised bone is ≈ 4000 Ω-cm (16). For *in vivo* bone, ρ is ≈ 300 Ω-cm, due to the blood forming elements it contains.[46]

The REG contains an extracranial component. In general, the extracranial-intracranial ratio is strongly dependent on electrode placement and size.[68] Small electrodes favor registration of superficial impedance changes.[46,68] The amount of extracranial component in the REG is one of the criticisms raised in clinical applications of this technique.

To summarize, interpretation of REG is more complex than other plethysmographic studies. The

vessels of the brain are surrounded by CSF and housed within a rigid container, the skull. The REG signal must be considered as a composite of the pulsatile changes in volume, the redistribution of blood and CSF to compensate for the increased volume, and, marginally, the velocity of blood flow.[27] These changes depend on the vascular resistance of cranial vessels. Therefore, the impedance changes and the REG reflect changes in cerebral vascular resistance.[25] The effect of acceleration stress on the system further complicates matters due to the bulk shifts of fluid.

REG CONFIGURATIONS

The basic design of the bipolar (two electrode) rheoencephalograph, is conceptually, very simple (see Figure 1). The body segment to be examined is connected to a resistance bridge. The excitation source of the bridge is generally sinusoidal in the frequency range of 15 to 150 kHz. Currents in this frequency range will not effectively stimulate the heart or skeletal muscle. According to Nyboer,[61,page24] when excited at frequencies between 100 kHz and 1 Mhz, a biological segment becomes a pure resistance and reactance of the tissue approaches zero. Therefore, changes in volume are directly related to conductance. The phase angle as measured between the excitation source (Figure 1, points b–d) and the bridge output (Figure 1, points a–c) does increase at frequencies greater than 1 MHz, though its sign is the same as at low frequencies. The output of the bridge is amplified and demodulated.[61] The major disadvantage to the classical design is that over time the bridge must be rebalanced and care must be taken that the impedance of the arm adjacent to the subject (Figure 1, points c–d) is much greater than the impedance between the electrodes. If the latter point is not addressed then the impedance change recorded will be due in some unknown amount to the undesirable interelectrode impedance. Advantages of this configuration include the ability to detect a wide range of impedances and great sensitivity to low level impedance changes.[17]

In bipolar systems, it is desirable to place the electrodes as closely as possible on a straight line joining opposite ends of the head. In this way the current flow through the interior of the head will be maximized. The longer undesirable current pathway around the head through the scalp and subcutaneous tissues will then be minimized. As the electrodes are brought closer together an increasing percentage of the superficial tissues will contribute to the overall REG signal[46] along with field effects from the electrodes themselves (*i.e.* nonuniform current lines). Seipel[68] conducted a series of experiments in which he varied electrode size and composition and he determined that increasing the size of the electrodes minimizes the extracranial contribution to the REG waveform.

In an effort to avoid the necessity of rebalancing and to minimize the measurement of superficial changes, a four electrode, or tetrapolar, configuration was developed (this is sometimes referred to as Rheoencephalography II). In this design two outer electrodes inject a current and two inner electrodes detect voltage changes when the signal is passed into a high input impedance amplifier (see Figure 2). Ideally, no current flows through the pickup electrodes. Therefore, the high impedance amplifier isolates the head and changes in voltages are directly due to changes in impedance by Ohm's Law. This occurs without introducing the effect of an impedance drop caused by current flow to the electrodes through more superficial tissues. However, events close to the detectors will distort potential current lines more than distant ones. Therefore, the current supplying electrodes and their voltage pickup counterparts should be spaced as far away as possible from their respective mates in tetrapolar systems, *i.e.* no closer than 3 cm.[46]

The four electrodes should also be placed in a linear array. This is particularly important when the electrodes are placed on an irregularly shaped object, such as the head. For simplicity, consider a spherical head of homogenous content and uniform ρ. If we placed the electrodes on either side of the head, the bulk of the current density would go directly through it. This would minimize the contribution

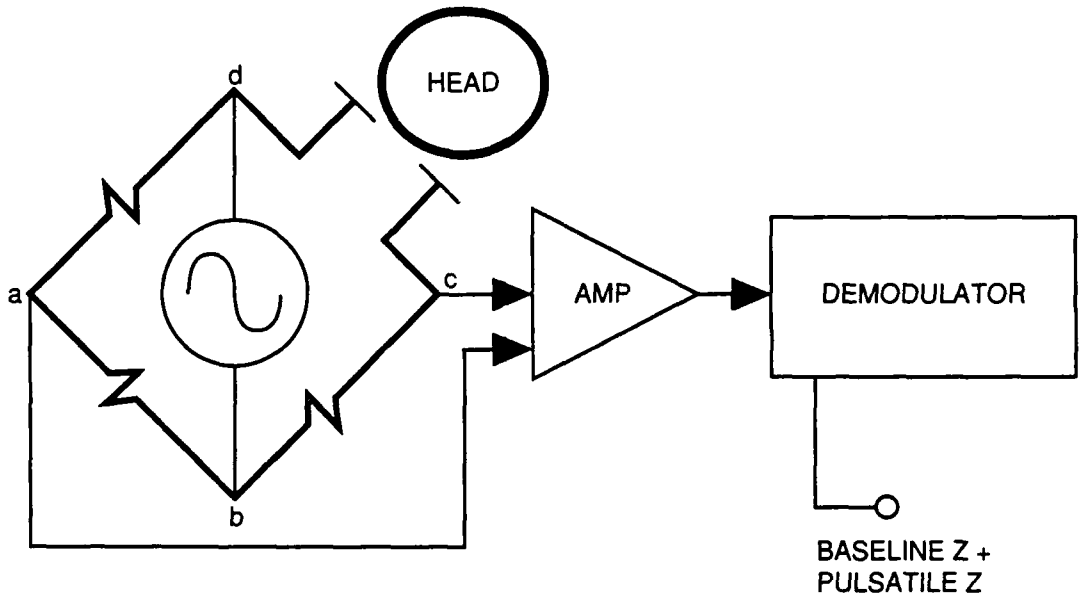

Figure 1. Basic 2 electrode rheoencephalograph.

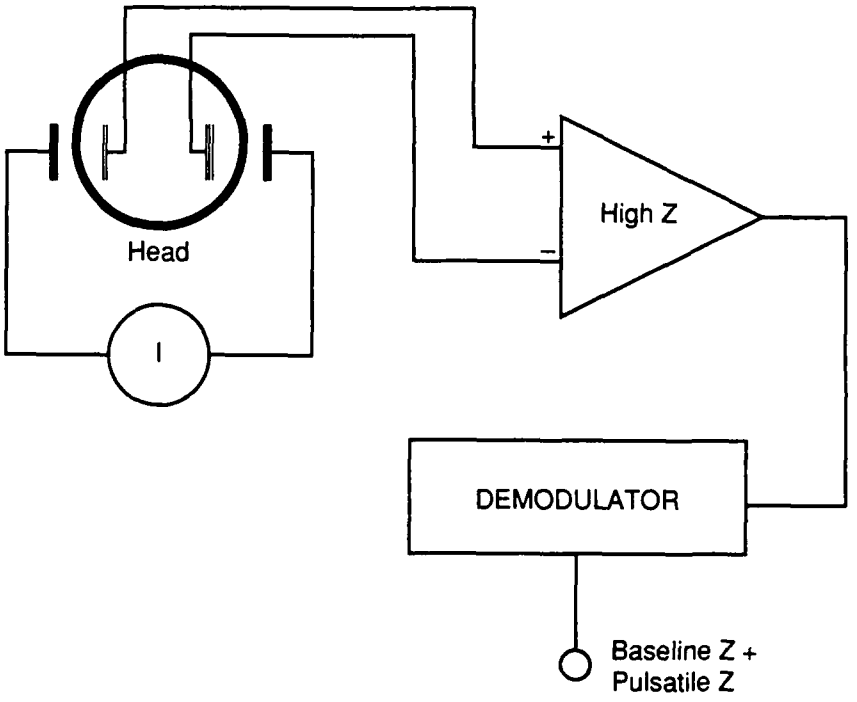

Figure 2. Basic 4 electrode rheoencephalograph.

of superficial tissues to overall impedance measurements.

The following are some possible electrode placements (these apply for both bipolar and tetrapolar configurations):

1) Fronto-mastoid — this presents a symmetrical view of the right and left cerebral hemispheres

2) Bi-temporal — this arrangement is considered to indicate primarily vascular changes in the internal carotids.

3) Bi-occipital — this primarily indicates vascular changes in the vertebral artery area.

4) Fronto-occipital or fronto-mastoid, with the two homologous electrodes tied together — may be considered to give an average representation of the entire cerebral circulation.[46]

CLINICAL PROBLEMS WITH REG

In the late 1960's and early 1970's, the use of Rheoencephalography held high promise in clinical neurology. The method is noninvasive, convenient, and adaptable to both patient monitoring and diagnosis of cerebral vascular disorders. It is non-intrusive and objective. Some problems attributed to the clinical use of REG include a relative lack of anatomic selectivity and rather major signal "artifacts" upon changes in posture (particularly in the craniocaudal axis) and respiratory efforts, such as the Valsalva maneuver. The use of REG for the evaluation of cephalic circulation under conditions of acceleration stress is warranted because the very same "artifact" which apparently interferes with the use of REG in clinical neurology is of critical interest in acceleration studies; namely, the bulk movement of blood between the head and the rest of the body with postural (gravitational field orientation) changes and respiratory maneuvers. Also, in acceleration studies, it is of interest to monitor the total cephalic circulation not just the intracranial component.

Historically, a major challenge in recording the REG has been the composite nature of the impedance changes that were measured. The resting baseline impedance is determined by the composition (blood, bone, *etc.*) of the body part being examined, its geometry, and the electrode interface. Bulk shifts of blood, such as those resulting from venous occlusion of a limb, the Vaisalva maneuver or high-G forces, cause changes in the range of 1–2% of the total baseline value. Resistance changes resulting from arterial pulsations are three orders of magnitude smaller than the baseline resistance. With previous circuits and display devices, acquisition of the pulsatile component resulted in loss of much information about the bulk blood shifts.

Seipel[68] proposed the following explanation to account for some of the clinical problems associated with REG. He stated that the extracranial circulatory component of the REG may increase ipsilaterally in cases where extracranial or intracranial lesions significantly restrict internal carotid blood flow without similarly altering the external carotid circulation (external carotid artery inversion). This ipsilateral increase can explain a large percentage of the reported clinical inaccuracies of REG, while collateral circulation supplied to the intracranial vasculature by the less involved major arteries and/or the deep branches of the external carotids accounts for much of the remainder.

VALIDATION OF REG TECHNIQUE

That the REG does indeed measure the state of cephalic circulation has been validated in a number of ways. The following are a few examples.

REG peak time (alpha or α) is defined as the time from the initial rise of the anacrotic portion of the REG waveform to the maximum peak amplitude. α is known to be related to the cerebral circulatory resistance and arteriographic and isotopic transit times.[33] Hadjiev[25] used a radioisotopic venous dilution technique (using I-131 as the indicator) to determine CVR. He took a series of bipolar fronto-mastoid recordings of REG and measured α. He then calculated the ratio of α to a single cardiac cycle ("T," in seconds). The ratio α/T is sometimes referred to as the "rheographic time." This parameter gives information on vascular tone and the cerebral vascular resistance of the investigated hemisphere. Hadjiev then performed a least squares correlation analysis on the CVR, as measured radioisotopically, and the relative portion of α to the R-R interval and found a reasonable ($r = 0.81$, $P < 0.001$) correlation between the two measures. Hadjiev[26] then argued in a later article that since cerebral vascular changes allow for fluctuations in cerebral blood flow and redistribution within the skull, one could obtain a measure of cerebral blood flow (CBF) in the following manner. If one measures the mean arterial pressure, Pm, CBF can be calculated as:

$$\mathrm{CBF(ml/min)} = \frac{(60)(\mathrm{Pm})}{\mathrm{CVR}} \qquad (6)$$

where $\mathrm{CVR} = (-2.57 + 1.39X) \pm (1.70Sy)$,

X = relative part of α to the R-R interval,

Sy = 4.25; which is one standard deviation from the regression line. The large deviation about the regression line can be attributed to extracranial blood flow and the movement of CSF.

In 1974, Jacquy *et al*[33] compared the use of REG with two dynamic methods of cerebral blood flow (CBF) measurement: isotopic mean transit time (MT) and isotopic regional CBF. They found significant correlation ($r = 0.93$, $P < 0.001$) between the isotopic transit time using the 133 Xe clearance method (intra-arterial injection) and the rheographic time. In these experiments, the REG was measured with a tetrapolar configuration in which the excitation electrodes (metal plates, 3 × 5 cm) were placed fronto-occipitally, and the pickups (1 cm needles inserted subcutaneously) were placed in the lateral fronto-occipital regions.

The state of the cerebral vessels is controlled to a large extent by the concentration of CO_2 in the tissues. Increasing pCO_2 is a powerful vasodilating agent.[37] Therefore, as pCO_2 rises, one would expect that the magnitude of the REG would decrease as the number of conducting species in the blood increased. Bostem and Thibaut,[6] in a study with normal patients, demonstrated an increase in amplitude of the REG as their subjects experienced hypocapnia caused by hyperventilation. Conversely, as their pCO_2 increased (by breathing a mixture of 7% CO_2 in oxygen), the REG was attenuated. Namon *et al*[59] in a study in 1967 was able to obtain similar results.

There is some question as to whether the REG waveform merely registers the motion of the electrodes as the skin moves in accordance with the heart beat. Geyer[18] performed a series of experiments to address this question. At first, he fashioned an *in vitro* apparatus in which blood vessels were simulated by a glass tube. Pulse-like flow pressure could be introduced and measured. Using a tetrapolar rheoencephalograph he found that only fresh whole blood could produce a REG-type waveform. As flow was increased, the rheographic conduction value (defined for blood as a speed-dependent change in electrical resistance without plethysmographic effect) decreased. As flow became uniform, the rheographic conduction value was unchanged. The magnitude of the impedance was shown to increase as the number of erythrocytes was increased. Finally, he stated that the occurrence of a rheo-

graphic conduction value was direction independent. This meant that the speed dependent value was always the same regardless of which direction the blood was perfused. In a series of similar experiments Gollan and Namon[22] confirmed much of Geyer's findings. Further, they discovered that the magnitude of the REG waveform is dependent on the RATIO of number of red blood cells to plasma. This was based on the finding that the introduction of osmotically swollen erythrocytes also increased the measured impedance. Based on these findings, it is clear that the REG is more than a simple reflection of changes in cross sectional area of blood vessels.

INTERPRETATION OF PULSATILE REG (ΔZ) WAVEFORM

The form of the pulsatile REG waveform, or ΔZ, is quite variable and is subject to change depending on the state of the cephalic vasculature, size and placement of the electrodes, and preparation of the electrode site. It has a few prominent features, the size and timing of each can give an indication of the ebb and flow of the cephalic circulation (see Figure 3).

There is an initial large peak, usually a global maximum, called an "A" wave. This occurs with the systolic phase of the cardiac cycle and the peak of the A wave follows the R wave of the ECG (under normal conditions) by an average of 300 msec. Under certain conditions (see below) a "pre-systolic wave" occurs during the rise of the A wave. A downward inflection, the "B" wave, follows the A wave and is similar in appearance to the dichrotic notch seen in arterial pressure waveforms. Following the B wave is another rising peak, usually smaller in magnitude than the A wave, called the "C" wave. Following this peak there can be a number of smaller inflections before the end of the period of the waveform. The period, "T," is the same length as the ECG R-R interval. The time from the initial rise of the A wave to the peak is called the REG peak time (α) and the ratio α/T is called the "rheographic time." Some authors also measure the angle of inclination of the rising A wave and use it to determine the "expansion rate" of cerebral vessels, expressed as the tangent of that angle.[62] It is important to realize that the REG in its present state ONLY provides information on the RELATIVE state of the cephalic circulation. Therefore, the REG contains valuable information as expressed by changes in rheographic indices that result when comparing unstressed waveforms to those measured during acceleration stress or functional testing. Many laboratories use different REG instruments and some of these have been used in correlative studies that form the basis for the following list. However, the REG device that was developed in the course of this thesis project is unique and awaits similar studies (see Recommendations for the Future, below).

Clinical investigators have used these features and along with the results of functional tests, *e.g.* orthostatic tests, inhalation of CO_2, performance of straining maneuvers, *etc.*, and correlative measurements[6,25,33,59] have proposed a number of indices to evaluate ΔZ as follows:

1. A wave: this is referable to the peak of the systolic inflow of blood into the cephalic circulation. This observation is based on studies employing vasodilators, such as CO_2;[59]

2. C wave: this is associated with overall venous pressure and the relative amount of impedance to venous outflow, based upon studies using intravenous injection of nicotinic acid;[27]

3. α/T: this gives information as to the elasticity and tone of large and intermediate size vessels, *i.e.* CVR.[33,57] Correlative studies by Hadjiev[25] and Jacquy *et al*,[33] using radioisotopic clearance mesurements, have been conducted to support this claim;

4. B/A: this ratio gives an indication of arteriolar tone,[56,33,57] based on experiments in which chemical agents affecting vascular tone altered the timing and amplitude of the REG "dichrotic notch;"

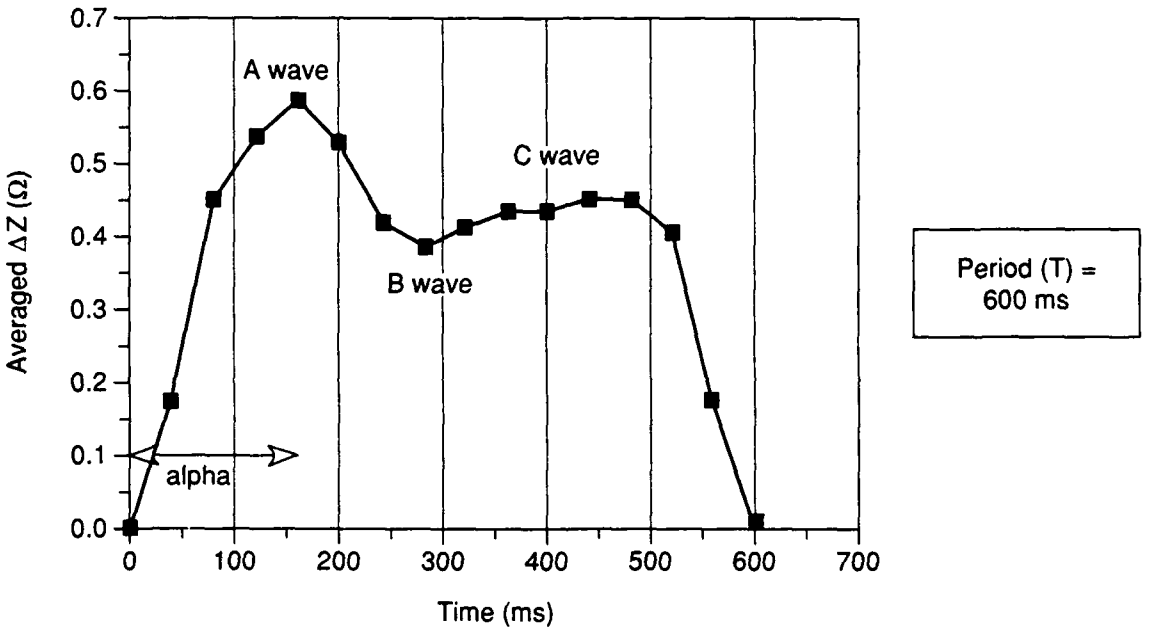

Figure 3. ΔZ waveform with indices labeled.

5. C/A: changes in this ratio indicate alterations in blood outflow and venous tone. This observation is based on the effects of functional testing, such as anti-orthostatic tests which promote venous congestion;[56,57]

6. α: a shorter α, and therefore a steeper A wave, is an indication of decreased vascular tone;[33]

7. Pulse wave delay: this is the time from the peak of the R wave of the ECG to the peak of the ΔZ A wave. McHenry[53] noted that this delay was prolonged with increased CSFP. He attributed this change to an increase in pulse propagation time or to an increase in venous pressure. This explanation may be inadequate in the case of an increase in pulse wave delay under a +Gz load;[32]

8. Pre-systolic wave: Hadjiev[27] noted that there was no direct association with this wave and overall venous pressure or changes in CSFP. He attributes this to regional fluctuations in the filling of cerebral veins.

Most of these measures will reflect changes in CVR. Pathologic deviations or exposure to a high +Gz field will be manifested by signs of dilated or constricted vascular lumen. Therefore, changes in the shape of ΔZ and the indices may give information on the existence of vascular dystonia and alterations in cephalic venous outflow.

To summarize, these are the alterations in ΔZ that accompany changes in CVR, according to Hadjiev:[27]

1. Reduced vascular tone:
   a. steep rise of ascending portion of the A wave (decreased α);
   b. increased blood filling (decreased impedance as reflected in the A wave);
   c. sharp peak of A wave;
   d. overt incisure (B wave) located in the lower third of the descending portion of the curve or very close to the baseline.

2. Increased vascular tone:
   a. slower rise of ascending portion of the A wave (impedance is altered more slowly due to impeded blood inflow);
   b. decreased blood filling (increased impedance as reflected in the A wave);
   c. rounded peak of A wave;
   d. poorly defined incisure (B wave) located in the upper third of the descending portion of the curve.

Factors other than those affecting CVR contribute to the overall state of the cephalic circulation and therefore indirectly affect ΔZ. The skull limits the amount of expansion of the brain to compensate for increased blood volume which leads to blood and CSF redistribution. The CSF acts to keep the venous circulation patent by following changes in venous pressure with similar changes in CSFP. Finally, the lumen and tone of the cerebral vessels are influenced by arterial and venous pressure, heart rate, and some metabolic factors, *e.g.* pCO_2 and arterial pH.

OTHER DEVICES CURRENTLY IN USE TO ESTIMATE +GZ-TOLERANCE

1. Direct *in situ* measurement: Both electromagnetic and ultrasonic flow probes are available for implantation on blood vessels such as the carotid artery. Their major disadvantage is, of course, the need for surgical implantation; absolutely precluding their use in humans. Another factor to be consid-

ered is the presence of multiple sources of cephalic blood flow (two each of the carotid and vertebral arteries along with the dorsal spinal artery).

2. Behavioral Methods: These rely upon a response or performance on the part of the subject. An example of such a method is the "NADC light bar." The NADC light bar is an instrument that is used to measure the peripheral vision of a subject who is exposed to acceleration stress in a human centrifuge. Mechanically, the bar is a fixed aluminum semi-circular channel with a 30 inch radius. It is mounted at eye level to give a peripheral coverage of 180 degrees. On the metal channel are 118 discrete light emitting diodes (LED), 59 on either side of the center line. The LEDs are spaced at increments of 1.5 degrees starting at 180°. The LEDs can appear to be red, green, or yellow. The +Gz-tolerance end-point is usually taken as the point where a subject's field of vision has collapsed to a 60 degree forward visual cone. The operation of the light bar is computer controlled. The computer acts to extinguish the lights from the periphery while the subject, by pulling back on a joystick, illuminates the lights to the farthest limits of his/her peripheral vision. Effective use of this instrument as a reliable and reproducible indicator of +Gz-tolerance is greatly dependent on the training and experience of the subject in its operation.[8]

Although generally non-invasive, these methods are intrusive — they require the attention and participation of the subject; thus they are not suitable for in-flight use, nor are they readily applicable to animal studies.

3. Neurophysiologic Methods: The electroencephalogram (EEG), in its conventional form, is complex to interpret. Alterations due to ischemic anoxia of the brain require four to fifteen seconds to appear.

Use of visual evoked potential (VEP) has shown some promise. Nelson, *et al*[60] have developed a method for objective real-time (4–5 seconds) monitoring of the steady state VEP. They employed the Fast Fourier Transform to develop a method to maximize the signal-to-noise ratio. That is, a digital frequency domain non-white noise matched filter is used to evaluate the signal only at the expected response peak. The coefficients of the matched filter have to be derived empirically by analysis of test data obtained in a test static centrifuge run performed prior to a dynamic run. Real-time processing of VEP is vital if this is to be used as a +Gz-tolerance end point indicator. This is due to the variable time course of visual symptoms and the fact that as blackout is approached, the visual evoked response progressively decreases. Obviously, this method shows promise but requires pre-run analysis and extensive computer support.

4. Transcutaneous Ultrasonic Blood Velocity Methods: Among conventional methods used in high +Gz studies, application of transcutaneous ultrasonic blood velocity measurement to the external carotid and/or superior temporal arteries provide the most precisely quantitative estimate of the cephalic circulation. Stability of the probe placement is a significant problem. Other uncertainties relating to the use of ultrasonic blood velocity measurement under +Gz have been discussed at length.[38]

Pulse Wave Delay: Hrebien[32] has developed a technique using a 8.2 MHz directional ultrasonic doppler flowmeter to measure +Gz-tolerance. In a centrifuge experiment in which the doppler, light bar, and plethysmograph recordings were taken, a consistent pulse wave delay was obtained between the peak of the ECG R wave and the peak of the doppler and plethysmographic waveforms. The most useful aspect of this "delta delay" is that the delay lengthens with increasing levels of acceleration as compared to the delta delay at 1 g. Also, with the addition of anti-G protective measures, such as the use of an AGS and a supinating seat, the delta delay increases at a reduced rate with increasing amounts of protection.

5. Moderately Invasive Clinical Methods: These include indicator dilution methods for blood flow and contrast radiography (carotid arteriogram). Not only are these unacceptably dangerous to the subject, but also the flow information is an average over five to twenty heartbeats — hardly acceptable for events of such rapid onset as PLL.

6. Reflectance Photoplethysmography: A reflectance plethysmograph (RP) senses changes in the opacity of flesh between a light source and a reflector, such as blood and bone. A photodetector responds to changes in blood volume and produces a signal that mirrors that change. Jaron, *et al*[34] used such a device in order to predict the onset of PLL. A variable (>2 seconds, depending on rate of +Gz onset) lead time occurred between the onset of PLL and a reduction in magnitude of the RP signal by 20%. This method produced successful prediction rates in both PLL and non-PLL centrifuge runs which favorably compare to similar doppler predictions. The authors admit that improvements need to be made in both detection and signal processing for more reliability.

7. Methods related to Ophthalmodynamometry: The basic method among these is compression ophthalmodynamometry (COPD). Intraocular pressure (IOP) is raised by applying pressure upon the globe with a spring tension device. The systolic and diastolic ophthalmic artery pressures are deduced by observing ophthalmoscopically the behavior of the central artery to the optic disc. Oculoplethysmography (OPG) is the first of a series of methods in which corneal or scleral cups are applied to the eyes. In OPG, the condition of the cephalic circulation is inferred from the symmetry, particularly with respect to timing, of the pulsations detected from each eye. With oculopneumoplethysmography (OPPG), IOP is manipulated by means of a scleral cup. Application of suction deforms the globe such that the IOP will rise. The onset of pulsations in a corneal sensing cup signals the point of systolic ophthalmic artery pressure. The IOP change is derived from the level of suction in the scleral cup by means of an empirical calibration chart. Oculocerebrovasculometry (OCVM) also uses a scleral cup to alter IOP along with a digital pneumotonometer to measure the IOP and to detect the onset of arterial pulsations. Proponents of this method claim that this technique provides a more direct measurement of IOP. All of these methods have the advantage that the phenomenon being measured is the central and basic issue in visual derangement with a +Gz load; namely, evaluation of circulation in the intraocular vessels. A major disadvantage is that the technical circumstances of these procedures are most unsuitable for in-flight or centrifuge testing. These techniques occlude the subject's vision and they require a mechanically stable and quiet environment.

USE OF REG IN ACCELERATION STRESS ENVIRONMENT

REG was studied intensively in the 1960's as a potential diagnostic tool in the diagnosis of cerebral vascular disease. Today, it is still widely used in the U.S.S.R. and Europe. A decline in interest in the U.S. may be attributed to two factors — one intrinsic and one extrinsic to the method itself. The former factor consists of the claim that the REG reflects primarily the extracranial circulation of the head. Some of the counter arguments to this statement have already been discussed. In addition, there are rather wide baseline swings coincident with the phases of normal respiration and the performance of respiratory maneuvers, such as the Valsalva and AGSM. In fact, many current designs of impedance plethysmographs go to great lengths to supress this variation.[40,63] Indeed, in the clinical setting, where a neurosurgeon may wish to decide which radicle of the internal carotid requires surgical attention, REG is not specific enough. However, where the basic question pertains to the general economy of the cephalic circulation, such a method is sufficient. The baseline variations, rather than being an annoying artifact, probably represent shifts of blood between the head and body. This information is potentially very useful in the +Gz environment. The extrinsic factor to the decline of interest in REG has been the development of new clinical modalities, including two dimensional ultrasonic imaging, computerized axial tomography, and magnetic resonance imaging. These provide very precise and

detailed information about the cephalic circulation. Their intensive requirements of computer time and elaborate and delicate equipment are not a problem in a clinical setting.

There are several advantages towards using the REG to measure the small impedance changes that arise due to changes in blood volume under acceleration stress. I have already described the temporal sensitivity of the device. The REG is virtually innocuous in terms of danger to the subject, discomfort, inconvenience, and constraints upon the performance of mission-oriented tasks. It is objective, in that it does not depend upon a response or participation of the subject. The equipment is relatively simple and inexpensive. The REG is also quite suitable for use in animal experimentation.

METHODS

REG CIRCUITRY

The first objective to satisfy in this project is the design and development of an impedance plethysmograph that can successfully record the small amplitude impedance changes arising from the head under normal conditions and while exposed to a +Gz load. A block diagram of the "NADC REG" is given in Figure 4. The principle underlying the operation of the device is as follows. The head comprises the unknown impedance arm of a modified Wheatstone bridge, which is excited by a 95.2 kHz sinusoidal voltage. The head can be considered as a series combination of impedances; a low frequency component coincident with heart rate, a dc value comprising the impedance of the head, skin, and neural tissues, and a baseline impedance which is modulated by the low frequency impedance. The bridge output therefore consists of an amplitude modulated high frequency carrier riding on a dc offset. This AM signal is passed to a high input impedance instrumentation amplifier. This stage does not load the bridge, *i.e.* draw current, and eliminates unwanted noise signals common to the differential bridge output. The AM signal is processed by a narrow (carrier ± 1 kHz) bandpass filter tuned to attenuate all but the carrier and the bandpass frequencies. The size of the bandpass was chosen as a compromise between employing a simple circuit design with reasonable component values and permitting passage of all physiologic frequencies (*e.g.* heart rate). The signal is then demodulated via a classic diode-lowpass filter combination to remove the carrier. The baseline impedance ($f \leq 0.1$ Hz) is separated from the low frequency impedance ($f \geq 1$ Hz) via a slow ($\tau = 74$ ms) integrator-subtraction circuit. This separation method was chosen rather than simple filtering due to the low frequency content of the waveforms[46] (a circuit with τ in this range operates at ten times the frequency of the baseline impedance). Both waveforms are then amplified and buffered for transfer to display and recording devices.

The acceleration "hardiness" of the REG has already been demonstrated.[72] In designing this device, among the major considerations were portability, safety (isolation), sensitivity, low noise and real-time processing of the impedance signals. The REG is battery operated and includes the use of low-power IC chips in order to avoid most patient isolation problems, particularly those associated with line frequency electric shock. All electrical connections to and from the head and the output signals are all buffered with operational amplifiers. Battery power allows the device to be portable and allows more flexibility when it comes to installing it in the centrifuge gondola at NADC for acceleration studies. A problem that occurs with these devices is that when one obtains a differential signal from the head of the subject, the signal can be eliminated by the patient touching a metal object. In order to overcome this phenomenon, the earlier versions of the device included placement of an additional ground electrode on the subject in an attempt to create a common reference level between the device and the centrifuge gondola. (See Figure 8a for details of the earlier version of the bridge detection circuit).

The newest version of the device, to be tested in 1989 at NADC, employs the use of a high frequency 1:1 matching transformer (3 MHz) to isolate the patient and a dual battery power supply. A ±9 volt power source consisting of two 9 volt batteries, will energize the front end. The front end (*i.e.* the oscillator) will then have a totally separate ground from the subject and any potential ground loops will be effectively eliminated. The currently used ±9 volt supply (12 "C" batteries) will power the back end (*i.e.* the processing circuitry). Figure 5 shows the details of the battery power supplies. The third electrode, the ground, will then be no longer necessary. Patient isolation will be assured and electrode application will be further simplified. Note that all data presented in subsequent sections of this thesis were obtained using the older version of the device.

The REG splits the impedance signal obtained from the head into two components in real time:

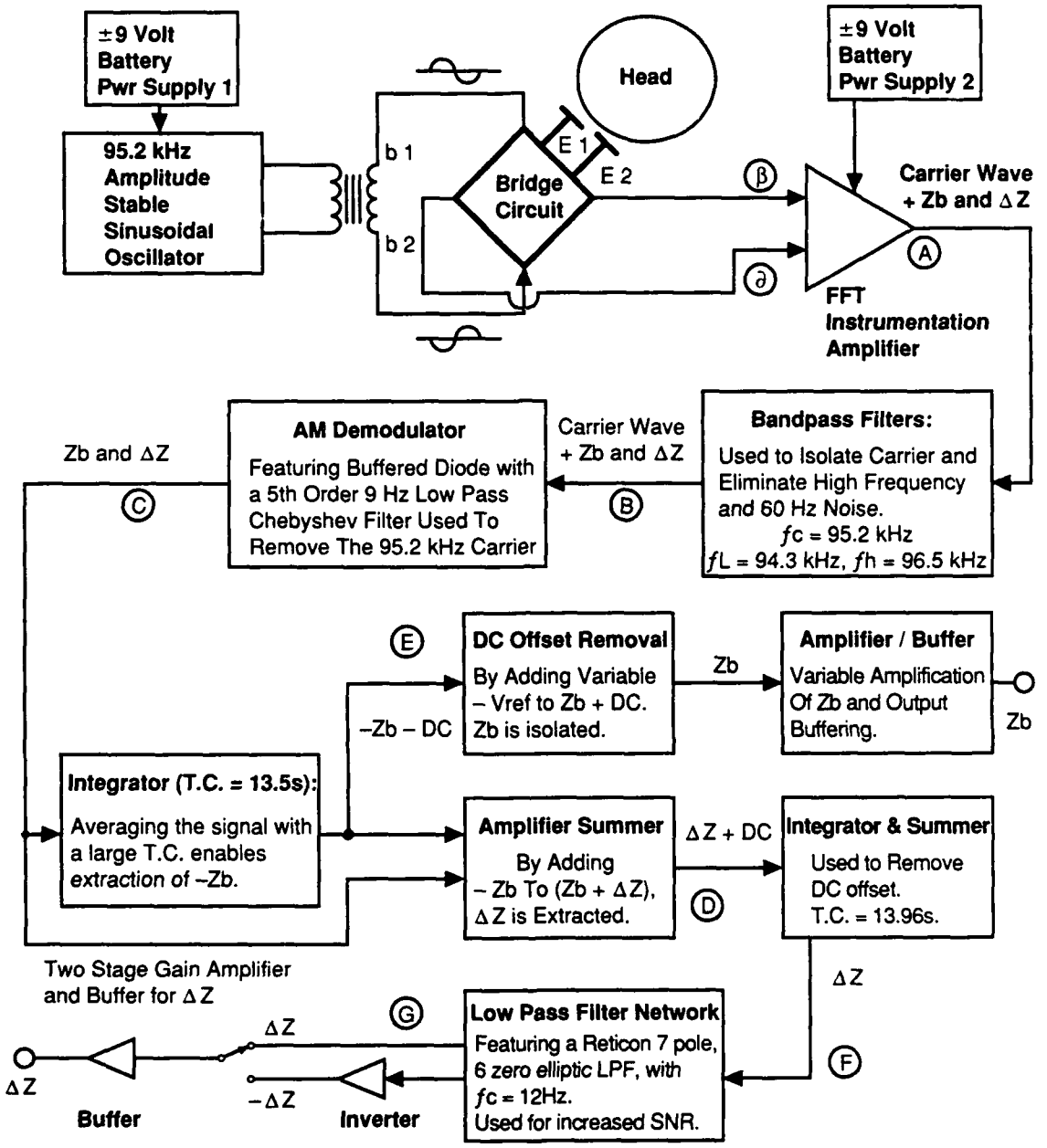

Figure 4. Block diagram of circuit used to detect impedance changes due to pulsatile changes in blood volume, cephalic baseline impedance shifts due to respiration and M1/L1 maneuvers, and bulk movement of cerebrospinal fluid in and out of the skull (REG).

KEY

E1-2 : Electrode connections from the bridge circuit to the subject's head.
Zb : Baseline impedance reflecting bulk movement of blood in and out of head.
ΔZ : Pulsatile impedance change (~ 20 – 200 mΩ).

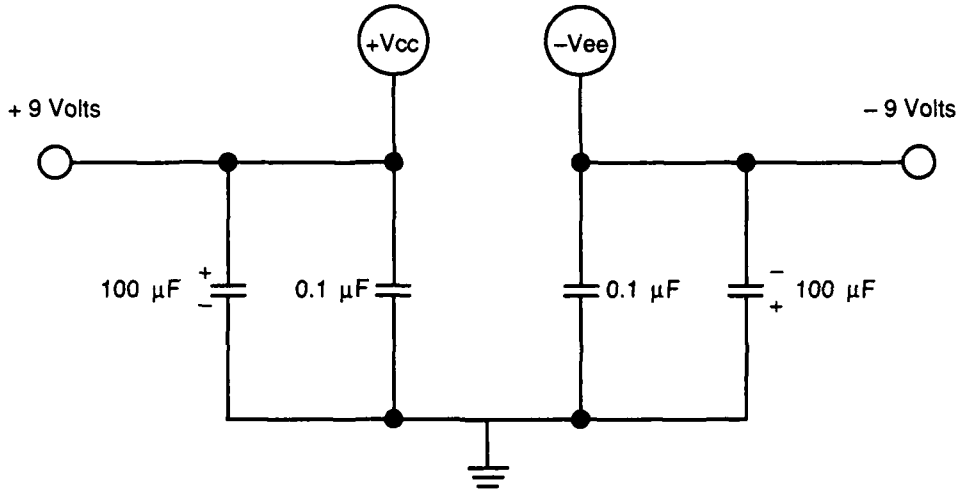

Figure 5. REG Battery Power Supply.
Back end includes 12 "C" Alkaline Batteries
Front end includes 2 9 volt Alkaline Batteries

1) impedance changes referable to the pulsatile variation in blood volume (ΔZ), and 2) the "baseline" impedance which is an indication of the bulk movement of blood between the head and the rest of the body (Zb). A strip chart of the composite ΔZ + Zb waveform (uppermost trace), ΔZ (middle trace), and Zb (bottom trace) is shown in Figure 6. In this figure, the head of the subject was tilted down, simulating –Gz exposure. The two electrodes were positioned bitemporally. ΔZ + Zb, measured at point C of Figure 4, is approximately 10 mVp-p riding on a –700 mV dc offset. In order to display it in Figure 6, ΔZ + Zb was ac coupled and amplified 100 times. Unstressed ΔZ ranges from approximately 470 to 530 mΩ. Note the decrease in ΔZ amplitude with an increase in blood flow under these conditions along with the shift in Zb as the head tilted down and then up (see arrows on Figure 6). ΔZ and Zb are primarily resistive quantities at 100 kHz as evidenced by the low phase shift measured between the oscillator output and the instrumentation amplifier output (point A in Figure 4). When the skin-electrode interface is properly prepared, *i.e.* skin cleansed with alcohol, good adhesion of the surface electrodes, *etc.*, the phase shift is approximately –3.5°. This indicates a capacitive shift in the signal caused by the head. If skin preparation is inadequate, the phase shift can be as high as –27°, due to skin capacitive effects.

Since the aim of this REG is to obtain a relative measure of the overall state of the cerebral blood circulation and not to diagnose deep cerebral incidents, a bipolar (two electrode) design for the excitation/receiving electrodes was chosen. A bipolar arrangement is highly sensitive and can detect very low level changes better than a tetrapolar system. The sensitivity of the bridge transducer is 0.7 mV/Ω. The output of the device is linear beyond the expected range of ΔZ, *i.e.* 0–50 Ω, assuming a basal resistance of the segment of 1 kΩ. This was derived by plotting a regression line for sensitivity ($S = dVout/dR$) versus change in resistance. The equation was

$$S = -7.07 \times 10^{-4} + 3.65 \times 10^{-6}\, dR, \qquad (7)$$

where the coefficient of determination, R^2, was 0.861. With amplification, the ΔZ output voltage ranges from 350 to 750 mV/Ω. This arrangement also has the added benefit of simpler circuit design and ease of experimental setup. With a bipolar configuration, the electrode placement on the subjects is simplified as compared to the tetrapolar arrangement (which uses a constant current source activating two stimulating, with two receiving electrodes between them).[64]

In order to promote safety and record a signal that essentially contains all real (no reactive) components,[83] a sinusoidal excitation frequency of 95.2 kHz, ±1.4 volts peak-to-peak, produced by an amplitude stable sinusoidal oscillator (see Figure 7), is used to energize a resistance bridge. This oscillator was derived from a design by Ravi Shankar and Webster.[63] A similar oscillator is also found in Linear Applications Handbook 1.[80]

In Figure 7, operational amplifier A_1 is connected as a two-pole low pass active filter (LPF) and A_2 is configured as an integrator. This combination of op amps oscillates when the loop gain is high enough at the frequency in which the phase lag of the amplifiers is 180°. The amplitude is stabilized via zener diodes D_1 and D_2. The distortion introduced by these diodes is reduced by the LPF. Since D_1 and D_2 have essentially equal breakdown voltages, the resulting symmetrical clipping virtually eliminates the even order harmonics. The third harmonic is approximately 40 dB down at the output of A_1, leading to a total harmonic distortion of about one percent. Oscillation frequency and threshold are set by R_1, R_2, R_3, C_1, C_2, C_3, and C_4. R_4 is set much smaller than R_2 so that the effective resistance at R_2 does not drop when the zener diodes conduct.

A_3 acts as an oscillator load and buffer stage. Half of A_4 serves to reduce the gain (Av = –3.01 kΩ/ 10 kΩ = 0.33) and current consumption. The other half of A_4 employs high precision (0.025%) resistors

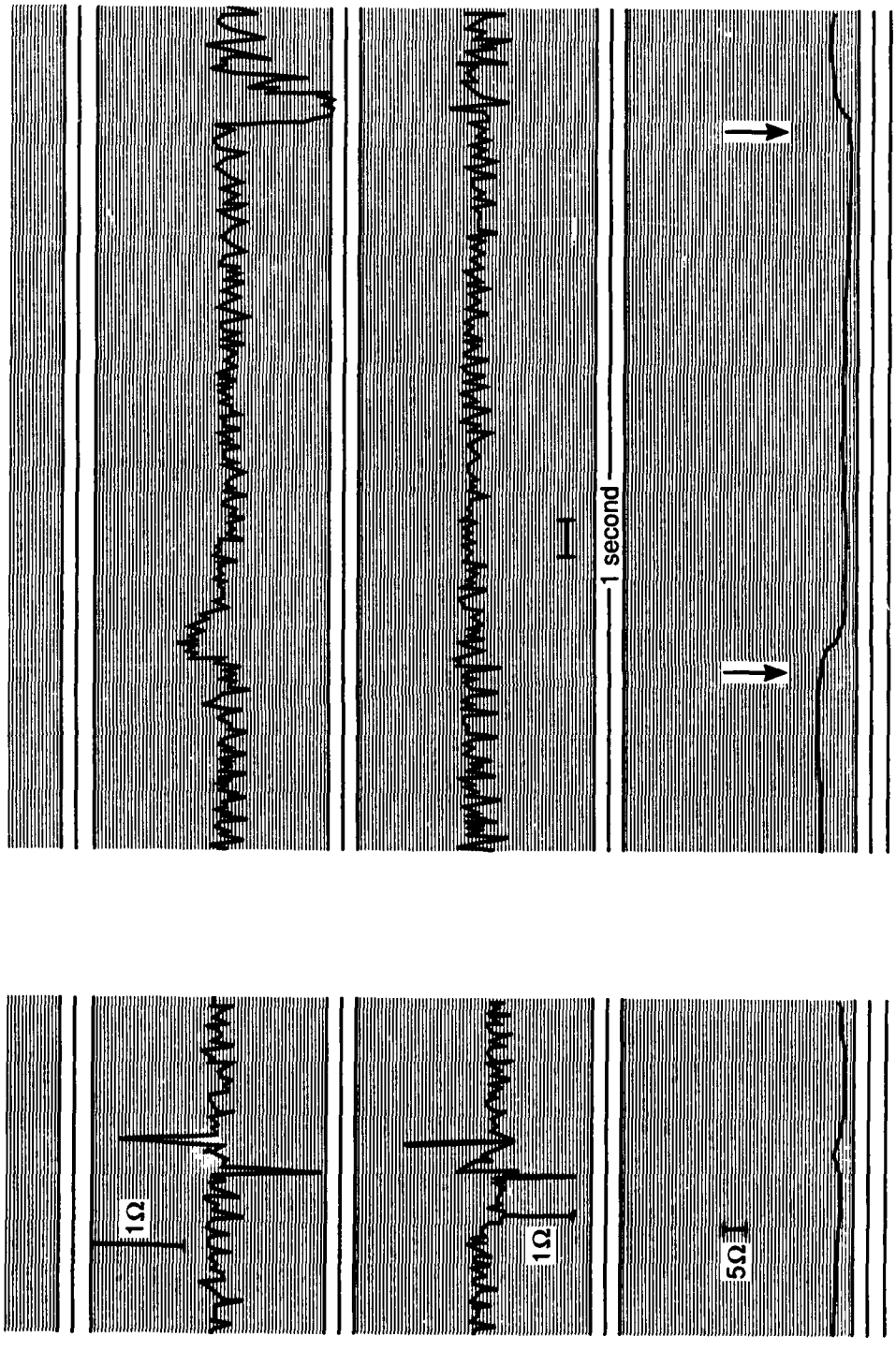

Figure 6. Unstressed REG waveforms. From top: composite of ΔZ + Zb amplified 100 times and ac coupled to remove –0.7 V dc offset (50 mΩ/div), ΔZ (59 mΩ/div), Zb (1 Ω/div).

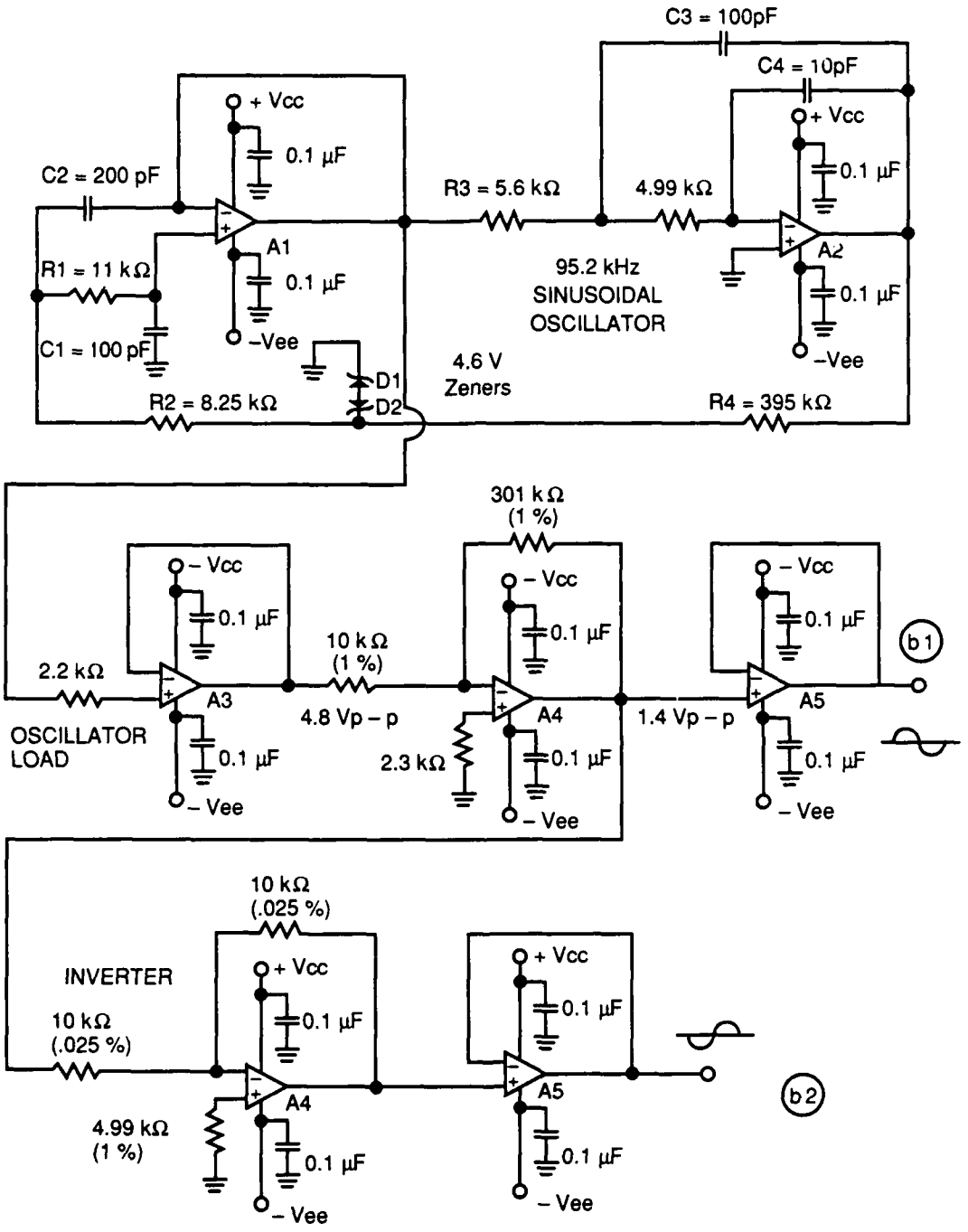

Figure 7. 95.2 kHz Amplitude Stable Sinusoidal Oscillator, Gain Reduction Stage, and Inverter for ± Signal Excitation To Detection Bridge

KEY

A1,2 : LF 351 Oscillator.
A3 : TL071 LOad/Buffer Stage.
A4 : 1/2 TL072 Gain Reduction/Buffer Stage.
A5 : 1/2 TL072 Signal Inversion/Buffer Stage.

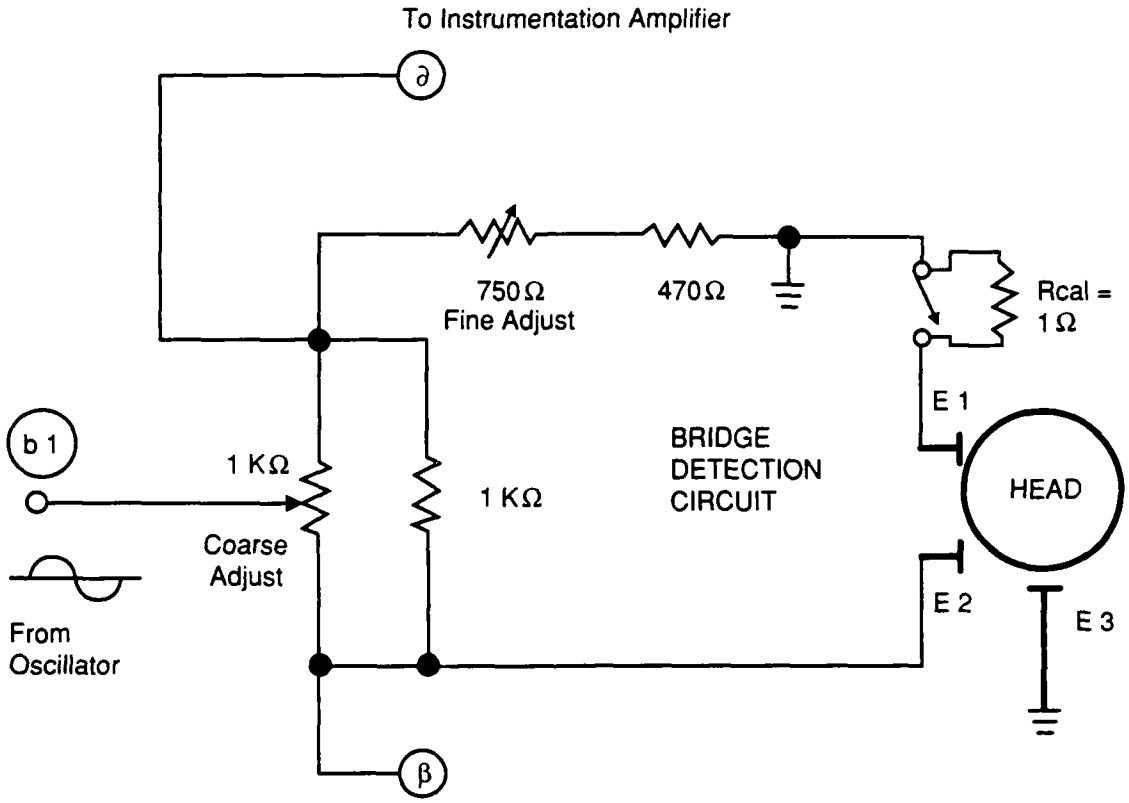

Figure 8a. Older version of Bridge Detection Circuit. Note bridge is excited by + sinusoid on one side and ground on the other. There is a ground electrode applied to the head (E3). A 1 kΩ resistor lies across the course adjustment potentiometer.

Rcal — Calibration Switch — Normally closed, when opened adds 1.0Ω to head.

E1–3 — Electrodes affixed to subject.

to shift the sine wave 180° for a ± excitation source for the bridge. The two output waveforms from A_4 are passed through buffer stages (A_5) prior to connection to the transformer (see Figure 7, points b_1 and b_2).

Details of the improved bridge detection circuit design can be found in Figure 8b. The major changes include a ± excitation voltage as opposed to a single ended approach. This effectively eliminates the previous need for an inversion switch prior to ΔZ output. The bridge also receives slightly more current than previously. The potential value of the variable resistance arm of the bridge has been increased. This will enable setting the bridge to correct operating levels with wider swings in the basal resistance of the head (primarily due to the skull and electrode interface). The elimination of the third electrode and the 1 kΩ resistance across the fine adjust potentiometer should increase detectable signal power.

Due to the small size of the signal in relation to the relatively large dc offset that occurs at this point in the circuit, the bridge is operated "off-null" and balancing the bridge entails changing its variable resistors (large swing and fine adjustment) until a maximum amplitude signal is obtained. Included in the bridge is a 0.1 Ω calibration resistor used to both correlate a fixed ohmic change to a voltage excursion and to provide a quick check that the device is operating properly. Since the value of the calibration resistor is so low, it is connected to a low resistance (10 mΩ) miniature SPDT toggle switch (ALCOSWITCH #MST-105E).

To describe the bridge output voltage, the resistors are described as follows. The "coarse adjust," a 1 kΩ 10-turn precision wirewound potentiometer (Spectrol model #534), is used to correct the output voltage based on the unknown resistance of the head. The excitation sinusoid is applied to the wipe of the potentiometer and its two portions can be described as 1 kΩ – XΩ(R_1) and XΩ(R_2). The unknown resistance is expressed as a series combination $R_3 + \Delta R_3$, where R_3 is the dc resistance and ΔR_3 is the small change due to changes in blood volume, of both pulsatile and bulk movement origins. R_4 is the series combination of the "fine adjust" potentiometer and a fixed 1 kΩ resistor. The latter is used to help keep the bridge off null. Typical base dc resistance of an entire mammalian head ranges from about 80–1000 Ω.[57] Assuming proper skin preparation, this arrangement requires very little bridge adjustment among individual subjects, a very useful feature when one considers the high cost of delays in human centrifuge experimentation. Classical analysis of the bridge[71] leads to the following equation for output voltage. Vout, which will vary based on ΔR3, based on the above fixed resistances which form two potentiometric dividers across the excitation voltage, Vin:

$$Vout = \frac{R_1 Vin}{(R_1 + R_4)} - \frac{R_2 Vin}{R2 + (R_3 + \Delta R_3)} \tag{8}$$

or

$$Vout = \frac{\left[\frac{R_1}{R_4} - \frac{R_2}{R_3 + \Delta R_3}\right] Vin}{\left(\frac{1 + R_1}{R_4}\right)\left(\frac{1 + R_2}{R_3 + \Delta R_3}\right)} \tag{9}$$

Once the head is excited, an amplitude modulated composite signal, Zt, (ΔZ + Zb + carrier) is passed into a FET instrumentation amplifier (IA) to detect a differential signal off of the head and to

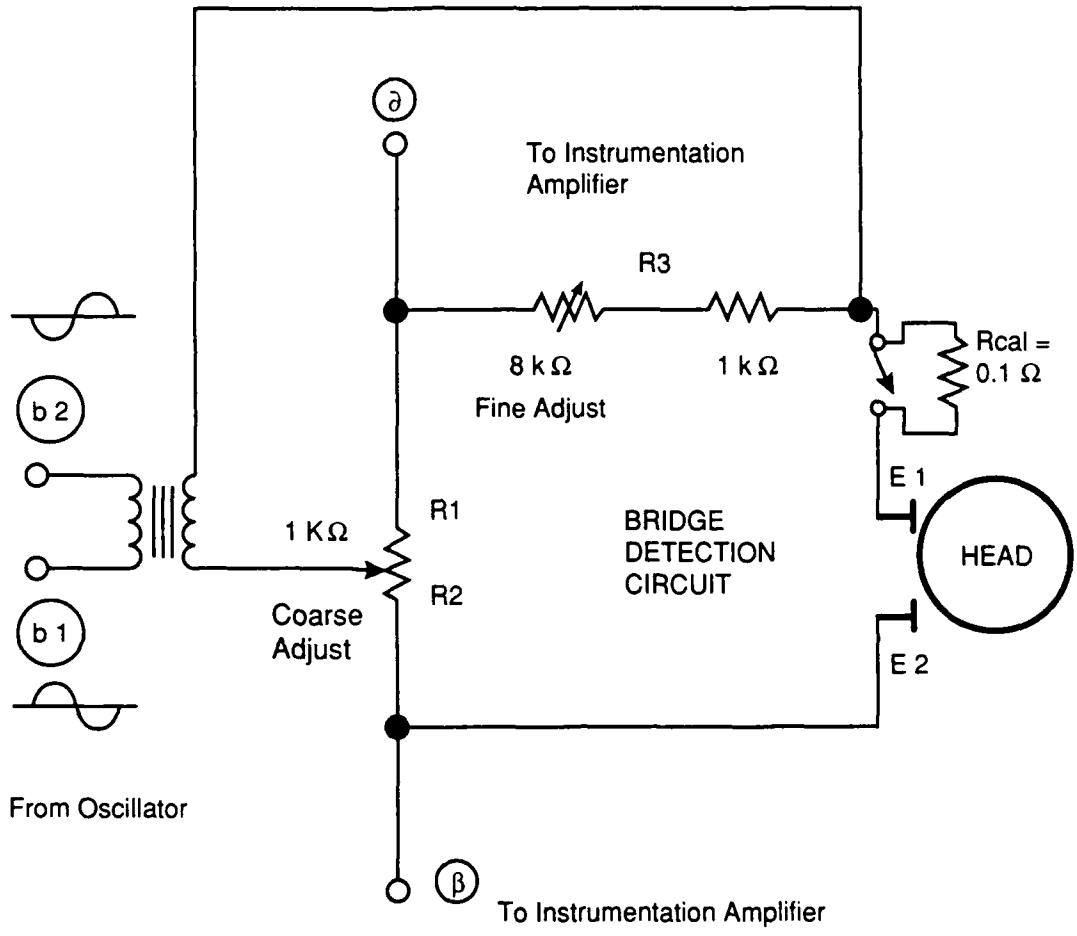

Figure 8b.	Newest version of Bridge Detection Circuit. Note bridge is excited by ± sinsuoidal voltage. There is no grounding electrode attached to the head. 1:1 matching transformer added to isolate excitation voltage from subject.
Rcal	Calibration Switch – Normally closed, when opened adds 0.1 Ω to head.
E1, E2	Electrodes affixed to subject.

ohmically isolate the subject (see Figure 9). Output offset voltage is removed from the IA from a voltage divider between pins 1 and 5 of op amp A_7. The overall voltage gain, Av, of the IA is

$$Av = \left[\frac{2Ra}{Rc} + 1\right]\left[\frac{R_8}{R_6}\right] \tag{10}$$

if Ra = Rb, $R_6 = R_7$, and $R_8 = R_9 + R_{10}$. R_{10} is used to maximize common mode rejection. Ra, Rb, R_6 and R_7 are 1% precision resistors to ensure that the equalities hold. Rc sets the gain. The capacitors used in A_8 serve to minimize the frequency response of the IA above 100 kHz. The overall gain is set at 42. This was a compromise between reasonable gain and the high input impedance of the FET op amps. The common mode rejection ratio is 60 dB at 100 kHz.

Zt is then placed through a cascade of two active filters comprising a narrow bandpass filter section (BPF), centered about the carrier frequency, which reduces high and 60 Hz frequency noise (see Figure 10). The first section is a biquad BPF, which is characterized by a constant absolute bandwidth.[78] The gain of the filter, K, is variable as determined by R_1 (series combination of a 20 kΩ potentiometer and a 3.9 kΩ fixed resistor) and R_2. The Q of the filter is set by R_2 and the center frequency, ω_0, is set by R_3 and C_1. The transfer function for this BPF is given by

$$H(s) = \frac{\frac{K\omega_0 s}{Q}}{\frac{s^2 + s\omega_0}{Q + \omega_0^2}} \tag{11}$$

where Q = 20, $1.4 \le K \le 8.6$, $\omega_0 = 613.2 \times 10^3$ rad/s (97.6 kHz), V_{out} = output voltage, V_{in} = input voltage, and bandwidth = 7 kHz. To choose the values of R_1–R_4 and C_1, these factors were first normalized: $\omega_0 = 1$ rad/s, $C_1 = 1$F, and $R_4 = 1\Omega$. Then $R_1 = Q/K$, $R_2 = Q$, and $R_3 = 1\Omega$. To denormalize these values, the frequency normalizing factor, μ, and the impedance scaling factor, ISF, were calculated as follows:

$$\mu = \frac{\omega_0}{\omega_n} \tag{12}$$

$$= \frac{2\pi f_0}{1\text{ rad/s}} = \frac{2\pi(100000)}{1\text{ rad/s}} = 200000\pi$$

where the subscript n refers to the normalized value and

$$ISF = \frac{f_0}{20\pi} \tag{13}$$

$$= \frac{100000}{20\pi} = 1591.55$$

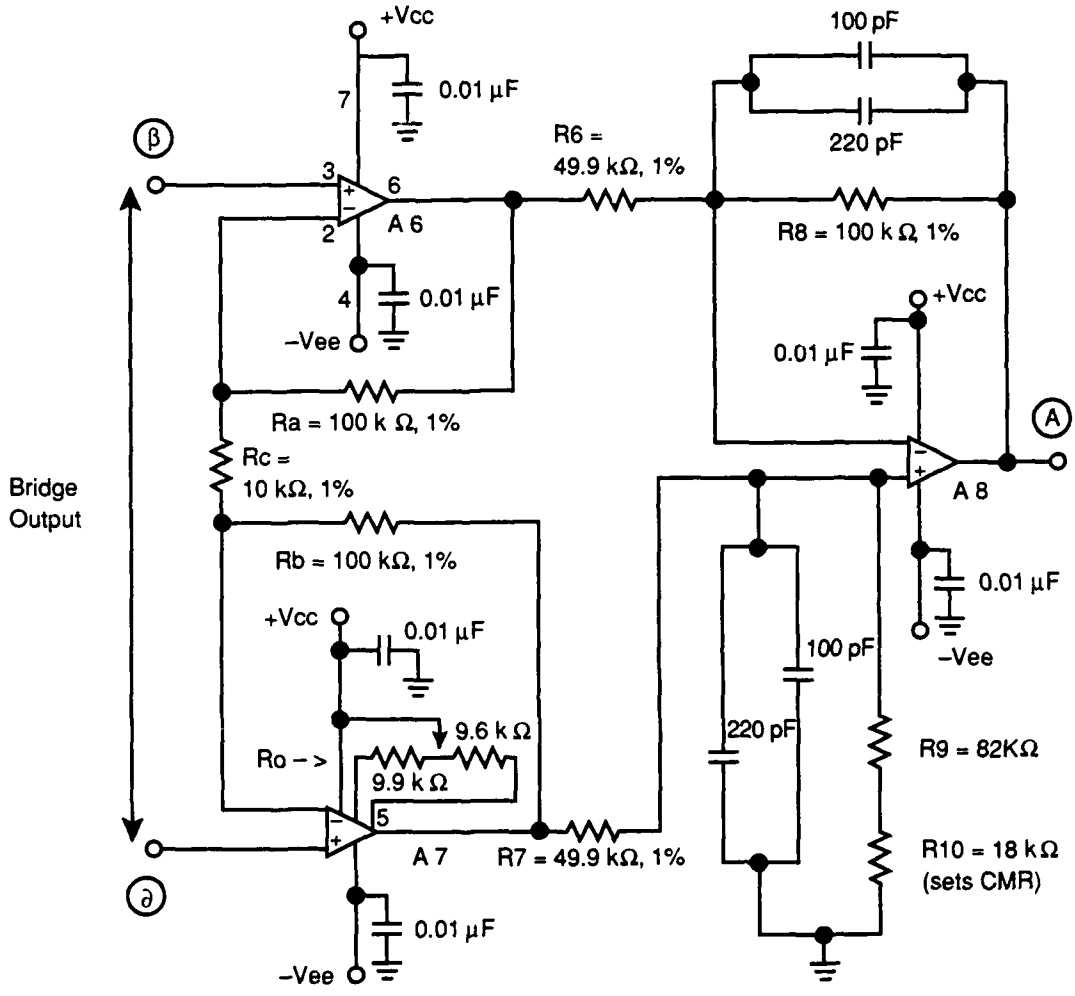

Figure 9. Instrument Amplifier — Low Pass Filtered To Eliminate High Frequency Noise.

KEY

A6–A8 : LF356N.
Rc sets the gain for the front end (Gain = 21).
R6 sets the gain for the back end (Gain = 2). Overall Gain – 42.
at Ro is a resistor pair that provides DC offset control.
Input voltage is on the order of 20 mV.

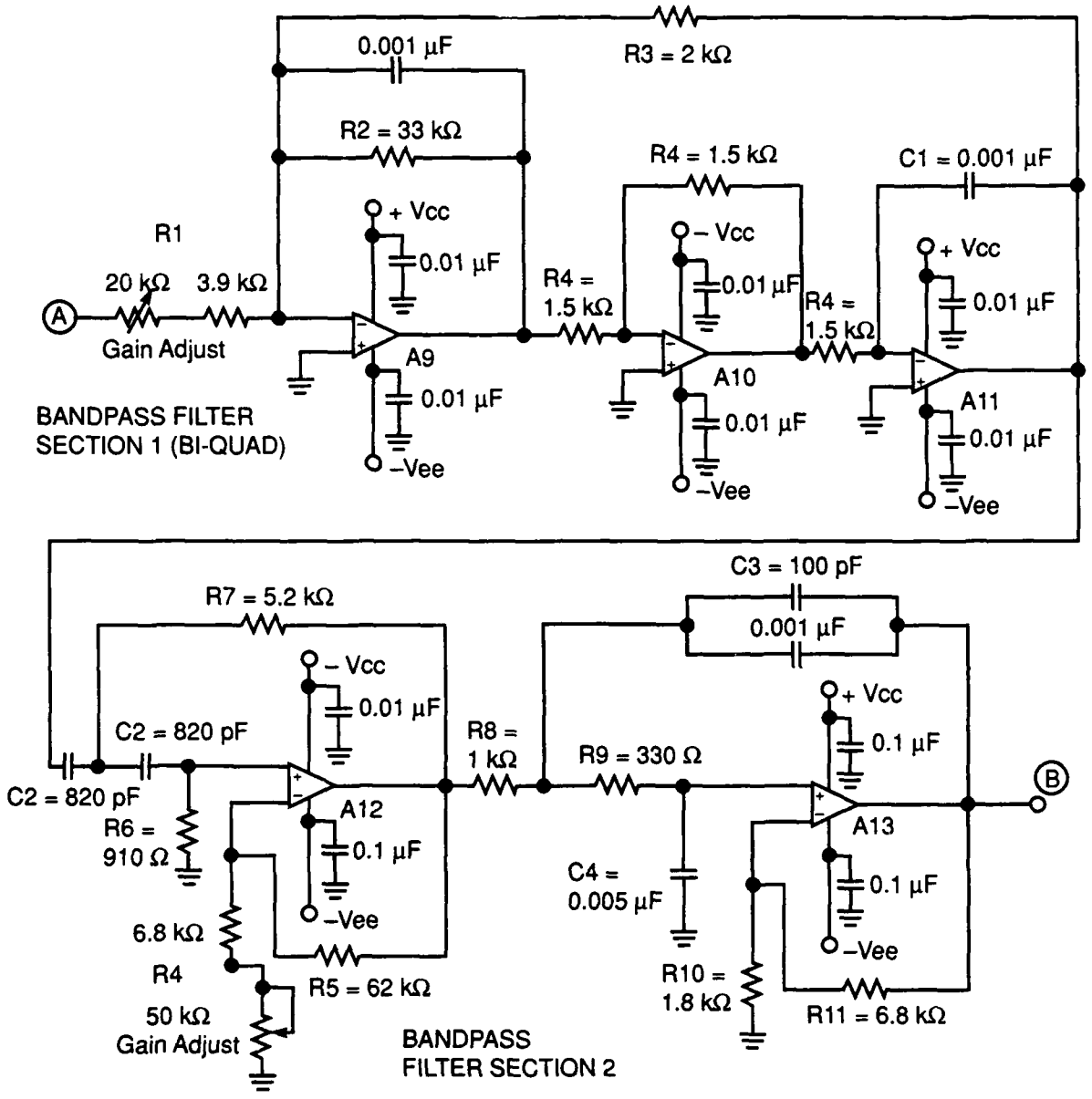

Figure 10. Bandpass Filters—Eliminates Both High and Low Frequency Noise Interference While Retaining AM Modulated Carrier.

KEY

A9-A13 : LM318N.
fl (Center Frequency) = 95.2 kHz Sinusoidal.
fl (Lower 3 dB Frequency) = 94.3 kHz Sinusoidal.
fh (Higher 3 dB Frequency) = 96.5 kHz Sinusoidal.

Then the capacitances and resistances were calculated as

$$C = \frac{Cn}{\mu ISF} \tag{14}$$

$$R = ISF(Rn). \tag{15}$$

To improve on this stage, a second active BPF was added which consists of a cascade of a second order Chebyshev voltage controlled voltage source (VCVS) high pass filter (HPF) and a second order VCVS LPF. The transfer function of the HPF is given by

$$H(s) = \frac{Ks^2}{a_0 + a_1 s + s^2} \tag{16}$$

where the variable gain, K, is set by $R_5/R_4 + 1$ and ranges from 2 to 10. R_4 is the series combination of a 50 kΩ potentiometer and a fixed 6.8 kΩ fixed resistor. The Chebyshev coefficients, for a 0.5 dB ripple width (ripple factor ≈ 0.349), are a0 = 0.66 and a1 = 0.94. The cutoff frequency is set at 90 kHz. C_2 was normalized to 1F. Normalized conductances were found by using Equations 17 and 18.

$$G_7 = \frac{\left\{a_1 + \left[a_1^2 + 8\,a_0\,(K-1)\right]^{\frac{1}{2}}\right\}}{4} \tag{17}$$

$$G_6 = \frac{a_0}{G_7}. \tag{18}$$

The denormalized capacitances and resistances were calculated as above with Equation 14 and

$$Ri = \frac{ISF}{Gi}, \tag{19}$$

where i = integer index, using μ and ISF with f_0 = 90 kHz.

The transfer function of the LPF is given by

$$H(s) = \frac{K\,b_0}{s^2 + b_1 s + b_0} \tag{20}$$

where the variable gain, K, is set by $R_{11}/R_{10} + 1 \approx 5$. For a ripple width of 0.5 dB, b0 = 1.516 and b1 = 1.426. The dc offset of the filter is minimized by choosing

$$R_{11} = K(R_8 + R_9) \tag{21}$$

$$R_{10} = \frac{K(R_8 + R_9)}{K-1}. \tag{22}$$

R_8 and R_9 are determined in a similar fashion to the HPF by solving for the following conductances

$$G_8 = \frac{\left\{b_1 + \left[b_1^2 + 8\, b_0 (C_4 + 1 - K)\right]^{\frac{1}{2}}\right\}}{2}. \tag{23}$$

$$G_9 = \frac{a_0}{G_8}. \tag{24}$$

To make the radical in Equation 21 positive, C_4 was set to 4F. The denormalized capacitances and resistances were determined by Equation 14 and 19, respectively, with f_0 = 100 kHz.

The overall bandwidth of the BPF section is center about 95.2 kHz with an upper –3 dB frequency of 96.5 kHz and a lower –3 dB frequency of 94.3 kHz.

Then Zt is AM demodulated to remove the carrier signal (see Figure 11). This is accomplished by the classic diode-LPF series combination. To improve on the carrier frequency rejection, the typical passive LPF has been replaced by a VCVS Chebyshev active LPF. Design requirements included a maximum attenuation in the pass band of 0.5 dB (ripple factor, ε = 0.349) and a minimum attentuation in the stop band of 60 dB. The cutoff frequency is 9 Hz ($\omega c = 20\pi$) and the stop frequency is 30 Hz ($\omega s = 60\pi$). To obtain these features, a fifth order filter was required, as determined by solving for N (filter order) in Equation 25 (78).

$$20 \log \varepsilon - 6\,(N-1) - 20\, N \log \frac{\omega s}{\omega c} \geq 60 \text{ dB} \tag{25}$$

Three active LPFs were cascaded, one first order stage, which included a gain of –6 (set by resistor R1), and two second order stages, both with a gain of one. The transfer function of each stage (H_1, H_2, H_3) is multiplied to obtain the overall H(s) as

$$H(s) = H_1 H_2 H_3 \tag{26}$$

$$H(s) = \frac{-K_0}{s + b_0} \; \frac{Kab}{s^2 + a_1 s + b_1} \; \frac{Kbb2}{s^2 + a_2 s + b_2} \tag{27}$$

where K_0, K_a, and K_b are the gains of stages 1, 2, and 3, respectively. For a 0.5 dB Chebyshev filter, the coefficients are: b_0 = 2.863, a_1 = 0.351, b_1 = 1.064, a_2 = 0.947, and b_2 = 0.356. Using a similar normalizing/denormalizing procedure are above, the circuit components are determined as follows. The

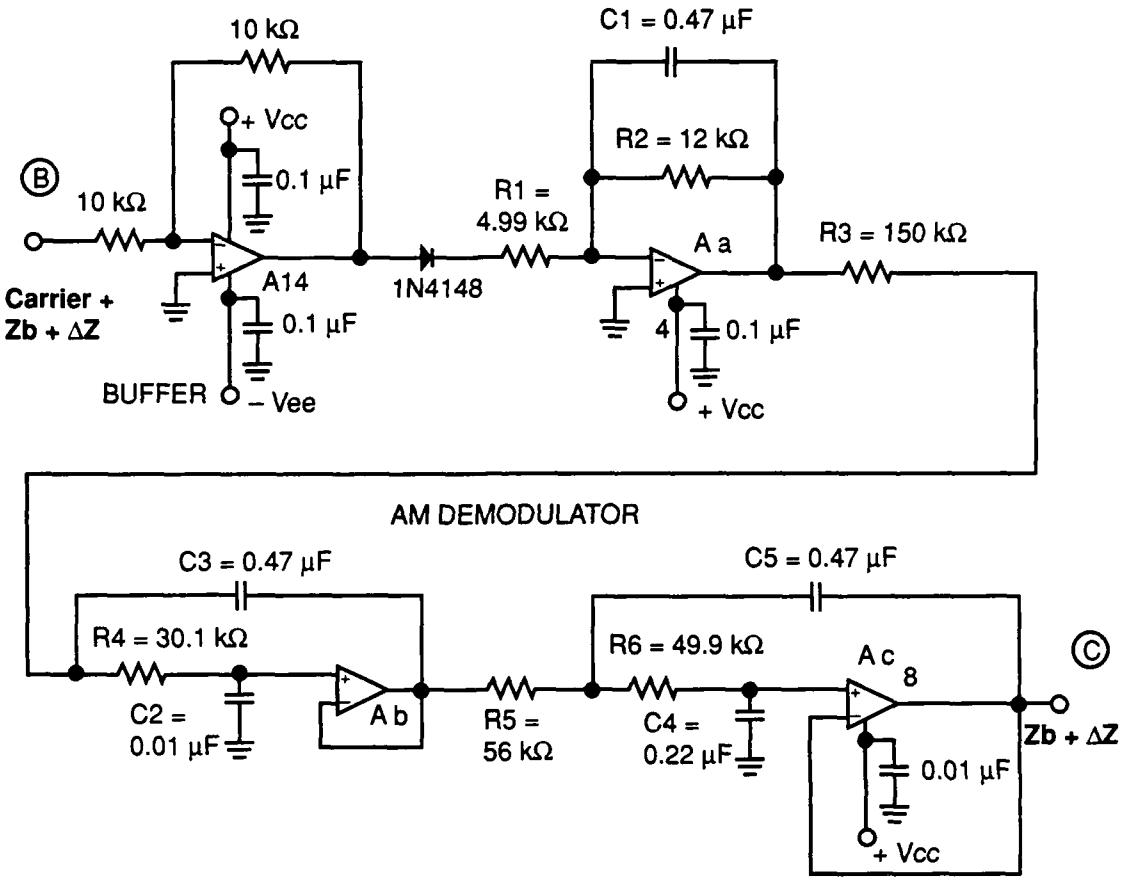

Figure 11. Buffer and AM Demodulator; Featuring A 5th Order 9 Hz Low Pass Chebyshev Filter.

KEY

A14 = LF356N.
A15 = Aa-Ac, formed using TL074CN JFET Quad Op Amp.
Zb = Baseline Impedance Signal.
ΔZ = Pulsatile Impedance Signal.
Carrier = 95.2 kHz Sinusoidal.
Filter Characteristics:
Theoretical Gain Aa = 6 (Set by value R1)
Gain of Kb and Kc = 1.
3 dB Pass Frequency = 9Hz.
Stop Frequency = 30 Hz.
Maximum Attenuation in Passband = 0.5 dB.
Minimum Attenuation in Stopband = 60 dB.
All Capacitors (except 0.1 µF & 0.01 µF) are Mylar

capacitors are normalized as $C_1 = C_3 = C_5 = 1F$, $C_2 = 0.025$ F, and $C_4 = 0.6$ F. The conductances are calculated by using Equations 28–33.

$$b_0 = \frac{G_2}{C_1} \tag{28}$$

$$K_0 = \frac{-G_1}{C_1} \tag{29}$$

$$G_3 = \frac{\left\{a_1 + \left[a_1^2 + 4\,b_1\,(C_2 + 1 - Ka)\right]^{\frac{1}{2}}\right\}}{2} \tag{30}$$

$$G_4 = \frac{C_2\,b_1}{G_3} \tag{31}$$

$$G_5 = \frac{\left\{a_2 + \left[a_2^2 + 4\,b_2\,(C_4 + 1 - Kb)\right]^{\frac{1}{2}}\right\}}{2} \tag{32}$$

$$G_6 = \frac{C_4\,b_2}{G_5} \tag{33}$$

Capacitor and resistance values were denormalized using Equations 14 and 19, respectively, for f_0 = 10 Hz. The higher value capacitors (0.22 and 0.47 μF) are mylar type for better filter stability.

To isolate ΔZ, the baseline impedance is removed by using a slow integrator (time constant ($\tau = R_1C_1$) = 74 ms) and an analog summer (see Figure 12a). A_{16} is a continuous integrator with matched high value resistors at the negative input terminal and in the feedback loop. A continuous integrator features a dc "gain stop" resistor, R_2, across C_1 to reduce the integrator gain from the full open-loop value.[39] In order to obtain such a long time constant, very large resistances were employed to prevent possible input failure by using a capacitance > 0.1 μF.[39] Error from input bias current is minimized by the use of a high input impedance op amp and mylar capacitors.[39] These resistors maintain identical dc offset amplitude of opposite polarity at points "a" and "b." This ensures that ΔZ is centered about Zb with a small dc offset. Integration over a relatively long time period acts to eliminate the pulsatile waveform while averaging Zt. Therefore, ΔZ drops out of Equation 34 during the long term continuous integration.

$$Vout = -\left(\frac{1}{R_1 C_1}\right)\int Vin\ dt \tag{34}$$

where V_{in} is the voltage at point "a," referable to ΔZ + Zb and Vout is the voltage at point "b," referable to −Zb + dc. The limits of integration are from any arbitrary point in time to 74 milliseconds later. −Zb + dc is then summed with Zt in an analog summer to produce ΔZ + dc, as seen in Equation 35.

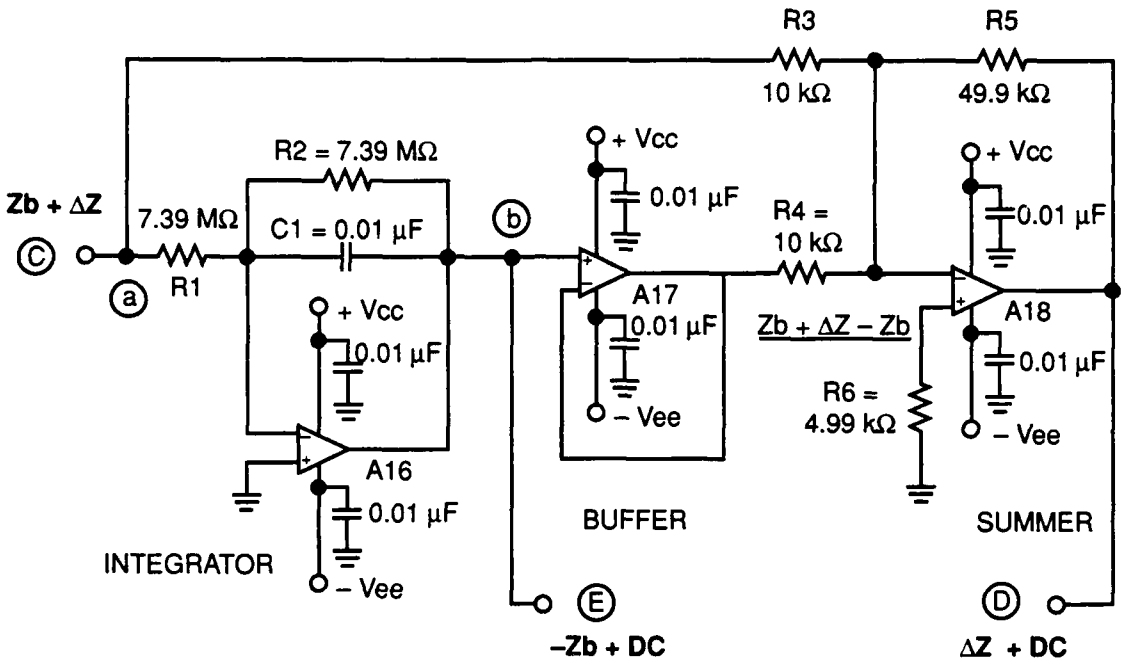

Figure 12a. Separation of Zb (Baseline Impedance Signal) From ΔZ (Pulsatile Impedance Signal).

KEY

A16-17 : TL071N JFET Input Wideband Op Amp.
A18 : LF356N

Features:
Continuous Integrator: Matched valued resistors maintain identical DC offset amplitude at opposite signs at points "a" and "b." This ensures that ΔZ is centered about Zb with a small DC offset remaining.
fc = 2.15 Hz. Time constant = 74 ms.
Amplifier Summer: Extracts ΔZ by removing Zb by simple subtraction.
Rc: Eliminates voltage offset by balancing impedance at input terminals of A18.

$$V_{(\Delta Z + dc)} = V_{(Zt)}\left(\frac{R_5}{R_3}\right) + V_{(-Zb + dc)}\left(\frac{R_5}{R_4}\right) \quad (35)$$

Note that the voltages listed in Equation 35 refer to their associated impedances. The gain of each input to A_{18} is –5 and R_6 acts to eliminate offset voltage error by balancing the impedance seen by the input terminals of A_{18}.

The negative dc offset that accompanies Zb is removed by a subtraction circuit with a variable positive voltage reference source, LM317, and is shown in Figure 12b. The output voltage of the LM317 (V_o) compensates for the negative offset according to Equation 36.

$$V_0 = Vref\left(1 + \frac{Ra}{R_1}\right) \quad (36)$$

where $V_{ref} = V_0 - V_{adj}$; reference voltage equals the difference between the voltage at the output and adjustment terminals of the LM317. The subtraction circuit is an analog summer which produces an amplified voltage referable to Zb without a dc offset, $V_{(Zb)}$, whose value is determined by Equation 37.

$$V_{(Zb)} = \frac{V_{(-Zb + dc)}(R_4 + R_5)}{R_2} + \frac{V_0(R_4 + R_5)}{R_3} \quad (37)$$

Zb is then buffered for output for passage to other devices.

The dc component that remains with ΔZ is also removed by a slow integrator and an analog summer in a circuit similar to that in Figure 12a (see Figure 13). The explanation accompanying the previous circuit is identical except that the voltage referable to ΔZ + dc is passed through an inverting amplifier with a gain of 10 and the time constant for this circuit is 72 ms ($\tau = R_1C_1$).

To increase signal-to-noise ratio, the pulsatile impedance signal is then low pass filtered using a Reticon© 7 pole-6 zero elliptic switched capacitor filter (RF5609A) (see Figure 14), which has a 75 dB stop band rejection and less than ±0.5 dB passband ripple. dc offset voltage is nulled by a voltage divider network between pins 1 and 7. Filter characteristics are controlled by an external clock circuit which is set to frequency f_{clk} = 1200 Hz. The cutoff frequency, f_c, is 0.1 f_{clk}, or 12 Hz. The sampling rate is 50 f_c, or f_s = 600 samples/sec. The square wave clock is an RC comparator oscillator consisting of a LM319 high speed linear comparator whose frequency is set by $f_{clk} = 0.56/R_1C_1$. This circuit produces an easily tuned, very accurate, stable square wave output.[41] For accurate reproduction by the sampling system of the filter, no frequencies greater than $f_s/2$ can be connected to the input of the filter.[41] To insure this, ΔZ is first passed through an antialiasing second order VCVS Butterworth LPF. The components of this filter are derived as above by using Equations 20–24 using Butterworth coefficients b_0 = 1.0 and b_1 = 1.414 and a gain of 1. The cutoff frequency is 200 Hz. Denormalized capacitances and resistances are found using Equations 14 and 19, respectively. To remove noise spikes generated by the clock, the filter output is passed through a passive R-C LPF, with a cutoff frequency $f_c \leq 0.1\ f_{clk}$.[41] Therefore, $f_c = 1/(2\pi R_2C_2)$ = 22.6 Hz.

The ΔZ waveform can be inverted if necessary by a switch connecting ΔZ to a unity gain analog

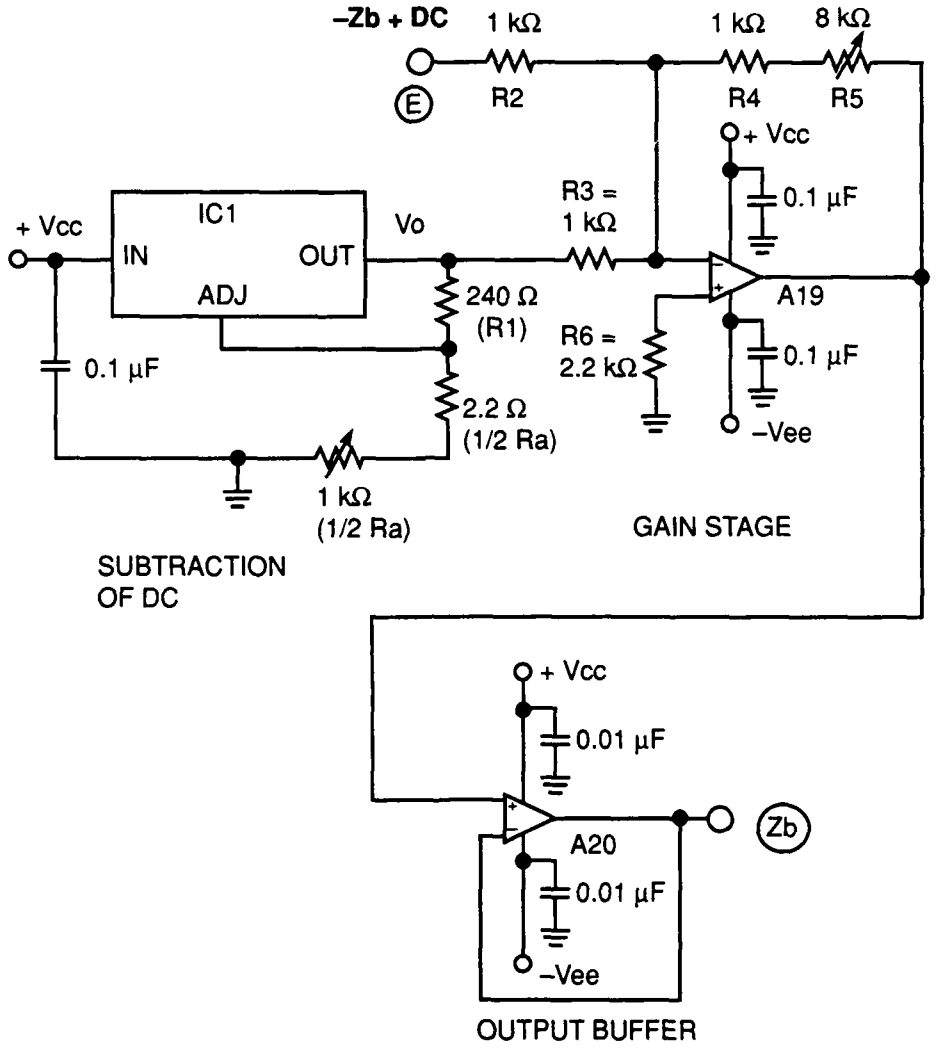

Figure 12b. Remove DC From Zb (Baseline Impedance Signal), Amplification and Buffering of Zb

KEY

A19-20 : LM741
IC1 : LM317 — Variable Positive Voltage Reference

Vo = Output voltage from LM317:
Vo = Vref (1 + (Ra/R1))
Vref = Vo – Vadj at terminals

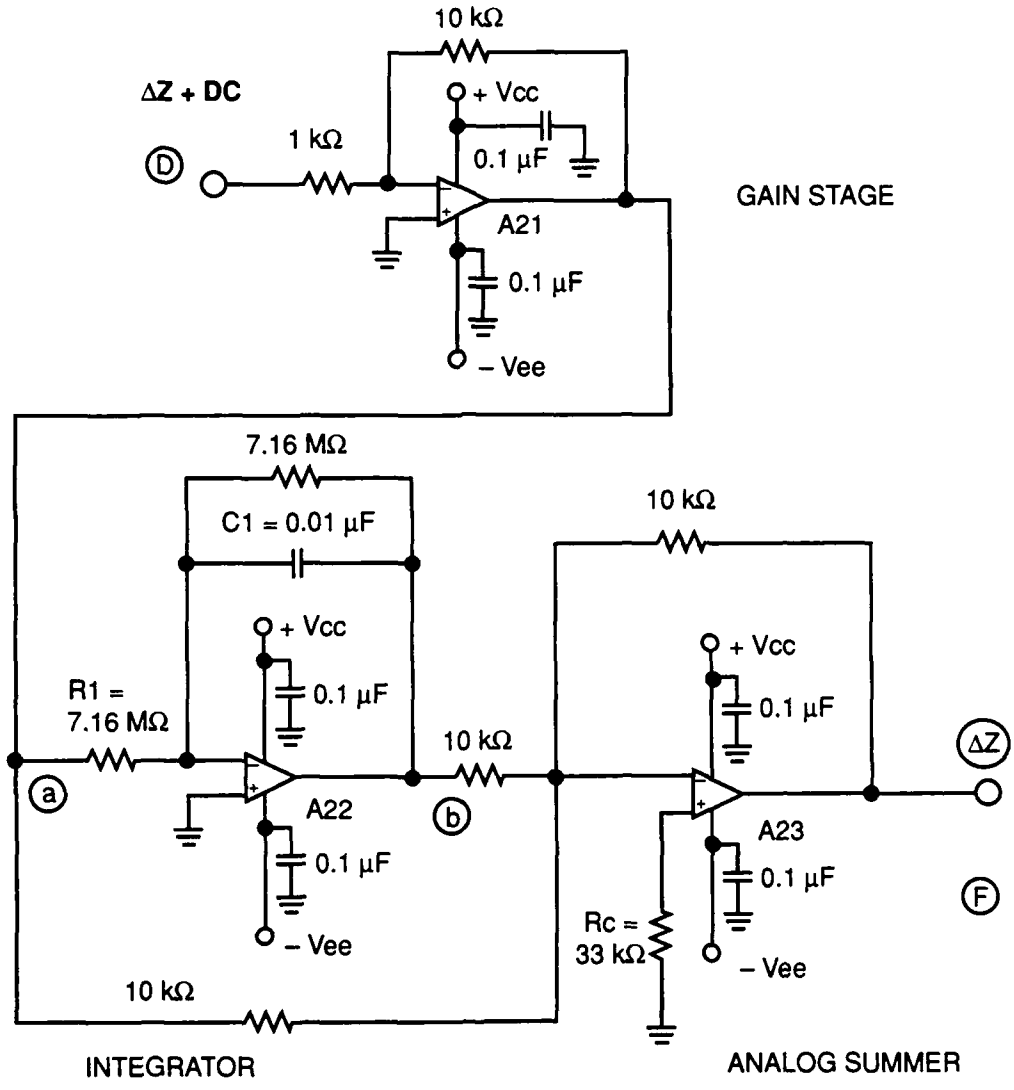

Figure 13. Separation of DC Offset From ΔZ (Pulsatile Impedance Signal).

KEY

A21 : LM318
A22, 23 : TL071N
Features:
— Gain stage of 10 to boost size of ΔZ.
— Continuous Integrator: Matched valued resistors maintain identical DC offset amplitude at opposite signs at points "a" and "b." This ensures that ΔZ is centered about 0 V. fc = 2.22 Hz, Time constant = 72 ms.
— Amplifier Summer: Extracts ΔZ by removing DC by simple subtraction.
— Rc: Eliminates voltage offset by balancing impedance at input terminals of A21.

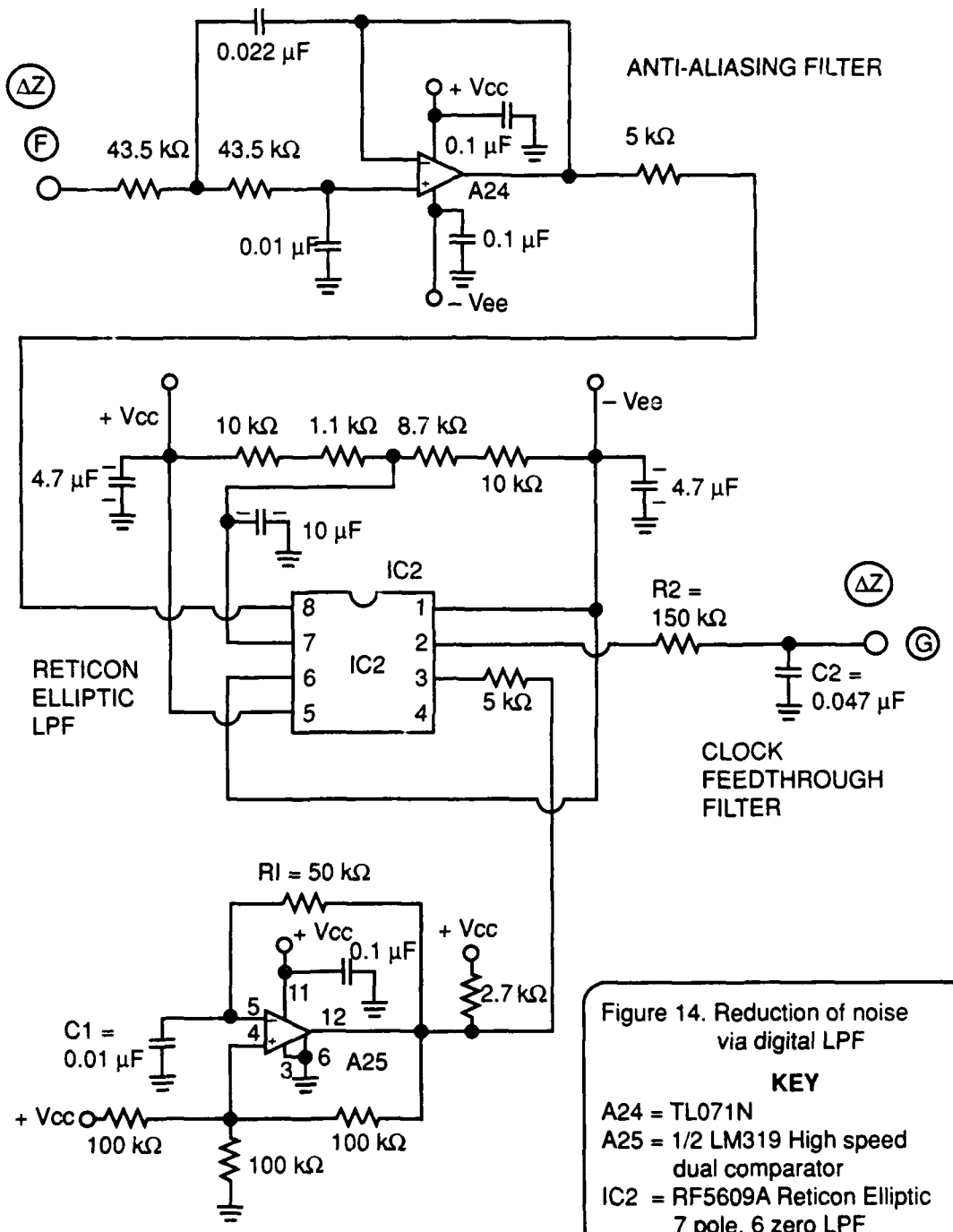

Figure 14. Reduction of noise via digital LPF

KEY

A24 = TL071N
A25 = 1/2 LM319 High speed dual comparator
IC2 = RF5609A Reticon Elliptic 7 pole, 6 zero LPF
fc = 12 Hz
— fs = Sampling rate of IC1 = 600/sec.
— Anti-aliasing filter is two pole Butterworth LPF
— fc of clock-feedthrough LPF ≤ 0.1 $f$clock

inverter (amplifier A_{26}) prior to amplification by amplifier A_{27} (see Figure 15). Output gain is set by a cascade of two noninverting op amps with a first stage fixed gain of 26 ($A_{V1} = 1 + R_4/R_3$) and a variable gain of 2 to 51 ($A_{V2} = 1 + R_6/R_5$). Therefore total gain ($A_V = A_{V1} + A_{V2}$), ranges from 28 to 77. R_6 is a series combination of a 50 kΩ potentiometer and a fixed 1 kΩ resistor. The output waveform is then passed through a voltage follower (A_{28}).

The waveform is then sent to a variety of recording devices. Data is stored onto FM tape, strip charts, or is passed to an automatic data acquisition system. One such system we have developed consists of the Macintosh Plus™ and a Micromint™ minicomputer. This system is an expanded refinement of an earlier Drexel Macintosh/Micromint system.[14]

DATA ACQUISITION SYSTEMS

Micromint-Macintosh (MAC): The current system uses an 8 channel–8-bit analog to digital (A/D) board under Z-80 microcomputer control manufactured by The Micromint Co. (25 Terrace Drive, Vernon, CT 06066). It can convert 3 channels at a sampling rate of 40 Hz. It transfers data to the MAC at 2400 baud. The MAC (Apple Computer Inc., 20525 Mariani Avenue, Cupertino, CA 95014) has a software package written in MEGAMAX C that can receive integer data and 1) store into text files, 2) display data (up to three channels) on the screen, like an oscilloscope, 3) read already stored data files, 4) has "smart mouse" function in which individual points can be selected and stored to file for later processing. This sampling rate is obviously too slow for good fidelity. The problem has been adequate communications between the two computers. The MAC is not configured for full RS-232C hardware handshake communications protocol. Another problem is that the MAC's video retrace occurs every 60th of a second regardless of what is occurring in the program. This effectively ruins any timing pattern that exists while the two computers are free running. To circumvent this problem, we will be packaging the data in a circular buffer array that will utilize the available memory on the Micromint. In this fashion, along with some error checking (*i.e.* a number count would be part of the data package — in the event that the number of bytes read does not equal the number count, the data will be discarded) we will not have to rely on the inadequate hardware handshaking available. This will sacrifice some real time processing but by optimizing the size of the circular buffer, the delay will be minimal. One advantage to the MAC is the capability of accessing the serial communications chip directly through 68000 machine language. In this way we can optimize the speed of the data transfer. To improve resolution of the data, the system is in the process of an upgrade to a 16 channel (16 single ended or 8 differential) 12 bit A/D system. It will also employ a more powerful computer controller that has a miniassembler to aid in programming. The results of this upgrade can be found in D. Walsh's master's thesis.[82]

The data collected from the dynamic flight simulator at NADC in April 1987 (see below in Centrifuge Experiments section) has been digitized and processed at NADC. The computer system consists of a Digital Equipment Corporation MINC™ (LSI-11/23™) computer (146 Main Street, Maynard, MA 01754), two 10.2 megabyte cartridge discs, and 800 & 1600 bpi magnetic tape transport, 12 bit A/D, digital to analog conversion, IEEE-488 interface with DMA, digital plotter, printer, and Sky™ Computer vector processor (Foot of John Street, Lowell, MA 01852). The A/D system includes a Data Translation™ (100 Locke Drive, Marlboro, MA 01752) DT2782 direct memory access (DMA) A/D converter. It has 16 channels (16 single ended or 8 differential), 12 bit resolution, and can sample as fast as 125 kHz to memory. It is fully supported by FORTRAN IV libraries that can be configured to run asychronously without stopping the host program. When one user defined A/D buffer is filled the data can be stored to virtual memory while the digitization continues unabated. The vector processor is capable of one million floating point operations per second, using DMA. (As a bench-mark example, a 1024 point complex floating point FFT requires 60 msec).

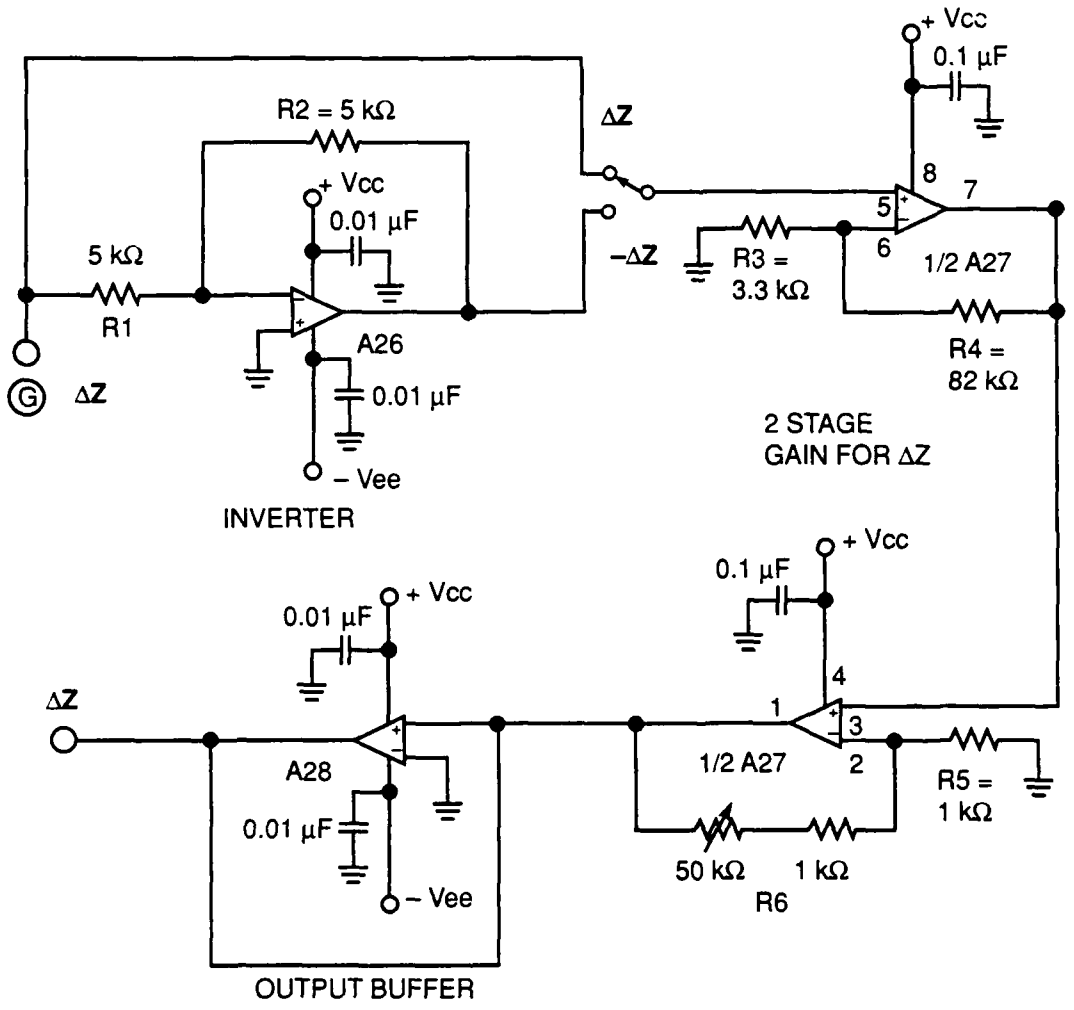

Figure 15. ΔZ Output Section — Signal Inversion and Gain

KEY

A26 : LF356N — Inverter.
A27 : TL072 Dual JFET Op Amp — Gain Stage.
A28 : µA741 — Output Buffer.

Overall Gain Range for ΔZ, Av = 26 to 77.

HUMAN CENTRIFUGE EXPERIMENTS

The first human centrifuge experiment (CE1) was performed on a single day (April 30, 1987) in conjunction with another experiment in which an inertia reel was tested. Acceleration runs were performed on six male adult subjects riding on the human centrifuge at NADC.[73] These were "familiarization" runs in which PLL was not seen nor expected. The subjects were exposed to gradual onset gravitational stresses (at a rate of 0.3 Gz/sec) from one to a maximum of three +Gz. They were maintained at +3 Gz for 25 second plateau and then returned to +1.03 Gz at a rate of 0.1 Gz/sec. During each insertion, two rapid onset runs, ROR, were also performed. In these maneuvers, gravitational stress was altered in the following manner: +Gz was decreased from +1.8 to +1 Gz in two seconds, maintained at +1 Gz for ten seconds, then increased to +1.8 Gz in two seconds. At the same time –Gx (acceleration from chest-to-spine) was changed from 0 to –1.5 Gx and back to 0 Gx, mimicing the change in +Gz.

The following data were recorded onto strip chart and FM tape for each experiment:

1. EKG (taken from the chest);
2. pulsatile impedance, ΔZ, recorded off of the forehead;
3. "baseline" impedance, Zb;
4. superficial temporal artery infrared plethysmograph (IRP);
5. acceleration in the +Gz and –Gx planes.

The purpose of this first series of runs was to demonstrate the ability of an early version of the REG device to perform under acceleration stress on humans. After successful completion of this task, data was examined and processed in a preliminary attempt to characterize acceleration induced changes in REG indices. Based on these results, the REG device underwent a few refinements, particularly in the area of control of the output waveforms, *i.e.* ΔZ baseline wander control and improved Zb quality.

The second experiment (CE2) was conducted in November of 1987 in conjunction with a study in which automatically reclining aircraft seats were evaluated. These included a tilt-back and PALE (pelvis and legs elevating) seats. The tilt-back seat design was based on the principle of counterbalancing of moments about an acceleration sensitive pivot point. Of most interest were the results obtained from the runs using the PALE seat, which in this experiment served as the control. These runs afforded an opportunity to not only test the REG instrument at higher onset rates and acceleration levels, but to determine the effects of anti-G protective devices on the impedance waveforms.

Five Navy corpsmen wore MA-2 harnesses and standard anti-G suits (AGS), which were inflated according to the equation:

$$\{[\cos (SBA)\ (Gz)] - 1\}\ (1.5). \qquad (38)$$

The maximum +Gz allowed was +7 Gz and maximum inflation pressure was 5.25 psi. The subjects were exposed to a series of ramp type profiles in which the onset/offset rates were 0.1 Gz/sec, 0.5 Gz/sec, and 2.3 Gz/sec. These profiles included a +7 Gz plateau that was maintained for five seconds. Subjects were also exposed to a series of low level simulated aerial combat maneuvers (SACM) that were used to test the ability of the tilt-back seat to rapidly and comfortably follow the +Gz load about the acceleration sensitive pivot point. This was in contrast to earlier experiments in which a reclining seat was simply set at larger than usual angle from the vertical, *e.g.* 60°.[31] The tilt-back seat was set at an initial SBA of 30° and reclined to a maximum of 70° at approximately +3.0 Gz. The PALE seat was

initially set at 25° and reclined to 65° at approximately +6 Gz ± 0.5 Gz, depending upon the onset rate. Physiological data (ECG, ΔZ, Zb, and respiration) and mechanical data (SBA, AGS pressure, and Gz) were recorded.

During these experiments two different electrode types were employed. One was a commercially produced 25 × 38 oval flexible, self adhesive, silver-silver chloride pediatric long-term monitoring type (Sentry Medical Products, #1071, 2615 So. Orange Ave., Santa Ana, CA 92707). The other was the author's own design consisting of a 20-mm diameter hypoallergenic stainless steel reuseable disk. Use of either design produced useable results though the former design proved to be more convenient to use.

The third experiment (CE3), held in February, 1988, was the most comprehensive series of centrifuge experiments to date. CE3 was performed along with a study conducted by the Naval Aerospace Medical Research Laboratory (NAMRL) in which the effects of exercise on +Gz-tolerance was investigated. These trials were held over two weeks and involved 20 volunteer subjects, 18 of which were aviators. Subjects were placed in a 15° SBA ESCAPAC seat, wore a MA-2 flight harness and no helmet, and performed a tracking task. There were two phases of each subject's high +Gz exposure. Relaxed tolerance, using an inflated AGS without performing AGSM, to 15 second plateau, two second onset/offset rate ROR profiles was determined. These runs started at +2.5 Gz and increased in 0.5 Gz increments until the highest level in which the subject could maintain peripheral vision (defined as a 60° forward visual cone) for the full 15 second plateau. This was the relaxed tolerance limit, or G_{15} level. Following these runs, two straining runs to G_{15} + 1 Gz and G_{15} + 2 Gz plateaus were conducted. After these runs, relaxed +Gz-tolerance determination was repeated. The next insertion, usually one to two days later, was a two part SACM in which a relatively equal amount of workload was imposed on each individual based on their G_{15} level. The first part consisted of a 15 second warm-up plateau of 1.75 Gz, then a two second rise to the G_{15} level for ten seconds, then alternating one second rise to G_{15} + 2 Gz for ten seconds and back down to G_{15} for ten seconds until the subject decided he was too fatigued to continue. After a one minute rest period, the second part of the SACM runs took place. These runs were an alternation from 1.75 Gz for ten seconds to G_{15} + 2 Gz for ten seconds and back to 1.75 Gz until the subject stopped the run. The latter SACM was run to ensure that the metabolism of motivated subjects would be functioning anaerobically.

Physiological data (ECG, ΔZ, Zb, IRP, doppler, blood pressure, before and after SACM blood lactate levels, and respiration) and mechanical data (AGS pressure, light bar tracking, and Gz) were recorded. The IRP was placed on the right temple over the superficial temporal artery, the doppler ultrasound velocimeter was placed over the left temple and the REG electrodes (Sentry Medical Products) were placed bi-occipitally. Respiration was measured as thoracic and abdominal excursions as measured by a strain gauge type device, a Respitrace©.

For these trials further improvements in the REG device were made including changes to both the ΔZ and Zb processing circuitry. These runs afforded an opportunity to test the REG on large numbers of individuals under conditions in which comparisons could be made in terms of the response of the REG device to relaxed vs stressed environments. Determination of the effects of anti-G protective maneuvers on the impedance waveforms was now also possible.

ANIMAL EXPERIMENTS

To demonstrate the development of the REG device, the results of two experiments performed on a dog and a rabbit in the laboratory at 1 g will be briefly described. Besides the obvious anatomical differences, detailed in the Aspects of the Cerebral Circulation section above, canines and rabbits[54] differ

from each other and humans[10] in their respiratory and heart rates and mean arterial blood pressure (see Table 1). These differences must be kept in focus when comparing the REG waveforms among different species. For all animals tested, ΔZ retained its pulsatile nature at a heart beat coincident rate. All ΔZ waveforms contained an A wave. However, the form of the descending branch of ΔZ was quite variable. The effects of respiration on REG signals were quite evident in the animal studies.

Dog and rabbit facial muscles are highly vascularized and highly moveable. One might expect that the extracranial component of the REG would be higher in animals as compared to man, though this was not specifically determined. References in the literature detailing REG studies using animals are few in number and are often not performed due to the differences in anatomical geometry and circulation.

One of the major difficulties we had during our animal experiments was electrode motion artifact. While the animals were sedated, they often moved their facial muscles while unconscious, thereby producing artifacts in the REG waveform. A variety of electrode types were used, including Beckman EEG needle electrodes, stainless steel surgical needles, acupuncture needles, alligator clips, and surface disk ECG type electrodes. Motion artifact remained an obstacle for all recordings regardless of the electrode types and whether recordings were obtained superficially or by piercing the skin.

Table 1. Comparison of resting physiological data among rabbits (New Zealand White),[54] dogs (beagle),[54] and humans.[37]

	Rabbit	Dog	Human
Respiratory Rate (/min)	36.8 ± 10.6	28.2 ± 3.3	12
Heart Rate (bpm)	246	155	65
Mean Arterial Blood Pressure (mmHg)	82–133	113 ± 2.7	100
Brain weight (gm)	8.2–10	76–81	1500

The first experiment employed an early version of the REG instrument in August of 1986 and used a 25-pound mongrel dog. The dog was anesthetized and intubated. Physiological recordings included ECG, aortic pressure, descending aortic flow, and ΔZ. A sample strip chart recording is found in Figures 16a and 16b. Note that in this recording, ΔZ is inverted such that blood inflow is represented by a downward deflection of the first peak. Stainless steel needles were used as electrodes and were inserted into the scalp bitemporally. The signal was of low amplitude and quite variable, specially on the descending branch. When the exhalation port of the respirator was temporarily closed (See the arrow in Figure 16a) and intrathoracic pressure increased, the A wave of the ΔZ waveform became much more sharply defined and the multiple inflections after the C wave were markedly dampened and very close to the baseline. This occurred about 13 seconds after the exhalation port of the respirator was blocked. By this time the ECG contained T wave inversions, indicating that the heart was distressed due to oxygen insufficiency.[52] Aortic pressure had dropped from a mean of about 125 mmHg to 60 mmHg. Unfortunately aortic flow went offscale during this functional test. Approximately 16 seconds into the test the amplitude of the A wave became too small to distinguish it from the rest of the ΔZ

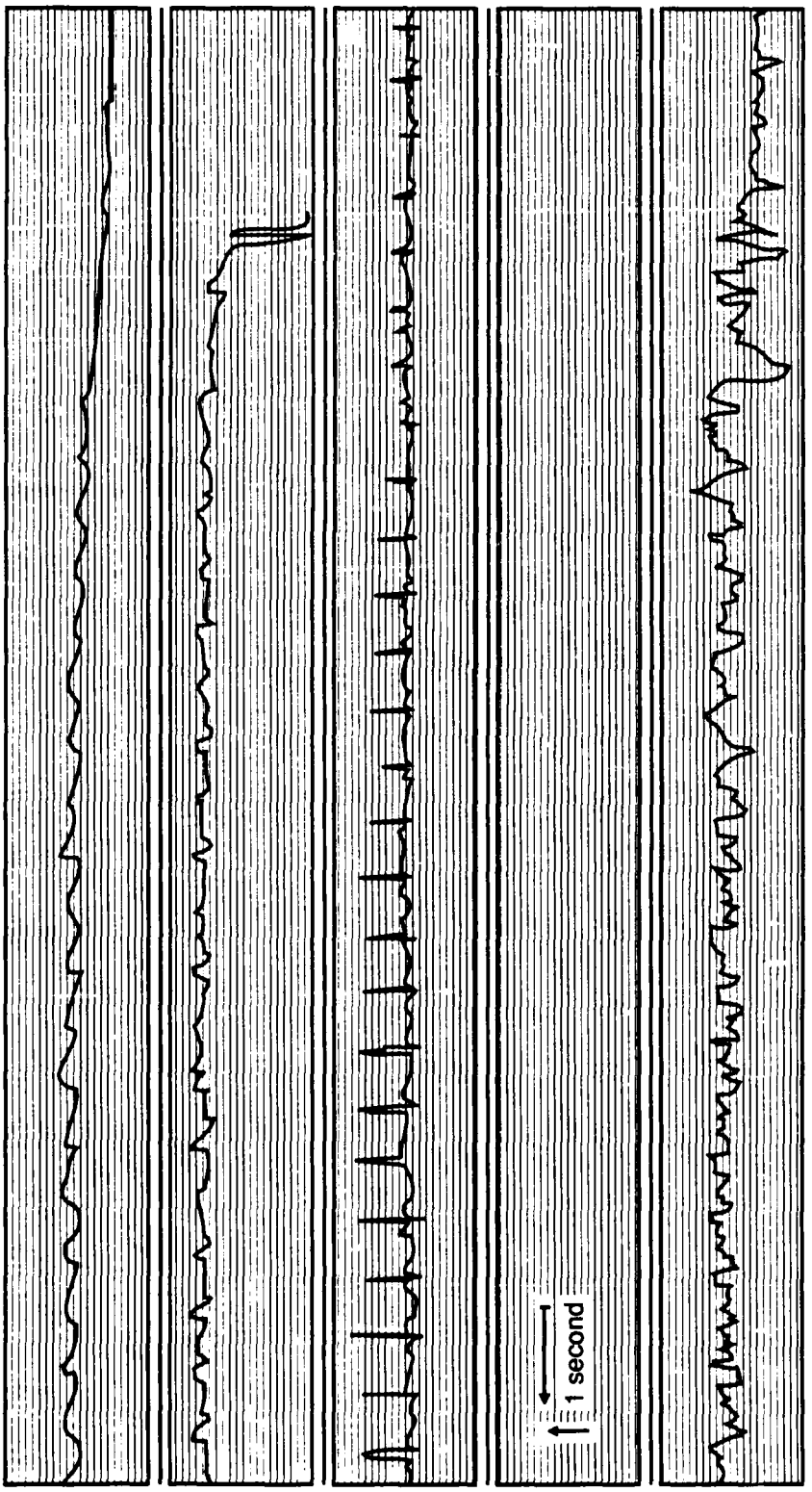

Figure 16a. Dog experiment in which intrathoracic pressure was increased. Figure includes onset of procedure. From top: aortic pressure, descending aortic flow, ECG, ΔZ.

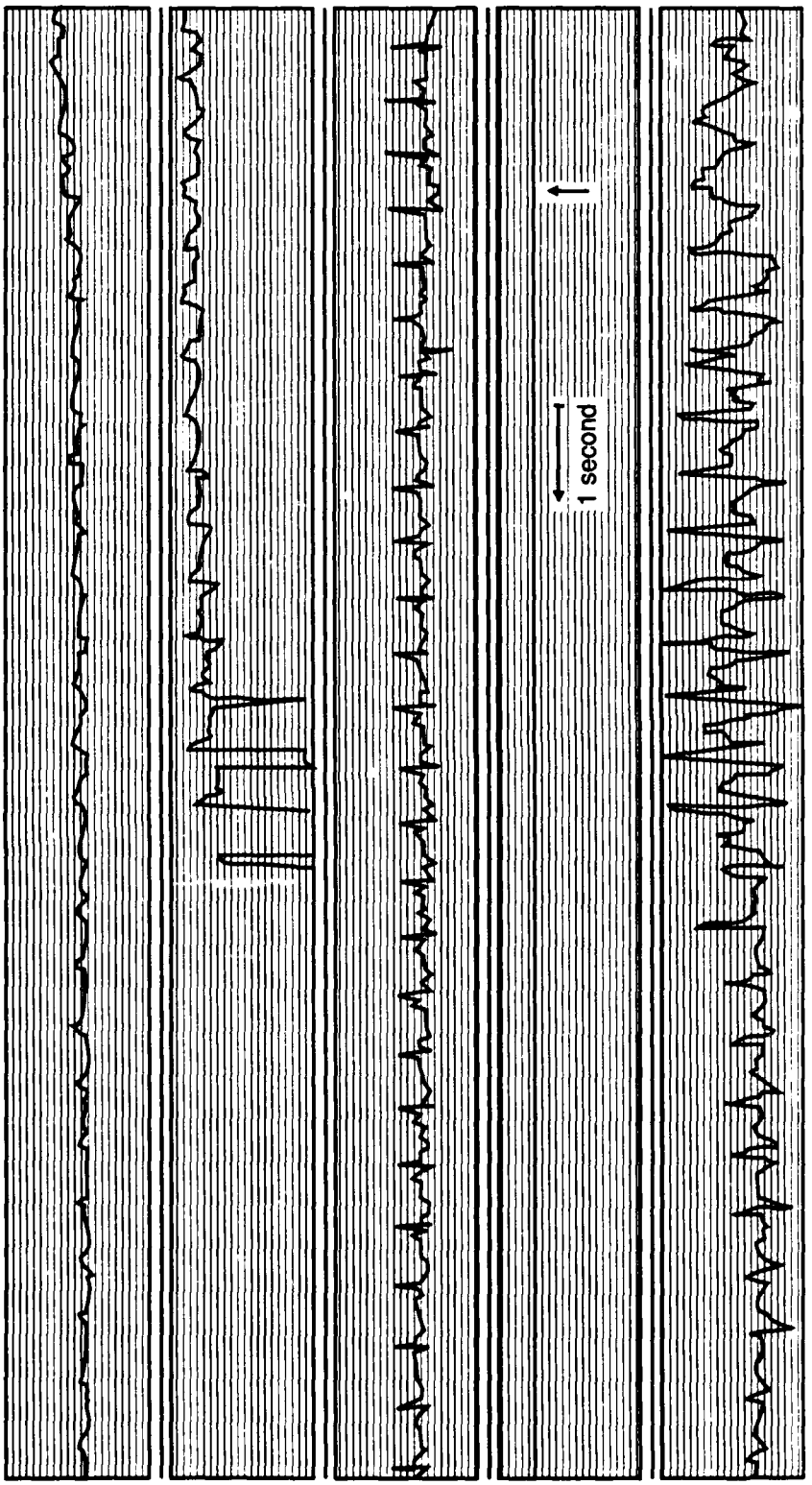

Figure 16b. Dog experiment in which intrathoracic pressure was increased.
Figure includes cardiac recovery and offset of procedure. From top:
aortic pressure, descending aortic flow, ECG, ΔZ.

waveform. After 20 seconds, the dog's heart began to recover and aortic flow increased approximately four times over the resting levels (peak systolic flow of 0.6 L/min *vs* 0.16 L/min). The A wave became exaggerated and the descending portion of the waveform became elevated with clearly defined B and C wavelets. In fact the amplitude of the C wave was greater than the A wave. This may be indicative of increased blood outflow. This difference persisted for five seconds until peak systolic aortic flow reduced to 0.5 L/min. When the expiration port was opened (See the arrow in Figure 16b), aortic pressure and flow returned to pretest levels, as did the REG. Peak systolic aortic flow recovered to 0.3 L/min when ΔZ returned to unstressed levels. Interpretation of these waveforms is complicated by the large swings in hydrostatic pressure this test creates.

The most recent procedure (December 1987) involved a five-pound rabbit. Physiological recordings included oxygen tension measurements, using recessed cathode oxygen microelectrodes,[7] ECG, ΔZ, and Zb. Respiration patterns were apparent by looking at the wide baseline swings of the ECG. Unstressed ECG, ΔZ, and Zb recordings on an anesthetized animal (ketamine and rompun) were made prior to any surgical intervention. EEG needle electrodes placed fronto-occipitally were used to record REG signals. The surgical procedure included reflecting the skin back over the skull and a burr hole was bored mid-sagittally between the eyes and ears, exposing the cerebrum. The carotid arteries were also exposed. Measurements were taken with the skull exposed and with and without the carotids occluded.

With the skull open the effect of tidal changes in intrathoracic pressure with respiration on the intracranial pressure of the exposed brain was manifested by a swelling of cerebral tissue up out of the hole upon exhalation.

B and C waves were much more sharply defined with the skull exposed as compared to the unstressed measurements. In fact the B wave was usually obscured prior to surgery. During carotid occlusion, most of the ΔZ waveforms were saturated. However, after the occlusion was released, the magnitude of ΔZ was slightly reduced ($\approx$16%). This decrease in impedance corresponds to the inrush of blood back into the cranial space from the carotids. The effects of respiration on Zb were very evident in that the baseline swings in the ECG referable to respiration were accompanied by similar excursions in Zb, though the signals were 180° out of phase.

Sample strip chart recordings of REG and ECG and the oxygen tension measurements are found in Figures 17 and 18. During occlusion, the oxygen tension fell from 37 to 22 mmHg at a disappearance rate of –4 mmHg/sec. This rate can be compared to a similar experiment performed by Nair *et al*[58] in which oxygen tension measurement were performed on gerbils. They report that the cerebral metabolic rate for oxygen ($CMRO_2$) was 8.3 ml O_2/100 gm/min in the cortex and the disappearance rate was –23 mmHg/sec. Even though the $CMRO_2$ for rabbits is about half that of gerbils, the disappearance rate appears to be somewhat too low. This result indicates that complete occlusion of the carotids was not attained.

This was a demonstration experiment to determine the potential difficulties involved with simultaneous REG and oxygen tension measurements. There was apparently no electrical interference between the two measurement techniques. It is difficult to make conclusions based upon an experiment in which there was only one subject. However, given the circumstances of the experiment, the results are not inconsistent with the case in which circulation to the brain is arrested while oxygen consumption proceeds at a normal rate.

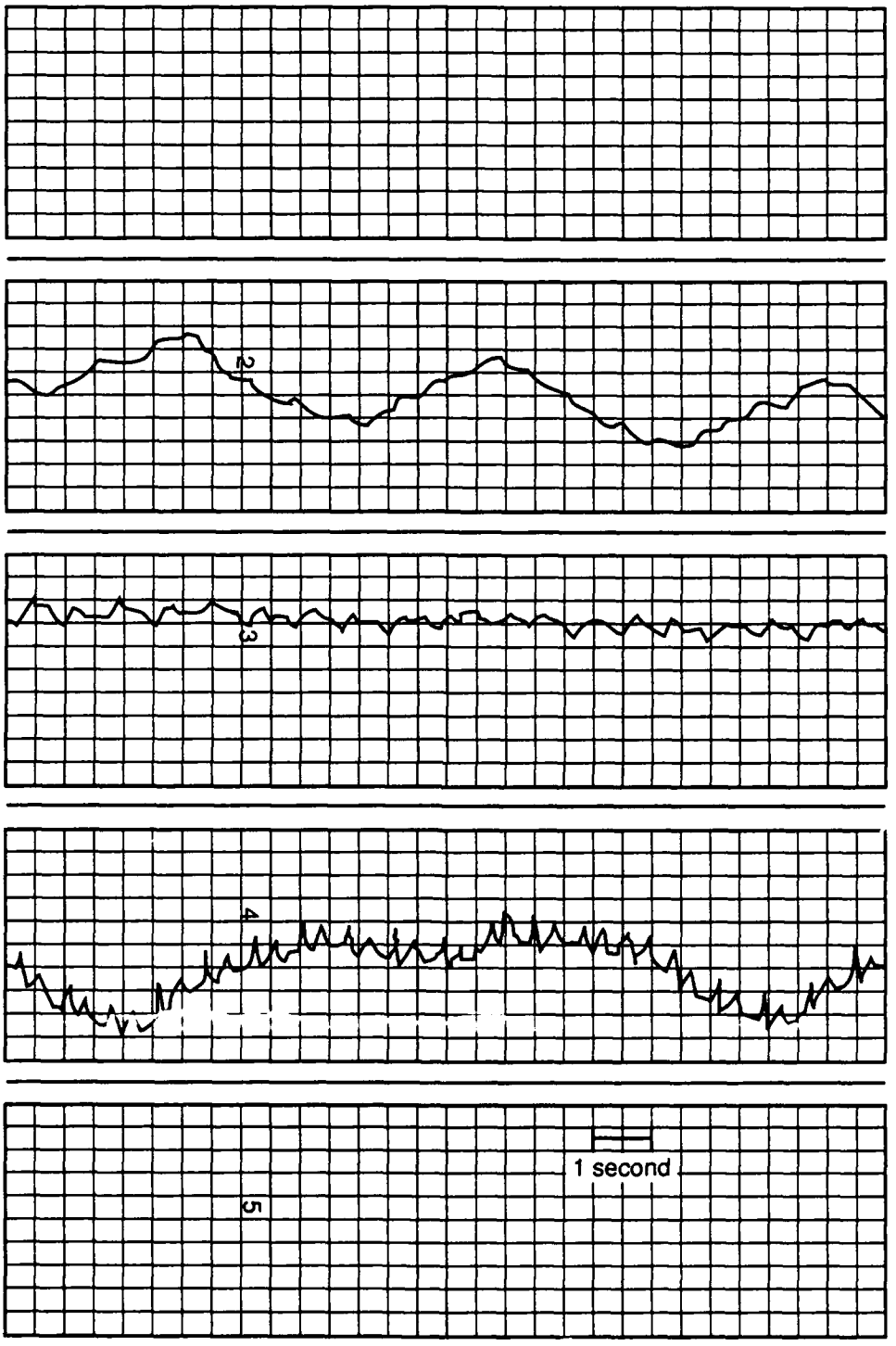

Figure 17. Demonstration of unstressed REG on rabbit. From top: Zb, ΔZ, ECG.

Figure 18. Rabbit cerebral oxygen tension measurements during carotid occlusion.

RESULTS AND DISCUSSION

CENTRIFUGE EXPERIMENT 1 (CE1)

The REG has been constructed and has undergone initial testing in both normal and simulated military stress environments. The REG has withstood stresses of at least +14 Gz. Measurements on human subjects have been taken at extremes of +8 Gz and –1.5 Gx. One of the most notable features of the ΔZ waveform is its highly variable nature. Automatic data processing must be used very carefully in order to trust its evaluations. Otherwise, data processing can be done by hand with certain, though more tediously obtained, results. In order to orient the reader a modified Wiggers diagram in which the timing of ΔZ with respect to other cardiovascular events (ECG, venous pulse, ventricular volume, aortic blood flow, and various pressures) is presented in Figure 19. The ΔZ waveform is an average of six waveforms obtained from one subject at 1 g.

The first version of the REG device had a few limitations in that ΔZ was presented in an inverted manner and the small changes in Zb were obscured by a large negative offset. The data from the first centrifuge experiment, CE1, was processed using the digital signal processing equipment at NADC, as described in the Data Acquisition section of this manuscript. Of the data recorded onto FM analog tape, only the ECG, pulsatile REG, infrared plethysmograph, and the baseline REG were readable. Data was organized into files consisting of 7–8 heartbeats (5.76 seconds, with each data point representing 5 msec). The range of the data was ±5 volts with a 12 bit resolution. Acceleration onset and offset were determined by using the strip charts and the audio recording of the subjects, the centrifuge operator, and the flight deck personnel.

The form of the ΔZ was very variable due in part to the existence of muscle and motion artifact. The simplest method for extracting the random noise out of a repetitive waveform is to average it. Six waveforms were averaged to obtain a template, representative of unstressed and stressed waveforms for ECG, ΔZ, and IRP. This procedure of averaging and using a template to compare other waveforms is similar to an approach used by Tarassenko, *et al*.[77]

As a fiducial point to commence averaging, the R wave of the ECG was chosen. The R wave was detected via an amplitude threshold method in which the maximum of the total record of ECGs was calculated (a 5.76 second slice of time). An R wave was "captured" if the amplitude of the waveform was 70% of the maximum. Once detected the algorithm skipped the next five data points to avoid registration of false positive detections before searching for the next R wave. Heart rate (HR) varies under the effects of acceleration. As acceleration increases, so does heart rate. During protracted runs, bradycardia can occur to some extent. The timing of the latter appears to coincide with the onset of cardiovascular compensation.[19] Since the HR was variable, after obtaining the template magnitude, the period of the shortest was chosen as the length of the template. For each record, the lengths of the six intervals, the length of the shortest, the maximum amplitude of the R wave, and HR were calculated. Both averaged and raw ECG signals could be saved to disk.

ΔZ and IRP were processed in a similar manner to the ECG. The maximum value of the A wave, ΔZ_{max}, was also calculated via a threshold detection algorithm. The threshold was set at 50% of the largest peak in the record. Once detected the algorithm skipped the next 25 data points to avoid registration of false positives prior to searching for the next ΔZ_{max}. Analogously, the threshold for IRPmax was set at 30% of the largest peak in the record and the next 80 points were skipped. The periods of ΔZ_{max}-ΔZ_{max} and IRP_{max}-IRP_{max} were calculated and compared to the R-R intervals. Theoretically, the timing of the R-R interval and the ΔZ_{max}-ΔZ_{max} period should be the same. By aligning the averaged ΔZ waveform to the start of the averaged ECG signal, *i.e.* the R wave, pulse wave delay is simply the time from the beginning of the record to ΔZ_{max}.

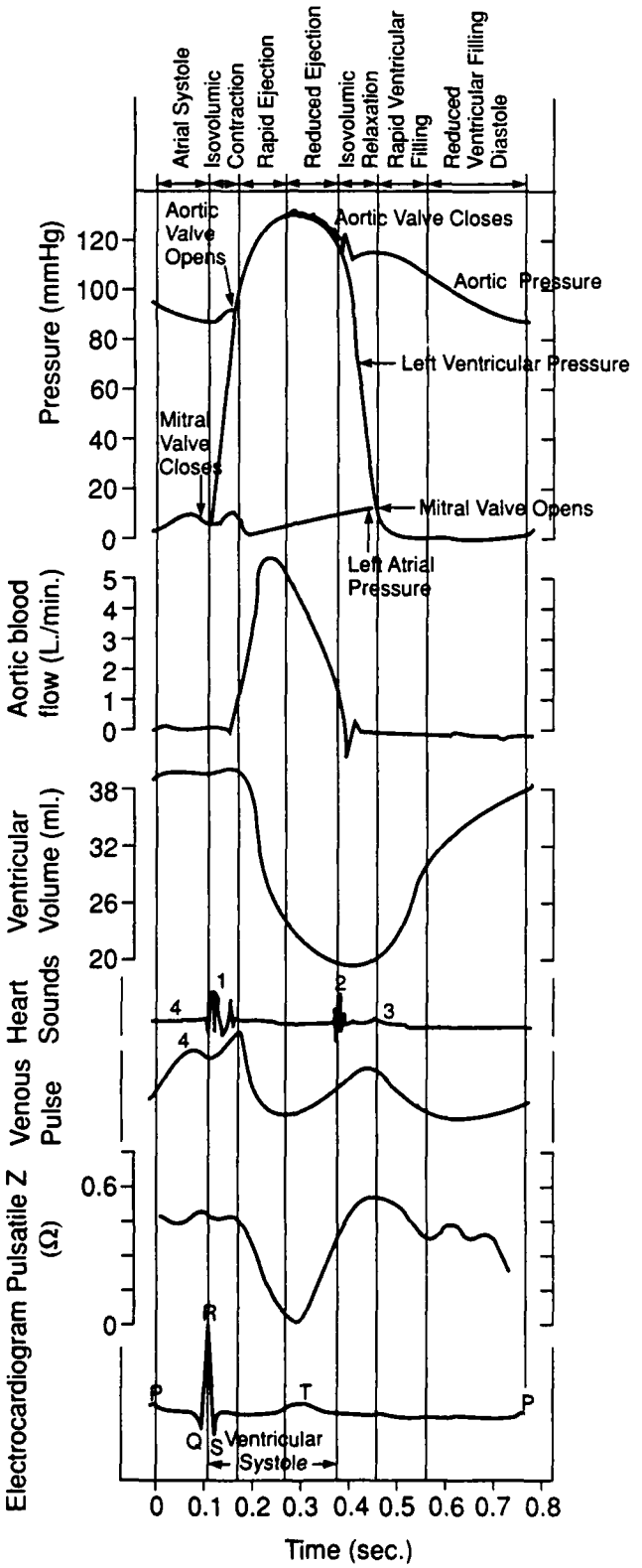

Figure 19. Modified Wigger's diagram including pulsatile REG.

Once the averages have been obtained, the waveforms can be analyzed in both the time and frequency domains. Correlations can be performed to determine the fit of the averaged as compared to the raw signal. The timing relationships between the ECG and pulsatile waveforms can also be verified via cross correlations.

Power spectral density functions (PSD) can be generated to determine the frequency content of the various signals. We can compare these spectra to each other and we can determine the effect of increasing acceleration load on the PSD of these waveforms.

The analysis of the data obtained during CE1 was centered on the best available data, *i.e.* from subjects S1 and S5. For this analysis, data used were from gradual onset runs (GOR) and rapid onset runs (ROR). See Appendices B and C for averaged values of ECG, output voltage referable to ΔZ and IRP for S1 and S5, respectively. (A calibration switch was not installed in the REG device when CE1 was performed. Therefore, all references to ΔZ are expressed in voltages not ohms.) For S1, these started at a +1.03 Gz level and for S5, these started at a +1.8 Gz level. Sample strip chart recordings for S1 and S5 are found in Figures 20 and 21. Analysis of IRP signals proved fruitless due to the low amplitude and lack of easily definable peaks. Threshold detection for this waveform was clearly not the best approach.

Zb contained a rather large dc offset that obscured the low level changes in Zb seen in subsequent experiments. However, upon careful examination of the strip charts, Zb changed in magnitude and followed the +Gz trend, indicating a shift of blood out of the head. Unfortunately, the magnitude of these changes with respect to those at a 1 g level was insignificant.

One expects that under a +Gz load, cephalic fluid volume should be reduced according to the hydrostatic column theory. This reduction in volume ought to accompany an increase in impedance which would be reflected by an increase in the amplitude of the A wave. Cardiovascular compensation can occur after about ten seconds of acceleration exposure, though the timing does depend on the onset rate and level of acceleration stress. Comparison of the effects of acceleration during GOR exposures to S1 and S5 on A wave amplitude were inconclusive. For both individuals the A wave initially decreased as acceleration approached +1.8 Gz. A wave amplitude for S1 then increased until the acceleration was offloaded (see Figure 22). In the case of S5, however, A wave amplitude oscillated (see Figure 23). There was certainly enough time for compensation to occur though it is difficult to conclusively state that from A wave analysis alone.

Another deficiency with the automatic data processing results was discovered when analyzing the difference in time periods between the R-R and the ΔZ_{max}-ΔZ_{max} intervals. When comparing the values obtained by the threshold detection algorithm, there was a significant difference between the two intervals for both S1 and S5 (determined by a paired t test, $p < .009$ and $p < .002$, respectively). However, hand analysis of the strip charts proved that the intervals were virtually the same and that as heart rate increased during acceleration, the ΔZ_{max}-ΔZ_{max} period decreased (determined by a paired t test, $p < .418$ and $p < .170$, for S1 and S5 respectively).

No such problem was found in the determination of the pulse wave delay or "delta delay," (ΔD). As found by Hrebien in doppler ultrasound studies,[32] there was a similar relationship between the time of the occurrence of the R wave and the subsequent peak of the A wave and the imposition of a high +Gz load. As acceleration increases, the delay also increases linearly. ΔZ_{max} occurs approximately 320 msec after the "R" wave at +1 Gz and about 360 msec after the "R" wave at +3 Gz. These values are somewhat higher than those reported by Hrebien but the acceleration profiles were also quite different. These trends are found for S1 and S5 in Figures 24 and 25.

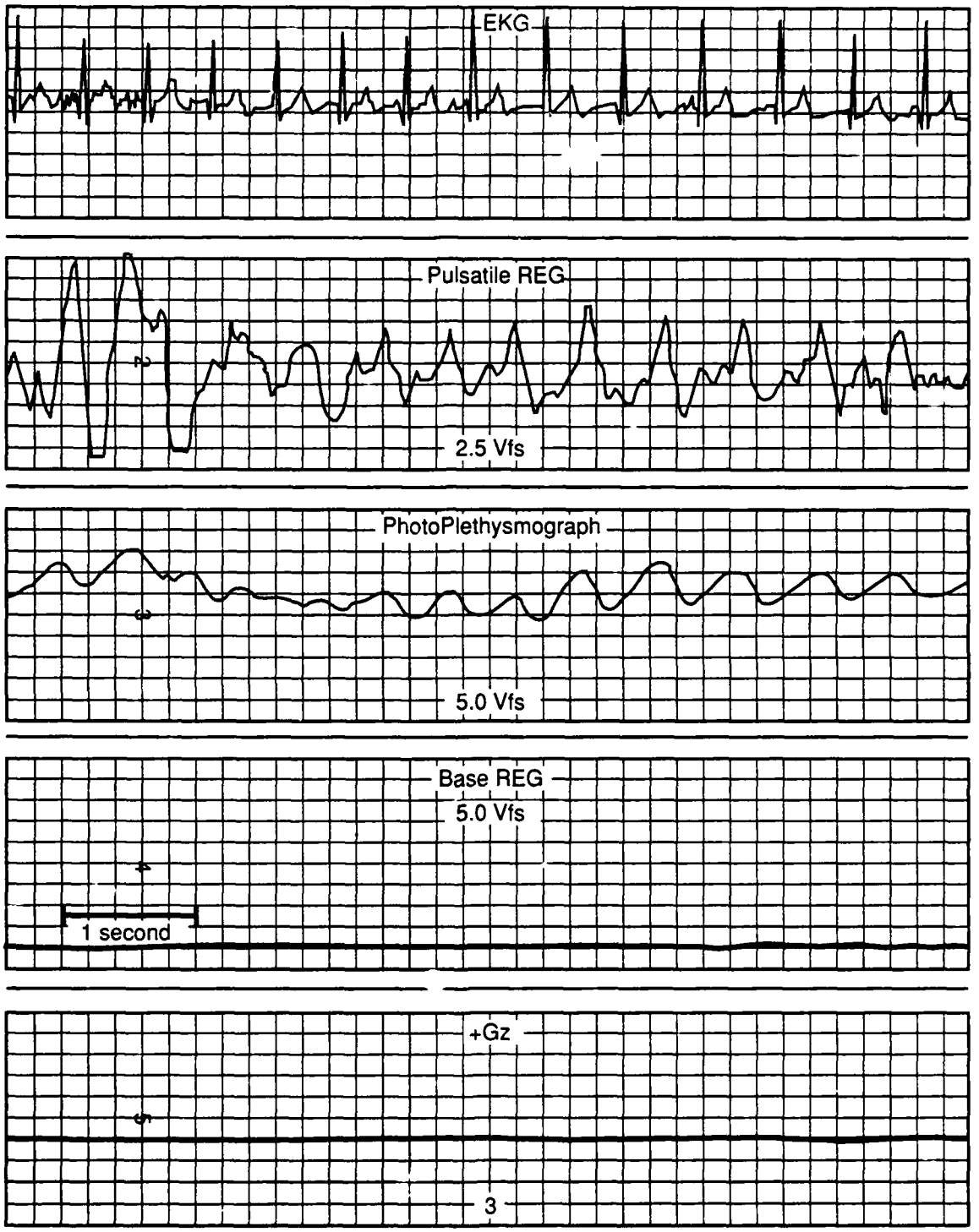

Figure 20. Example of first human centrifuge experimental data (subject S1). Note that ΔZ is inverted. From top: ECG, ΔZ, photoplethysmograph of right superficial temporal artery, Zb, Gz (+3.0 maximum).

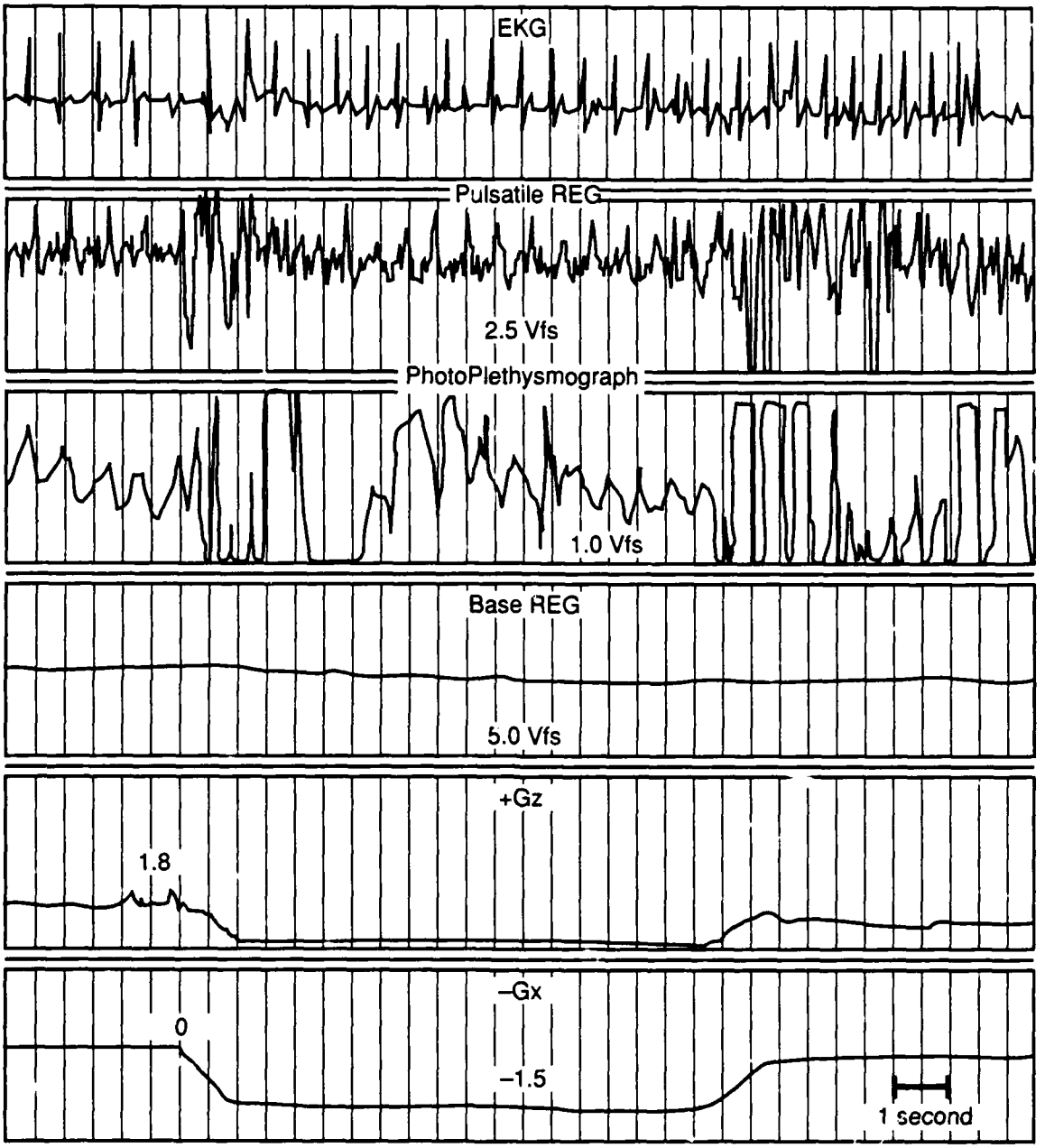

Figure 21. Example of first human centrifuge experimental data (subject S5). Note that ΔZ is inverted. From top: ECG, ΔZ, photoplethysmograph of right superficial temporal artery, Zb, Gz (+1.8 maximum), –Gx(–1.5 maximum).

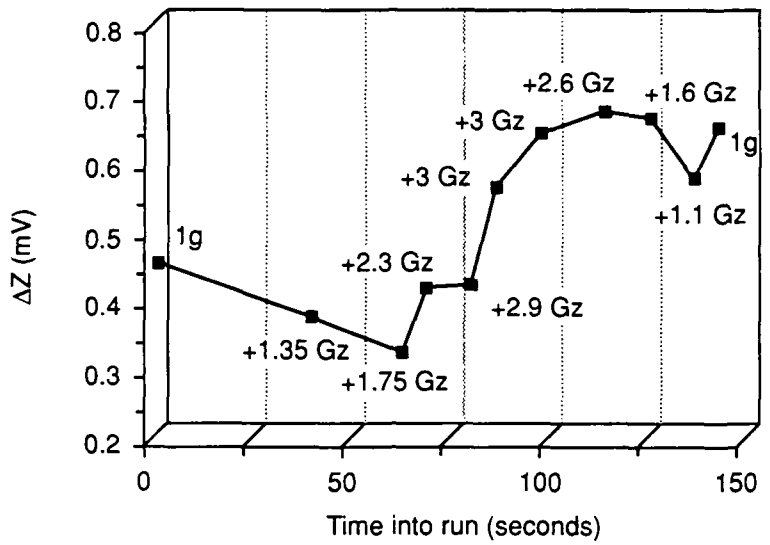

Figure 22. Effects of increasing +Gz stress during GOR on the amplitude of averaged A wave: experiment CE1 — subject S1.

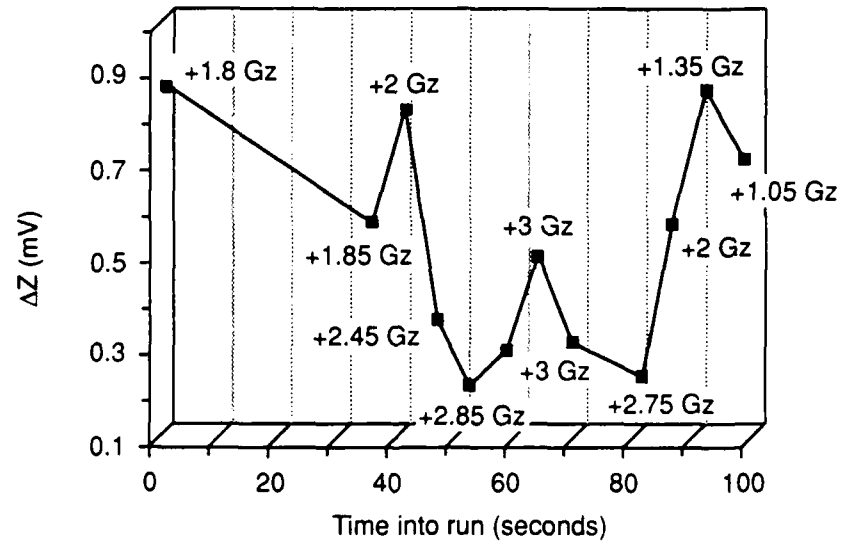

Figure 23. Effects of increasing +Gz stress during GOR on the amplitude of averaged A wave: experiment CE1 — subject S5.

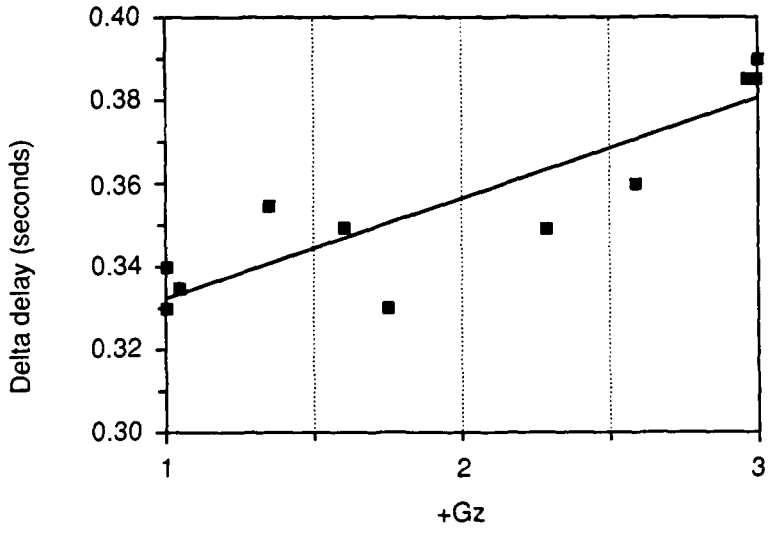

Figure 24. Pulse wave (delta) delay (ΔD) during experiment CE1: subject S1.
Regression equation: ΔD = 0.31 + 0.23 GZ

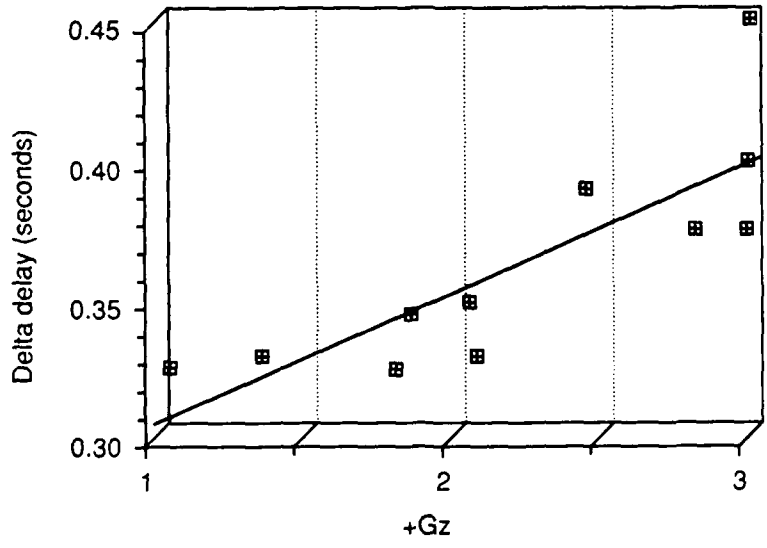

Figure 25. Pulse wave (delta) delay (ΔD) during experiment CE1: subject S5.
Regression equation: ΔD = 0.25 + 0.05 GZ

The linear regression equations are:

$$S1: \Delta D = 0.31 + 0.23\ Gz;\ R^2 = 0.89, \quad (39)$$

$$S5: \Delta D = 0.25 + 0.05\ Gz;\ R^2 = 0.80. \quad (40)$$

In the course of examining the frequency content of the signals, several interesting features became apparent. The frequency content for GORs is shown in Tables 2 and 3. Under acceleration stress the frequency content of ΔZ changed whereas the frequency content of both the ECG and the IRP remained the same. Waterfall plots of the effect of increasing acceleration stress on frequency content are shown for ΔZ in Figure 26 and for the IRP in Figure 27. This alteration occurred even though heart rate only rose, during the onset to plateau periods, from 88.9 to 108 bpm (S1) and from 86.3 to 101.7 bpm (S5). The most notable change seen under a +Gz load included an increase in frequency content of the primary lobe at +3 Gz (from ≈2 Hz to 4 Hz, for S1, to 5.8 for S5) and a reversal from minima to maxima at +3 Gz at ≈9.5 Hz. There was another change from an unstressed frequency maxima to a stressed frequency minima, though these occurred at different frequencies (S1: 6.4–6.8 Hz and S5: 8.6 Hz).

In an attempt to discover whether or not the changes in frequency content outlined above are related to the time domain change in the ratio α/T, cross correlation analysis (R_{xy}) was performed.[47] Frequency content data could be described on the basis of the peak of the fundamental frequency band (f) or the −3 dB (f_{-3dB}) decline from that fundamental. This data can be found in Appendix D. Plots of f and f_{-3dB} with respect to rising and falling levels of acceleration, expressed in +0.1 Gz steps, for subjects S1 and S5 are found in Figures 28a, b and 29a, b, respectively. In these figures α/T is expressed as 10 α/T for a clearer plot. Since f consists of a band of frequencies, frequency content is expressed as two curves. 'Low peak f' refers to the low frequency bound of f and 'high peak f' is the corresponding upper bound. Note that these and the f_{-3dB} plots are similar in appearance. Since f is characterized by a range of frequencies, a cross correlation is difficult to determine and weight properly with such a continuum of values. Therefore, a cross correlation was performed between f_{-3dB} and 10 α/T.

Table 2. Subject S1: ΔZ frequency content changes with increased +Gz load. Reversals from maxima to minima and vice versa at +3 Gz are shown in bold face. Runs were gradual onset.

+Gz	FREQUENCY (Hz)	MAGNITUDE (dB)	MAXIMA/MINIMA
any	2–2.6	0– –1	maxima
3	**2–4**	**0**	**maxima**
any	4–4.5	0– –5	maxima
any	7.2–8.2	–11– –20	maxima
any	10.6–11.6	–20– –31	maxima
any	5.4–7	–12.5– –34	minima
any	9–10.6	–22– –34	minima
<3	6.2–6.4	–12.25	maxima
3	**6.4– 6.8**	**–21.5**	**minima**
<3	9.4–10	–30.1	minima
3	**9.6**	**–14.5**	**maxima**

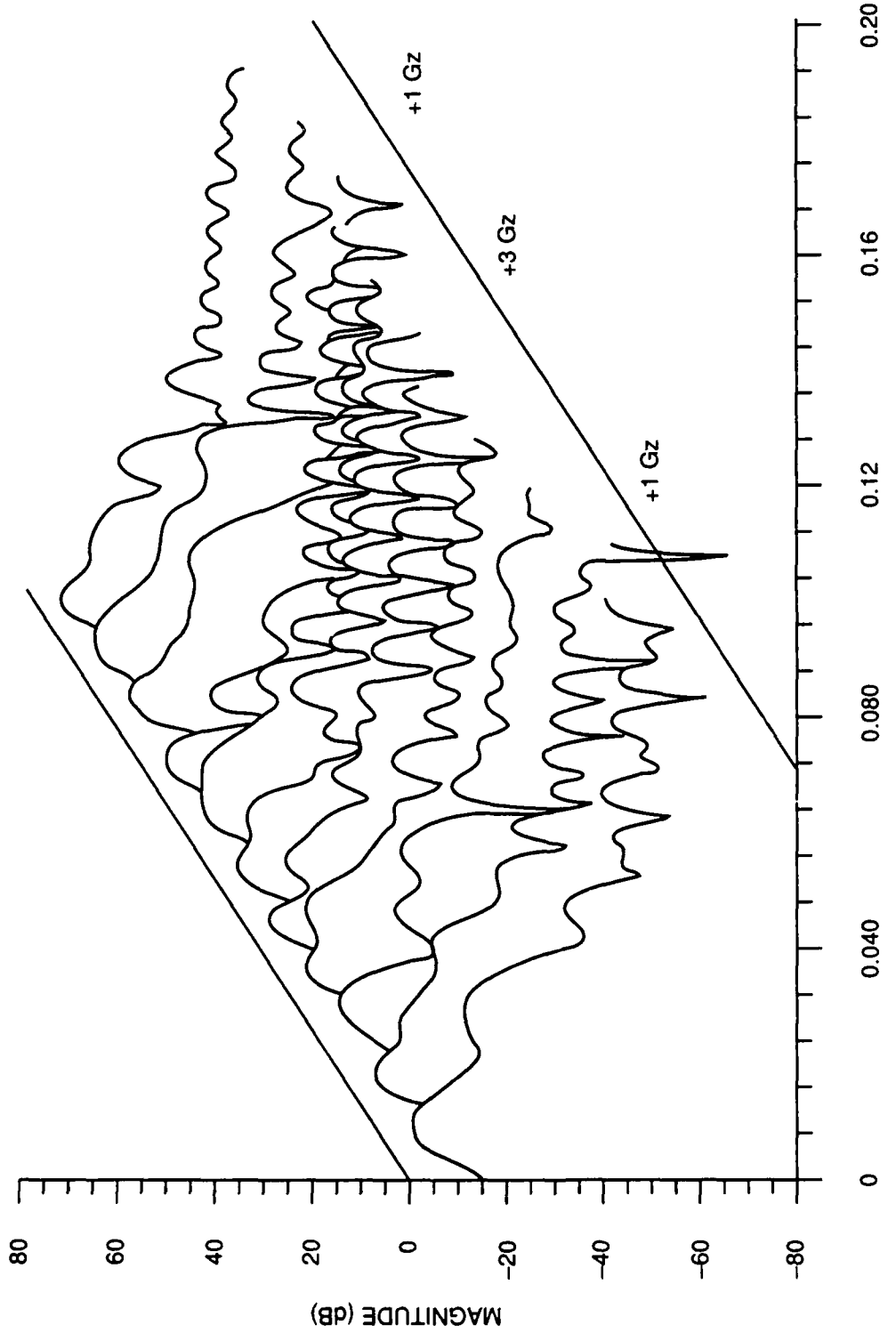

Figure 26. PSD ofΔZ as acceleration load varies from +1 to +3 to +1 Gz.

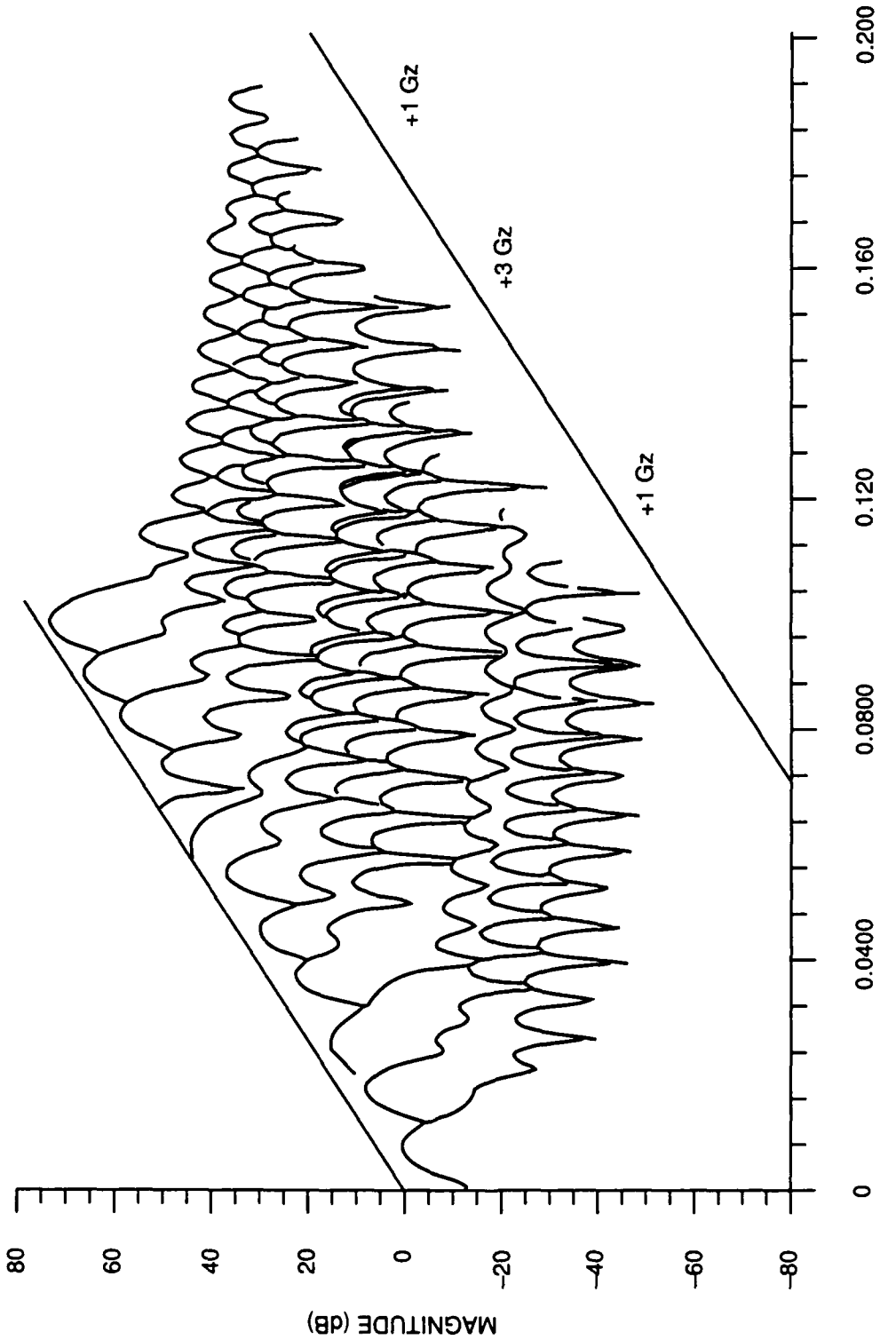

Figure 27. PSD of infrared plethysmograph of superficial temporal artery as acceleration load varies from +1 to +3 to +1 Gz.

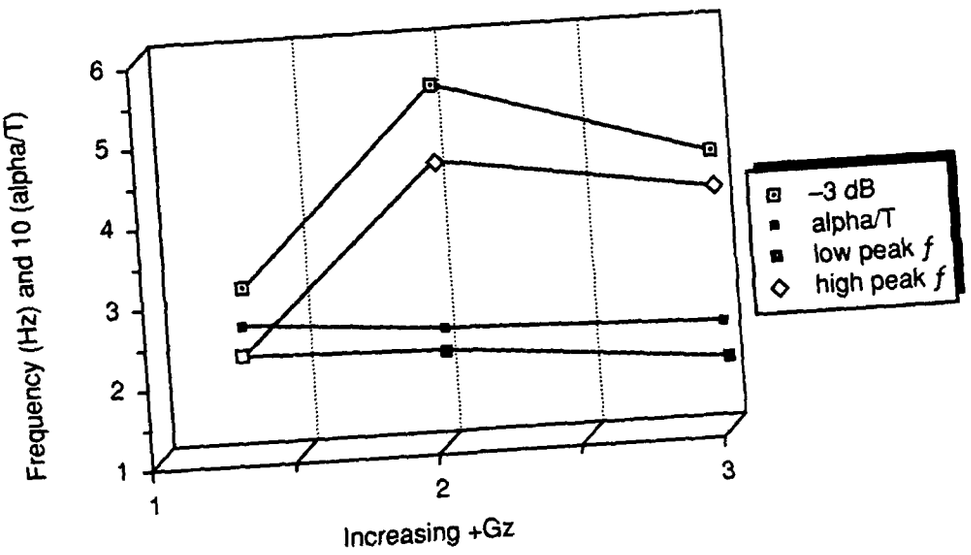

Figure 28a. Frequency content and alpha/T changes as acceleration increases: subject S1.

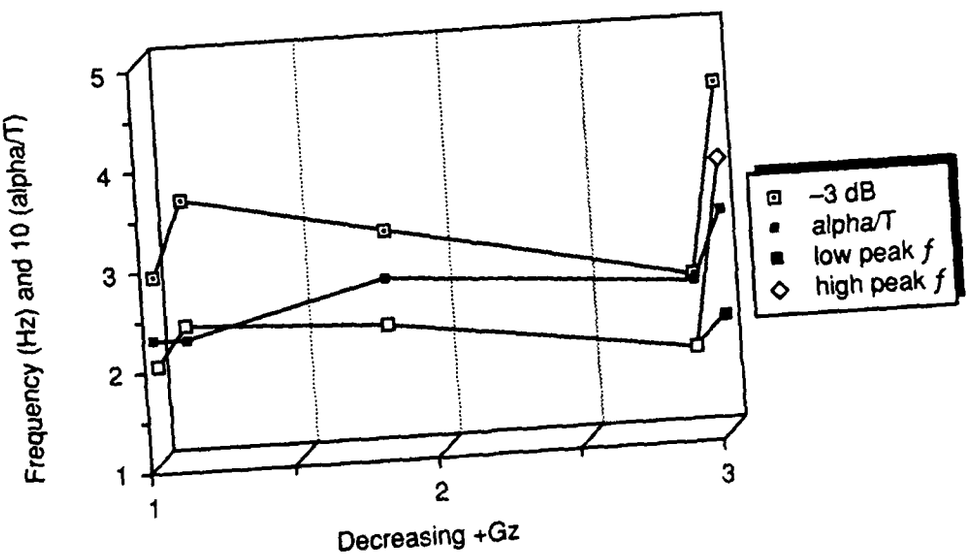

Figure 28b. Frequency content and alpha/T changes as acceleration decreases from +3 to +1 Gz: subject S1.

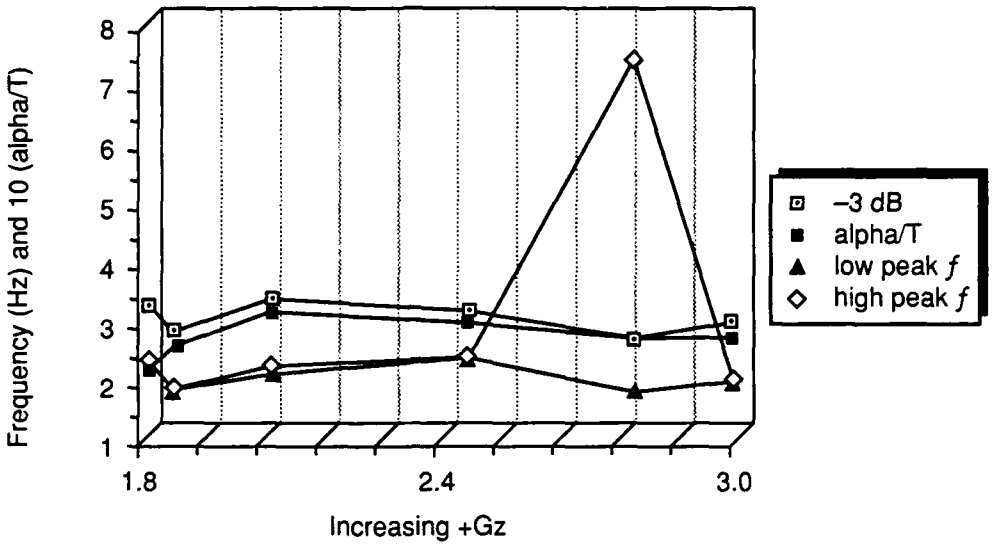

Figure 29a. Frequency content and alpha/T changes as acceleration increases: subject S5.

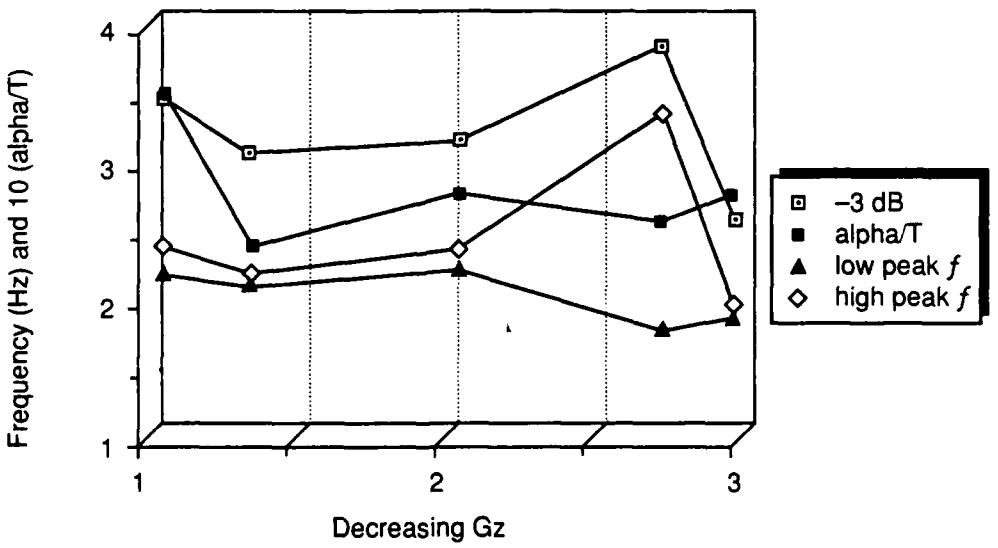

Figure 29b. Frequency content and alpha/T changes as acceleration decreases from +3 to +1 Gz: subject S5.

Table 3. Subject S5: ΔZ frequency content changes with increased +Gz load. Reversals from maxima to minima and vice versa at +3 Gz are shown in bold face. Runs were gradual onset.

+Gz	FREQUENCY (Hz)	MAGNITUDE (dB)	MAXIMA/MINIMA
any	1.8–2.4	0	maxima
<3	4–5.4	–15.5	minima
3	**1.8–5.8**	**0**	**maxima**
any	5.4–6.2	–7.75	maxima
any	10.6–11.4	–17.5	maxima
any	6.4–6.8	–19.25	minima
3	**9.4–9.8**	**–16.5**	**maxima**
<3	9.4–9.8	–30.4	minima
3	**8.6–9.2**	**–25.9**	**minima**
<3	8.6–9.2	–18	maxima

To calculate R_{xy}, the sum of the dot products was taken between all points of f_{-3dB}, *i.e.* the kernal, and each point of the 10 α/T waveform ($t_{10\alpha/T}$). This included a total of 2N – 1 points, where N is the number of data points. R_{xy} ranges from –N to N. If the correlation was perfect, the result would be the same as the kernal squared, *i.e.* each data point matches between the kernal and f_{-3dB}. Therefore, the sum of the dot products was normalized to 1.0 by dividing each point in the sum by the sum of the squared magnitudes of the kernal points (see Equation 41).

$$Rxy(k) = \left(\sum_{j=1}^{N} \left| f_{-3dB}(j) \right| \right)^{-1} \left\{ \sum_{i=-N}^{N} f_{-3dB}(i) \cdot t_{10\alpha/T}(i+k) \right\} \tag{41}$$

Therefore, a perfect positive cross correlation function would resemble an impulse function with a value of 1.0 positioned at the center of the function, *i.e.* $R_{xy}(0)$.

R_{xy} for S1 ($R_{xy:S1}$) and S5 ($R_{xy:S5}$) are plotted in Figures 30 and 31, respectively. While these functions do not indicate a perfect positive correlation as defined above, they do show that f_{-3dB} and $t_{10\alpha/T}$ are probably (in the statistical sense) weakly correlated with $R_{xy:S1}(0) = 0.64$ and $R_{xy:S5}(0) = 0.84$. Since there is no "figure of merit" for nonlinear cross correlation and the fact that the bulk of the power of the signal should be at Rxy(0), the area under the Rxy curve was calculated and compared to the area bounded by one standard deviation (±1 σ) centered about $R_{xy}(0)$. Each R_{xy} waveform was fitted to a fourth order polynomial (Equations 42 and 43). Equations 44 and 45 were used to determine the relative amount of the waveform that was within ±1 σ, *i.e.* 68% of the distribution.

$$R_{xy:S1} = 0.581 + 0.0245x - 0.073x^2 - 0.002x^3 + 0.002x^4 \quad \text{for } -N \le x \le N;\ R^2 = 0.994 \tag{42}$$

$$R_{xy:S5} = 0.743 + 0.014x - 0.018x^2 - 0.002x^3 + 0.005x^4 \quad \text{for } -N \le x \le N;\ R^2 = 0.993 \tag{43}$$

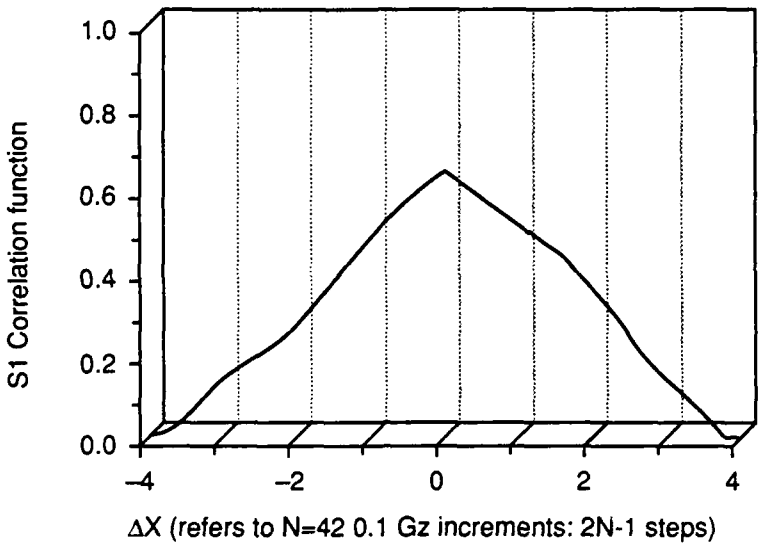

Figure 30. Cross correlation function between changes in −3dB frequency and alpha/T: subject S1.

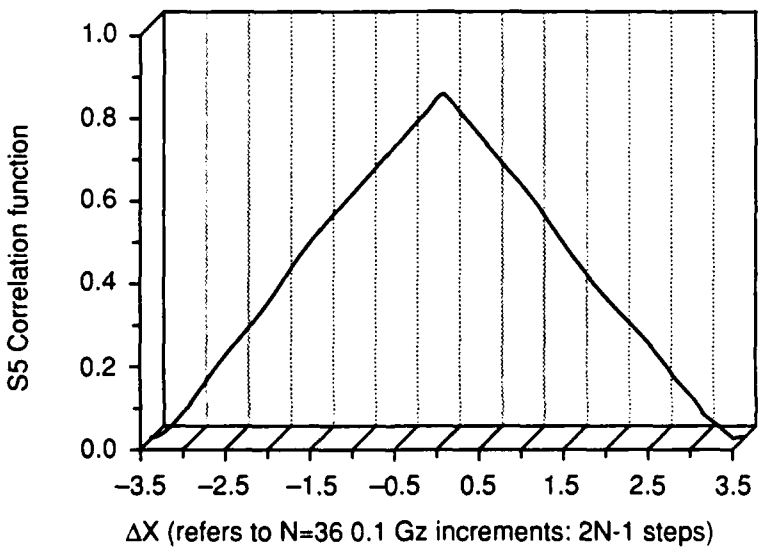

Figure 31. Cross correlation function between changes in −3dB frequency and alpha/T: subject S5.

$$\%S_1 = 1 - \frac{\left\{\int (Rxy : S_1\, dx)\Big|_{-4.0,4.0} - \int (Rxy : S_1\, dx)\Big|_{-2.5,2.5}\right\}}{\int (Rxy : S_1\, dx)\Big|_{-4.0,4.0}} \tag{44}$$

$$\%S_5 = 1 - \frac{\left\{\int (Rxy : S_5\, dx)\Big|_{-3.5,3.5} - \int (Rxy : S_5\, dx)\Big|_{-2.2,2.2}\right\}}{\int (Rxy : S_5\, dx)\Big|_{-3.5,3.5}} \tag{45}$$

It was found that 92.8% of $R_{xy:S1}$ lies within ±1 σ of $R_{xy:S1}(0)$ and 88.1% of $R_{xy:S5}$ lies within ±1 σ of $R_{xy:S5}(0)$. These values tend to support the validity of the cross correlation, assuming that Equations 41 and 42 are good representations of the actual curves.

CENTRIFUGE EXPERIMENT 2 (CE2)

Following the mixed success of automatic data processing for experiment CE1, experiment CE2 was processed by hand, with the help of automated statistical packages. It is important to point out at the onset of this discussion that demonstration of statistical significance does not imply clinical or experimental significance. Statistical significance can merely determine whether or not events occur due to chance alone. In this study, we were able to investigate the effects on the REG waveforms of a common technique to increase +Gz-tolerance, *i.e.,* reclining the seat back from the vertical. Of most interest in this study was the effects of changing seat-back-angle (SBA) under acceleration on Zb while the subjects were seated in a PALE (pelvis and legs elevated) seat. Results from this experiment were presented at the 1988 Annual Scientific Meeting of the Aerospace Medical Association (see page 74 for the abstract).

As a +Gz load is applied to a subject, there is a fluid shift out of the head down towards the abdomen and large capacitance veins of the legs. If Zb does indeed reflect the bulk movement of blood in and out of the head, then one should see a change in inflection in the waveform in conjunction with applied stress. Under 1 g conditions, Zb remains fairly stable without much change in the overall voltage level. With the application of stress, Zb decreases along with the increasing +Gz load during a "relaxed" run (see Figure 32). A relaxed acceleration exposure usually consists of a subject wearing a standard anti-G suit, which may or may not be inflated, a flight harness, and the subject does not perform an anti-G straining maneuver. In fact, as acceleration increases so does the magnitude of change in Zb. As the +Gz load is lifted, Zb returns back to a consistent level that is approximately the same as the prestress levels. Prior to attaining this level, there is an overshoot in the waveform. This overshoot is consistent with the onrush of blood back into the head and increased blood pressure (19, page 622) that occurs to compensate for the temporary acceleration induced loss in volume. Signal overshoot has also been seen in doppler ultrasound velocimetry recordings under a +Gz load performed in the human centrifuge at NADC.

In experiment CE2, as seen in the relaxed +Gz exposures, as the load is applied the magnitude of Zb changes along with the applied stress. However, as the seat approached a 40° to 50° SBA, the decline in Zb reversed and Zb either started a slow rise or maintained a consistent level higher than under relaxed conditions but lower than unstressed values. A sample strip chart recording of a +1.0 Gz/second onset rise to a +7 Gz, 5 second plateau run is shown in Figure 33. This change in inflection (marked with an arrow in the figure) occurred at this range of angles regardless of onset rate and corresponding +Gz level. For clarity, plots of percent change in Zb, %ΔZb, ((|Zb at +1.03 Gz| – |Zb at Gz > +1.03|)/|Zb at +1.03 Gz|) versus run time, SBA, and +Gz level for two subjects (MB and ES)

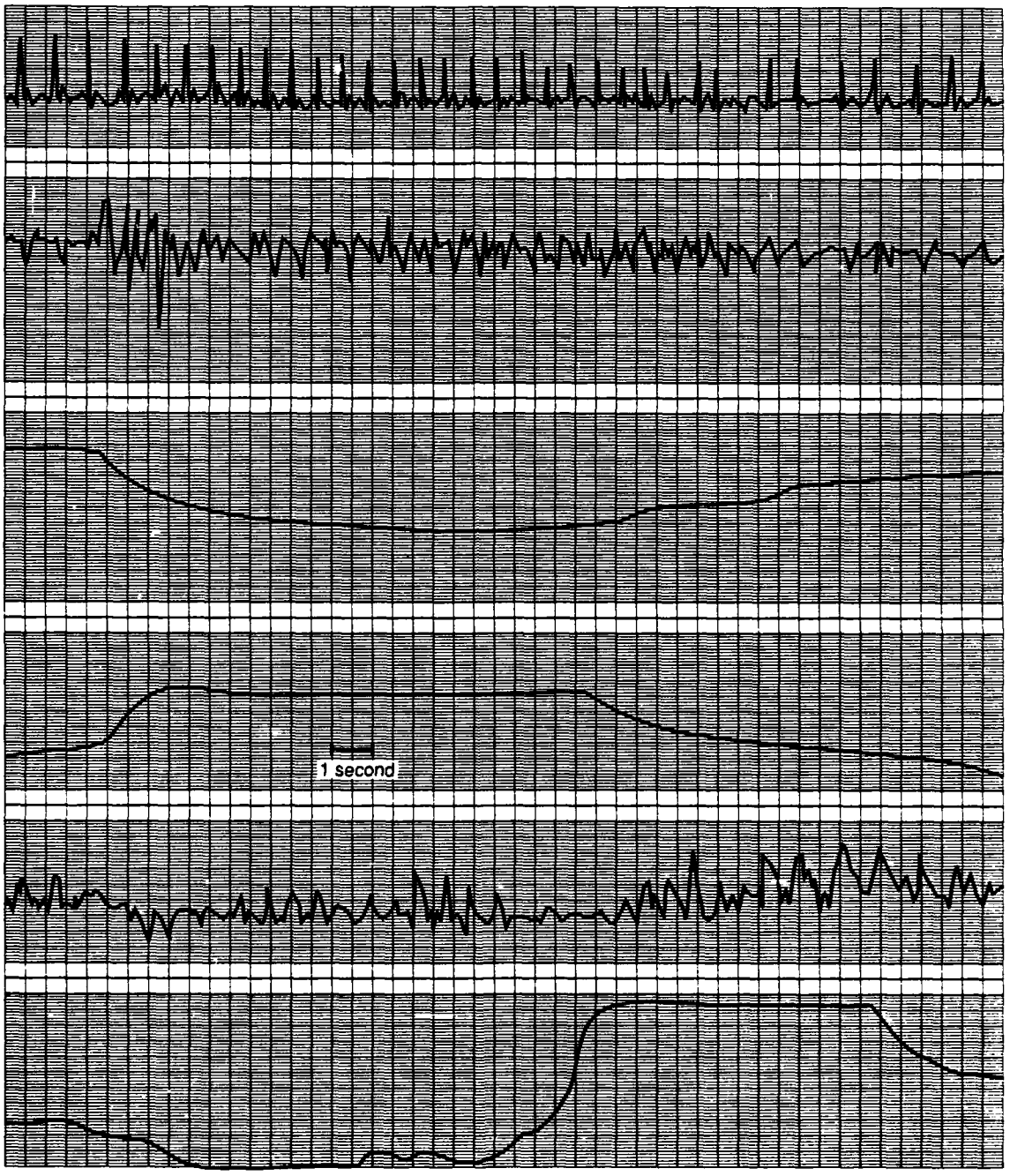

Figure 32. Effect of +Gz on Zb. This example taken during a run ending due to a reduction in peripheral light of >60°. From top: ECG, ΔZ, Zb, Gz (+5.0 plateau), doppler of superficial temporal artery,

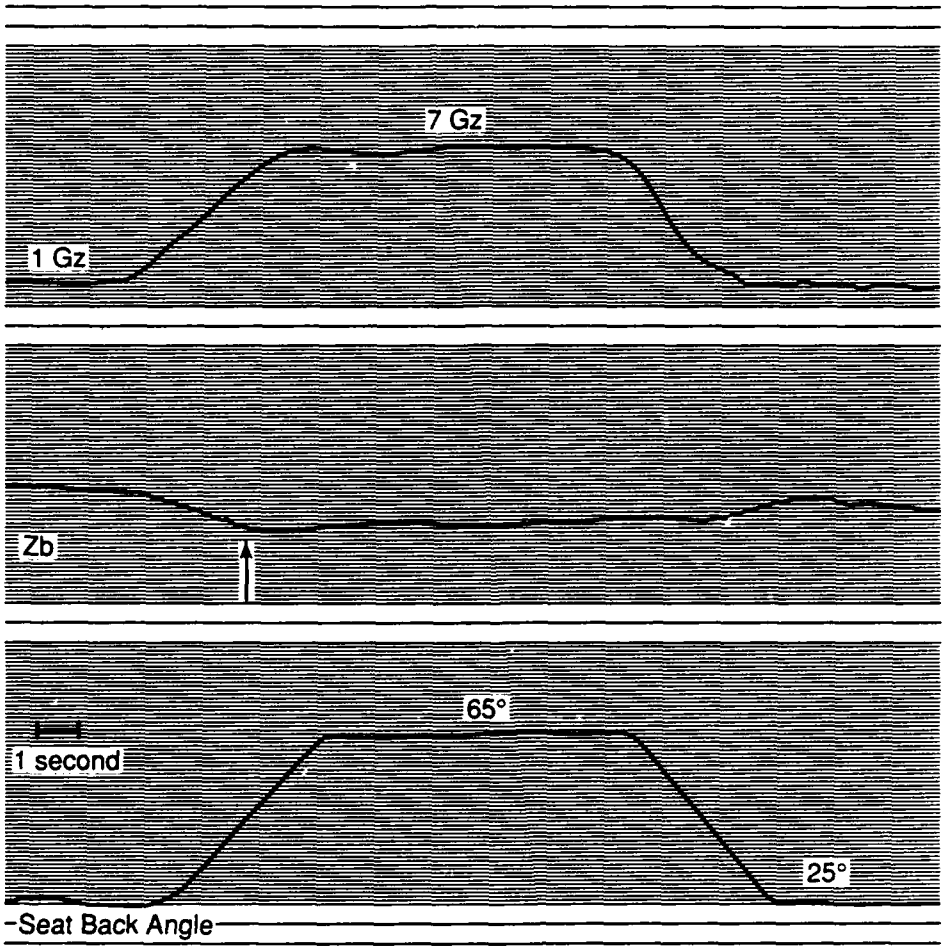

Figure 33. Strip chart recording on effects of reclining SBA on Zb. From top: Gz (+7.0 plateau), Zb, SBA (65° maximum).

during a GOR (+0.5 Gz/second) are shown in Figure 34. This indication of increased cephalic circulation and therefore ability to withstand higher acceleration stress occurs at an angle which is consistent with the studies done by Harald von Beckh at NADC in the 1970's.[81] In that study he reported an increase in +Gz-tolerance at a SBA of 45°. During experiment CE2, the average SBA in which there is an indication of the reversal of outward blood flow from the head is 49.25°. In Table 4, a summary of the SBA, Gz level and onset rate for ramp-type centrifuge runs at the point of inflection of Zb is presented. The changes in output voltage referable to Zb as acceleration load is increased and decreased, %ΔZb, SBA, and time from acceleration onset are presented in Appendix E. Upon offloading of the stress, the Zb waveform demonstrates a similar overshoot and subsequent return to prestress levels as seen in relaxed runs. These changes in Zb may allow us in future studies to use REG waveforms as an aid in determining the efficiency of anti-G protective devices.

Table 4. +Gz and seat-back-angle (SBA) at which there is a change in inflection of Zb during ramp-type acceleration exposures in experiment CE2.

ONSET RATE	+Gz at Zb INFLECTION	SBA
+2.3 Gz/sec	6.8	50°
+2.3 Gz/sec	6.8	48°
+0.5 Gz/sec	5.5	54°
+0.5 Gz/sec	4.7	48°
+0.5 Gz/sec	4.6	48°
+0.1 Gz/sec	4.8	51°
+0.1 Gz/sec	4.6	49°
+0.1 Gz/sec	4.4	46°

CENTRIFUGE EXPERIMENT 3 (CE3)

Circuitry improvements in the REG device permitted the collection of the best ΔZ and Zb data to date during experiment CE3. Specifically, enough data to characterize the magnitude and timing changes in impedance signals under acceleration stress was collected under relaxed and straining conditions.

Baseline REG, Zb

In the REG device, Zb is derived from a hardware combination of subtraction from and a slow (*i.e.* a long time constant) integration of ΔZ (see Figure 12a). Measurements are expressed as a percentage change in baseline from unstressed (*i.e.* 1 g) to a high +Gz load environment.

As mentioned previously, as acceleration load increases, so does the magnitude of the change in Zb. Zb data from four of the subjects was used to describe the change in Zb with respect to unstressed (+1.03 Gz) values taken five seconds prior to acceleration onset. These values were expressed as a percent change (%ΔZb), with the unstressed levels arbitrarily set to zero. According to the hydrostatic column theory, CV compensation can occur after about ten seconds of acceleration exposure, assuming that the onset rate was not so great as to overwhelm the CV system, which leads to loss of consciousness. Therefore, readings were taken five seconds prior to acceleration onset, during the two second onset, during the first, second, and third five second periods at plateau, during the two second acceleration offset, at the peak of the overshoot, and at the point of baseline recovery. The average

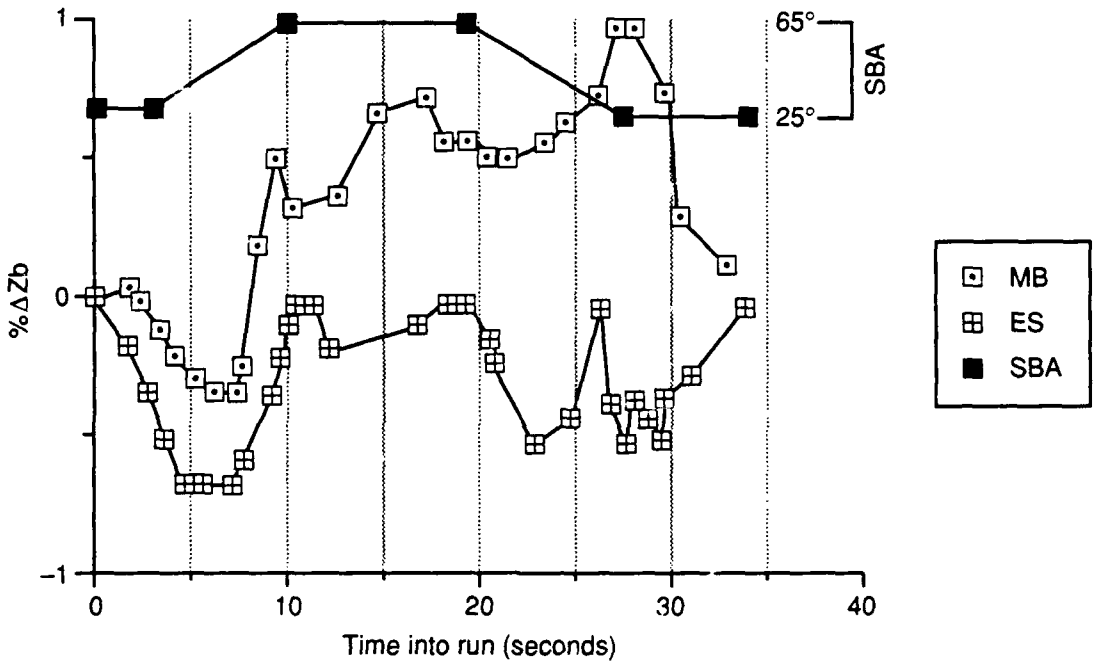

Figure 34. Plot of effects of increasing seat-back-angle (SBA) on Zb for subjects MB and ES during 0.5 Gz/sec ROR.

values of %ΔZb at +2.5 to +4.5 Gz for four relaxed subjects are presented in Table 5. These averages were determined from the raw data found in Appendix F. Appendix G contains the %ΔZb values for each individual subject. Also in Table 5 are values for runs that were stopped because the subjects' peripheral vision closed down to a 60° forward visual cone (labelled PLL, peripheral light loss, in the table). This endpoint occurred at an average level of +5.17 Gz after approximately ten seconds at plateau. The last line in the table, labelled AGSM, are the values of %ΔZb obtained while the subjects performed an L-1 maneuver. These values are taken during the forced exhalation period of the straining maneuver. A plot of %ΔZb with respect to run time and acceleration level is presented in Figure 35.

Table 5. Percent change in Zb with respect to +1.03 Gz levels during various points throughout the ROR. See text for explanation.

	Time Into Run From +Gz Onset						
+Gz	0–2s	2–7s	7–12s	12–17s	17–19s	peak	settle
2.5	−.222	−.200	−.247	−.295	−.148	−.05	−.122
3.0	−.142	−.152	−.186	−.22	−.062	−.006	.026
3.5	−.291	−.300	−.379	−.416	−.009	.129	.05
4.0	−.516	−.571	−.572	−.611	−.186	.121	.008
4.5	−.367	−.509	−.547	−.556	−.184	.184	.084
PLL	−.451	−.634	−.621	x	x	x	.053
AGSM	−.180	.132	.266	.348	.214	.440	.040

From this data several observations can be made. As acceleration stress increases, so does the magnitude of %ΔZb. Upon offloading of acceleration stress, there is an overshoot corresponding to the influx of blood reentering the head due to the effects of CV compensation. The relative amount of this overshoot tends to rise with increasing acceleration load, which corresponds to the increased amount of CV compensation necessary to restore the neural tissues to normal conditions. After the run, %ΔZb returns to the previous unstressed level within approximately 10%. This change in Zb level indicates that the subject's CV system has readjusted and blood flow has been restored. An example of one subject's Zb measurements both relaxed and straining can be found in Figure 36. Unfortunately, with this measure we cannot conclusively predict just by the magnitude of %ΔZb whether or not the onset of 60° PLL is imminent.

One way analysis of variance (ANOVA) was performed on %ΔZb with respect to acceleration load to discover if a significant statistical relationship exists between the baseline impedance and increasing acceleration level at plateau. We can see that while is there some biological variability in the data, *i.e.* %ΔZb at +2.5 Gz is greater than at +3 Gz, the relationship between increasing acceleration load and rising %ΔZb is highly significant (see Table 6).

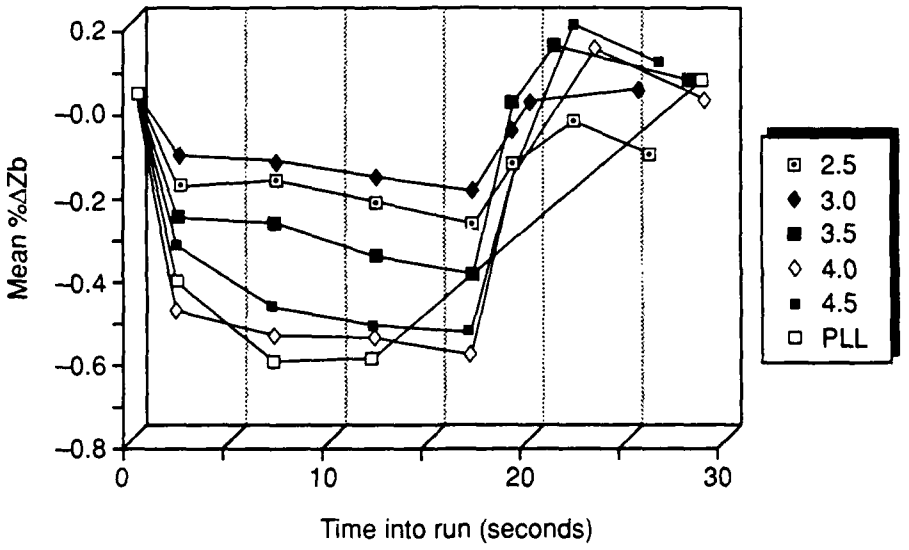

Figure 35. %ΔZb during ROR (average of four subjects). +Gz plateau from 0 to 15 seconds and recovery period from 15 to 30 seconds.

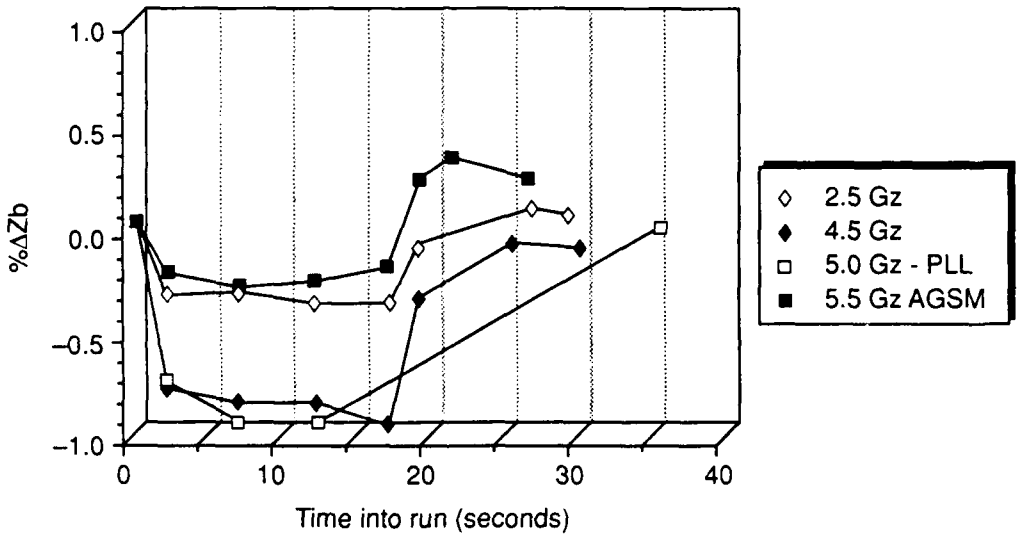

Figure 36. Effects of +Gz on %ΔZb during ROR: subject P5. +Gz plateau from 0 to 15 seconds and recovery period from 15 to 30 seconds.

Table 6. One way ANOVA comparing percent difference in the averaged baseline impedance with respect to +Gz level. dof = degrees of freedom.

Source	Sum of Squares	dof	Mean Squares	F	Prob > F
between +Gz	.439	4	.110	34.7	.000
Error	.048	15	.003		
Total	.487	19			

The plot in Figure 36 would seem to indicate that %ΔZb during straining is different from relaxed runs. The fact that at two seconds into the run no difference is apparent is probably due to inefficient straining technique during acceleration onset. Two tailed paired t tests were performed comparing relaxed runs (all grouped together) with straining runs. These tests were performed for each time period during plateau. As expected, at two seconds, the difference was insignificant ($p < 0.12$) while at plateau the difference between the means was highly significant ($p < 0.005$). One would like to be able to predict the onset of a PLL terminated run from the previous run time performance. Again, two tailed paired t tests were performed to judge the significance between the means at +4.0 and at +4.5 Gz with the PLL terminated run. These results were somewhat confusing due to the biological variability inherent in the data. The magnitude of %ΔZb values, while close, are greater at +4.0 than at +4.5 Gz. Therefore, while comparison between PLL and +4.0 Gz runs proved to be insignificant ($p < .736$), the results between PLL and +4.5 Gz were significant ($p < .026$). More data needs to be obtained to show that this reduction in %ΔZb prior to PLL runs is due to subject variability or is a consistent indication of potential cephalic circulation compromise.

Therefore, this measure gives a good indication of the relative state of the cephalic circulation with increasing acceleration load and shows that straining is indeed an effective means to increase cephalic blood flow.

EFFECTS OF STRAINING ON ZB

During the performance of an AGSM, such as the L-1, there are very definite changes in the form and level of Zb that can be used as a gauge to aid in the evaluation of the effectiveness of the respiratory portion of the AGSM. The form and reference points for the straining Zb waveform are shown in Figure 37 and are as follows:

1. I wave: Following a relatively flat or slightly sloped period corresponding to the forced expiration portion of the maneuver, there is a rise, the I wave, corresponding to the rapid expiration immediately preceeding the inhalation phase (the "KAH").

2. II wave: Next is a depression that corresponds to the first part of the rapid (<30 sec) inspiratory phase, the II wave.

3. III wave: The second part of the inspiratory phase including the beginning of the forced expiration and muscle tensing is manifested by a large peak, the III wave, that corresponds to the "HOOK."

4. IV wave: This is a relatively flat portion of the curve that corresponds to the forced expiratory phase of the L1.

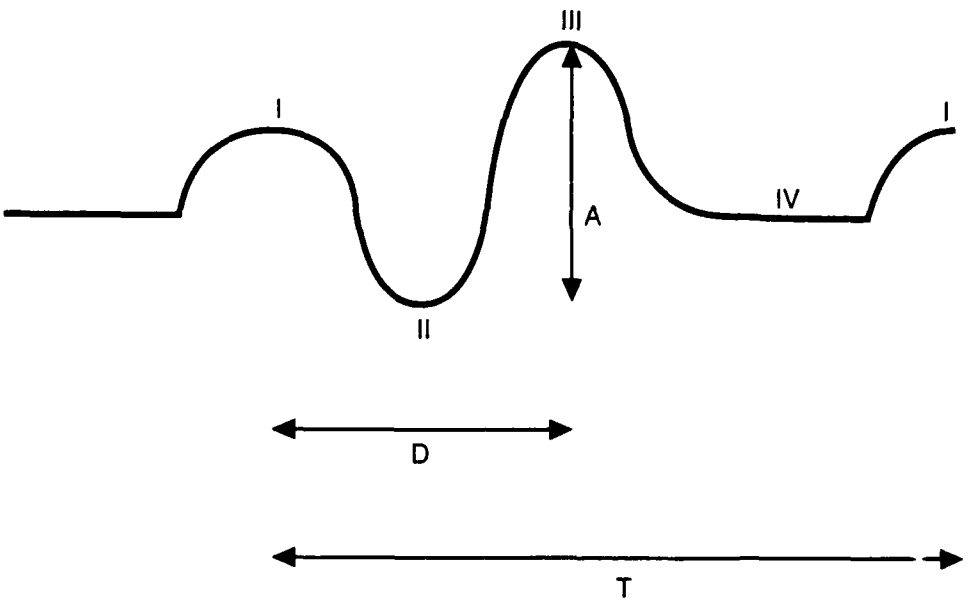

Figure 37. Zb waveform during the performance of an AGSM.

KEY

I	:	End of forced expiration period, the "Kah" sound.
II	:	Start of inspiration, the "Hook" sound.
III	:	Peak of inspiration.
IV	:	Start of forced exhalation period.
A	:	Magnitude of strain, i.e. relative strength of the strain.
D	:	Duration of strain, i.e. speed of breath exchange.
T	:	Period of strain, length of maneuver.

5. Strain amplitude: The difference between the minimum of the II wave and the peak of the III wave gives a relative indication of the strength of the strain during the breath exchange portion of the AGSM.

6. Strain duration: This is measured from the peak of the I wave to the end of the III wave. An indication of the speed of the air exchange is evident from this measure. Ideally, this takes about 0.5 seconds.[21]

7. Strain period: Measured between two I wave minima, this indicated the length of time the entire maneuver takes. Ideally, this should take three seconds.[21]

In order to compare the effects of straining on bulk movement of blood under acceleration, one can compare Zb levels when relaxed under stress to IV waves when performing an AGSM.

Figure 38 shows the changes in Zb during straining along with a respiration trace. The latter was obtained by placing a strain gauge type device across the thorax of the subject. The timing and patterns recorded with this device were mirrored by changes in Zb. By studying the Zb traces one can determine the speed of air exchange, relative strength of the respiratory effort, and the length of the strain. As an example, during the SACM phase of CE3, as time progressed during the runs and the subjects started to tire, some subjects exhibited some or all of the following responses: the straining period (I wave–I wave interval) decreased, strain duration (*i.e.* speed of breath exchange) lengthened, and the top of the strain amplitude wave (III wave) decreased in magnitude and flattened. Clearly, exhibition of these trends would indicate that the effectiveness of their straining technique was diminished. However, while straining amplitude and period both declined as SACM time increased, strain duration either lengthened or shortened depending upon the individual. The amount of straining effort an individual produces in the centrifuge, however, depends in large part to their level of motivation. During these trials, blood lactate measurements were made before and after SACM runs in order to determine whether subjects were engaged in anaerobic metabolism. These indicated that some subjects expended much more energy than others. It was difficult to determine for most of the subjects who truely reached a fatigue end point.

Therefore, while these changes in Zb are indeed promising and worthy of future investigation, more data needs to be obtained from a group of well trained clearly motivated individuals to reduce the variability seen in these indices, specially strain duration. Further, in order to gain a complete assessment of straining effort, electromyographic recordings of the arms, legs, and neck muscles are needed to complement the Zb respiratory information.

Once the additional information has been attained and baseline values and trends are known, may be possible to employ the REG as a training aid in the instruction of effective AGSM techniques in a noninvasive unobtrusive manner. Currently, one can monitor AGSM performance by measuring intrathoracic pressure by using an intraesophageal balloon. As one might imagine, it is difficult if not impossible to persuade volunteer subjects to use such a device.

Pulsatile Impedance, ΔZ

Analysis of the pulsatile impedance waveform, ΔZ, focused upon characterization of acceleration induced changes in magnitude and timing and attempting to explain those alterations with respect to the hydrostatic column theory of physiological response to acceleration stress. Sample strip charts showing the effects of two levels of Gz (+2.5 and +4.5 Gz) on ΔZ are found in Figures 39 and 40.

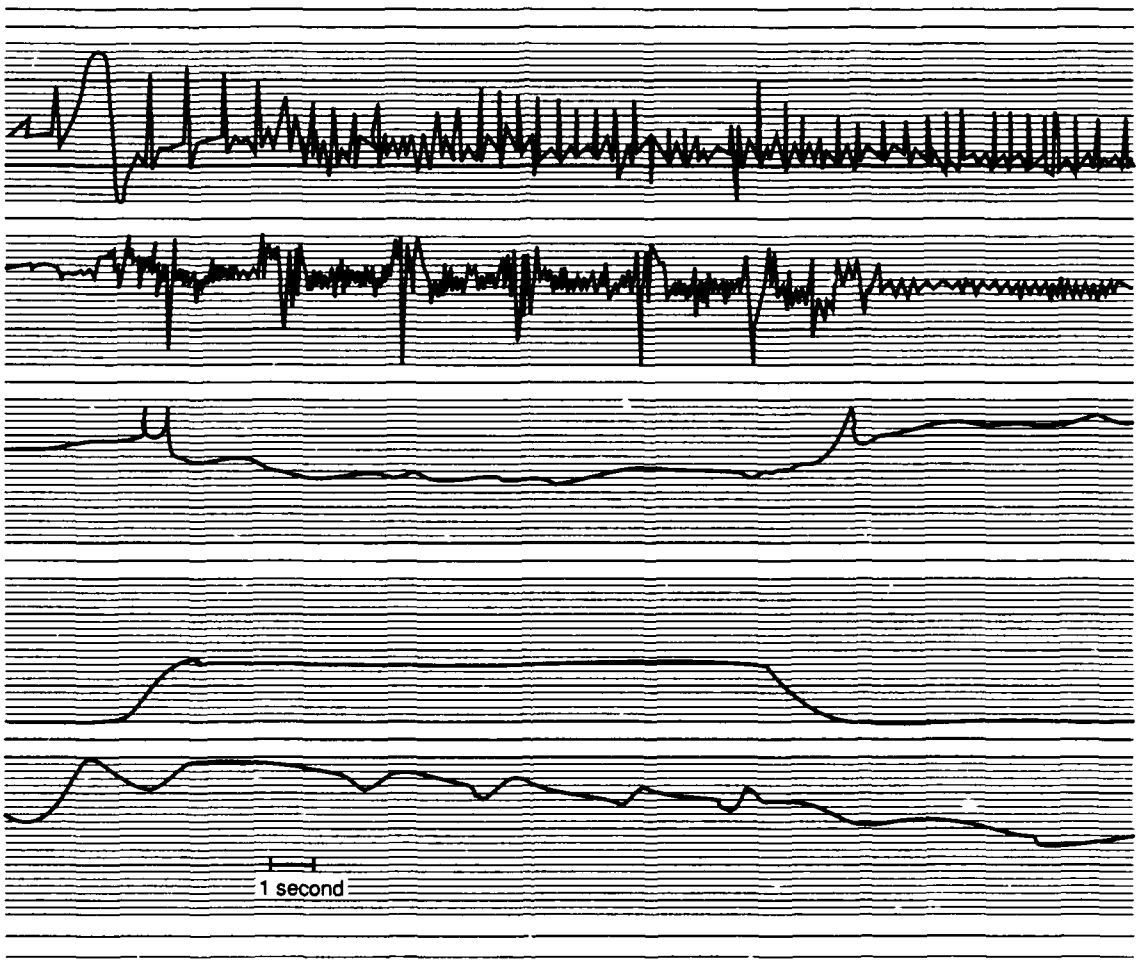

Figure 38. Effect of AGSMs on Zb. Respiration trace shown for comparision. From top: ECG, ΔZ, Zb, Gz (+5.5 plateau), thoracic respiration.

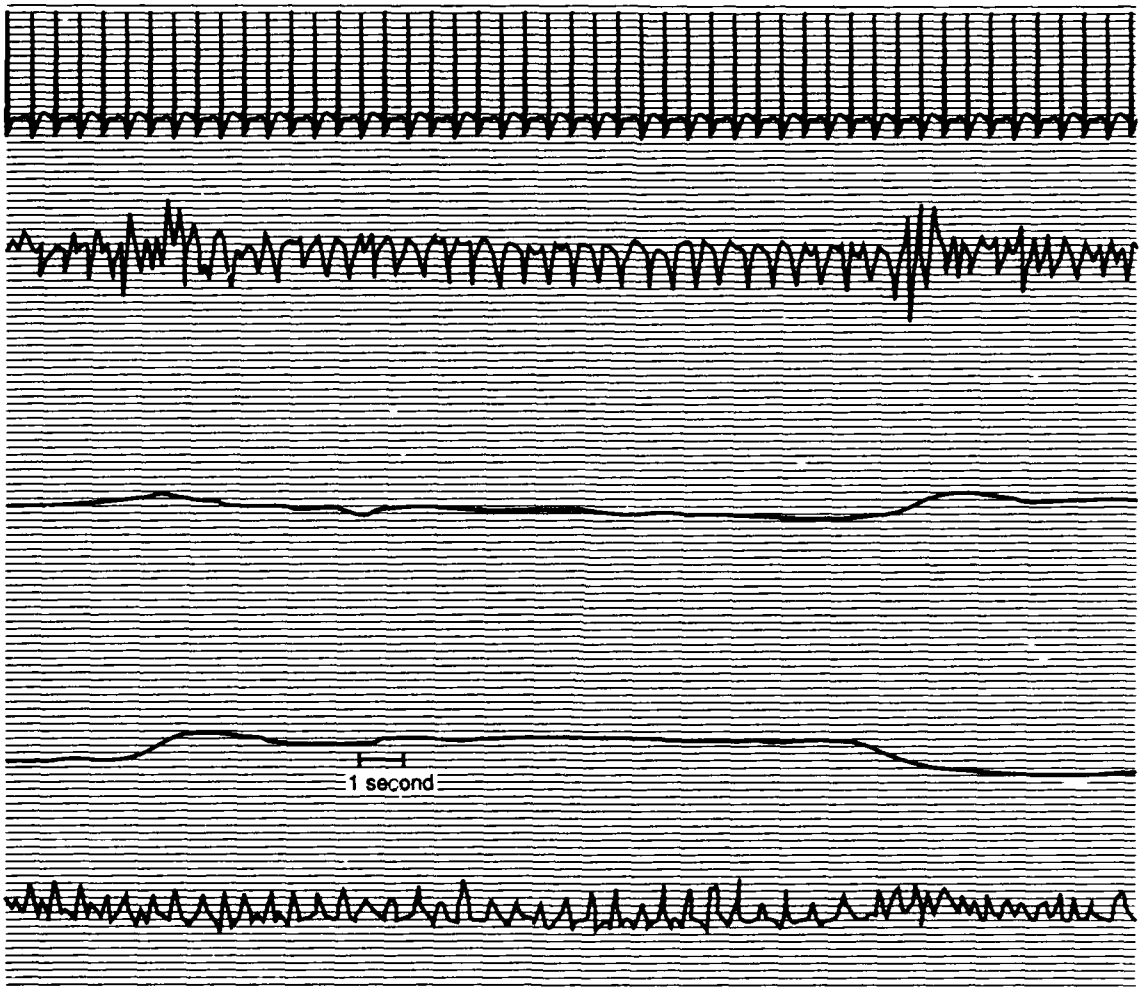

Figure 39. Effects of + 2.5 Gz on ΔZ. From top: ECG. Z, Zb, Gz (+ 2.5 plateau), ultrasound doppler of superficial temporal artery.

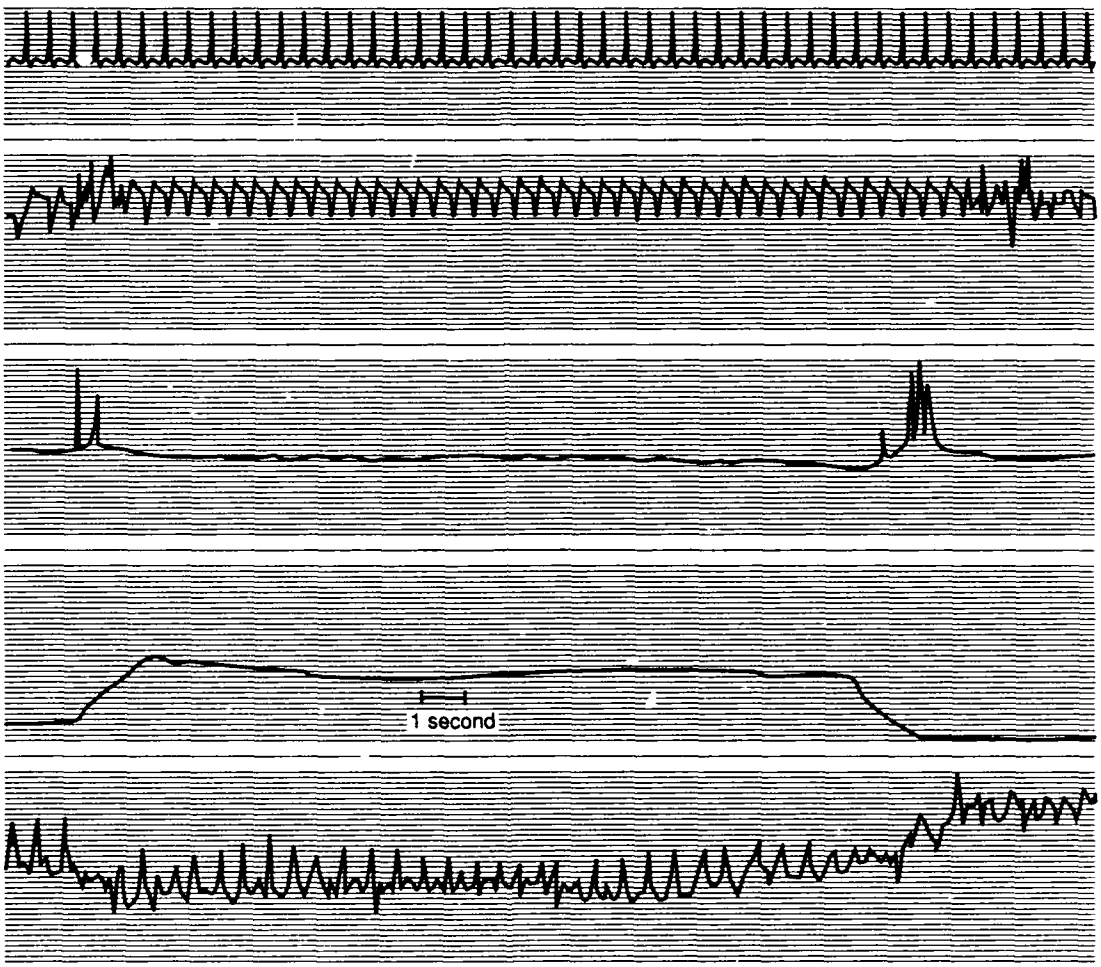

Figure 40. Effects of +4.5 Gz on ΔZ. From top: ECG, ΔZ, Zb, GZ (+4.5 plateau), ultrasound doppler of superficial temporal artery.

In order to get a general idea of the overall nature of the unstressed ΔZ waveform, six clean waveforms (3.6 seconds overall) from one subject, P7, were averaged (one point every 40 msec) and a fourth order polynomial equation was fit to the data. The results of the averaging and curve fit are found in Figure 41. The regression equation is

$$\Delta Z(\Omega) = -0.049 + 0.0102\,t - 6.14\times10^{-5}\,t^2 + 1.43\times10^{-7}\,t^3 - 1.15\times10^{-10}\,t^4 \qquad (46)$$

where t is time in msec. The coefficient of correlation is r = 0.97, the coefficient of determination, r^2 = 0.94, and the standard error of estimate is 0.050 Ω.

Rheoencephalographic Indices: A, B, C Wavelets

Under high a + Gz load, the ΔZ wavelets A, B, and C all increase in magnitude. As the level of stress rises, more and more of the relatively highly conductive blood plasma and cerebrospinal fluid is redistributed within the skull or is drained out of the cephalic space. Therefore, the impedance of the head rises with respect to an increase in acceleration stress.

For each index, five waveforms were averaged to eliminate the effects of random noise for each of four subjects for nine relaxed runs and six straining runs each. While there was some variability among these subjects, their respective values for each +Gz level and point in time during the runs were averaged together since the overall trend in these indices was the same. Impedance data was then expressed in terms of the percent change between prestress and stressed values since the objective was to determine relative changes with respect to acceleration load. In this way, it made no difference whether we expressed the raw data in terms of voltage or resistance. This presentation is similar to one taken by Lifshitz.[46] Also, evaluating data in this fashion tended to reduce the bias that occurs when one set of figures was obtained with a higher gain setting on the REG device.

Tables 7, 8, and 9 contain the percentage change from prestressed to stressed levels for wavelets A, B, and C, respectively. This information is also displayed graphically in Figures 42, 43, and 44. The raw data is presented in Appendix H. The prestress period is defined as five seconds prior to acceleration onset. In these tables, run time is broken down as follows: 0–5 seconds, 5–10 seconds, and 10–15 seconds at +Gz plateau, 5–10 seconds and 15–20 seconds after acceleration offset. In this way, it ought to be possible to see any effects of cardiovascular compensation occurring after ten seconds of high +Gz exposure. Recall that the onset of this compensation, on average, can occur after approximately ten seconds of exposure.[15] We also wanted to monitor how ΔZ reflects physiological recovery after acceleration offset.

Table 7. Percent change from prestress levels (+1.03 Gz) of the A wave of ΔZ with respect to run time and +Gz.

+Gz	0–5 s	5–10 s	10–15 s	20–25 s	30–35 s
2.5	.152	.222	.265	.027	
3.0	.319	.391	.434	.207	.128
3.5	.299	.445	.393	.044	−.022
4.0	.308	.487	.503	.061	−.034
4.5	.491	.547	.595	.166	.098
PLL	.410	.434		.073	−.179

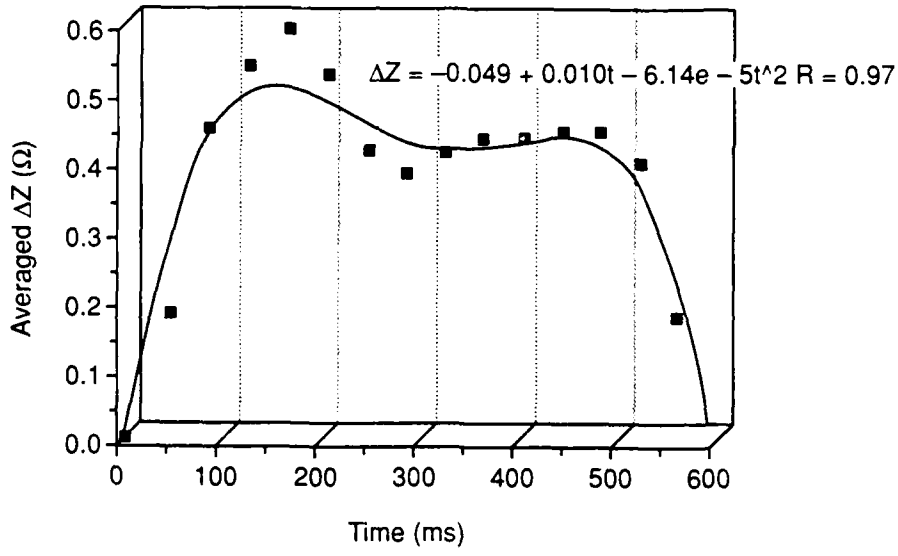

Figure 41. Fourth order polynominal curve fit of averaged ΔZ at 1 g: subject P7.

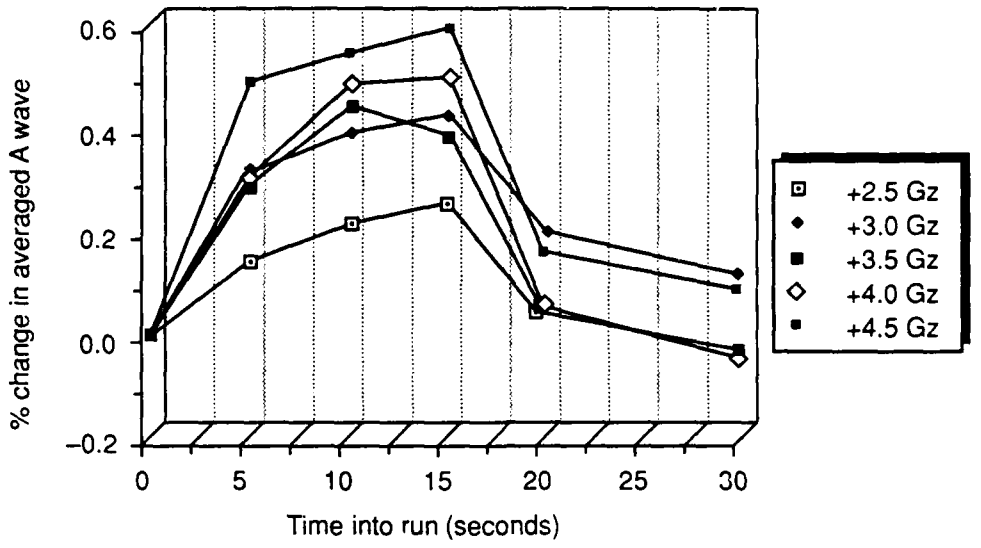

Figure 42. Effects on increasing +Gz on percentage change in A wave amplitude from prestress to high +Gz levels (average of four subjects). +Gz plateau from 0 to15 seconds and recovery period from 15 to 30 seconds.

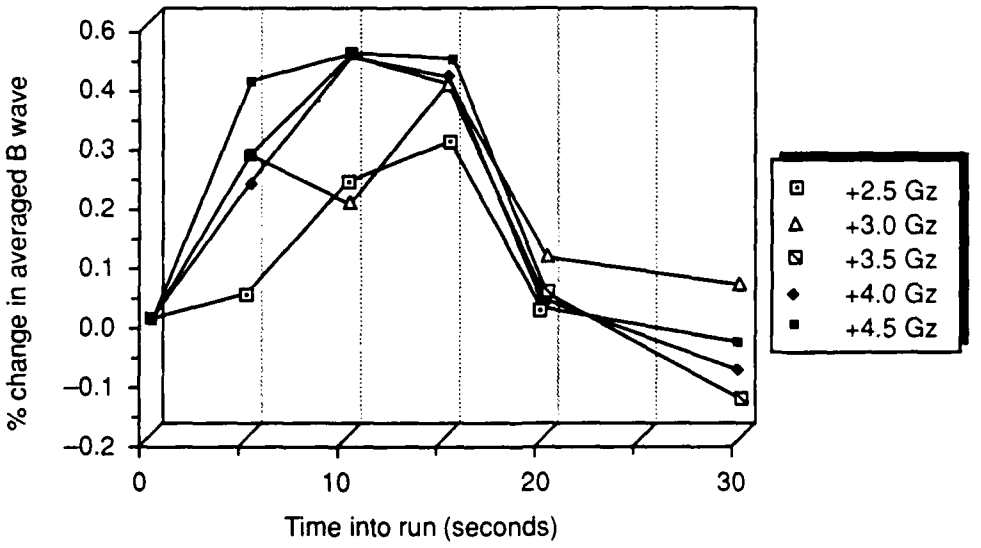

Figure 43. Effects on increasing +Gz on percentage change in B wave amplitude from prestress to high +Gz levels (average of four subjects). +Gz plateau from 0 to 15 seconds and recovery period from 15 to 30 seconds.

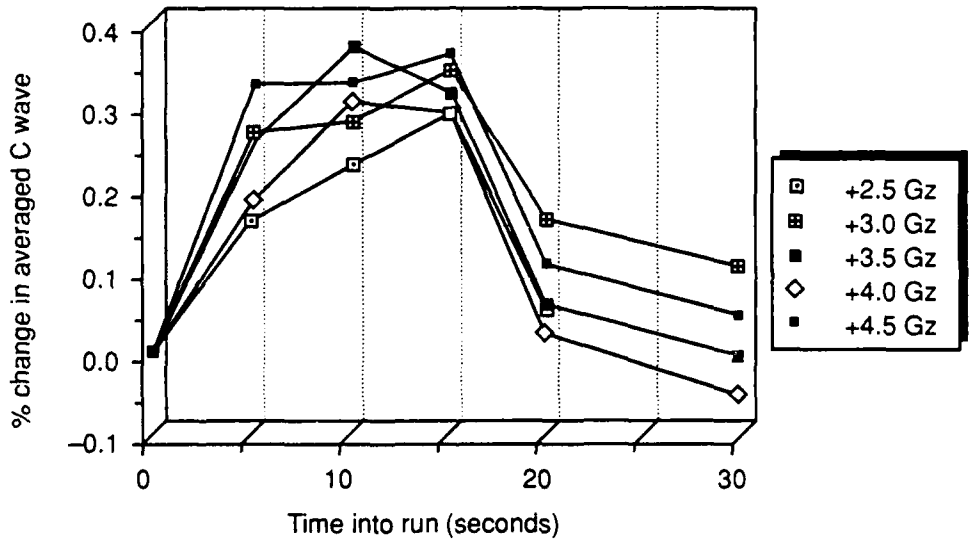

Figure 44. Effects on increasing +Gz on percentage change in C wave amplitude from prestress to high +Gz levels (average of four subjects). +Gz plateau from 0 to 15 seconds and recovery period from 15 to 30 seconds.

Table 8. Percent change from prestress levels (+1.03 Gz) of the B wave of ΔZ with respect to run time and +Gz.

+Gz	0–5 s	5–10 s	10–15 s	20–25 s	30–35 s
2.5	.047	.236	.305	0.0	
3.0	.275	.197	.388	.108	.066
3.5	.275	.453	.398	.055	−.119
4.0	.227	.453	.411	.024	−.077
4.5	.404	.45	.441	.024	−.022
PLL	.360	.343		.048	−.163

Table 9. Percent change from prestress levels (+1.03 Gz) of the C wave of ΔZ with respect to run time and +Gz.

+Gz	0–5 s	5–10 s	10–15 s	20–25 s	30–35 s
2.5	.161	.228	.289	.054	
3.0	.264	.279	.338	.161	.108
3.5	.253	.367	.315	.059	0.0
4.0	.182	.301	.288	023	−.049
4.5	.320	.325	.359	.107	.045
PLL	.274	.247		.064	−.154

No effects of CV compensation were seen with the A wave. At +3.5 Gz and above, the B wave did indicate increased tone after ten seconds at plateau with respect to the first ten seconds of stress. The C wave was a bit more variable in that during some of the runs, at +3.5 and +4.0 Gz, compensation may have begun, also after ten seconds at plateau. It is important to emphasize that compensation *may* have occurred. There is great variability within individuals as to when their cardiovascular compensatory responses begin in earnest. The nature of this response also depends upon the rate of onset and level of acceleration stress. Impedance changes can be quite useful in determining these responses if they are used in conjunction with other correlative measures. This is brought out by the fact that the A wave showed no changes similar to those seen with B and C waves. By fifteen seconds after offloading from high +Gz, all wavelets return to within approximately 15% of the previous unstressed levels.

ANOVA for each time period and wavelet were performed to assess the differences between ΔZ and run time and/or +Gz value (see Tables 10 and 11). One way ANOVA tests comparing the means of the percent changes in A, B, and C wavelets with respect to run time show that the pulsatile impedance waveform changes significantly as the length of time under acceleration stress continues. The results of two way ANOVA comparisons between percent changes in A, B, and C wavelets with respect to run time and +Gz level indicate significant differences between calculated impedance values and run time. However, only analysis of the A and C waves demonstrated a significant difference between impedance, run time, and acceleration load. One cannot state that changes in the B wave, as analyzed under conditions of this test, did not occur due to chance alone.

AD-A221 150 RHEOENCEPHALOGRAPHY IN SIMULATED AVIATION ENVIRONMENTAL STRESS(U) NAVAL AIR DEVELOPMENT CENTER WARMINSTER PA AIR VEHICLE AND CR.. B S SHENDER 01 JUN 89 2/2

UNCLASSIFIED NADC-89042-60 F/G 6/10 NL

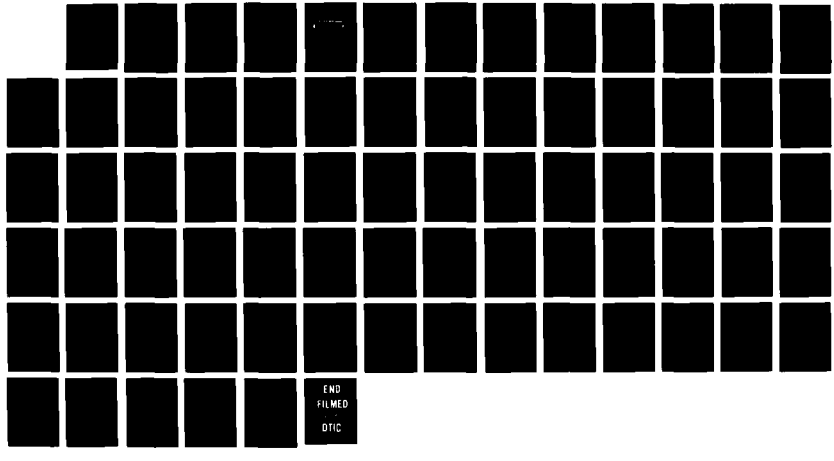

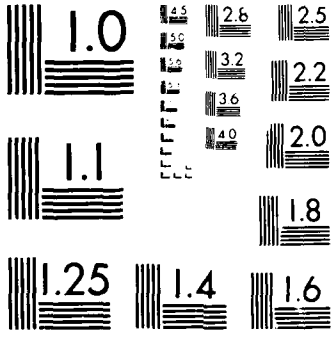

MICROCOPY RESOLUTION TEST CHART
NATIONAL BUREAU OF STANDARDS-1963-A

Table 10a. One way ANOVA comparing percent difference in the A wave with respect to run time. dof = degrees of freedom.

Source	Sum of Squares	dof	Mean Squares	F	Prob > F
between run time	.917	5	.183	18.64	.000
error	.226	23	.01		
total	1.143	28			

Table 10b. One way ANOVA comparing percent difference in the B wave with respect to run time. dof = degrees of freedom.

Source	Sum of Squares	dof	Mean Squares	F	Prob > F
between run time	.847	5	.169	22.91	.000
error	.170	23	.007		
total	1.046	28			

Table 10c. One way ANOVA comparing percent difference in the C wave with respect to run time. dof = degrees of freedom.

Source	Sum of Squares	dof	Mean Squares	F	Prob > F
between run time	.482	5	.096	39.39	.000
error	.056	23	.002		
total	.538	28			

Table 11a. Two way ANOVA comparing percent difference in the A wave with respect to run time and +Gz. dof = degrees of freedom.

Source	Sum of Squares	dof	Mean Squares	F	Prob > F
between run time	.964	5	.193	41.70	.000
between +Gz	.135	4	.034	7.31	.001
error	.092	20	.005		
total	1.192	29			

Table 11b. Two way ANOVA comparing percent difference in the B wave with respect to run time and +Gz. dof = degrees of freedom.

Source	Sum of Squares	dof	Mean Squares	F	Prob > F
between run time	.875	5	.175	27.26	.000
between +Gz	.043	4	.011	1.679	.194
error	.128	20	.006		
total	1.046	29			

Table 11c. Two way ANOVA comparing percent difference in the C wave with respect to run time and +Gz. dof = degrees of freedom.

Source	Sum of Squares	dof	Mean Squares	F	Prob > F
between run time	.508	5	.102	72.89	.000
between +Gz	.029	4	.007	5.198	.005
error	.028	20	.007		
total	.564	29			

Third order polynominal regression equations for each wavelet with respect to time into the +Gz exposure ('run time') and +Gz load level have been calculated and are found in Table 12. The t^3 terms were all on the order 10^{-5} and less and were omitted from the table. With these equations expressing the acceleration induced changes in the indices and Equation 40, it should be possible to construct a preliminary mathematical model describing the appearance of the ΔZ waveform for various levels of +Gz. While the coefficient of determinations for these equations are reasonably good (ranging from 0.684, percent change in B wave at +3 Gz, to 1.0, percent change in B wave at +2.5 Gz), how well this combination of equations predicts ΔZ under acceleration stress awaits further investigation.

Table 12a. Polynomial regression describing the effects of +Gz on the A wave of ΔZ as expressed as the percent change in ΔZ with respect to +1.03 Gz levels ($\%\Delta Z_A$). Where r = coefficient of correlation, r^2 = coefficient of determination, SEE = standard error of estimate, F = F ratio, Prob > F = significance.

+Gz	Equation	r	r^2	SEE	F	Prob > F
2.5	$\%\Delta ZA = -.015 + .049t - .002t^2$	.950	.903	.052	9.26	.097
3.0	$\%\Delta ZA = -.006 + .095t - .006t^2$	.975	.95	.059	12.69	.074
3.5	$\%\Delta ZA = -.025 + .117t - .009t^2$	.963	.926	.09	8.39	.108
4.0	$\%\Delta ZA = -.034 + .126t - .009t^2$	.937	.878	.135	4.80	.177
4.5	$\%\Delta ZA = -.010 + .152t - .011t^2$	.962	.926	.111	8.35	.109
PL	$\%\Delta ZA = .006 + .118t - .009t^2$	.999	.998	.026	142.9	.061

Table 12b. Polynomial regression describing the effects of +Gz on the B wave of ΔZ as expressed as the percent change in ΔZ with respect to +1.03 Gz levels (%ΔZB). Where r = coefficient of correlation, r^2 = coefficient of determination, SEE = standard error of estimate, F = F ratio, Prob > F = significance.

+Gz	Equation	r	r^2	SEE	F	Prob > F
2.5	$\%\Delta ZB = -.022t + .008t^2$	1.0	1.0	.001	29815	.004
3.0	$\%\Delta ZB = .004 + .067t - .005t^2$	.827	.684	.127	1.44	.435
3.5	$\%\Delta ZB = -.028 + .111t - .008t^2$	.967	.936	.093	9.68	.095
4.0	$\%\Delta ZB = -.040 + .111t - .008t^2$	.93	.865	.131	4.27	.196
4.5	$\%\Delta ZB = -.013 + .135t - .010t^2$	.966	.933	.098	9.35	.098
PLL	$\%\Delta ZB = .010 + .099t - .008t^2$	.995	.991	.044	35.08	.123

Table 12c. Polynomial regression describing the effects of +Gz on the C wave of ΔZ as expressed as the percent change in ΔZ with respect to +1.03 Gz levels (%ΔZc). Where r = coefficient of correlation, r^2 = coefficient of determination, SEE = standard error of estimate, F = F ratio, Prob > F = significance.

+Gz	Equation	r	r^2	SEE	F	Prob > F
2.5	$\%\Delta ZC = -.015 + .050t - .002t^2$	.945	.893	.055	8.34	.107
3.0	$\%\Delta ZC = .001 + .072t - .005t^2$	.96	.923	.055	7.94	.114
3.5	$\%\Delta ZC = -.017 + .094t - .007t^2$	.973	.947	.06	11.85	.079
4.0	$\%\Delta ZC = -.022 + .077t - .006t^2$	.945	.893	.079	5.58	.156
4.5	$\%\Delta ZC = -.001 + .093t - .007t^2$	.965	.931	.067	8.95	.102
PLL	$\%\Delta ZC = .011 + .069t - .005t^2$	.99	.98	.05	16.57	.178

During the performance of an AGSM during a two second rise, 15 second plateau ROR, reductions in magnitude of the A, B, and C wavelets indicate an elevated level of blood flow towards the head as straining time increases. (See Figure 45 for an example strip chart recording of a straining run). During each approximately three second strain, one to four ΔZ waveforms were readable and measured for subjects P7 and P10. These values have been expressed as percentages as above and are displayed in Appendix I. The effects of straining on the A, B, and C wavelets for subject P10 are found in Figures 46, 47, and 48. In general, during the performance of an effective AGSM the overall percentage magnitude change declines within an individual straining period and during the entire +Gz exposure at plateau. Note that there was an increase in index magnitude during the post-stress recovery period which then returns to values close to prestress levels. This change indicates that after performance of AGSMs over a fifteen second period, which caused an abnormal increase of blood flow into the head, a compensatory response to decrease this extra volume occurs, causing a rise in measured impedance.

Rheoencephalographic Ratios: B/A, C/A, α/T

Several rheoencephalographic indices have been proposed to express the state of the resistance bed and the cephalic circulation. These include the ratios B/A (indication of arteriolar tone), C/A (indication of blood outflow and venous tone), and α/T (indication of elasticity and vascular tone of large and intermediate vessels).[27] Changes in α/T have been related to overall changes in cerebral vascular resistance (CVR).[57]

Figure 45. Strip chart recording of effects of AGSMs on ΔZ and Zb. From top: ECG, ΔZ, Zb, Gz (+5.5 plateau), ultrasound doppler of superficial temporal artery.

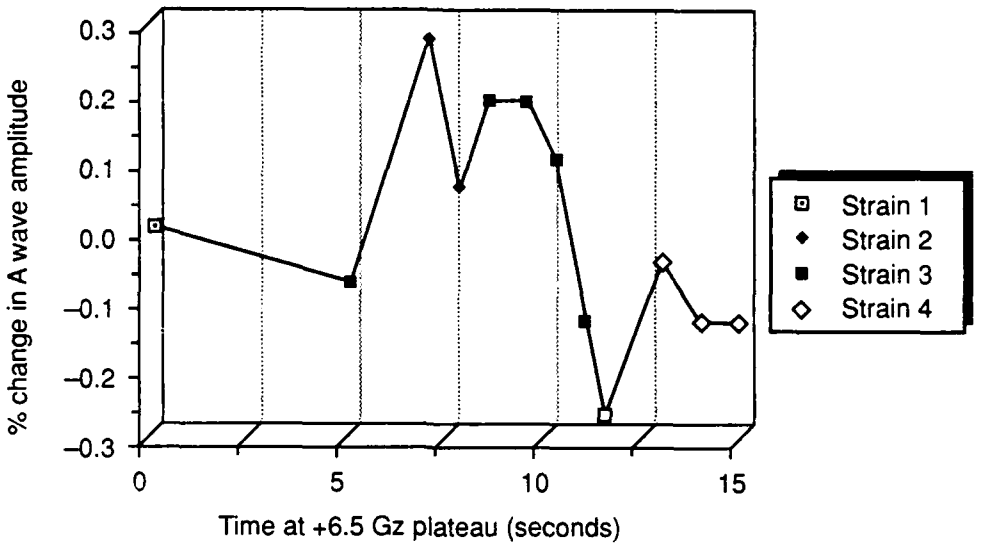

Figure 46. Effect of AGSMs on A wave amplitude during 15 seconds at +6.5 Gz: subject P10.

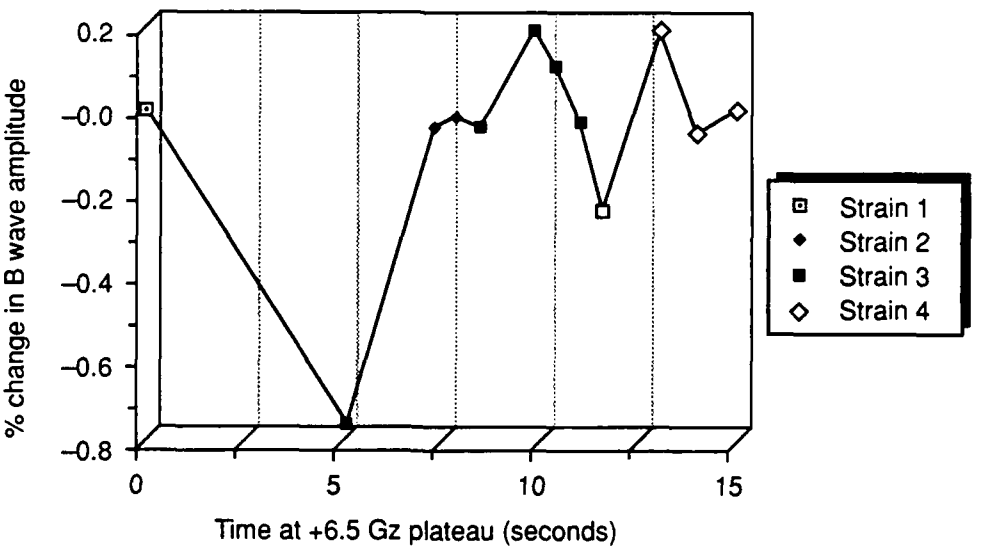

Figure 47. Effect of AGSMs on B wave amplitude during 15 seconds at +6.5 Gz: subject P10.

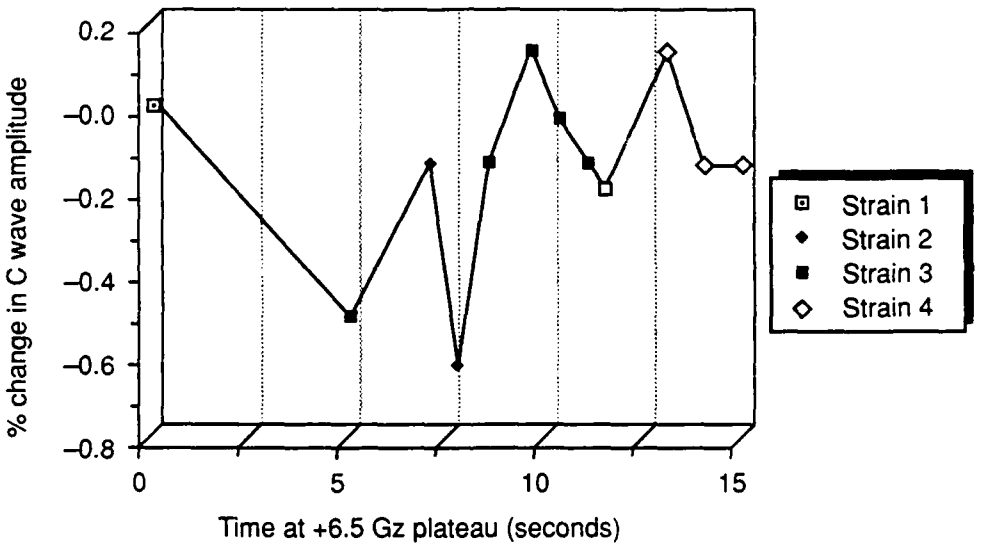

Figure 48. Effect of AGSMs on C wave amplitude during 15 seconds at +6.5 Gz: subject P10.

The main physiological responses of the body to positive acceleration stress are tachycardia and a rise in arterial pressure that occurs was a consequence of increased vasoconstriction. Concurrently with this rise in pressure in the lower regions of the body is a decrease in blood pressure in the head. Recall that the venous and, to a lesser extent, the arterial circulation of the head is protected under a high +Gz load by the CSFP.[66] Gillies[19,page599] cites experiments that showed decreased vasoconstriction, particularly in the pial system, occurs in the cranium under acceleration stress. Therefore, inaccurate interpretation of CVR based on the above indices alone without having other measurements to support the findings is possible.

With above cautions in mind, the following are the results of analysis of the various ratios. Table 13 contains the averaged percent change in B/A for four subjects from prestress to stressed values for acceleration levels ranging from +2.5 to +4.5 Gz. Also included are values from runs terminated due to 60° PLL. Appendix J contains the B/A ratios for each subject for the various acceleration loads. The changes in B/A during relaxed +Gz runs were quite variable. For all +Gz levels, during the first five seconds at plateau, arteriolar tone, as indicated by B/A, decreased. During the rest of the time at plateau and during recovery, arteriolar tone either increased or decreased depending upon the acceleration load, though not in any particular pattern. A plot of the percent change in B/A under high +Gz with respect to prestress levels is found in Figure 49. A two way ANOVA comparing these values to run time and acceleration level is shown in Table 14. Results of this analysis show that there was no significant change in B/A with respect to +Gz levels during relaxed acceleration exposures.

Table 13. Percent change from prestress levels (+1.03 Gz) of the averaged ratio B/A with respect to run time and +Gz.

+Gz	0–5 s	5–10 s	10–15 s	20–25 s	30–35 s
2.5	−.125	.007	−.018	−.082	−.071
3.0	−.058	−.121	−.068	−.056	−.081
3.5	−.028	−.047	−.036	−.033	−.104
4.0	−.109	−.016	−.059	−.039	−.047
4.5	−.063	−.044	−.122	−.133	−.111
PLL	−.066	−.075		.055	.023

Table 14. Two way ANOVA comparing percent difference in the B/A ratio with respect to run time and +Gz. dof = degrees of freedom.

Source	Sum of Squares	dof	Mean Squares	F	Prob > F
between run time	.023	5	.005	3.64	.017
between +Gz	.006	4	.001	1.165	.356
error	.025	20	.001		
total	.054	29			

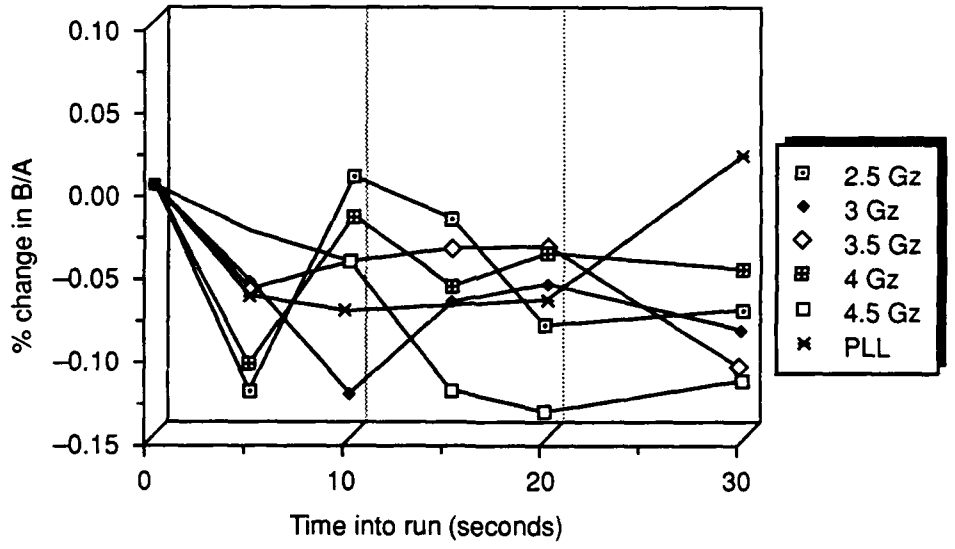

Figure 49. Percentage change in B/A from prestress to high +Gz levels. +Gz plateau from 0 to 15 seconds and recovery period fom 15 to 30 seconds.

The results determining the effects on changing venous tone, C/A, under high +Gz were quite different. The ratio C/A were expressed as percentages in the same manner as above. These values are presented in Table 15. Appendix K contains the raw data. With each +0.5 Gz increase, C/A indicated a decrease in tone, except for the first run at +2.5 Gz. A plot of these values is shown in Figure 50. Two way ANOVA comparing these values to run time and acceleration level is shown in Table 16. Results of this analysis show that there was a highly significant change in percent change of C/A with respect to acceleration levels.

Table 15. Percent change from prestress levels (+1.03 Gz) of the averaged ratio C/A with respect to run time and +Gz.

+Gz	0–5 s	5–10 s	10–15 s	20–25 s	30–35 s
2.5	–.004	.023	–.013	.006	.014
3.0	–.027	–.071	–.071	–.063	–.023
3.5	–.086	–.074	–.083	–.015	–.021
4.0	–.103	–.105	–.126	.001	–.006
4.5	–.128	–.134	–.159	–.025	–.040
PLL	–.138	–.168		–.043	.025

Table 16. Two way ANOVA comparing percent difference in the C/A ratio with respect to run time and +Gz. dof = degrees of freedom.

Source	Sum of Squares	dof	Mean Squares	F	Prob > F
between run time	.035	5	.007	7.46	0.0
between +Gz	.023	4	.006	6.20	.002
error	.019	20	.001		
total	.077	29			

The third index of CVR is the rheographic time α/T. These values were averaged for each time period during the run as above (see Table 17 and Appendix L). In contrast to the rheographic ratio results above which indicated a decrease in tone, α/T tends to increase under acceleration. According to Hadjiev,[27] this increase is indicative of greater levels of CVR. His measurements were performed on patients with ischemic cerebrovascular disorders and there was no indication of the heart rate of these subjects. Figure 51 displays the change in α/T with increasing acceleration load. Note on this figure that there is a change in inflection after ten seconds at plateau. This may be due to a decrease in tone with the onset of cardiovascular compensation or may only be due to biological variability. Figure 52 is a 'blowup' of Figure 51 in which α/T responses at +4.0 and +4.5 Gz can be compared with α/T during PLL runs. In this case, the PLL values were quite different during the first ten seconds at plateau. More data needs to be obtained to objectively verify this change. One sample t tests performed comparing prestress levels to stressed levels showed highly significant differences ($p < 0.01$ or better) at +3.5 Gz and above. By 15 seconds after offset of acceleration, α/T returned to prestress values. However, a two way ANOVA comparing α/T with time at plateau and +Gz showed there was no significant interaction between α/T and acceleration load (see Table 18).

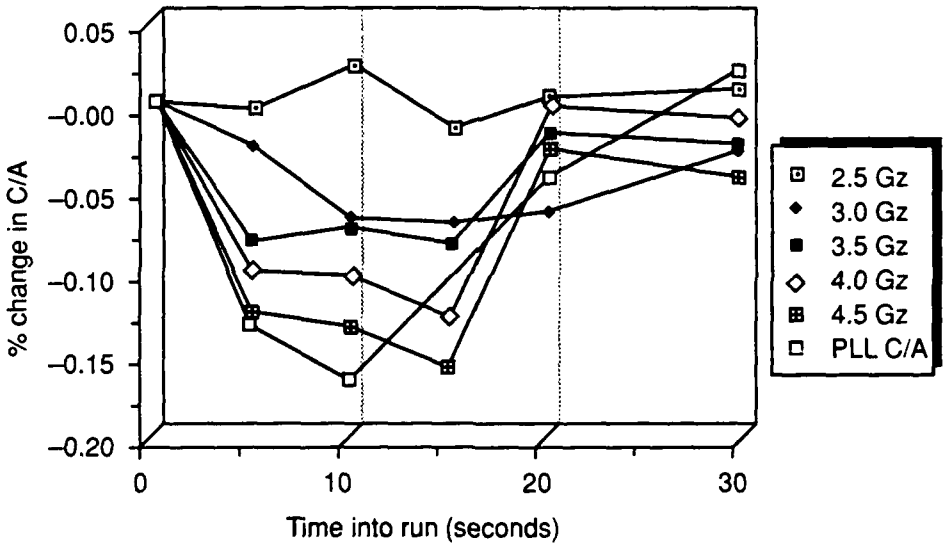

Figure 50. Percentage change in C/A from prestress to high +Gz levels. +Gz plateau from 0 to 15 seconds and recovery period from 15 to 30 seconds.

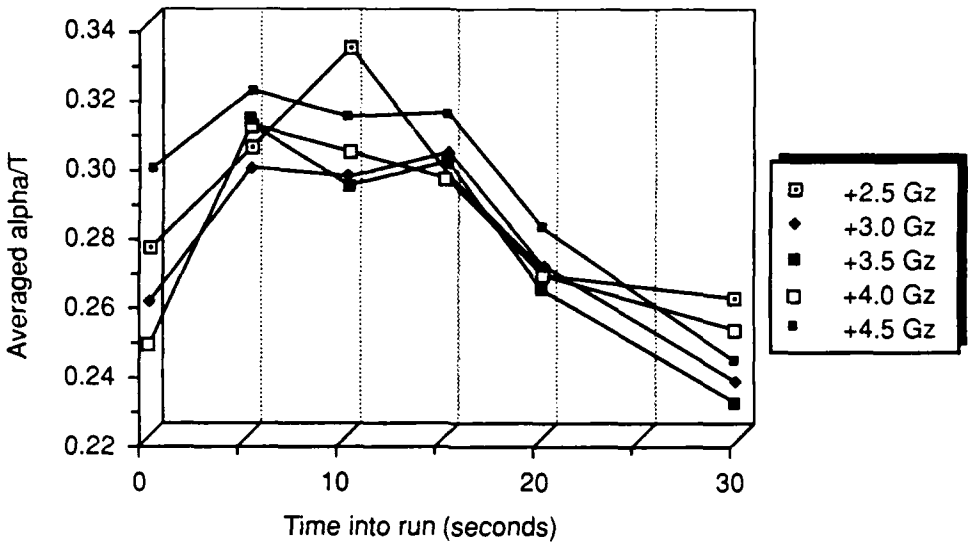

Figure 51. Effects of increasing +Gz on alpha/T (average of four subjects). +Gz plateau from 0 to 15 seconds and recovery period from 15 to 30 seconds.

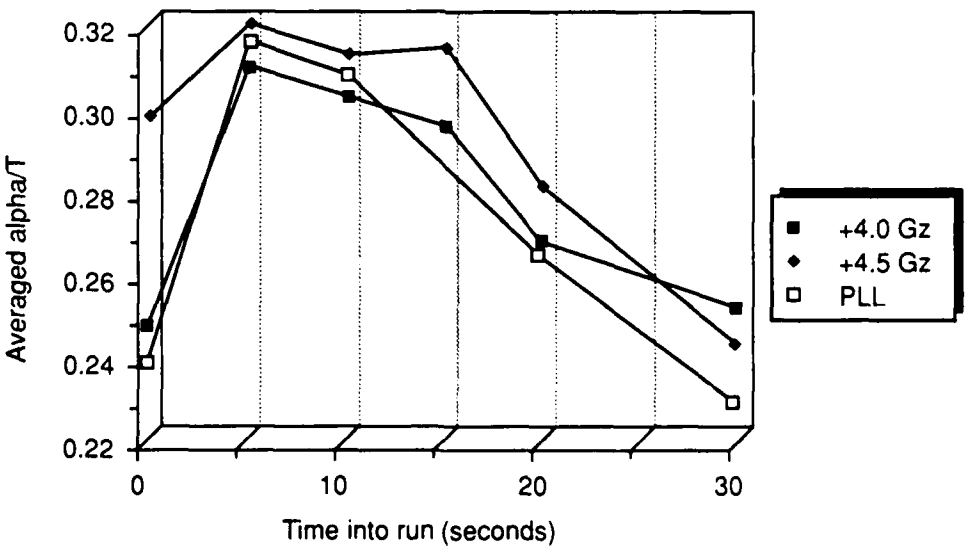

Figure 52. Change in alpha/T as +Gz load approaches PLL level (average of four subjects). +Gz plateau from 0 to 15 seconds and recovery period from 15 to 30 seconds.

Table 17. Percent change from prestress levels (+1.03 Gz) of the averaged ratio α/T with respect to run time and +Gz.

+Gz	0–5 s	5–10 s	10–15 s	20–25 s	30–35 s
2.5	.113	.215	.084	−.018	−.040
3.0	.151	.143	.170	.046	−.077
3.5	.263	.186	.215	.069	−.057
4.0	.255	.227	.198	.089	.028
4.5	.077	.054	.061	−.051	−.175
PLL	.328	.294		.113	−.029

Table 18. Two way ANOVA comparing α/T with respect to run time and +Gz. dof = degrees of freedom.

Source	Sum of Squares	dof	Mean Squares	F	Prob > F
between time at plateau	.674	4	.168	18.60	0.0
between +Gz	.035	3	.012	1.31	.285
Interaction	.061	12	.005	.561	.864
error	.498	55	.009		
total	1.268	74			

In order to place any real faith in these rheographic ratios more correlative studies must be performed with our device to characterize these responses. As an example, inhalation of CO_2 at 1 g would cause vasodilatation and enable us to set baseline responses of the ratios with respect to one variable as opposed to attempting to characterize these indices in the complicated environment of the human centrifuge.

Rheoencephalographic Indices And Relaxed +Gz-Tolerance

One might ask if there is a detectable change in impedance measurements between the highest relaxed +Gz level attained, G15, and data from the next run in which a peripheral light loss end of run (PLLeor) occurred (see Figure 33). To determine this, two tailed paired t tests comparing G15 with PLLeor for the A, B, and C wavelets and for the ratios B/A, C/A, and α/T were performed. One can compare the responses in the A, B, and C waves between higher relaxed acceleration levels and PLL runs by referring to Figures 53, 54, and 55. The results are summarized in Table 19. At best, there is a marginal difference in A and C waves and no significant difference in the other indices. Therefore, while a decrease in A wave magnitude at a higher +Gz plateau than the one just completed might indicate the onset of 60° PLL, it would not be a conclusive and reliable indicator in and of itself. For example, during the first five seconds at plateau, A wave magnitude was higher at +3.0 Gz than at +3.5 or +4.0 Gz for the averaged magnitude data.

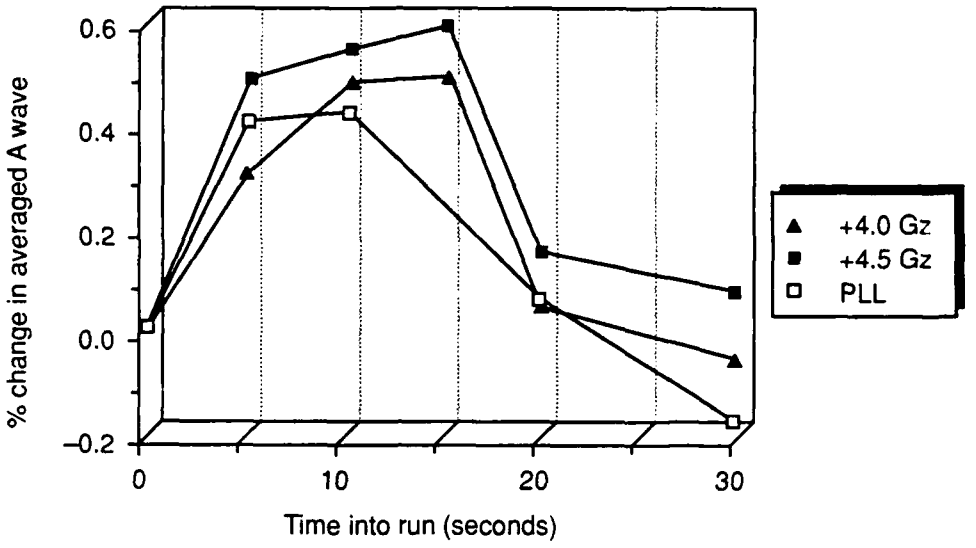

Figure 53. Percentage change in A wave amplitude from prestress level to point in which +Gz load approaches PLL level (average of four subjects). +Gz plateau from 0 to 15 seconds and recovery period from 15 to 30 seconds.

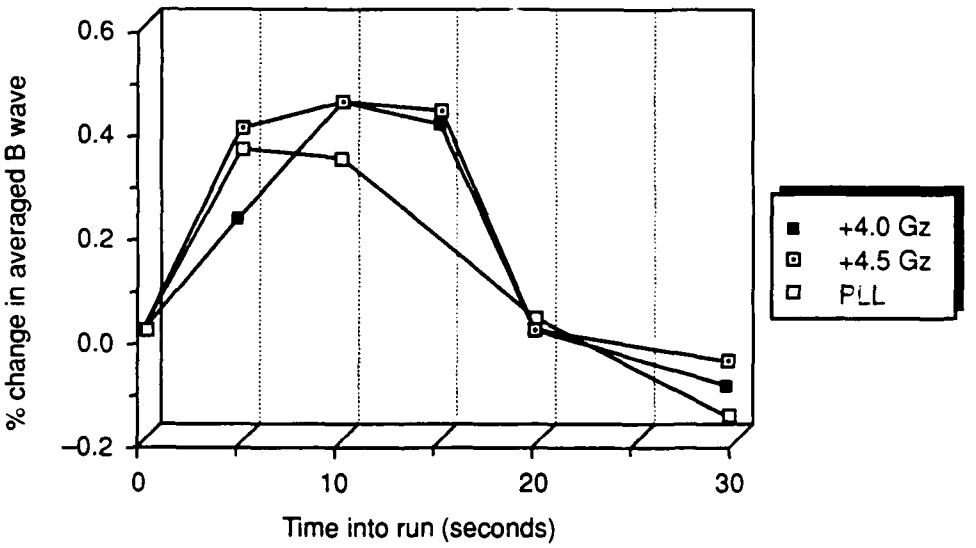

Figure 54. Percentage change in B wave amplitude from prestress level to point in which +Gz load approaches PLL level (average of four subjects). +Gz plateau from 0 to 15 seconds and recovery period from 15 to 30 seconds.

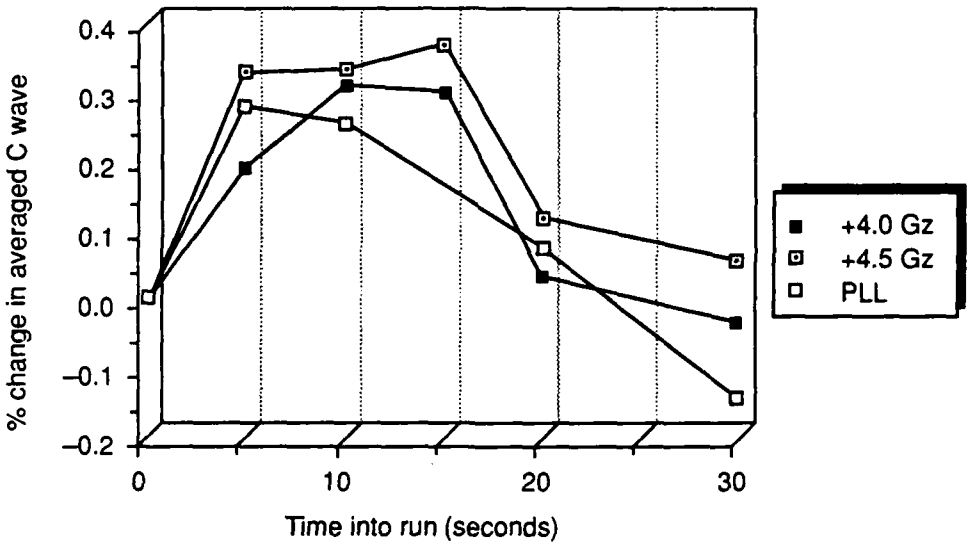

Figure 55. Percentage change in C wave amplitude from prestress level to point in which +Gz load approaches PLL level (average of four subjects). +Gz plateau from 0 to 15 seconds and recovery period from 15 to 30 seconds.

Table 19. Two tailed paired t tests to determine the significance of the difference in rheographic indices between G15 and PLLeor levels. dof = degrees of freedom.

Index	t	dof	Significance
A wave	–2.489	4	0.068
B wave	–1.729	4	0.159
C wave	–2.165	4	0.096
B/A	–1.118	4	0.326
C/A	–0.915	4	0.412
α/T	–1.211	4	0.293

OUTLINE FOR PROPOSED MODELING OF RHEOENCEPHALOGRAPHY, INCLUDING THE EFFECTS OF THE CEREBROSPINAL FLUID SYSTEM, UNDER ACCELERATION STRESS

CLASSICAL MODELING OF REG WAVEFORM: $\rho = L/A$

As mentioned in the section entitled "Rheoencephalography (REG), EIP measurements are classically interpreted from the definition of resistivity,

$$\rho = \frac{E}{J} = \frac{\frac{V}{L}}{\frac{I}{A}} = \frac{RA}{L} \quad \text{or} \quad R = \frac{\rho L}{A} \tag{47}$$

where ρ is the resistivity of the material (Ω-cm), E is electric field (volts (v)/cm), J is current density (current (I) amps/cm^2), L is the distance between the electrodes (cm), and A is cross sectional area (cm^2). Resistance is then related to volume changes (ml) as per Equation 5 assuming that L remains constant while volume varies. Since this is the traditional first approach, an attempt was made to apply this basic formula to REG analysis. The assumptions outlined in the section entitled "Background" (page 00) apply here along with the following constraints. We assume that the head is a perfect sphere with homogenous contents with a volume, V, given by

$$V = \frac{\pi D^3}{6} = \left(\frac{2D}{3}\right)\left(\frac{\pi D^2}{4}\right) = \frac{2}{3}(AD) \tag{48}$$

where D is the diameter of the sphere and cross sectional area is given by $A = \pi r^2 = \pi D^2/4$, (r = sphere radius, cm). Within this sphere are two spheres of identical volume which occupy the same physical space. These spheres represent the blood and the CSF. Further, overall volume is held constant, *i.e.* blood inflow is offset by a CSF shift towards the spine. It is assumed that all volumes change equally and at the same rate. Contributions of the extracranial circulation are simply lumped together with the overall blood volume since it occupies a relatively small cross sectional area as compared with the head as a sphere. (If one considers the skin covering the head as a spherical shell with an average diameter of 0.5 cm, the volume of the skin would be 306 cm^3 for a 20 cm diameter head. The corresponding volume of a spherical head is 4189 cm^3. Therefore, neglecting this term would lead to an error of only 7%). Also, all impedance changes due to membrane interfaces, which can be considerable, are assumed to be negligible. Finally, it is assumed that the reactance of the head and its contents at 100 kHz excitation frequency is also negligible and that only resistance changes are determined.

It is assumed that the head contains a homogenous mixture of components consisting of blood, CSF, bone, neural tissue, and skin. The volume of these individual components can vary only over a limited range in order to maintain an approximately constant total volume. The head can be modeled by a combination of resistances as seen in Figure 56, where Rt represents the combined resistance of the bone, skin, and neural tissues; Rs represents the resistance of the small part of the skull between the electrode and the interior of the sphere; Rb refers to the resistance of the blood; and Rc represents the resistance due to CSF. The resistivities of *in vivo* bone, skin, and neural tissue can be combined

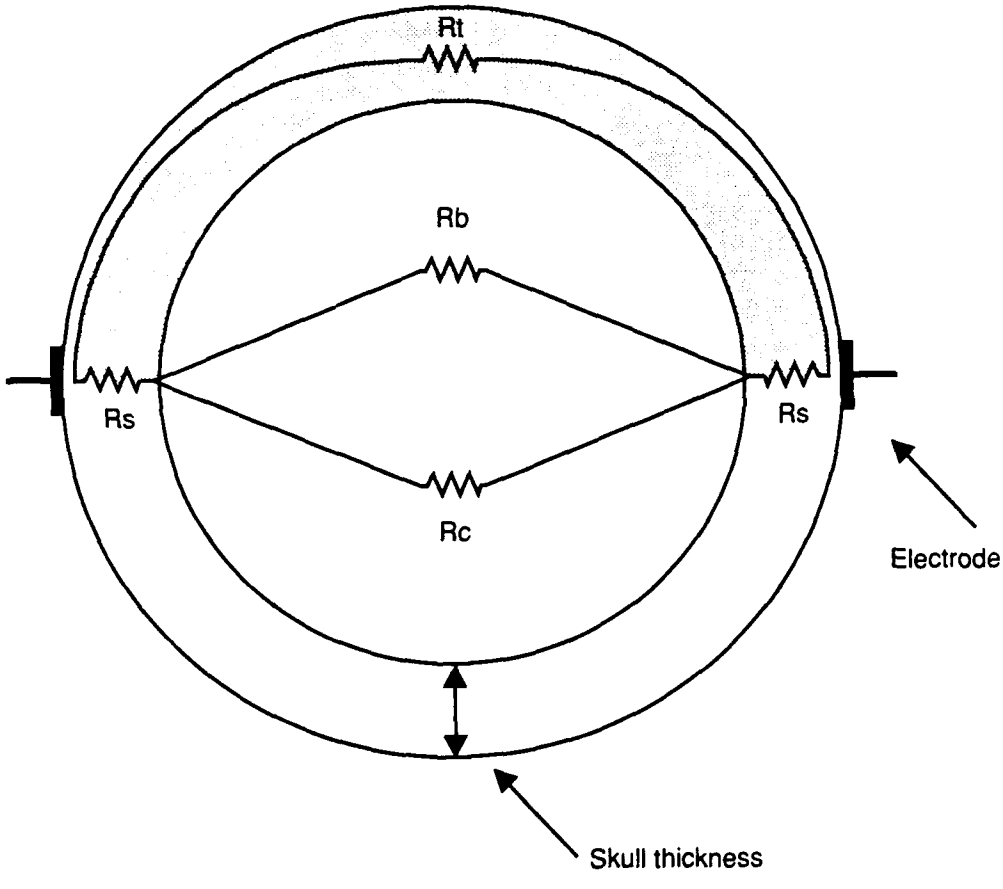

Figure 56. The head as represented by parallel resistances. Rt: combined resistance of bone, skin,and neural tissues; Rs: resitance of bone between electrode and interior of skull; Rb: resistance due to the blood; Rc: resistance due to CSF.

since they are all in the range of 200–300 Ω-cm. For a 5-cm radius circular electrode (cross sectional area = 78.5 cm^2) and an average skull thickness of 0.4 cm (as measured on an excised adult skull), Rs = 1.5 Ω as calculated using Equation 47 with ρ = 300 Ω-cm and L = 0.4 cm. The total contribution to the overall resistance of the small bone sections is 3 Ω (2Rs). When compared to the overall range of base resistance of the human skull (80–1000Ω (57)), this amounts to a maximum contribution of 3.8%. Therefore, one can neglect the resistance due to the short straight current path through the bone, Rs, when compared to Rt. For modeling purposes, it is assumed that current flows through three parallel resistance paths: Rt || Rb || Rc. Therefore, the overall resistance, Ro, is given by

$$\frac{1}{Ro} = \frac{1}{Rt} + \frac{1}{Rb} + \frac{1}{Rc} \tag{49}$$

To calculate the change in pulsatile resistance with systole, the overall resistance changes by a small amount (ΔR), Rb changes to Rb′ and Rc changes to Rc′. So the net overall resistance is now

$$\frac{1}{(Ro + \Delta R)} = \frac{1}{Rt} + \frac{1}{Rb'} + \frac{1}{Rc'} \tag{50}$$

Solving Equation 49 for Rt gives

$$\frac{1}{Rt} = \frac{1}{Ro} - \frac{1}{Rb} - \frac{1}{Rc} \tag{51}$$

Substituting Equation 51 into Equation 50 leads to

$$\frac{1}{(Ro + \Delta R)} = \frac{1}{Ro} - \frac{1}{Rb} - \frac{1}{Rc} + \frac{1}{Rb'} + \frac{1}{Rc'} \tag{52}$$

Equation 52 can be rearranged as

$$\frac{-\Delta R}{Ro(Ro + \Delta R)} = \frac{1}{Rb'} - \frac{1}{Rb} + \frac{1}{Rc'} - \frac{1}{Rc} \tag{53}$$

Since ΔR << Ro, Equation 53 simplifies to

$$\frac{-\Delta R}{Ro^2} = \frac{1}{Rb'} - \frac{1}{Rb} + \frac{1}{Rc'} - \frac{1}{Rc} \tag{54}$$

If the electrodes are placed on either end of the sphere at the equator, L in Equation 47 becomes D. By substituting the expression for volume, Equation 48, into Equation 47 gives Equation 55, which expresses resistance in terms of spherical volume.

$$R = \frac{\rho D}{A} = \left[\frac{\rho D}{A}\right]\left[\frac{\frac{2D}{3}}{\frac{2D}{3}}\right] = \frac{\left[\frac{\rho 2D^2}{3}\right]}{V} = \frac{\rho 2D^2}{3V} \tag{55}$$

Defining Rb and Rc in terms of Equation 55 gives

$$R_{b'} = \frac{\rho_b 2D^2}{3V_{b'}} \tag{56}$$

$$Rb = \frac{\rho_b 2D^2}{3Vb} \tag{57}$$

$$R_{c'} = \frac{\rho_c 2D^2}{3V_{c'}} \tag{58}$$

$$Rc = \frac{\rho_c 2D^2}{3Vc} \tag{59}$$

where Vb′ is the new blood volume, Vb′ = Vb + ΔVb, (diastolic volume + systolic pulse volume), Vc′ is the new CSF volume, ρ_b is the resistivity of blood (150 Ω-cm) and ρ_c is the resistivity of CSF (60 Ω-cm). Equation 54 can then be expressed as

$$\frac{-\Delta R}{R_0^2} = \frac{3V_{b'}}{\rho_b 2D^2} - \frac{3Vb}{\rho_b 2D^2} + \frac{3V_{c'}}{\rho_c 2D^2} - \frac{3Vc}{\rho_c 2D^2} \tag{60}$$

Or,

$$\frac{-2D^2\Delta R}{3R_0^2} = \frac{V_{b'}}{\rho_b} - \frac{Vb}{\rho_b} + \frac{V_{c'}}{\rho_c} - \frac{Vc}{\rho_c} \tag{61}$$

Substituting ΔVb = Vb′ – Vb and ΔVc = Vc′ – Vc gives

$$\frac{-2D^2\Delta R}{3R_0^2} = \frac{\Delta Vb}{\rho_b} + \frac{\Delta Vc}{\rho_c} \tag{62}$$

If we assume that blood and CSF travel in opposite directions during systole, Equation 62 becomes

$$\frac{-2D^2\Delta R}{3R_0^2} = \frac{\Delta Vb}{\rho_b} - \frac{\Delta Vc}{\rho_c} \tag{63}$$

Placing the right side of Equation 63 under a common denominator and multiplying on both sides gives

$$\frac{-2\rho_b\rho_c D^2\Delta R}{3R_0^2} = \rho_c\Delta Vb - \rho_b\Delta V \tag{64}$$

Recall that the overall volume of the head is held constant so that $\Delta Vb = \Delta Vc = \Delta V$. Or,

$$\frac{-2\rho_b\rho_c D^2\Delta R}{3R_0^2} = (\rho_c - \rho_b)\Delta V \tag{65}$$

Using this assumption, Equation 66 is the expression relating ΔR to ΔV.

$$\Delta V = \frac{-2\rho_b\rho_c D^2\Delta R}{3(\rho_c - \rho_b)R_0^2} \tag{66}$$

The values of Ro and D are critical for accurate calculation of volumes. Unfortunately these measurements were not performed during experiment CE3. However, using 12 ml for systolic pulse volume, as reported by Moskalenko,[57] and solving Equation 66 for ΔR values as measured at 1g for subjects P5, P7, P8, and S11, estimates of Ro were made. Acceleration induced volume changes were calculated using the averaged magnitude of A wavelets taken during the plateau of various RORs as a measure of ΔR. (See Appendix H for these values). D was arbitrarily set at 20 cm based on anthropometry data compiled from military male aviators.[87] In interpreting these values recall that in the classical analysis these changes in resistance, and hence volume, refer to changes in inflow or outflow of the body segment of a single conducting medium. Usually in these analyses, either inflow or outflow is occluded prior to taking measurements. This occlusion was not performed on these subjects. These values are listed in Table 20 a–d for these four subjects during relaxed acceleration exposures ranging from +2.5 to +5.5 Gz.

Table 20a. Change in volume (ml) with increasing acceleration level as predicted by Equation 66 for subject P5. R_{ocalc} for Run1: 12.74 Ω; R_{ocalc} for Run2: 12.20 Ω.

+Gz:	1.0	2.5	3.0	3.5	4.0	4.5	5.0
Run 1:							
$\Delta R_{ave}(\Omega)$:	0.073	0.108	0.112	0.124	0.118	0.140	0.139
ΔV_{calc}(ml):	12.0	17.74	18.4	20.37	19.39	23.0	22.84
Run2:							
$\Delta R_{ave}(\Omega)$:	0.067	0.102	0.094	0.108	0.106	0.118	0.141
ΔV_{calc}(ml):	12.0	21.5	16.84	19.35	18.99	21.14	25.26

Table 20b. Change in volume (ml) with increasing acceleration level as predicted by Equation 66 for subject P7. R_{ocalc} for Run1: 28.44 Ω; R_{ocalc} for Run2: 27.93 Ω.

+Gz:	1.0	2.5	3.0	3.5	4.0	4.5	5.0
Run 1:							
$\Delta R_{ave}(\Omega)$:	0.364	0.424	0.531	0.545	0.526	0.548	0.545
ΔV_{calc}(ml):	12.0	13.98	17.51	17.97	17.34	18.07	17.97
Run2:							
$\Delta R_{ave}(\Omega)$:	0.351			0.456	0.399		
ΔV_{calc}(ml):	12.0			15.60	13.65		

Table 20c. Change in volume (ml) with increasing acceleration level as predicted by Equation 66 for subject P8. R_{ocalc} for Run1: 21.13 Ω; R_{ocalc} for Run2: 21.76 Ω.

+Gz:	1.0	2.5	3.0	3.5	4.0	4.5	5.0	5.5
Run 1:								
$\Delta R_{ave}(\Omega)$:	0.201	0.227	0.222	0.240	0.244	0.264	0.252	0.289
ΔV_{calc}(ml):	12.0	13.56	13.26	14.33	14.57	15.77	15.05	17.26
Run2:								
$\Delta R_{ave}(\Omega)$:	0.213		0.275	0.257	0.280	0.268	0.267	
ΔV_{calc}(ml):	12.0		15.49	14.47	15.77	15.09	15.04	

Table 20d. Change in volume (ml) with increasing acceleration level as predicted by Equation 66 for subject S11. $R_{o_{calc}}$ for Run1: 17.06 Ω; $R_{o_{calc}}$ for Run2: 14.22 Ω.

+Gz:	1.0	2.5	3.0	3.5	4.0	4.5	5.0	5.5
Run 1:								
$\Delta R_{ave}(\Omega)$:	0.131	0.176	0.196	0.182	0.183	0.198	0.194	0.200
ΔV_{calc}(ml):	12.0	16.13	17.96	16.68	16.77	18.14	17.78	18.32
Run2:								
$\Delta R_{ave}(\Omega)$:	0.091		0.127	0.117	0.126	0.151	0.148	
ΔV_{calc}(ml):	12.0		16.75	15.43	16.62	19.91	19.52	

A plot of calculated ΔR versus ΔV, based on Equation 66, was constructed using D = 20 cm and Ro = 19.44 Ω (the average of the four subjects over eight exposures). This is shown in Figure 57. The "goodness of fit" of the experimental ΔR as compared to the estimated values shown in Figure 57 depends to a large extent upon the value of Ro and therefore the accuracy of the original assumption that an average systolic pulse contains 12 ml of blood.

It is somewhat difficult to classically interpret these changes in pulsatile blood volume under conditions of high acceleration stress. A comparison of the calculated volume changes with respect to 1 g levels (*i.e.* 12 ml), to the averaged change in volume at highest +Gz level attained for each subject is shown in Table 21. These values represent a percentage change in pulsatile volume ranging from 32% (subject P7) to 100% (subject P5). Since blood outflow or inflow out of the segment was not completely stopped, one cannot interpret these percentages to represent total pulsatile volume change in either direction. In the conditions of these trials, these high percentages are misleading when one considers that the hydrostatic column theory refers to a bulk shift of blood out of the head and does not specifically consider pulsatile volume changes. One might expect that the pulsatile volume would not change as much as the overall volume since the CV system attempts to maintain cardiac output by increasing aortic pressure to offset the reduced blood flow.[19] Gillies[19,page596] speculates that at +3 to +4 Gz, the heart may have reached its capacity to increase its work load to counter the stress. Note that there were no cardiac abnormalities, except for the expected tachycardia seen at high acceleration levels, apparent in the ECG recordings of these four subjects.

Clearly, the classical approach is inadequate to describe pulsatile REG changes under acceleration stress. However, can this method be used to determine changes in bulk movement of blood under these conditions?

Following similar reasoning as above, Equation 49 was solved for a change in baseline rather than pulsatile resistance under elevated acceleration stress.

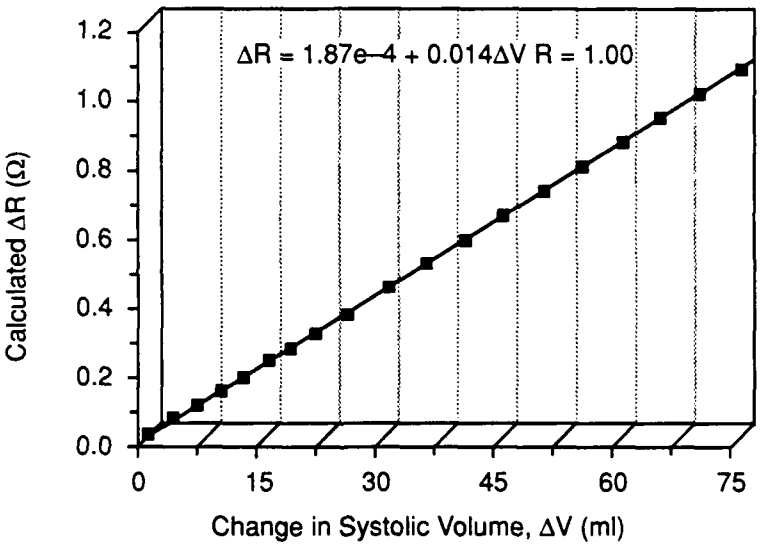

Figure 57. Pulsatile ΔR as Determined From Equation 66.

Table 21. Average and percentage change in calculated pulsatile blood volume from 1 g to peak +Gz (Gz_{pk}) for four subjects during RORs.

Subj.	Peak + Gz (Gz_{pk})	Average Volume Change at Gz_{pk}	Percent Change
P5	5.0	12.05 ml	100
P7	5.0	3.81 ml	32
P8	5.5	4.15 ml	35
S11	5.5	6.92 ml	58

To calculate the change in baseline resistance under increased acceleration level, the overall resistance changes to Ro′, Rb changes to Rb′ and Rc changes to Rc′. So the net overall resistance is now

$$\frac{1}{R_{o'}} = \frac{1}{Rt} + \frac{1}{R_{b'}} + \frac{1}{R_{c'}} \tag{67}$$

Substituting Equation 51 into Equation 67 leads to

$$\frac{1}{R_{o'}} = \frac{1}{R_o} - \frac{1}{Rb} - \frac{1}{Rc} + \frac{1}{R_{b'}} + \frac{1}{R_{c'}} \tag{68}$$

Equation 68 can be rearranged as

$$\frac{1}{R_{o'}} - \frac{1}{R_o} = \frac{1}{R_{b'}} - \frac{1}{Rb} + \frac{1}{R_{c'}} - \frac{1}{Rc} \tag{69}$$

Or,

$$\frac{R_o - R_{o'}}{R_{o'} R_o} = \frac{1}{R_{b'}} - \frac{1}{Rb} + \frac{1}{R_{c'}} - \frac{1}{Rc} \tag{70}$$

Or,

$$\frac{R_o - R_{o'}}{R_{o'}} = R_o\left[\frac{1}{R_{b'}} - \frac{1}{Rb} + \frac{1}{R_{c'}} - \frac{1}{Rc}\right] \tag{71}$$

Or,

$$\frac{Ro}{Ro' - 1} = Ro\left[\frac{1}{Rb'} - \frac{1}{Rb} + \frac{1}{Rc'} - \frac{1}{Rc}\right] \tag{72}$$

Rearranging Equation 72 to isolate Ro′ leads to

$$\frac{Ro' = Ro}{\left[1 + Ro\left(\frac{1}{Rb'} - \frac{1}{Rb} + \frac{1}{Rc'} - \frac{1}{Rc}\right)\right]} \tag{73}$$

Substituting Equations 56–59 for Rb′, Rb, Rc′, Rc, respectively, leads to

$$Ro' = \frac{Ro}{1 + Ro\left(\frac{3Vb'}{\rho_b 2D^2} - \frac{3Vb}{\rho_b 2D^2} + \frac{3Vc'}{\rho_c 2D^2} - \frac{3Vc}{\rho_c 2D^2}\right)} \tag{74}$$

Factoring out the common terms gives

$$Ro' = \frac{Ro}{1 + \left(\frac{3Ro}{2D^2}\right)\left(\frac{Vb'}{\rho_{b'}} - \frac{Vb}{\rho_b} + \frac{Vc'}{\rho_c} - \frac{3Vc}{\rho_c}\right)} \tag{75}$$

Substituting ΔVb and ΔVc as in Equation 62 gives

$$Ro' = \frac{Ro}{1 + \left(\frac{3Ro}{2D^2}\right)\left(\frac{\Delta Vb}{\rho_b} + \frac{\Delta Vc}{\rho_c}\right)} \tag{76}$$

If we assume that blood and CSF travel in opposite compensatory directions to maintain constant volume, Equation 76 becomes

$$Ro' = \frac{Ro}{1 + \left(\frac{3Ro}{2D^2}\right)\left(\frac{\Delta Vb}{\rho_b} - \frac{\Delta Vc}{\rho_c}\right)} \tag{77}$$

Placing the volume terms in Equation 77 under a common denominator leads to

$$R_{o'} = \frac{R_o}{1+\left(\frac{3R_o}{2D^2}\right)\left(\frac{\rho_c \Delta Vb - \rho_b \Delta Vc}{\rho_b \rho_c}\right)} \tag{78}$$

Recall that the overall volume of the head is held constant so that $\Delta Vb = \Delta Vc = \Delta V$. Using this assumption and rearranging Equation 78 leads to an expression for the change in overall resistance with increasing acceleration:

$$R_{o'} = \frac{R_o}{\left[1+\left(\frac{3R_o \Delta V(\rho_c - \rho_b)}{2D^2 \rho_b \rho_c}\right)\right]} \tag{79}$$

Solving Equation 79 for ΔV leads to an expression for acceleration induced change in cephalic volume:

$$\Delta V = \left[\frac{R_o}{R_{o'}} - 1\right]\left[\frac{2D^2 \rho_b \rho_c}{3R_o(\rho_c - \rho_b)}\right] \tag{80}$$

As in the above treatment, estimates of Ro were made for subjects P5, P8, S5, and S8. Acceleration induced volume changes were calculated using the value of Zb midway during the ROR plateau (during 5–10 seconds at plateau). (See Appendix F for these values). Ro′ was determined by adding the change in resistance from the unstressed levels to the calculated Ro. As above, D was arbitrarily set at 20 cm based on anthropometry data compiled from military male aviators.[87] These values are listed in Table 22 a–d for these four subjects during relaxed acceleration exposures ranging from +2.5 to +6.5 Gz. These calculated values appear to be too large, particularly for subject P5. Unfortunately, quantitative measurements of acceleration induced cephalic bulk blood volume shifts have not been previously published with which to compare these figures. When interpreting these values, recall that blackout was not seen. Therefore, blood pressure was theoretically greater than 20–25 mmHg at eye level.[19] Also, recall that inflow was not arrested and that these resistance measures may be not solely represent the change from the instantaneous blood volume of 75 ml at 1 g. To do that, one would have to assume (incorrectly) that the head was a closed 75 ml sphere with only a single opening at its bottom.

It appears quite clear that the classic approach for constructing a model to relate resistance to volume changes contains far too many assumptions to adequately describe the experimental data.

Table 22a. Change in volume (ml) with increasing acceleration level as predicted by Equation 80 for subject P5. R_o' for Run1: 12.74 Ω; R_o' for Run2: 12.20 Ω.

+Gz:	2.5	3.0	3.5	4.0	4.5	5.0
Run 1:						
$\Delta R_o'$ (Ω):	14.74		15.84	16.49		
ΔV_{calc} (ml):	284		410	476		
Run2:						
$\Delta R_o'$ (Ω):	13.9		14.7	15.4	16.3	16.6
ΔV_{calc} (ml):	267		372	454	550	579

Table 22b. Change in volume (ml) with increasing acceleration level as predicted by Equation 80 for subject P8. R_o' for Run1: 21.13 Ω; R_o' for Run2: 21.76 Ω; R_o' for Run 3: 21.45 Ω.

+Gz	2.5	3.0	3.5	4.0	4.5	5.0	5.5	6.0
Run 1:								
$\Delta R_o'$ (Ω):	21.63	21.88	23.13	23.38	22.38	22.63	23.38	
ΔV_{calc} (ml):	29.2	43.3	109	121	70.5	83.7	121	
Run2:								
$\Delta R_o'$ (Ω):		22.51	23.26	24.76	23.51	23.51		
ΔV_{calc} (ml):		40.8	79	148	91	91		
Run3:								
$\Delta R_o'$ (Ω):	22.19	22.70	23.70	24.08		23.95	25.70	24.83
ΔV_{calc} (ml):	41.5	68.5	118	136		130	206	169

Table 22c. Change in volume (ml) with increasing acceleration level as predicted by Equation 80 for subject S5. R_o' = 16.67 Ω.

+Gz:	2.5	3.0	3.5	4.0	4.5
$\Delta R_o'$ (Ω):	17.87	17.67	16.92	17.67	17.92
ΔV_{calc} (ml):	107	91	23.6	91	112

Table 22d. Change in volume (ml) with increasing acceleration level as predicted by Equation 80 for subject S8. R_o' for Run1 and Run 2: 19.32 Ω.

+Gz:	3.0	3.5	4.0	4.5	5.0	5.5	6.0	6.5
Run 1:								
$\Delta R_o'$ (Ω):	19.92	19.32		20.52	20.12	19.92	20.12	20.52
ΔV_{calc} (ml):	41.6	0		80.7	54.9	41.6	54.9	80.7
Run2:								
$\Delta R_o'$ (Ω):			20.92	20.82			20.92	
ΔV_{calc} (ml):			106	99			106	

Experimental Evidence For The Hydrostatic Column Theory

Much of the work in the field of acceleration physiology refers to the response of the body to the hydrostatic effects of the difference in blood pressure between the heart and at eye level in order to interpret the visual symptoms that accompany acceleration stress. In order to confirm this, the eye-heart distance (EHD), in millimeters, and arterial blood pressure (at the arm) were recorded for six subjects during experiment CE3. The drop in blood pressure from the heart to the base of the brain was determined according to Equation 81.

$$Pressure_{eyelevel} = \frac{(EHD)(d_{blood})}{d_{Hg}} \qquad (81)$$

d_{blood} is the density of blood (1.055 gm/cm^3) and d_{Hg} is the density of mercury (13.6 gm/cm^3). Values for these subjects are listed in Table 23. Considering that 60° PLL theoretically appears when blood pressure at the eye level drops below 20 mmHg, this simple relation is a quite good approximation within ±0.5 Gz for these individuals.

Table 23. Predicted drop in eye-level blood pressure according to Equation 81. EHD = eye-heart distance (cm), PHS = hydrostatic pressure drop from heart to eye level (mmHg), Psys = mean systolic blood pressure (mmHg), Pei = eye-level pressure at i^{th} acceleration level (+1 Gz ≤ i ≤ +6 Gz) (mmHg), PLL = level of +Gz in which 60° light loss occurred.

Subj.	EHD	PHS	Psys	Pe1	Pe2	Pe3	Pe4	Pe5	Pe6	PLL
P5	25	19.4	117	97.6	78.2	58.8	39.4	20	0.6	5.0
P7	27	20.9	123	102.1	81.2	60.3	39.4	18.5	−2.4	5.0
P8	27	20.9	120	99.1	78.2	57.3	36.4	15.5	−5.4	5.0
S5	28	21.7	132	110.3	88.6	66.9	45.2	23.5	1.8	5.5
S8	26	20.2	123	102.8	82.6	62.4	42.2	22.0	1.8	6.5
S11	28.5	22.1	130	107.9	85.8	63.7	41.6	19.5	−2.6	5.0

CONSIDERATIONS FOR MODELING OF REG WAVEFORM UNDER +GZ ACCELERATION

A mathematical description of the REG under acceleration stress must take into account many variables. The nature of the waveform changes in many facets under acceleration stress and these changes are augmented as the stress increases. One must account for the shifts of both blood AND cerebrospinal fluid within and in and out of the head to completely characterize cerebral fluid flow. It has been theorized that CSF pressure supports the cephalic venous circulation and allows subjects to withstand high +Gz forces that otherwise would clamp off circulation at a low level of acceleration. Another major component that must be addressed is the changes in HR which accompany acceleration stress. Several of the REG timing indices that have been discussed in the Results section depend upon the HR: the ΔZ period, T, the rheographic time, α/T, and the delta delay, ΔD.

Since this system is so complex, the available published cerebral circulation models either cannot explain the effects of acceleration stress or they neglect to include the CSF system. In our studies, we have described an impedance method to conveniently and noninvasively investigate changes in cephalic fluid volume under such a stress. These measures have been related to estimates of the state of the CVR. A description of determinants of CVR and CSF system status must by definition include the following variables: blood pressure, perfusion pressure, vascular compliance, and CSF compliance. All of these factors are, in turn, related to vascular and CSF volume changes. These components are all reflected in pulsatile pressure and blood waveforms. Moskalenko *et al*[57,page83] have shown, using REG, that pulsatile fluctuations in pressure are reflected by similar changes in pulsatile volume changes. Van Eijndhoven and Avezaat[79] point out that measures of CSF pulse pressure (CSFPP) can be used as an indication of intracranial elastance. Further, CSFPP depends upon the magnitude of the pulsatile variation in cerebral blood volume. Therefore, the first step in the development of our model will include a mathematical description of ΔZ under normal conditions and under acceleration stress. This waveform also contains a CSF volume component and this will be determined with the use of animal experimentation. Once this portion of the model is complete, the next refinement will include descriptions of the cerebral vascular tree and cranial and spinal CSF systems. Insight into the development of the second stage of the model will be aided by use of rheoencephalography; in particular, how bulk shifts of blood under acceleration stress are reflected in the changes in the Zb waveform. The use of REG in conjunction with other modalities, such as oxygen tension measurements and manipulations of the cerebral vasculature and CSF system with functional testing, will provide information which may aid in the description of the metabolic changes that occur under acceleration stress.

With the data currently obtained, we can begin the development of our REG model with a mathematical description of the waveform at 1 g. The waveform is quite variable between individuals in that the various indices are more or less defined. The overall shape of the waveform can be fit to a multi-order polynomial, as seen in Equation 46. This particular approach needs to be performed with better data resolution (this equation was derived from a strip chart record made at 25 mm/sec for a resolution of 25 Hz). Once unstressed data is processed, similar data sets for at least four individual subjects at each acceleration level recorded (+2.5 to +4.5 Gz) in a relaxed posture must be calculated. Runs in which a peripheral light loss of greater than 60° occurred and/or straining was performed also need to be characterized.

Since there is such a great variability between individuals, it probably is necessary to correct the curves for the changes in rheographic indices, as described in the Results section above. A progressive change in the A, B, and C wavelets as well as changes in heart rate and rheographic time should be included. The latter is an important variable in that it includes HR as well as the slope of the rising part of the REG curve. An indication of the change in the delta delay should also be factored in so that

the timing of changes in cephalic fluid flows are kept in agreement with ECG temporal patterns. Changes in the indices while riding at a +Gz plateau should also be considered, particularly since there was an indication that some factors (B and C wavelets) did change while at plateau. More data needs to be collected to better quantify these changes.

All of the above is possible to accomplish and only requires the availability of computer time to construct better calculation and detection algorithms to perform the data manipulations. To date, this has been somewhat of a problem, but not an insurmountable one.

A number of 1 g tests can be performed to aid in the characterization of the REG waveform. These include orthostatic tests, such as those employing the use of a tilt table. Functional tests can be performed including inhalation of 5–7% CO_2 and air for 5–10 min to promote vasodilation. Hyperventilation for 3–5 minutes can elevate vascular tone by decreasing $PaCO_2$ in the blood.

CEREBROSPINAL FLUID SYSTEM

The part of the model related to cephalic blood volume changes is only part of the story. As Jenkner pointed out in 1968,[36] a major component of ΔZ is CSF volume due to its higher level of conductivity. As blood enters the skull, to make room for it, there must be a shift in CSF and/or venous blood volume. He goes on to claim that, "... changes in CSF volume multiply the impedance changes of the blood and present them in an integrated somewhat delayed fashion. Thus redistribution of volume is apparently dependent on the pulse wave volume and ... changes in the elasticity (or rigidity) of vessel walls, patency (or obstruction) of lumen and changes in peripheral vascular resistance."[36,page129]

The model will also include the following physical characteristics. The brain is housed in an "unexpandable enclosed" space undergoing volume and pressure changes. Quotes have been placed about the words "unexpandable enclosed" because the brain does in fact expand slightly with volume shifts, contrary to the Munro-Kellie hypothesis. (This hypothesis states that under normal conditions the total volume of brain mass, blood, and CSF is a constant). The cephalic circulation and its support system, *i.e.* the CSF compartment, is in intimate contact with the spinal spaces. On the other hand, we must be sure that the laws of conservation of matter and energy prevail. The total amount of CSF and blood in the body are relatively constant. Under normal conditions CSF is continually being formed and absorbed. In abnormal conditions, bulk shifts of blood in and out of the head may also be accompanied by shifts of CSF. It has yet to be determined how the CSF moves, in terms of direction and rate of flow, under high +Gz load. Under periods of acceleration stress as described in this thesis, there probably is not enough time for a formation/reabsorption cycle to occur. There is, however, evidence that the CSF pressures change in concert with venous pressures under acceleration.[66] One might assume that CSF volume must change in some as yet undetermined fashion. Another factor which influences CSFP is respiration. During inspiration, CSFP falls and CSFP rises during expiration.[57] This factor is of considerable interest, though its magnitude is as yet unknown, during the performance of an AGSM. For conservation of energy, one must take into account the resistance of the cephalic bed and the elasticity of the vascular and support tissues. Of particular importance is the state of the pial and intracerebral vessels. These are the most resistive of the cerebral circulation and they exert the most control in maintaining the regulation of the cerebral blood flow.

Marmarou developed an electrical analog model of the CSF system[48] in which the interrelationships between the static and dynamic processes of formation, storage, and absorption were described. This description can form a starting point for determining whether or not there is time under short periods of acceleration stress for these processes to affect the cephalic response to that stress

or whether it is merely a dynamic redistribution of fluid.

The compliance coefficient (C), the ratio of a change in volume (ΔV) to a corresponding change in pressure, (ΔP) is a measure of the distensibility of the CSF space. Knowledge of this factor is important because when changes in volume in the cranial space (blood, brain, or CSF) occur, the compensatory change in CSFP required to return the compartments to their original dimensions will be given by the compliance coefficient. Marmarou *et al*[49] defined the pressure-volume index (PVI) as the slope of the linear volume-log pressure plot. Using this transformation, compliance can be related to CSFP by

$$C = \frac{0.4343\ PVI}{CSFP}. \tag{82}$$

Note that a high PVI is associated with a high level of compliance. In one study (70), PVI was measured in adults and was estimated at 25.9 ± 3.7 ml. Compliance and absorption (change in volume per unit time) are intimately related and govern the dynamics of the intracranial pressure (ICP). The CSF outflow resistance (Ro) can also be determined from the CSFP. Ro is equal to the effective perfusion pressure (CSFP — venous exit pressure) divided by the rate of outflow (CSF formation rate). (There is some evidence that the venous exit pressure equals the absolute magnitude of the sagittal sinus pressure). Resistance is expressed in mmHg/ml/min. The authors claim that CSF compliance and blood vessel compliance are directly related. Also, CSF compliance can be divided into cranial (comprising 68%) and spinal (32%) components. Further, most of the absorption (84%) occurs within the cerebral compartment.

A description of proposed animal studies using a rabbit model to invasively manipulate the CSF system in order to characterize it and its effects on the REG waveform is presented in the Recommendations for the Future section of this report.

SECOND GENERATION MODEL

In accordance with the hydrostatic column theory of physiologic response to acceleration stress, we must incorporate into the model the onset of cardiovascular compensation that occurs on average after ten seconds of high +Gz exposure. This assumes that the individual has not lost consciousness due to high onset rates and acceleration levels. Under rapidly applied acceleration stress (*e.g.* +2 Gz/second), the oxygen reserve will been exhausted after an average of seven seconds. To further outline the criticality of timing relationships, note that Dewey, *et al*[11] claim that cerebral vasomotor responses require approximately fifteen seconds to occur and that changing pressures during this time do not permit autoregulatory responses. These figures come from experiments performed at normal acceleration levels.

Dewey also states that as vascular pressure falls, it can reach a "critical closing pressure (CCP)." Once this level is attained (43 mm Hg in normotensive man, with a range of 10–95 mm Hg) pre-resistance vessels (*e.g.* pre-capillary arterioles) may even exhibit retrograde flow. After this collapse, tone is reduced and the vessels open at a lower pressure than they close. This pressure is determined by the vasomotor tone and the ICP. Cerebral perfusion pressure, according to Dewey, is more accurately determined by the difference between mean arterial pressure (MAP) and CCP rather than the more commonly used MAP–ICP. The latter difference is only accurate when there is no vasomotor tone. In this analysis, cerebral perfusion pressure, not vascular bed resistance, is the primary variable affecting cerebral blood flow.

Therefore, the second generation model must take into account the CSF system, acceleration level, rate of onset, availability of oxygen, and onset and extent of autoregulatory processes. Availability of oxygen can be linked to the volume of blood within the brain and the hemoglobin concentration therein. Autoregulation is also related to metabolic factors, such as $PaCO_2$, PaO_2 and pH as well as physical characteristics, such as cephalic vascular resistance, perfusion pressure, vasomotor tone, and compliance.

Other factors of importance include knowledge of the resistivity of the various components comprising the head. These are found in Table 24. Biophysical data, including flows and volumes, is presented in Table 25.

Table 24. Resistivity of various human anatomical components (from (16)).

Human Substance	Resistivity (Ω-cm)	Measurement Frequency
CSF	64.6	1–30 kHz
Blood	154	120 kHz
Skeletal muscle	110–675	1 MHz–0.1–1 kHz
Fat	1100–5000	>200 MHz
Bone	1800	1 MHz
Skin	289	1 MHz
Head	840	dc
Scalp	230	dc
Neck	280	dc

Table 25. Physical constants of interest in cerebral circulation modeling (from 76). * value taken from (86), ** value taken from (57) *** values taken from (70).

Factor	Value
Volume of brain tissue	1500 gm
Volume of blood in brain	75 ml
Volume of CSF	75 ml
Cerebral Blood Flow (CBF) Rate	750 ml/min or 54 ml/100 gm/min*
Cerebral metabolic consumption rate for O_2	3 ml/100 gm/min
Volume of blood entering brain with each systole	12–15 ml**
MBP at entrance to cerebral arterial bed	100 mmHg
MBP at entrance to cerebral arteriolar bed	85 mmHg
MBP at entrance to cerebral venous bed	10 mmHg
MBP exiting the cerebral venous bed	2 mmHg
Compliance of the arterial bed	0.04 ml/mmHg
Compliance of the venous bed	1.1 ml/mmHg
Compliance of the arteriolar bed	0.04 ml/mmHg
Active CSF production rate	0.36 ml/min***
Resistance to absorption of CSF	2.8 mmHg/ml/min***

Along with the variables and concerns denoted above, the following is a summary of the anatomical and physiological variables that should be included in a complete description of the cerebral circulation: 1) blood pressure in the arteries at the base of the skull, in the jugular veins, and the veins of the spinal canal; 2) the total hydraulic resistance, which is determined by the difference between pressure in the arteries at the base of the skull and pressure in the pial veins; 3) the volume of blood in the cerebral arteries and veins and in the veins of the spinal canal; 4) the total volume of the brain tissue; and 5) the fluid volume within the CSF compartment of the skull and spinal canal. The vessels of the head can be divided into five groups: 1) large cerebral arteries, characterized by low resistance and large blood pulsatile pressure variations (*e.g.* the carotids and vertebrals and their branches off of the circle of Willis); 2) small arteries and arterioles which comprise the major source of vascular resistance; 3) the tissues that effect metabolic exchanges between blood and tissues (*e.g.* capillaries); 4) the terminal cerebral veins (*e.g.* pial veins); and 5) the large collecting veins at the base of the brain. Geometric values, approximate number of vessels, and estimates of elastance are available (86, human) and (57, canine).

A number of the variables may not change under acceleration stress which may simplify the model. These include the basal resistance values of the components of the head (see Table 24). The volume of the brain will not change under acceleration stress. It may not be necessary to calculate CSF formation and absorption changes due to the brief time period. However, CSF flow rate between the cranial and spinal compartments must be included. The variables that are time dependent may only become a factor for certain rates of acceleration onset and durations. Very rapid rates of onset (>6g/sec), in most individuals, will overwhelm the cardiovascular system leading to loss of consciousness. Therefore, compensation effects only need to be taken into account if the exposure is prolonged beyond approximately five seconds.

Obviously, a full description of the effects of acceleration on the impedance measurements of the cephalic circulation is quite complicated. For example, the metabolic and neurologic mechanism preceeding loss of consciousness is not presently understood. However, a few models already exist which describe portions of the cerebral circulation under normal conditions. These models might be used to form the basis for an expanded model which can describe the system in the high +Gz environment.

Other Models

Takemae *et al*[76] constructed an electrical analog of the cerebral circulation to investigate the effects of changing ICP on the intracranial pressure pulsatile wave and the pulsatile wave of the CBV. Pressure-volume relationships were assumed to be linear with respect to small changes in the pulsatile wave and that the hydrodynamic elements within the cranial space could be lumped into a few parameters. These included a single resistance and compliance term (change in vessel volume/ change in intravascular pressure) for the cerebral arteries (Ra, Ca), arterioles and capillaries (Rk, Ck), and veins (Rv, Cv). Note that vessel compliance is a function of internal pressure, radius, and wall tension. A separate resistance term related to venous outflow (Rvo) and a term expressing the compliance of the intracranial space (Cb) were also included. They claimed that Ra refered to inflow resistance and Rk represented autoregulation. They neglected the effects of CSF.

In this study, a change in ICP was expressed as the following:

$ICP = ICPo\ e^{aV}$, where (83)

ICPo = ICP under normal conditions,

a = constant (≈0.092.ml, evaluated from the pressure-volume curve of a human brain),

V = additions to the volume of the intracranial compartment.

Further, the intracranial compliance, Cb, was given as

$$Cb = \frac{dV}{dP} = \left(a\ ICP_0\ e^{aV}\right)^{-1} = (a\ ICP)^{-1}. \quad (84)$$

A small change in CBV (ΔV) and in pulsatile wave ICP (ΔP) was assumed to be

$$\Delta V = Cb\ \Delta P. \quad (85)$$

It was found that changes in pressure and volume pulsatile waveforms principally depended upon intracranial compliance, arterial and venous outflow resistance. They then used REG (recorded during apnea just after voluntary hyperventilation) to determine which had the greater effect on the pulsatile wave of the cerebral blood volume (CBVPW), intracranial compliance or venous outflow resistance. They claimed that changes in CBVPW (as reflected by the change in amplitude of the REG) will be determined by which factor is dominant, *i.e.* CBVPW amplitude increases when the effect of an increase in Rvo is stronger than the decrease in Cb.

This model reinforces the importance of gaining knowledge of the state of the compliance and resistance beds of the brain which are in turn controlled by the ICP and by the transmural pressure. While this model provides insight into our investigation, it is too simplified for direct application in the acceleration stress environment due to its lack of a CSF model and the fact that no provision is given for variation in the distribution of the flow within the brain. It is not known whether the brain is uniformly emptied under acceleration or whether certain areas are affected first.

Another model was proposed by Zagzoule *et al*[86] in 1986 to mathematically characterize the cerebral circulation in terms of fluid mechanic concepts.[86] Some of this description may be useful towards characterizing the cerebral circulation. This is due to the fact that the main thrust of this model is an attempt to account for changes in blood flow and vasomotion. It describes normal autoregulation of the cerebral circulation and its predictions are in reasonable agreement with known values of blood flows and pressure waveforms. The authors tested the ability of the model to account for regulatory changes under conditions of arterial hypotension and it performed adequately. However, the model does not take into account CSF pressure or the effects of acceleration stress or changes in posture.

CONCLUSIONS

A convenient, unencumbering, noninvasive, real time, and unobtrusive method for investigating the redistribution of cephalic fluid volume in humans that accompanies exposure to acceleration has been demonstrated. This is the first successful use of this technique at high acceleration levels and onset rates. The REG device has successfully withstood acceleration stresses as high as +14 Gz and −1.5 Gx without compromise. In contrast to the clinical difficulties reported in the literature of the past, rheoencephalography is a useful and easily applied technique in acceleration studies. In the past, the slow moving, or baseline, component of the REG signal has been considered to be an annoying artifact that was removed within the clinical devices. This baseline has been successfully separated from the composite signal in hardware and the utility of monitoring it has been demonstrated. It is now possible to estimate the extent of the bulk movement of cranial blood that occurs under acceleration stress under relaxed conditions and with the performance of AGSM by monitoring changes in the baseline impedance, Zb. The bulk movement of blood out of the head towards the large capacitance veins of the legs has been postulated in accordance with the hydrostatic column theory of the physiological responses to acceleration stress. This is the first demonstration of the ability to estimate these shifts, whether directly or indirectly. Further, changes in Zb have been shown to be useful in determining the effects of anti-G protective devices, *e.g.* a reclining seat, and anti-G protective maneuvers, *e.g.* as an aid in determining with effectiveness of the performance of the respiratory portion of a AGSM.

The pulsatile component of the REG waveform, ΔZ, has been subjected to both classical and contemporary analysis. The form of ΔZ shows definite temporal and morphological changes with increasing levels of acceleration stress, particularly those indications related to changes in blood volume and vascular tone. It was even possible to demonstrate a frequency content change in ΔZ as acceleration load increases. Further, changes seen with other modalities, *i.e.* pulse wave delay using pulsed doppler ultrasound, were also seen with ΔZ.

The instrument has been worn by thirty volunteer subjects during three different human centrifuge experiments. A variety of electrode types have been investigated. Large surface area silver-silver chloride electrodes seem to work the best. In all of the configurations, whether placed on the forehead or on the occipital region of the head, none of the subjects experienced any discomfort or after-effects as a consequence of using the REG device.

A plan for modeling the cerebral circulation under acceleration stress based on rheoencephalographic changes has been outlined. Complete characterization of the REG waveform awaits the performance of animal experimentation to determine the contribution of CSF volume changes.

In summation, an old technique configured and used in a new environment has been developed and tested. Use of this device has enhanced the potential for further exploration into the mysteries of the cerebral circulation in both normal and acceleration environments.

RECOMMENDATIONS FOR THE FUTURE

The next step in the evaluation of the use of rheoencephalography under acceleration stress will be the planned human centrifuge experiments, scheduled for 1989, in conjunction with the second phase of the NAMRL exercise conditioning experiment. Hopefully, we will see the effects of physical conditioning and will be able to have a larger body of data at higher levels of +Gz. During these trials the improved REG device will be employed and even better results without annoying grounding artifacts should be obtained. From this potentially larger body of data, the mathematical representation of ΔZ, during both prestressed and stressed conditions, will be refined.

Obviously, it has been impossible to characterize the contribution of CSF to the REG waveform while only performing human trials. Only by the use of animal models in both normal and acceleration stress environments can this be determined.

An appropriate choice of animal model would be the rabbit. Rabbits are good subjects for neurological studies because they are reasonably small and of uniform size. Successful demonstration of REG recordings with a rabbit have been discussed above. The topology of the rabbit brain is well known and anatomic atlases are available to aid in the precise placement and manipulation of cranial probes.

To overcome the motion artifact problem that has been observed by the author with the use of surface or large needle recording electrodes, the skulls of adult white New Zealand rabbits would be prepared for study in the laboratory and on the animal centrifuge at NADC in the following manner. The skin and muscles overlying the cranium would be incised and reflected to expose the skull. Holes would be drilled through the skull and stainless steel screws would be implanted in contact with the dura. These screws and electrode cables attached to them would serve as the REG transducer interface. Bone wax would then be applied to the bony defects in the skull. A dental acrylic cap would then be formed enclosing the montage. After the acrylic has cured, the muscles would be sutured to the cap (see reference 69 for an example of this surgical procedure). Once the rabbits have healed it would then be possible to demonstrate the robustness of the arrangement on the animal centrifuge to discover the nature of the rabbit REG under a +Gz load.

Once this procedure has been performed successfully, the next step would be to investigate the role of CSF formation, absorption, and movement on the REG signal. Specific procedures for manipulation of the CSF compartment can be found in the Ph.D. Thesis of A. Marmarou.[48] Under acceleration stress, the latter should be the most important for short term (≈15 seconds) exposures. There probably is not enough time to see the effects of CSF formation or absorption under acceleration. A relatively simple procedure can be performed in which, using the rigid platform as a staging area, measurement of the cisterna magna CSFP can be taken inside of the meninges without entering the brain. If possible, intraventricular pressures, a more invasive and difficult procedure, can be measured by inserting probes into the intraventricular spaces. In order to manipulate the conductivity of the head, it is possible to remove portions of the CSF and replace it with nonconductors, such as CO_2 or air, and measure the REG without the contributions of CSF. One can simply open CSF system to atmosphere thereby clamping one of the pressure variables to zero.

Further analysis on humans can be performed noninvasively. For example, tests on a tilt table to simulate higher acceleration stress can be performed without having to schedule human centrifuge time. Volunteers can inhale 5–7% CO_2 and O_2 mixtures to increase vasodilation while REG, ECG, etc. is recorded. It should be possible to fashion useful electrodes that can be fitted to the nose to measure

REG signals. The nose is highly vascularized and contains no CSF. Obviously obtaining this kind of data would be enormously useful.

Once isolated CSF data is obtained, then the cephalic impedance mathematical model can be expanded to include the two major sources of conductance in the head. With this information it should be possible to more knowledgeably monitor the hemodynamic state of the head under stress in the most simple, noninvasive, unobtrusive, and inexpensive manner currently available. The ultimate goal would be to use this information to predict when the circulation of an individual is about to be dangerously compromised, leading to blackout of visual systems or eventual loss of consciousness.

Several technical refinements and additions should be incorporated into the REG design. Exciting the purposely off-null detection bridge with a ±1.4 Vp-p signal has led to a minimum of adjustments necessary for good reproduction of the signal. However, no adjustment would be best. Therefore, some automatic control mechanism for optimally setting the bridge should be considered. In order to compare the results currently obtained with those contained in some previously published clinical studies, a tetrapolar constant current version of the REG ought to be developed. This could use most of the currently installed hardware. This device would probably be less sensitive and more difficult to set up on a subject due to the necessity of good linear alignment of four electrodes on a curved surface, *i.e.* the head.

Finally, some consideration might be given for outfitting the REG electrodes in such a way that they do not have to be affixed to a individual in the current fashion. The current method can lead to problems when a subject dons a flight helmet. *e.g.* wires and electrodes may move and become disconnected. It may be possible to fit electrodes onto a pair of sunglasses with sensors places on the ear pieces. This arrangement should not conflict with other operational gear currently worn.

REFERENCES

1. Albery, W.B., Van Patten, R.E., Gordon, T.A., and Frazier, J.W. "Advanced Protection Concepts for the High +Gz Onset, High Sustained +Gz Flight Environment." Aviat. Space Env. Med. 58:505, 1987.

2. Akesson, S. Acta. Physiol. Scand. 15:237, 1948.

3. Beckman, E.L., Duane, T.D., Ziegler, J.E., and Hunter, H.N. "Some Observations On Human Tolerance To Accelerative Stress." J. Aviat. Med. 25:50, 1954.

4. Bergey, G.E., Sipple, W.C., Hamilton, W.A., and Squires, R.D. "A Quantitative Impedance Pneumograph." Naval Air Systems Command Report No. NADC-MR-6222, 1966.

5. Blomqvist, C.G. and Stone, H.L. "Cardiovascular Adjustments To Gravitational Stress." *in:* Handbook of Physiology, Section 2: The Cardiovascular System, Vol III. Peripheral Circulation and Organ Blood Flow, Part 2. *eds:* Shepherd, J.T. and Abboud, F.A. Bethesda: Physiological Society, Ch. 28, 1988.

6. Bostem, F. and Thibaut, A. "Tentative Application Of An Averaging Method In Rheoencephalography II." *in:* Rheoencephalography And Plethysmographic Methods. *eds.* H. Lechner, N. Geyer, E. Lugaresi, F. Martin, K. Lifshitz, S. Markovich, Amsterdam: Excerpta Medica Foundation, p. 37–45, 1969.

7. Buerk, D.G., Dubin, S., and Gealow, K. "Metabolism in Blood Vessel Walls With Stenosis." Proc. 14th. N.E. Bioeng. Conf. 1988, in press.

8. Cammarota, J. "A Training Method For The Dynamic Tracking Of Peripheral Vision Limits." NADC Report No. NADC-86072-60, 1985.

9. Cammarota, J.P. "The Effects of AGS Inflation Speed on G-Tolerance." Aviat. Space Env. Med. 58:505, 1987.

10. Cooney, D.O. Biomedical Engineering Principles. New York: Marcel Dekker, Inc. p. 22, 1976.

11. Dewey, R.C., Pieper, H.P., and Hunt, W.E. "Experimental Cerebral Hemodynamics. Vasomotor Tone, Critical Closing Pressure, and Vascular Bed Resistance." J. Neurosurg. 41:597, 1974.

12. Dhenin, G. *ed.* Aviation Medicine: Physiology and Human Factors. London: Tri-Med Books Ltd., Ch. 10, 1978.

13. Duane, T.D. Arch. Ophthal., N.Y. 51:343, 1954.

14. Dubin, S., Moore, T.W., Yeager, H., Shender, B.S., Kepics, F. "Data Conversion In The Surgical Research Laboratory." Proc. 2nd. Sci. Sess. Aca. Surg. Res. Clemson, S.C. 1986. p.51–54.

15. Gauer, O.H. and Zuidema, G.D. "The Physiology Of Positive Acceleration" *in:* Gravitational Stress In Aerospace Medicine. *eds.* Gauer and Zuidema, Boston: Little, Brown and Co., 1961.

16. Geddes, L.A. and Baker, L.E. "The Specific Resistance of Biological Material." Med. and Biol. Eng. 5:271, 1967.

17. Geddes, L.A. and Baker. L.E. Principles of Applied Biomedical Instrumentation. New York: John Wiley and Sons, Ch. 10, 1968.

18. Geyer, N. "The Rheographic Conduction Value." *in:* Rheoencephalography And Plethysmographic Methods. *eds.* H. Lechner, N. Geyer, E. Lugaresi, F. Martin, K. Lifshitz, S. Markovich, Amsterdam: Excerpta Medica Foundation, p. 62–66, 1969.

19. Gillies, J.A. A Textbook Of Aviation Physiology. Oxford: Pergamon Press, 1965.

20. Gillingham, K.K., and Krutz, R.W. "Effects Of The Abnormal Acceleratory Environment Of Flight." Aeromedical Review 10–74 USAF School Of Aerospace Medicine, Aerospace Medical Division Brooks Air Force Base, p. 24, 1974.

21. Gillingham, K.K., and Fosdick, J.P. "High-G Training for Fighter Aircrew." Aviat. Space Env. Med. 59:12–19, 1988.

22. Gollan, F. and Namon, R. "Electrical Impedance Of Pulsatile Blood Flow In Rigid Tubes And In Isolated Organs." Ann. Of The N.Y. Acad. of Sci. 170:568, 1970.

23. Gonzalez deMendoza, S. Significance of the Respiratory Synchronous Oscillations in Electro-Rheometry. M.S. Thesis, Philadelphia: Drexel University, 1972.

24. Gregg, D.E. and Huvos, A. "Special Features Of The Circulation In Different Regions. Brain, Skeletal Muscle, Skin." *in:* The Physiological Basis Of Medical Practice. *eds.* C.H. Best and N.B. Taylor. Baltimore: The Williams & Wilkins Co., Ch. 25, 1961.

25. Hadjiev, D. "A New Method For Quantitative Evaluation Of Cerebral Blood Flow By Rheoencephalography." Brain Research, 8:213, 1968.

26. Hadjiev, D. "Quantitative Evaluation Of Cerebral Blood Flow By Rheoencephalography." Ann. Of The N.Y. Acad. of Sci. 170:622, 1970.

27. Hadjiev, D. "Impedance Methods and Cerebral Circulation." Prog. in Brain Res. 35:25, 1972.

28. Heistad, D.D. and Kontos, H.A. "Cerebral Circulation." *in:* Handbook of Physiology. Section 2: The Cardiovascular System. Vol III. Peripheral Circulation and Organ Blood Flow, Part I. *eds:* Shepherd, J.T. and Abboud, F.A. Bethesda: Physiological Society, Ch. 5, 1988.

29. Henry, J.P., Gauer, O.H., Kety, S.S., and Kramer, K. "Factors Maintaining Cerebral Circulation During Gravitational Stress." J. Clin. Invest. 30:292, 1951.

30. Honig, C.R. Modern Cardiovascular Physiology. Boston: Little, Brown & Co, 1981.

31. Hrebien, L. and Hendler, E. "Factors Affecting Human Tolerance to Sustained Acceleration." Aviat. Space Env. Med. 56:19–26, 1985.

32. Hrebien, L. "Pulse Wave Delay For +Gz Tolerance Assessment." NADC Report No. NADC-86140-60, 1986.

33. Jacquy, J., Dekoninck, W.J., Piraux, A., Calay, R., Bacq, J., Levy, D., and Noel, G. "Cerebral Blood Flow And Quantitative Rheoencephalography." EEG and Clin Neurophys. 37:507, 1974.

34. Jaron, D., Moore, T., Shankara Reddy, B.R., Hrebien, L., Kepics, F. "Reflectance Photoplethysmography As An Adjunct To Assessment Of Gravitational Acceleration Tolerance: Preliminary Findings." Aviat. Space Env. Med. 58:604, 1987.

35. Jaron, D., Moore, T.W., Reddy B.R.S., Hrebien, L., and Kepics, F. "Increased Acceleration Protection With An Improved Pulsating Anti-G Suit." Aviat. Space Env. Med. 59:480, 1988.

36. Jenkner, F.L. "Rheoencephalography: Present Status." Prog. In Brain Res. 30:127, 1968.

37. Jensen, D. The Principles Of Physiology, 2nd ed. New York: Appleton-Century-Crofts, p. 250, 1980.

38. Johanson, D.C. An Investigation Of The Apparent Negative Velocities Of Cerebral Blood Flow During Exposure To +Gz Acceleration. M.S. Thesis, Philadelphia: Drexel University, 1982.

39. Jung, W.G. IC Op-Amp Cookbook. Indianapolis: Howard W. Sams and Co., Inc., 1980.

40. Kubicek, W.G., Kottle, F.J., Ramos, M.U., Patterson, R.P., Witsoe, D.A., Labree, J.W., Remole, W., Layman, T.E., Schoening, H., and Garamela, J.T. "The Minnesota Impedance Cardiograph — Theory and Applications." Biomed. Eng. 9:410, 1974.

41. Lacanette, K., *ed.* The Switched-Capacitor Filter Handbook. Santa Clara: National Semiconductor Corporation, 1985.

42. Lambert, E.H. "The Physiological Basis Of "Blackout" As It Occurs In Aviators." Fed. Proc. 4:43, 1945.

43. Leverett, S.D. Aerospace Physiology and Medicine In Medical Engineering. *ed.* C.D. Ray Chicago: Year Book Medical Publishers, p. 827, 1974.

44. Levitan, B.M., Montgomery, L.D., Bhagat, P.K., and Zieglschmid, J.F. "A Comparison Of Limb Plethysmograph Systems Proposed For Use On The Space Shuttle." Aviat. Space. Environ. Med. 54:6, 1983.

45. Lifshitz, K. "Rheoencephalography: I. Review Of The Technique." J. Nervous and Mental Disease. 136:388, 1963.

46. Lifshitz, K. "Electrical – Impedance Cephalography (Rheoencephalography)." *in:* Biomedical Engineering Systems *eds.* M. Clynes, and J.H. Milsum New York: McGraw Hill, Co. p. 21–64, 1970.

47. Lynn, P.A. An Introduction To The Analysis And Processing Of Signals. Indianapolis: Howard W. Sams & Co., Inc., 1982.

48. Marmarou, A. A Theoretical Model and Experimental Evaluation of The Cerebrospinal Fluid System. Ph.D. Thesis, Philadelphia: Drexel University, 1973.

49. Marmarou, A., Shulman, K., and LaMorgese, J. "Compartmental Analysis of Compliance and Outflow Resistance of the Cerebrospinal Fluid System." J. Neurosurg. 43:523, 1975.

50. Martin, A.N. Physical Pharmacy. Philadelphia: Lea and Febiger, p. 34, 1960.

51. Mayr, F. "Rheoencephalography and C.S.F. Pressure." *in:* Rheoencephalography And Plethysmographic Methods. *eds.* H. Lechner, N. Geyer, E. Lugaresi, F. Martin, K. Lifshitz, S. Markovich, Amsterdam: Excerpta Medica Foundation, p. 127–30, 1969.

52. McArdle, W.D., Katch, F.I., and Katch, V.L. Exercise Physiology. Energy, Nutrition, and Human Performance. 2nd ed. Philadelphia: Lea and Febiger, 1986.

53. McHenry, L.C. "Rheoencephalography. A Clinical Appraisal." Neurology. 15:507, 1965.

54. Melby, Jr., E.C. and Altman, N.H. *eds.* Handbook of Laboratory Animal Science, Volume III. Cleveland: CRC Press, p. 23–64, 1976.

55. Mohapatra, Surya N. Non-invasive Cardiovascular Monitoring By Electrical Impedance Technique. London: Pitman Medical, 1981.

56. Montgomery, L.D., Parmet, A.J., Booker, J.W., Harvey, W.T., and Peck, E.L. "Segmental Hemodynamic Responses To Antiorthostatic Simulation Of Weightlessness." Aviat. Space Env. Med. 55:466, 1984.

57. Moskalenko, Y.E., Weinstein, G.B., Demchenko, I.T., Kisyakov, Y.Y., and Krivchenko, A.I. Biophysical Aspects of Cerebral Circulation. Oxford: Pergamon Press, 1980.

58. Nair, P.K., Buerk, D.G., and Halsey, Jr., J.H. "Comparisons of Oxygen Metabolism and Tissue PO_2 in Cortex and Hippocampus of Gerbil Brain." Stroke. 18:616, 1987.

59. Namon, R., Gollan, F., Shimojyo, S., Sano, R., Markovich, S.E., and Scheinberg, P. "Basic Studies In Rheoencephalography." Neurology. 17:239, 1967.

60. Nelson, J.G., Cammarota, J.P., Hrebien, L. "Detection Of Acceleration (+Gz) Induced Blackout By Matched-Filtering Of Visual Evoked Potentials." AGARD/AMP Symposium. Trondheim, Norway 1987.

61. Nyboer, J. Electrical Impedance Plethysmography. Springfield: Charles C. Thomas, Publisher. 1970.

62. Perez-Borja, C. and Meyer, J.S. "A Critical Evaluation of Rheoencephalography in Control Subjects and in Proven Cases of Cerebrovascular Disease." J. Neurol. Neurosurg. Psychiat. 27:66, 1964.

63. Ravi Shankar, T.M. and Webster, J.G. "Design of an Automatically Resetting Electrical Impedance Plethysmograph." IEEE 1980 Frontiers of Engineering in Health Care. p. 346–349, 1980.

64. Rodler, H. "Methods For Rheoencephalography II And Their Further Development." *in:* Rheoencephalography And Plethysmographic Methods, *eds.* H. Lechner, N. Geyer, E. Lugaresi, F. Martin, K. Lifshitz, S. Markovich, Amsterdam: Excerpta Medica Foundation, p. 17, 1969.

65. Rossen, R., Kabat, H., and Anderson, J.P. "Acute Arrest Of Cerebral Circulation In Man." Arch. Neurol. and Psychiat. 50:510, 1943.

66. Rushmer, R.F., Beckman, E.L., and Lee, D. "Protection of the Cerebral Circulation by the Cerebrospinal Fluid Under the Influence of Radial Acceleration." Am. J. Phys. 151:355, 1947.

67. Seipel, J.H. "The Biophysical Basis And Clinical Applications Of Rheoencephalography." Neurology, 17:443,1967.

68. Seipel, J. "The Influence Of Electrode Size And Material On The Rheoencephalogram." Ann. Of The N.Y. Acad. of Sci. 170:604, 1970.

69. Sgro, O. Energy Optimization in Brain Pacemakers. M.S. Thesis. Philadelphia: Drexel University, p. 49–57, 1976.

70. Shapiro, K., Marmarou, A., and Shulman, K. "Characterization of Clinical CSF Dynamics and Neural Axis Compliance Using the Pressure-Volume Index: I. The Normal Pressure-Volume Index." Ann. Neurol. 7:508, 1980.

71. Sheingold, D.H. Transducer Interface Handbook. Norwood: Analog Devices, Ch. 2, 1981.

72. Shender, B., Dubin, S., Hrebien, L., Barnea, O., and Kepics, F. "Rheoencephalography: The Jury is Still Out." Proc. 13th. N.E. Bioeng. Conf. p. 420, 1987.

73. Shender, B.S., Hrebien, L., and Dubin, S. "The Use of Rheoencephalography In Simulated Military Environmental Stress." Proc. IEEE/9th Ann. Conf. of EMBS. p. 1134–5, 1987.

74. Shender, B.S., Hrebien, L. and Dubin, S. "Cephalic Impedance Changes As A Consequence Of +Gz Stress." Aviat. Space Env. Med. 59:489, 1988.

75. Stoll, Alice M. "Human Tolerance To Positive G As Determined By The Physiological End Points." J. Aviat. Med., 27:356, 1956.

76. Takemae, T., Kosugi, Y., Ikebe, J., Kumagai, Y., Matsuyama, K., and Saito, H. "A Simulation Study of Intracranial Pressure Increment Using an Electrical Circuit Model of Cerebral Circulation." IEEE Trans. Biomed. Eng. BME-34:958, 1987.

77. Tarassenko, L., Rolfe, P., Bristow, C.J., and Weindling, A.M. "Use of Digital Techniques to Process Cerebral Electrical Impedance Signals in the Newborn." Med. and Biol. Eng. and Comput. 22:55–62, 1984.

78. Tedeschi, F.P. The Active Filter Handbook. Blue Ridge Summit: TAB Books Inc., 1979.

79. van Eijndhoven, J.H.M. and Avezaat, C.J.J. "Cerebrospinal Fluid Pulse Pressure and the Pulsatile Variation in Cerebral Blood Volume: An Experimental Study in Dogs." Neurosurg. 19:507, 1986.

80. Vander Kooi, M.K. *ed.* Linear Applications Handbook 1. Santa Clara: National Semiconductor Corporation, p. AN29-9, 10, AN 31-5, 1973.

81. von Beckh, H.J. "The Development and Airborne Testing Of The PALE Seat." NADC Report No. NADC-81200-60, 1981.

82. Walsh, D.F. A Multi-Channel Data Acquisition System for Biological Signals. M.S. Thesis. Philadelphia: Drexel University, 1988.

83. Webster, J.G., *ed.* Medical Instrumentation Application and Design. Boston: Houghton Mifflin Co., p. 420, 1978.

84. Wood, E.H. "Evolution of Instrumentation and Techniques for the Study of Cardiovascular Dynamics From the Thirties to 1980, Alza Lecture, April 10, 1978." Ann. Biomed. Eng. 6:250–309, 1978.

85. Wood, E.H., Lambert, E.H., and Code, C.F. "The Hydro- And Resulting Bio-dynamics Of +Gz Induced Losses Of Consciousness And Its History." Proceedings of the IEEE 1987 National Aerospace and Electronics Conference p. 988–995, 1987.

86. Zagzoule, M. and Marc-Vergnes, J. "A Global Mathematical Model Of The Cerebral Circulation In Man." J. Biomech. 19:1015, 1986.

87. "Anthropometry and Mass Distribution for Human Analogues. Volume I: Military Male Aviators." NADC Report No. NADC-88036-60, 1988.

APPENDIX A

Determination of amount of dissolved oxygen in neural tissue, based on a technique outlined in Martin.[50]

Bunsen solubility coefficient (BSC) = volume (V) of gas in liters (at 0° C and 760 mmHg) / volume of solvent (sol) in liters / partial presure (p) at 1 atm

for O_2, at 0°C, BSC = 0.0478
at 25°C, BSC = 0.0283
at 37°C, BSC = 0.0189

i.e., the linear regression formula is BSC = –0.00078 T (C°) + 0.0478

and

$$BSC = \frac{Vgas}{Vsol\,p} = \frac{\left\{(amt/32\,mole)\,(0.08205\,liter\,atm/mole\,deg\,(273.16\,°K))\right\}}{1(80[average\,partial\,pressure\,of\,oxygen\,in\,tissue]/760)}$$

Solving for amt with BSC = 0.0189, gives
amount of dissolved oxygen in neural tissue = 2.8 ml.

APPENDIX B

Gz	ECG			ΔZ			IRP		
	Rmax	R-R	HR	A	A-A	R-A	IRPmax	P-P	R-P
1.0	0.965	0.615	97.6	0.450	0.615	0.330	0.909	0.555	0.320
1.3-1.4	0.934	0.675	88.9	0.369	0.670	0.355	0.658	0.64	0.325
1.5-2.0	1.027	0.590	101.7	0.319	0.450	0.330	0.608	0.450	0.320
2.0-2.6	1.049	0.555	108.1	0.415	0.400	0.350	0.629	0.405	0.350
2.9-3.0	1.120	0.555	108.1	0.416	0.440	0.385	0.749	0.405	0.375
3.0	1.042	0.565	106.2	0.559	0.575	0.390	0.864	0.405	0.365
3.0	1.038	0.575	104.4	0.637	0.555	0.385	0.926	0.595	0.370
2.9-2.3	1.068	0.590	101.7	0.669	0.445	0.360	1.173	0.405	0.335
1.8-1.4	0.949	0.595	100.8	0.658	0.570	0.350	0.948	0.460	0.295
1.1-1.0	0.883	0.700	85.7	0.571	0.670	0.335	0.659	0.680	0.290
1.0	0.940	0.745	80.5	0.647	0.685	0.340	0.772	0.405	0.280

Centrifuge experiment 1: subject S1 data

KEY

ECG: Electrocardiograph
Rmax = maximum amplitude of R wave (volts)
R-R = R to R interval (seconds)
HR = heart rate (beats/minute)

ΔZ: Pulsatile REG
A = amplitude of averaged A wave (volts)
A-A = A to A interval (seconds)
R-A = R to A wave interval, i.e. delta delay (seconds)

IRP: Infrared plethysmograph
IRPmax = maximum amplitude of peak of IRP (volts)
P-P = IRPmax-IRPmax interval (seconds)
R-P = R to IRPmax interval, i.e. delta delay (seconds)

APPENDIX C

Gz	ECG			ΔZ			IRP		
	Rmax	R-R	HR	A	A-A	R-A	IRPmax	P-P	R-P
1.8	0.765	0.600	100.0	0.856	0.510	0.325	0.322	0.460	0.260
1.8-1.9	0.757	0.695	86.3	0.562	0.445	0.345	1.038	0.405	0.330
1.9-2.2	0.845	0.615	97.6	0.808	0.400	0.330	0.990	0.405	0.135
2.2-2.7	0.820	0.660	90.9	0.352	0.620	0.390	0.435	0.580	0.290
2.7-2.9	0.808	0.610	98.4	0.212	0.400	0.375	0.422	0.495	0.305
3.0	0.788	0.620	96.8	0.296	0.425	0.400	0.482	0.600	0.300
3.0	0.764	0.590	101.7	0.503	0.585	0.375	0.706	0.440	0.330
3.0	0.755	0.613	97.6	0.309	0.505	0.450	0.478	0.520	0.315
3.0-2.5	0.740	0.590	101.7	0.238	0.450	0.700	0.387	0.410	0.305
2.5-1.6	0.713	0.560	107.1	0.567	0.520	0.350	0.447	0.405	0.320
1.6-1.1	0.734	0.680	88.2	0.850	0.660	0.330	0.489	0.595	0.315

Centrifuge experiment 1: subject S5 data

KEY

ECG: Electrocardiograph
Rmax = maximum amplitude of R wave (volts)
R-R = R to R interval (seconds)
HR = heart rate (beats/minute)

ΔZ: Pulsatile REG
A = amplitude of averaged A wave (volts)
A-A = A to A interval (seconds)
R-A = R to A wave interval, i.e. delta delay (seconds)

IRP: Infrared plethysmograph
IRPmax = maximum amplitude of peak of IRP (volts)
P-P = IRPmax-IRPmax interval (seconds)
R-P = R to IRPmax interval, i.e. delta delay (seconds)

APPENDIX D

Centrifuge experiment 1: Frequency content and alpha/T data.

Subject S1

+Gz	Fundamental Frequency (Hz)	–3 dB (Hz)	alpha (s)	T (s)	alpha/T	HR (bpm)
1.3-1.4	2.2	3.03	0.15	0.56	0.26	88.9
2.0-2.6	2.15/4.4-4.6	5.45	0.14	0.61	0.24	108.1
3.0	1.8-2.0/3.9-4.0	4.4	0.15	0.64	0.23	106.2
3.0	2.2-3.7	4.5	0.18	0.56	0.32	104.4
2.9-2.3	1.7-2.0	2.58	0.13	0.53	0.25	101.7
1.8-1.4	2.1-2.4	3.15	0.17	0.62	0.27	100.8
1.1-1.0	2.2-2.5	3.6	0.16	0.74	0.22	85.7
1.0	1.9-2.0	2.81	0.16	0.72	0.22	80.5

Subject S5

+Gz	Fundamental Frequency (Hz)	–3 dB (Hz)	alpha (s)	T (s)	alpha/T	HR (bpm)
1.8	2.1-2.3	3.25	0.13	0.60	0.21	100.0
1.8-1.9	1.8	2.72	0.19	0.74	0.25	86.3
1.9-2.2	2.0-2.15	3.30	0.20	0.64	0.31	97.6
2.2-2.7	2.4	3.14	0.20	0.70	0.29	90.0
2.7-2.9	1.75-1.85/7.4	2.63/8.34	0.16	0.60	0.27	98.4
3.0	2.0/6.6-6.8	2.89	?	?	?	96.8
3.0	1.9-2.1	2.97	0.16	0.60	0.27	101.7
3.0	1.8-2.0	2.63	0.18	0.63	0.28	97.6
3.0-2.5	1.75-1.85/ 3.3-3.5/5.4	3.89/5.92	0.19	0.74	0.26	101.7
2.5-1.6	2.1-2.4	3.20	0.16	0.57	0.28	107.1
1.6-1.1	2.0-2.2	3.09	0.18	0.74	0.24	88.2
1.1-1.0	2.3-2.4	3.49	0.24	0.69	0.35	98.4

APPENDIX E

Centrifuge experiment 2:
Baseline impedance data for subjects riding
in a Pelvis and Legs Elevating (PALE) seat.
Subject ES.
Onset Rate: 0.1 Gz/sec

+Gz	Zb (mV)	%Δ Zb	SBA	Time into run (s)
1.0	0	0	25	0
2.0	–30	–0.25	25	4.6
2.4	–40	–0.34	25	6.4
2.8	–40	–0.34	30	8.4
3.0	–60	–0.50	31	9.0
3.3	–80	–0.67	34	10.6
4.0	–80	–0.67	42	14.0
4.2	–80	–0.67	44	15.0
4.4	–70	–0.58	47	15.8
4.6	–60	–0.50	49	17.0
5.0	–50	–0.42	54	19.0
5.4	–40	–0.34	58	21.0
6.0	–20	–0.17	65	24.0
6.2	–40	–0.34	65	25.0
7.0	–40	–0.34	65	29.0
7.0	–30	–0.25	65	34.0
6.4	–20	–0.17	65	37.0
6.0	–20	–0.17	65	39.0
5.8	–20	–0.17	65	40.0
5.4	–40	–0.34	61	42.0
5.0	–60	–0.50	56	44.0
4.2	–100	–0.83	48	47.8
4.0	–80	–0.67	46	48.8
3.2	–60	–0.50	36	53.0
3.0	–50	–0.42	34	53.8
2.8	–40	–0.34	32	54.6
2.6	–20	–0.17	32	55.8
2.2	0	0.00	25	57.4
2.0	0	0.00	25	58.4
1.0	0	0.00	25	63.4

APPENDIX E (cont'd)

Centrifuge experiment 2:
Baseline impedance data for subjects riding
in a Pelvis and Legs Elevating (PALE) seat.
Subject MB.
Onset Rate: 0.5 Gz/sec

+Gz	Zb (mV)	%Δ Zb	SBA	Time into run (s)
1.0	0	0	25	0
1.8	10	0.05	25	1.9
2.0	0	0	25	2.2
2.5	–20	–0.11	25	3.2
3.0	–40	–0.21	25	4.1
3.5	–55	–0.29	31	5.1
4.0	–65	–0.34	38	6.1
4.6	–65	–0.34	43	7.3
4.7	–45	–0.24	44	7.5
5.0	4.0	0.21	48	8.2
5.5	100	0.53	54	9.2
6.0	60	0.32	55	10.2
7.0	70	0.37	65	12.2
7.0	130	0.68	65	14.4
7.0	140	0.74	65	16.8
6.6	110	0.58	65	18.3
6.0	110	0.58	63	19.5
5.5	100	0.53	59	20.5
5.0	100	0.53	54	21.5
4.0	115	0.61	43	23.5
3.5	130	0.68	37	24.5
3.0	140	0.74	32	25.5
2.5	190	1.00	26	26.5
2.0	190	1.00	25	27.4
1.0	140	0.74	25	29.6
1.0	60	0.32	25	30.5
1.0	30	0.16	25	32.3

APPENDIX E (cont'd)

Centrifuge experiment 2:
Baseline impedance data for subjects riding
in a Pelvis and Legs Elevating (PALE) seat.
Subject ES, run 1.
Onset Rate: 0.5 Gz/sec

+Gz	Zb (mV)	%Δ Zb	SBA	Time into run (s)
1.0	0	0	25	0
2.0	–20	–0.17	25	1.8
3.0	–60	–0.50	30	3.6
4.0	–80	–0.67	41	5.6
4.4	–110	–0.92	46	6.4
4.8	–100	–0.83	50	7.2
5.0	–100	–0.83	55	7.6
6.0	–60	–0.50	63	9.8
6.2	–60	–0.50	65	10.2
7.0	–60	–0.50	65	11.6
6.0	–60	–0.50	65	17.2
3.6	–60	–0.50	43	23.4
3.0	–40	–0.34	36	23.8
2.4	0	0.00	31	26.0
1.8	40	0.34	25	26.8
1.0	40	0.34	25	28.6
1.0	0	0.00	25	30.0

APPENDIX E (cont'd)

Centrifuge experiment 2:
Baseline impedance data for subjects riding
in a Pelvis and Legs Elevating (PALE) seat.
Subject ES, run 2.
Onset Rate: 0.5 Gz/sec

+Gz	Zb (mV)	%Δ Zb	SBA	Time into run (s)
1.0	0	0	25	0
2.0	–20	–0.17	25	1.7
2.5	–40	–0.34	25	2.7
3.0	–60	–0.50	30	3.6
3.6	–80	–0.67	36	4.7
4.0	–80	–0.67	42	5.7
4.8	–80	–0.67	49	7.1
5.0	–70	–0.58	52	7.6
5.8	–40	–0.34	60	9.2
6.0	–20	–0.17	64	9.6
6.2	–10	–0.08	65	10.0
6.3	0	0.00	65	10.2
6.8	0	–0.00	65	11.2
7.0	–20	–0.17	65	11.9
7.0	–10	–0.08	65	16.2
7.0	–10	–0.08	65	16.5
6.4	0	0.00	65	17.7
6.0	0	0.00	65	18.7
5.8	0	–0.00	65	19.2
5.2	–20	–0.17	60	20.4
5.0	–30	–0.25	58	20.7
4.2	–60	–0.50	49	22.4
4.0	–60	–0.50	47	22.7
3.2	–50	–0.42	38	24.4
3.0	–50	–0.42	36	24.7
2.4	0	0.00	29	25.9
2.0	40	0.34	25	26.7
1.6	60	0.50	25	27.4
1.4	40	0.34	25	27.8
1.0	50	0.42	25	28.7
1.0	60	0.50	25	29.2
1.0	40	0.34	25	29.5
1.0	30	0.25	25	30.7
1.0	0	0.00	25	33.2

APPENDIX E (cont'd)

Centrifuge experiment 2:
Baseline impedance data for subjects riding
in a Pelvis and Legs Elevating (PALE) seat.
Subject ES, run 1.
Onset Rate: 2.3 Gz/sec

+Gz	Zb (mV)	%Δ Zb	SBA	Time into run (s)
1.0	0	0	25	0
2.0	–20	–0.17	25	0.8
3.0	–80	–0.67	27	1.2
4.0	–100	–0.83	29	1.4
5.0	–100	–0.83	36	1.6
6.0	–120	–1.00	40	2.0
6.6	–120	–1.00	48	2.4
6.8	–110	–0.92	54	2.6
6.8	–90	–0.75	65	2.5
6.8	–80	–0.67	65	3.8
6.0	–80	–0.67	65	8.2
5.0	–70	–0.58	62	8.6
4.0	–60	–0.50	59	8.8
3.0	–40	–0.33	50	9.1
2.0	0	0.00	43	9.4
1.0	60	0.50	25	10.6
1.0	40	0.33	25	11.0
1.0	20	0.17	25	12.0
1.0	0	0.00	25	14.8

APPENDIX E (cont'd)

Centrifuge experiment 2:
Baseline impedance data for subjects riding
in a Pelvis and Legs Elevating (PALE) seat.
Subject ES, run 2.
Onset Rate: 2.3 Gz/sec

+Gz	Zb (mV)	%Δ Zb	SBA	Time into run (s)
1.0	0	0	25	0
1.2	20	0.17	25	0.3
2.0	0	0.00	25	0.9
2.8	–40	–0.34	25	1.2
3.0	–50	–0.42	27	1.3
4.0	–60	–0.50	31	1.6
5.0	–80	–0.67	35	1.9
6.0	–90	–0.75	42	2.2
6.6	–100	–0.83	48	2.5
6.8	–85	–0.71	51	2.8
6.8	–80	–0.67	56	3.0
6.8	–80	–0.67	64	3.5
6.8	–70	–0.58	65	3.6
6.8	–60	–0.50	65	3.7
6.0	-60	-0.50	65	8.2
5.0	–40	–0.34	63	8.6
4.0	–40	–0.34	59	8.9
3.0	–40	–0.34	54	9.2
2.0	–20	–0.17	44	9.7
1.7	0	0.00	39	10.0
1.0	100	0.83	27	10.7
1.0	100	0.83	25	11.0
1.0	60	0.50	25	12.5

APPENDIX F

Centrifuge experiment 3: Baseline impedance (ohm)

Subject S5 (run 1)
Calibration Factor: 60 mV/ohm

Time (sec)	2.5 Gz	3.0 Gz	3.5 Gz	4.0 Gz	4.5 Gz	5.0 Gz	5.5 Gz
prestress	0	0	0	0	0		
0-2	–0.67	–0.67	–0.17	–1.33	–0.83		
2-7	–0.50	–0.83	0	–1.00	–1.00		
7-12	–0.67	–0.67	0.17	–0.67	–1.00		
12-17	–0.83	–0.67	–0.17	–0.67	–0.83		
17-19	–0.33	0	0.67	0	0.17		
recovery	–0.67	–0.17	0.67	0.17	0.33		

Subject S5 (run 2)
Calibration Factor: 60 mV/ohm

Time (sec)	2.5 Gz	3.0 Gz	3.5 Gz	4.0 Gz	4.5 Gz	5.0 Gz	5.5 Gz
prestress			0	0	0	0	0
0-2			–0.33	0.33	–0.33	–0.17	–0.67
2-7			–0.17	0.17	0.33	0	–0.83
7-12			–0.25	0.50	0.67	–0.17	–0.50
12-17			–0.33	0.67	0.83	0.33	*PLL*
17-19			0.50	0.50	1.17	0.67	
recovery			0.50	0.33	0.83	0.50	–0.33

Subject S8 (run 1)
Calibration Factor: 60 mV/ohm

Time (sec)	2.5 Gz	3.0 Gz	3.5 Gz	4.0 Gz	4.5 Gz	5.0 Gz	5.5 Gz	6.0 Gz	6.5 Gz
prestress		0	0		0	0	0	0	0
0-2		–0.67	0		–1.00	0.67	0.50	–0.50	–1.00
2-7		–0.17	0.50		–1.17	–0.75	–0.67	–1.00	–1.00
7-12		–0.50	0.17		–1.00	–5.00	–0.83	–0.83	–1.50
12-17		–0.50	0		–1.00	–0.67	–0.50	–0.67	–1.00
17-19		0	?		0	–0.17	1.00	?	*PLL*
recovery		–0.42	–0.17		0	0.67	0	?	0.50

APPENDIX F (cont'd)

Subject S8 (run 2)
Calibration Factor: 60 mV/ohm

Time (sec)	2.5 Gz	3.0 Gz	3.5 Gz	4.0 Gz	4.5 Gz	5.0 Gz	5.5 Gz	6.0 Gz	6.5 Gz
prestress				0	0			0	
0-2				–0.67	–0.50			–1.00	
2-7				–1.17	–0.92			–1.17	
7-12				–1.50	–1.25			–1.50	
12-17				–1.33	–1.25			–1.33	
17-19				0	0			*PLL*	
recovery				0.17	0.33			0	

Subject P5 (run 1)
Calibration Factor: 100 mV/ohm

Time (sec)	2.5 Gz	3.0 Gz	3.5 Gz	4.0 Gz	4.5 Gz	5.0 Gz
prestress	0		0	0		
0-2	–1.70		–2.90	–3.45		
2-7	–1.70		–2.80	–3.55		
7-12	–2.00		–3.10	–3.75		
12-17	–2.10		–3.20	–3.65		
17-19	–0.80		–0.80	–0.55		
recovery	–0.10		0	0.60		

Subject P5 (run 2)
Calibration Factor: 100 mV/ohm

Time (sec)	2.5 Gz	3.0 Gz	3.5 Gz	4.0 Gz	4.5 Gz	5.0 Gz
prestress	0		0	0	0	0
0-2	–1.60		–2.30	–3.20	–3.80	–0.36
2-7	–1.55		–2.30	–3.15	–4.10	–4.40
7-12	–1.70		–2.50	–3.20	–4.10	–4.40
12-17	–1.50		–2.55	–3.40	–4.40	*PLL*
17-19	–0.20		–0.40	–1.10	–1.70	
recovery	0.40		0.30	0.70	–0.60	–0.10

APPENDIX F (cont'd)

Subject P8 (run 1)
Calibration Factor: 20 mV/ohm

Time (sec)	2.5 Gz	3.0 Gz	3.5 Gz	4.0 Gz	4.5 Gz	5.0 Gz	5.5 Gz
prestress	0	0	0	0	0	0	0
0-2	–1.00	–1.00	–2.25	–2.25	–1.25	–1.75	–2.25
2-7	–0.50	–0.50	–2.00	–2.25	–1.25	–1.25	–2.25
7-12	–0.50	–0.75	–2.00	–2.25	–1.25	–1.50	–2.25
12-17	–0.75	–0.75	–2.00	–2.25	–1.25	–1.50	*PLL*
17-19	0	0.25	–1.50	0	–1.75	0.75	
recovery	0	1.25	–1.50	0	0	0.50	0.75

Subject P8 (run 2)
Calibration Factor: 20 mV/ohm

Time (sec)	2.5 Gz	3.0 Gz	3.5 Gz	4.0 Gz	4.5 Gz	5.0 Gz	5.5 Gz
prestress		0	0	0	0	0	
0-2		?	?	–2.75	–1.25	–1.25	
2-7		–0.50	–1.00	–2.75	–1.50	–1.75	
7-12		–0.75	–1.50	–3.00	–1.75	–1.75	
12-17		–0.75	–1.25	–3.00	–1.75	*PLL*	
17-19		?	?	–0.50	–0.25	1.75	
recovery		0.50	0.50	–0.50	0.50	1.25	

Subject P8 (run 3)
Calibration Factor: 40 mV/ohm

Time (sec)	2.5 Gz	3.0 Gz	3.5 Gz	4.0 Gz	4.5 Gz	5.0 Gz	5.5 Gz	6.0 Gz
prestress	0	0	0	0		0	0	0
0-2	–0.63	–0.88	–1.75	–2.38		–2.13	–3.50	–3.13
2-7	–0.63	–1.13	–1.75	–3.25		–2.75	–4.38	–3.88
7-12	–0.75	–1.25	2.25	–2.63		–2.50	–4.25	–3.38
12-17	–0.75	–1.38	1.75	–2.75		–2.50	–4.13	–3.63
17-19	–0.50	–0.75	–1.25	–2.00		–0.75	–1.88	*PLL*
recovery	–0.50	–0.38	–1.00	–0.88		–0.75	–1.63	–0.63

APPENDIX G

Centrifuge experiment 3: Percentage change (from prestress levels) in averaged baseline impedance

Maximum Overshoot: Peak value after acceleration offset
Recovery: Poststress value after acceleration offset
Overshoot and Recovery Time: Seconds elapsed until peak and poststress values, respectively

2.5Gz

Subject	0-2 sec	2-7 sec	7-12 sec	12-17 sec	17-19 sec	Maximum Overshoot	Recovery	Overshoot Time (sec)	Recovery Time (sec)
S1 (run 1)	0.30	0.15	0.10	0	–0.40	–0.20	–0.30	–0.20	1.8
S5 (run 1)	–0.44	–0.33	–0.44	–0.56	–0.22	–0.44	–0.44	0	7.3
P5 (run 1)	–0.37	–0.37	–0.43	–0.46	–0.17	0	–0.02	5.3	7.3
P5 (run 2)	–0.35	–0.34	–0.37	–0.33	–0.04	0.11	0.09	10.5	13.2
P8 (run 1)	–0.33	–0.17	–0.17	–0.25	0	0.17	0	2.2	9.0
P8 (run 3)	–0.14	–0.14	–0.17	–0.17	–0.06	0.06	–0.06	0.4	3.5

3.0Gz

Subject	0-2 sec	2-7 sec	7-12 sec	12-17 sec	17-19 sec	Maximum Overshoot	Recovery	Overshoot Time (sec)	Recovery Time (sec)
S1 (run 1)	0.25	0.10	0	–0.10	–0.30	–0.20	0	0.4	10.2
S5 (run 1)	–0.44	–0.56	–0.44	–0.44	0	–0.11	–0.11	0	9.2
S8 (run 1)	0	0.12	0.04	0	0.08	–0.16	–0.10	2.5	5.5
P8 (run 1)	–0.33	–0.17	–0.25	–0.25	0.08	0.50	0.42	0.4	3.2
P8 (run 3)	–0.19	–0.25	–0.28	–0.31	–0.17	–0.06	–0.08	0.7	3.6

3.5Gz

Subject	0-2 sec	2-7 sec	7-12 sec	12-17 sec	17-19 sec	Maximum Overshoot	Recovery	Overshoot Time (sec)	Recovery Time (sec)
S1 (run 1)	0.25	0.10	–0.15	–0.10	0	0.2	0	1.8	10.1
S1 (run 2)	–0.20	–0.45	–0.65	–0.70	–0.55	–0.35	–0.35	0	7.5
S5 (run 1)	–0.11	0	0.11	–0.11	0.44	0.56	0.44	1.0	9.7
S8 (run 1)	0	0.12	0.04	0	0.08	0.08	–0.04	0	7.0
P5 (run 1)	–0.63	–0.61	–0.67	–0.70	–0.17	0.02	0	5.4	11.6
P5 (run 2)	–0.50	–0.50	–0.54	–0.55	–0.09	0.11	0.07	7.9	11.6
P8 (run 1)	–0.75	–0.67	–0.67	–0.67	0.50	0.58	0.50	0	10.6
P8 (run 3)	–0.39	–0.39	–0.50	–0.50	–0.28	–0.17	–0.22	0.9	4.8

APPENDIX G (cont'd)

4.0Gz

Subject	0-2 sec	2-7 sec	7-12 sec	12-17 sec	17-19 sec	Maximum Overshoot	Recovery	Overshoot Time (sec)	Recovery Time (sec)
S1 (run 1)	0.35	0.15	0.10	0	–0.10	0.35	0.10	3.2	13.0
S1 (run 2)	–0.25	–0.50	–0.60	–0.85	–0.60	0	–0.10	8.7	11.2
S5 (run 1)	–0.89	–0.67	–0.44	–0.44	0	0.22	0.11	1.1	3.6
S8 (run 2)	–0.20	–0.28	–0.36	–0.32	0	0.12	0.04	3.0	9.9
P5 (run 1)	–0.75	–0.77	–0.82	–0.79	–0.12	0.2	0.13	9.7	12.9
P5 (run 2)	–0.70	–0.68	–0.70	–0.74	–0.24	0.20	0.15	5.6	14.6
P8 (run 1)	–0.75	–0.75	–0.75	–0.75	0	0.17	0	3.8	7.5
P8 (run 2)	–0.92	–0.92	–1.0	–1.0	–0.17	0	–0.17	1.3	8.2
P8 (run 3)	–0.53	–0.72	–0.58	–0.61	–0.44	–0.17	–0.19	1.5	7.9

4.5 Gz

Subject	0-2 sec	2-7 sec	7-12 sec	12-17 sec	17-19 sec	Maximum Overshoot	Recovery	Overshoot Time (sec)	Recovery Time (sec)
S1 (run 1)	0	–0.30	–0.40	–0.55	–0.50	–0.30	0	5.0	11.1
S1 (run 2)	–0.40	–0.70	–0.75	–0.70	–0.45	0.10	0.25	3.1	4.2
S5 (run 1)	–0.56	–0.67	–0.67	–0.56	0.11	0.44	0.22	1.7	9.0
S8 (run 1)	–0.24	–0.28	–0.24	–0.24	0	0	0	0	0
S8 (run 2)	–0.12	–0.22	–0.30	–0.30	0	0.14	0.08	3.0	9.6
P5 (run 2)	–0.83	–0.89	–0.89	–0.96	–0.37	–0.11	–0.13	6.5	11.2
P8 (run 2)	–0.42	–0.50	–0.58	–0.58	–0.08	0.42	0.17	1.5	6.7

Runs Ending Due To PLL

Subject	0-2 sec	2-7 sec	7-12 sec	12-17 sec	17-19 sec	Sec at Plateau	Recovery Time	Gz
P5 (run 2)	–0.78	–0.96	–0.96	—	–0.02	10.0	16.6	5.0
P8 (run 2)	–0.42	–0.58	–0.58	—	0.33	10.5	31.3	5.0
S1 (run 2)	–0.40	–0.65	–0.70	—	?	7.9	?	5.5
S5 (run 2)	–0.44	–0.56	–0.33	—	–0.22	9.7	14.4	5.5
P8 (run 1)	–0.75	–0.75	–0.75	—	0.25	8.5	9.7	5.5
S1 (run 1)	–0.10	–0.75	–0.80	—	0.10	8.4	11.2	6.0
S8 (run 2)	–0.24	–0.28	–0.36	–0.32	0	11.7	25.7	6.0
P8 (run 3)	–0.69	–0.86	–0.75	–0.81	–0.14	11.1		6.0
S8 (run 2)	–0.24	–0.32	–0.36	–0.24	0.12	11.7	7.8	6.5

APPENDIX H

Centrifuge Experiment 3: A, B, and C wave magnitudes (ohm) for increasing +Gz load obtained before, during, and after ROR profiles. Values are averaged of five waveforms per time period.
Time periods measured in seconds from beginning of 15 second +Gz plateau.

Subject P5 / Run 1. Calibration factor: 700 mV/ohm

Gz	Prestress			Plateau									Poststress					
				0-5 s			5-10 s			10-15 s			20-25 s			30-35 s		
	A	B	C	A	B	C	A	B	C	A	B	C	A	B	C	A	B	C
2.5	0.076	0.050	0.056	0.106	0.059	0.094	0.109	0.071	0.097	0.109	0.074	0.111	0.097	0.037	0.074	0.084	0.051	0.074
3.0	0.069	0.051	0.069	0.106	0.060	0.094	0.123	0.071	0.106	0.106	0.063	0.091	0.094	0.063	0.080	0.081	0.043	0.077
3.5	0.076	0.057	0.080	0.117	0.074	0.110	0.126	0.077	0.097	0.129	0.083	0.109	0.089	0.047	0.081	0.090	0.056	0.069
4.0	0.075	0.053	0.067	0.124	0.064	0.093	0.117	0.087	0.104	0.113	0.071	0.083	0.079	0.050	0.093	0.083	0.050	0.069
4.5	0.068	0.051	0.061	0.127	0.091	0.109	0.133	0.100	0.113	0.160	0.097	0.119	0.073	0.039	0.067	0.079	0.053	0.071
5.0	0.073	0.049	0.066	0.134	0.061	0.077	0.144	0.090	0.097	*PLL*			0.077	0.043	0.059	0.080	0.047	0.074

Subject P5 / Run 2. Calibration factor: 700 mV/ohm

Gz	Prestress			Plateau									Poststress					
				0-5 s			5-10 s			10-15 s			20-25 s			30-35 s		
	A	B	C	A	B	C	A	B	C	A	B	C	A	B	C	A	B	C
2.5	0.073	0.050	0.066	0.093	0.043	0.079	0.089	0.059	0.080	0.124	0.074	0.089	0.080	0.051	0.071	0.077	0.044	0.066
3.0	0.060	0.039	0.050	0.090	0.054	0.094	0.087	0.063	0.079	0.106	0.064	0.090	0.091	0.064	0.080	0.076	0.044	0.064
3.5	0.066	0.049	0.064	0.111	0.091	0.107	0.107	0.066	0.089	0.106	0.071	0.103	0.080	0.053	0.071	0.066	0.043	0.064
4.0	0.069	0.043	0.059	0.107	0.053	0.087	0.100	0.061	0.080	0.111	0.071	0.099	0.071	0.049	0.080	0.069	0.041	0.066
4.5	0.066	0.049	0.061	0.111	0.053	0.087	0.121	0.086	0.091	0.123	0.081	0.080	0.083	0.057	0.074	0.079	0.047	0.071
5.0	0.066	0.050	0.063	0.129	0.089	0.110	0.153	0.086	0.101	*PLL*			0.077	0.053	0.067	0.063	0.049	0.061

APPENDIX H (cont'd)

Subject P7 / Run 1. Calibration factor: 550 mV/ohm

Gz	Prestress			Plateau									Poststress					
				0-5 s			5-10 s			10-15 s			20-25 s			30-35 s		
	A	B	C	A	B	C	A	B	C	A	B	C	A	B	C	A	B	C
2.5	0.382	0.265	0.305	0.389	0.287	0.338	0.451	0.331	0.356	0.433	0.338	0.360	0.364	0.273	0.309	?	?	?
3.0	0.345	0.247	0.291	0.495	0.367	0.400	0.542	0.302	0.422	0.556	0.447	0.462	0.375	0.269	0.313	0.393	0.305	0.335
3.5	0.353	0.251	0.276	0.520	0.371	0.385	0.585	0.440	0.447	0.531	0.400	0.429	0.338	0.265	0.284	0.356	0.240	0.295
4.0	0.353	0.240	0.287	0.487	0.371	0.385	0.545	0.353	0.371	0.545	0.396	0.415	0.342	0.255	0.295	?	?	?
4.5	0.356	0.265	0.295	0.542	0.409	0.415	0.571	0.389	0.393	0.531	0.396	0.396	0.335	0.244	0.276	0.351	0.245	0.278
5.0	0.393	0.280	0.309	0.545	0.422	0.436	*PLL*						0.451	0.320	0.356	0.353	0.247	0.280

Subject P7 / Run 2. Calibration factor: 550 mV/ohm

Gz	Prestress			Plateau									Poststress					
				0-5 s			5-10 s			10-15 s			20-25 s			30-35 s		
	A	B	C	A	B	C	A	B	C	A	B	C	A	B	C	A	B	C
3.5	0.349	0.240	0.287	0.407	0.295	0.331	0.502	0.353	0.375	0.460	0.333	0.364	0.269	0.193	0.225	0.255	0.169	0.209
4.0	0.353	0.175	0.240	0.349	0.251	0.291	0.455	0.320	0.360	0.393	0.258	0.309	0.255	0.182	0.218	0.309	0.195	0.260

Subject P8 / Run 1. Calibration factor: 750 mV/ohm

Gz	Prestress			Plateau									Poststress					
				0-5 s			5-10 s			10-15 s			20-25 s			30-35 s		
	A	B	C	A	B	C	A	B	C	A	B	C	A	B	C	A	B	C
2.5	0.201	0.145	0.175	0.225	0.161	0.189	0.205	0.159	0.179	0.251	0.168	0.184	0.255	0.173	0.213	0.233	0.177	0.187
3.0	0.169	0.128	0.157	0.223	0.181	0.199	0.225	0.161	0.175	0.219	0.157	0.200	0.245	0.159	0.191	0.239	0.157	0.197
3.5	0.203	0.136	0.163	0.213	0.156	0.193	0.263	0.187	0.201	0.243	0.183	0.200	0.244	0.171	0.203	0.207	0.125	0.187
4.0	0.207	0.152	0.177	0.229	0.175	0.179	0.244	0.164	0.171	0.260	0.181	0.195	0.220	0.135	0.159	0.212	0.157	0.185
4.5	0.179	0.153	0.176	0.237	0.169	0.183	0.271	0.209	0.220	0.284	0.180	0.193	0.252	0.165	0.207	?	?	?
5.0	0.207	0.155	0.183	0.249	0.175	0.191	0.245	0.171	0.180	0.263	0.189	0.212	0.224	0.160	0.185	?	?	?
5.5	0.244	0.177	0.201	0.292	0.203	0.231	0.285	0.205	0.237	*PLL*			0.249	0.176	0.203	?	?	?

Subject P8 / Run 2. Calibration factor: 750 mV/ohm

Gz	Prestress			Plateau									Poststress					
				0-5 s			5-10 s			10-15 s			20-25 s			30-35 s		
	A	B	C	A	B	C	A	B	C	A	B	C	A	B	C	A	B	C
3.0	0.245	0.184	0.219	0.248	0.171	0.189	0.275	0.192	0.229	0.301	0.211	0.237	0.288	0.179	0.227	0.256	0.176	0.216
3.5	0.211	0.152	0.184	0.248	0.136	0.187	0.261	0.192	0.224	0.261	0.176	0.195	0.256	0.192	0.227	0.235	0.128	0.219
4.0	0.197	0.152	0.184	0.229	0.139	0.179	0.277	0.213	0.229	0.333	0.197	0.213	0.251	0.171	0.205	0.221	0.149	0.184
4.5	0.200	0.141	0.176	0.280	0.197	0.217	0.237	0.019	0.184	0.288	0.224	0.237	0.275	0.176	0.213	0.253	0.153	0.220
5.0	0.211	0.141	0.168	0.261	0.192	0.021	0.272	0.163	0.189	*PLL*			0.229	0.160	0.200	0.223	0.151	0.183

APPENDIX H (cont'd)

Subject S11 / Run 1. Calibration factor: 700 mV/ohm

Gz	Prestress			Plateau									Poststress					
				0-5 s			5-10 s			10-15 s			20-25 s			30-35 s		
	A	B	C	A	B	C	A	B	C	A	B	C	A	B	C	A	B	C
2.5	0.144	0.103	0.124	0.179	0.104	0.126	0.173	0.119	0.139	0.177	0.123	0.143	0.146	0.109	0.123	?	?	?
3.0	0.131	0.097	0.109	0.194	0.129	0.154	0.191	0.114	0.154	0.203	0.131	0.149	0.143	0.089	0.117	0.126	0.089	0.103
3.5	0.123	0.069	0.097	0.180	0.114	0.137	0.171	0.126	0.160	0.194	0.120	0.146	0.143	0.094	0.120	0.106	0.071	0.093
4.0	0.129	0.089	0.114	0.157	0.086	0.126	0.194	0.126	0.149	0.197	0.117	0.151	0.131	0.091	0.114	0.117	0.081	0.107
4.5	0.126	0.089	0.106	0.189	0.114	0.146	0.211	0.129	0.146	0.194	0.120	0.157	0.129	0.080	0.114	?	?	?
5.0	0.131	0.094	0.114	0.206	0.134	0.166	0.197	0.140	0.157	0.180	0.111	0.134	0.131	0.083	0.111	0.114	0.077	0.100
5.5	0.134	0.083	0.114	0.209	0.143	0.160	0.191	0.133	0.147	*PLL*			0.146	0.106	0.129	0.106	0.100	0.107

Subject S11 / Run 2. Calibration factor: 700 mV/ohm

Gz	Prestress			Plateau									Poststress					
				0-5 s			5-10 s			10-15 s			20-25 s			30-35 s		
	A	B	C	A	B	C	A	B	C	A	B	C	A	B	C	A	B	C
3.0	0.094	0.066	0.084	0.129	0.089	0.119	0.126	0.071	0.103	0.126	0.080	0.100	0.097	0.077	0.086	0.086	0.600	0.080
3.5	0.083	0.071	0.081	0.111	0.083	0.100	0.119	0.069	0.107	0.121	0.080	0.093	0.076	0.054	0.071	0.097	0.066	0.086
4.0	0.083	0.057	0.076	0.126	0.069	0.100	0.134	0.090	0.117	0.117	0.080	0.100	0.094	0.054	0.076	0.099	0.067	0.089
4.5	0.096	0.064	0.081	0.146	0.089	0.109	0.153	0.120	0.126	0.154	0.077	0.120	0.100	0.063	0.094	0.113	0.080	0.089
5.0	0.100	0.077	0.097	0.149	0.100	0.114	0.147	0.103	0.114	*PLL*			0.110	0.067	0.097	0.101	0.061	0.080

APPENDIX I

Centrifuge Experiment 3: Magnitude of Rheographic Indices During AGSM (ohm)
Subject P7
Calibration Factor: 400 mV/ohm
G level: +5.5 Gz

Condition	Lentgth of Strain (s)	A	B	C	A	B	C	A	B	C	A	B	C
Prestress		0.46	0.30	0.34									
Strain 1	3.0	0.77	0.42	0.45	0.62	0.37	0.40						
Strain 2	2.6	0.95	0.67	0.70	0.82	0.65	0.77	0.82	0.52	0.60			
Strain 3	3.3	0.72	0.50	0.62	0.47	0.20	0.22	0.45	0.25	0.30	0.32	0.12	0.22
Strain 4	3.3	0.77	0.35	0.40	0.55	0.25	0.32	0.47	0.35	0.35	0.37	0.12	0.27
Strain 5	3.0	0.52	0.37	0.37	0.50	0.30	0.37	0.40	0.25	0.27	0.32	0.20	0.30
Recovery		0.40	0.25	0.26	0.51	0.34	0.37	1.00	0.70	0.86	0.53	0.37	0.40
		a	T	a/T	a	T	a/T	a	T	a/T	a	T	a/T
Prestress		0.16	0.53	0.30									
Strain 1	3.0	0.18	0.52	0.34	0.15	0.48	0.31						
Strain 2	2.6	0.23	0.45	0.51	0.15	0.58	0.26	0.18	0.50	0.35			
Strain 3	3.3	0.18	0.45	0.39	0.15	0.40	0.38	0.12	0.43	0.28	0.14	0.40	0.35
Strain 4	3.3	0.13	0.40	0.31	0.13	0.42	0.30	0.13	0.40	0.31	0.12	0.40	0.30
Strain 5	3.0	0.10	0.40	0.25	0.10	0.40	0.25	0.10	0.38	0.26	0.13	0.40	0.31
Recovery		0.18	0.44	0.40	0.15	0.43	0.35	0.13	0.43	0.30	0.15	0.54	0.28

NOTE: a = alpha (s) T = period (s)
Total recovery time measured from acceleration offset = 42-45 sec
Recovery period ends when values reach a constant poststress level

APPENDIX I (cont'd)

Centrifuge Experiment 3: Magnitude of Rheographic Indices During AGSM (ohm)
Subject P10
Calibration Factor: 500 mV/ohm
G level: +6.5 Gz

Condition	Lentgth of Strain (s)	A	B	C	A	B	C	A	B	C	A	B	C
Prestress		0.21	0.15	0.18									
Strain 1	2.5	0.20	0.05	0.09									
Strain 2	2.8	0.28	0.14	0.16	0.23	0.06	0.07	0.26	0.14	0.16			
Strain 3	3.0	0.26	0.18	0.21	0.24	0.16	0.18	0.19	0.15	0.16	0.16	0.11	0.15
Strain 4	3.0	0.21	0.18	0.21	0.19	0.13	0.16	0.19	0.14	0.16			
Recovery		0.27	0.16	0.21	0.17	0.16	0.21						
		a	T	a/T	a	T	a/T	a	T	a/T	a	T	a/T
Prestress		0.19	.06	0.31									
Strain 1	2.5	0.15	0.47	0.32									
Strain 2	2.8	0.13	0.47	0.27	0.13	0.47	0.27	0.10	0.47	0.21			
Strain 3	3.0	0.15	0.44	0.34	0.15	0.44	0.34	0.13	0.44	0.28	0.13	0.44	0.28
Strain 4	3.0	0.15	0.43	0.35	0.13	0.43	0.29	0.13	0.43	0.29			
Recovery		0.13	0.61	0.21	0.17	0.81	0.21						

NOTE: a = alpha (s) T = period (s)
Total recovery time = 47 sec
Recovery period ends when values reach a constant poststress level

APPENDIX J

Centrifuge experiment 3: B/A for four subjects
Time periods measured in seconds from beginning of 15 second +Gz plateau.

Subject P5: run 1

Gz	Prestress	Plateau			Poststress	
		0-5 s	5-10 s	10-15 s	20-25 s	30-35 s
2.5	0.660	0.554	0.658	0.684	0.382	0.610
3.0	0.750	0.568	0.581	0.595	0.667	0.526
3.5	0.755	0.634	0.614	0.644	0.532	0.619
4.0	0.698	0.517	0.744	0.633	0.636	0.603
4.5	0.750	0.719	0.753	0.607	0.529	0.673
5.0	0.667	0.457	0.624	*PLL*	0.556	0.589

Subject P5: run 2

Gz	Prestress	Plateau			Poststress	
		0-5 s	5-10 s	10-15 s	20-25 s	30-35 s
2.5	0.686	0.462	0.661	0.598	0.643	0.574
3.0	0.643	0.595	0.721	0.608	0.703	0.585
3.5	0.739	0.821	0.613	0.676	0.661	0.652
4.0	0.625	0.493	0.614	0.641	0.680	0.604
4.5	0.739	0.744	0.706	0.663	0.690	0.600
5.0	0.761	0.689	0.561	*PLL*	0.685	0.773

Subject P7: run 1

Gz	Prestress	Plateau			Poststress	
		0-5 s	5-10 s	10-15 s	20-25 s	30-35 s
2.5	0.695	0.738	0.734	0.782	0.750	?
3.0	0.716	0.743	0.557	0.804	0.718	0.778
3.5	0.711	0.713	0.752	0.753	0.785	0.673
4.0	0.680	0.761	0.647	0.727	0.745	?
4.5	0.745	0.755	0.682	0.747	0.728	0.699
5.0	0.713	0.773	*PLL*		0.710	0.701

APPENDIX J (cont'd)

Subject P7: run 2

Gz	Prestress	Plateau			Poststress	
		0-5 s	5-10 s	10-15 s	20-25 s	30-35 s
3.5	0.688	0.723	0.703	0.723	0.716	0.664
4.0	0.667	0.719	0.704	0.657	0.714	0.629

Subject P8: run 1

Gz	Prestress	Plateau			Poststress	
		0-5 s	5-10 s	10-15 s	20-25 s	30-35 s
2.5	0.722	0.716	0.773	0.670	0.681	0.760
3.0	0.756	0.814	0.716	0.720	0.647	0.659
3.5	0.671	0.731	0.711	0.753	0.699	0.606
4.0	0.735	0.762	0.672	0.697	0.612	0.742
4.5	0.858	0.713	0.773	0.634	0.649	?
5.0	0.748	0.701	0.696	0.721	0.714	?
5.5	0.727	0.694	0.720	*PLL*	0.706	?

Subject P8: run 2

Gz	Prestress	Plateau			Poststress	
		0-5 s	5-10 s	10-15 s	20-25 s	30-35 s
3.0	0.750	0.688	0.699	0.699	0.620	0.688
3.5	0.722	0.548	0.735	0.673	0.750	0.545
4.0	0.770	0.605	0.769	0.592	0.681	0.675
4.5	0.707	0.705	0.640	0.778	0.641	0.605
5.0	0.671	0.735	0.598	*PLL*	0.698	0.677

APPENDIX J (cont'd)

Subject S11: run 1

Gz	Prestress	Plateau			Poststress	
		0-5 s	5-10 s	10-15 s	20-25 s	30-35 s
2.5	0.713	0.580	0.686	0.691	0.745	?
3.0	0.739	0.662	0.597	0.648	0.620	0.705
3.5	0.56	0.64	0.73	0.62	0.660	0.68
4.0	0.689	0.545	0.647	0.594	0.696	0.695
4.5	0.705	0.606	0.608	0.618	0.622	?
5.0	0.717	0.653	0.710	0.609	0.630	0.675
5.5	0.617	0.685	0.694	*PLL*	0.725	0.946

Subject S11: run 2

Gz	Prestress	Plateau			Poststress	
		0-5 s	5-10 s	10-15 s	20-25 s	30-35 s
3.0	0.697	0.689	0.568	0.636	0.794	0.700
3.5	0.862	0.744	0.578	0.659	0.717	0.676
4.0	0.690	0.545	0.670	0.683	0.576	0.681
4.5	0.672	0.608	0.785	0.500	0.629	0.709
5.0	0.771	0.674	0.699	*PLL*	0.610	0.606

APPENDIX K

Centrifuge experiment 3: C/A for four subjects
Time periods measured in seconds from beginning of 15 second +Gz plateau.

Subject P5: run 1

Gz	Prestress	Plateau			Poststress	
		0-5 s	5-10 s	10-15 s	20-25 s	30-35 s
2.5	0.736	0.892	0.895	1.026	0.765	0.881
3.0	1.000	0.892	0.860	0.865	0.848	0.947
3.5	1.057	0.939	0.773	0.844	0.919	0.762
4.0	0.887	0.747	0.890	0.734	1.018	0.828
4.5	0.896	0.854	0.849	0.741	0.922	0.909
5.0	0.902	0.574	0.673	*PLL*	0.756	0.929

Subject P5: run 2

Gz	Prestress	Plateau			Poststress	
		0-5 s	5-10 s	10-15 s	20-25 s	30-35 s
2.5	0.902	0.846	0.903	0.713	0.893	0.852
3.0	0.833	1.048	0.902	0.851	0.875	0.849
3.5	0.978	0.962	0.827	0.973	0.893	0.978
4.0	0.854	0.813	0.800	0.885	1.120	0.958
4.5	0.935	0.859	0.753	0.651	0.897	0.909
5.0	0.957	0.856	0.664	*PLL*	0.870	0.997

Subject P7: run 1

Gz	Prestress	Plateau			Poststress	
		0-5 s	5-10 s	10-15 s	20-25 s	30-35 s
2.5	0.800	0.869	0.790	0.832	0.850	?
3.0	0.842	0.809	0.779	0.830	0.835	0.852
3.5	0.784	0.741	0.764	0.808	0.839	0.827
4.0	0.814	0.791	0.680	0.760	0.862	?
4.5	0.827	0.765	0.688	0.747	0.826	0.793
5.0	0.787	0.800	*PLL*		0.790	0.794

APPENDIX K (cont'd)

Subject P7: run 2

Gz	Prestress	Plateau			Poststress	
		0-5 s	5-10 s	10-15 s	20-25 s	30-35 s
3.5	0.823	0.813	0.746	0.791	0.838	0.821
4.0	0.917	0.833	0.792	0.787	0.857	0.841

Subject P8: run 1

Gz	Prestress	Plateau			Poststress	
		0-5 s	5-10 s	10-15 s	20-25 s	30-35 s
2.5	0.868	0.840	0.870	0.734	0.838	0.800
3.0	0.929	0.892	0.775	0.915	0.777	0.827
3.5	0.803	0.906	0.766	0.824	0.831	0.903
4.0	0.858	0.779	0.699	0.749	0.721	0.874
4.5	0.985	0.770	0.813	0.681	0.812	?
5.0	0.884	0.765	0.734	0.807	0.827	?
5.5	0.825	0.790	0.832	*PLL*	0.813	?

Subject P8: run 2

Gz	Prestress	Plateau			Poststress	
		0-5 s	5-10 s	10-15 s	20-25 s	30-35 s
3.0	0.891	0.763	0.835	0.788	0.787	0.844
3.5	0.873	0.753	0.857	0.745	0.885	0.932
4.0	0.932	0.779	0.827	0.640	0.819	0.831
4.5	0.880	0.776	0.775	0.824	0.777	0.868
5.0	0.797	0.816	0.696	*PLL*	0.872	0.820

APPENDIX K (cont'd)

Subject S11: run 1

Gz	Prestress	Plateau			Poststress	
		0-5 s	5-10 s	10-15 s	20-25 s	30-35 s
2.5	0.858	0.700	0.802	0.806	0.843	?
3.0	0.826	0.794	0.806	0.732	0.820	0.818
3.5	0.791	0.762	0.933	0.750	0.840	0.838
4.0	0.889	0.800	0.765	0.768	0.870	0.915
4.5	0.841	0.773	0.689	0.809	0.889	?
5.0	0.870	0.806	0.797	0.734	0.848	0.875
5.5	0.851	0.767	0.769	*PLL*	0.882	1.014

Subject S11: run 2

Gz	Prestress	Plateau			Poststress	
		0-5 s	5-10 s	10-15 s	20-25 s	30-35 s
3.0	0.894	0.922	0.818	0.795	0.882	0.933
3.5	0.983	0.897	0.904	0.765	0.943	0.882
4.0	0.914	0.795	0.872	0.854	0.803	0.899
4.5	0.857	0.745	0.822	0.778	0.943	0.785
5.0	0.971	0.769	0.777	*PLL*	0.883	0.789

APPENDIX L

Centrifuge experiment 3:
α, T, and α/T values (sec) for increasing +Gz load obtained before, during, and after ROR profiles. Values are averages of five waveforms per time period. Timing is measured with respect to the beginning of the +Gz plateau.
Subject P5

Gz	Prestress			Plateau									Post Stress					
				0-5 sec			5-10 sec			10-15 sec			20-25 sec			30-35 sec		
	α	T	α/T	α	T	α/T	α	T	α/T	α	T	α/T	α	T	α/T	α	T	α/T
2.5	.210	.780	.300	.190	.680	.279	.210	.610	.344	.210	.750	.280	.180	.760	.237	.200	.780	.256
3.0	.190	.880	.216	.140	.650	.215	.200	.750	.267	.200	.700	.286	.170	.660	.258	.150	.690	.217
3.5	.190	.850	.224	.200	.630	.317	.200	.660	.303	.160	.640	.250	.180	.730	.247	.150	.700	.214
4.0	.205	.840	.244	.175	.630	.278	.160	.630	.254	.160	.595	.269	.190	.700	.271	.170	.680	.250
4.5	.180	.915	.197	.200	.625	.320	.185	.600	.308	.165	.590	.280	.155	.590	.263	.165	.850	.194
5.0.	.170	.860	.198	.180	.605	.298	.169	.590	.286	*			.150	.605	.248	.155	.670	.231
2.5	.175	.870	.201	.210	.730	.288	.230	.730	.315	.190	.695	.273	.155	.660	.235	.170	.680	.250
3.0	.190	.850	.244	.200	.700	.286	.210	.710	.296	.195	.640	.305	.180	.720	.250	.165	.735	.224
3.5	.205	.925	.222	.222	.680	.324	.175	.720	.243	.200	.695	.288	.160	.665	.241	.130	.725	.179
4.0	.180	.840	.214	.180	.670	.269	.190	.680	.279	.180	.650	.277	.175	.685	.255	.160	.740	.216
4.5	.180	.810	.222	.200	.620	.323	.190	.620	.306	.170	.590	.288	.170	.660	.258	.150	.660	.227
5.0	.190	.840	.226	.175	.600	.292	.170	.600	.283	*			.175	.850	.206	.150	.850	.176

* : PLL ended run.

APPENDIX L (cont'd)

Centrifuge experiment 3:
α, T, and α/T values (sec) for increasing +Gz load obtained before, during, and after ROR profiles. Values are averages of five waveforms per time period. Timing is measured with respect to the beginning of the +Gz plateau.
Subject P7

Gz	Prestress			Plateau									Post Stress					
				0-5 sec			5-10 sec			10-15 sec			20-25 sec			30-35 sec		
	α	T	α/T	α	T	α/T	α	T	α/T	α	T	α/T	α	T	α/T	α	T	α/T
2.5	.160	.560	.286	.190	.560	.339	.185	.585	.316	.190	.590	.322	.180	.575	.313	?	?	?
3.0	.180	.580	.310	.190	.540	.352	.175	.575	.304	.195	.590	.331	.195	.630	.310	.155	.660	.235
3.5	.160	.590	.271	.190	.530	.358	.185	.545	.339	.190	.570	.333	.170	.610	.279	.150	.590	.254
4.0	.160	.590	.271	.185	.560	.330	.175	.580	.302	190	600	.317	.180	.620	.290	?	?	?
4.5	.175	.650	.269	.185	.560	.330	.170	.560	.304	.185	.580	.319	.175	.620	.282	.160	.600	.267
5.0	.155	.550	.282	.165	.510	.324	*						.160	.550	.291	.155	.565	.274
3.5	.157	.620	.253	.185	.600	.308	.154	.600	.257	.167.	.630	.265	.160	.650	.246	.163	.640	.255
4.0	.165	.630	.262	.180	.635	.283	.175	.620	.282	.175	.660	.265	.170	.680	.250	.167	.680	.246

* : PLL ended run.

APPENDIX L (cont'd)

Centrifuge experiment 3:
α, T, and α/T values (sec) for increasing +Gz load obtained before, during, and after ROR profiles. Values are averages of five waveforms per time period. Timing is measured with respect to the beginning of the +Gz plateau.
Subject P8

Gz	Prestress			Plateau									Post Stress					
				0-5 sec			5-10 sec			10-15 sec			20-25 sec			30-35 sec		
	α	T	α/T	α	T	α/T	α	T	α/T	α	T	α/T	α	T	α/T	α	T	α/T
2.5	.180	.630	.286	.170	.540	.315	.195	.550	.355	.175	.560	.313	.165	.570	.289	.165	.670	.246
3.0	.190	.690	.275	.205	.530	.387	.185	.550	.336	.175	.570	.307	.155	.580	.267	.155	.600	.258
3.5	.165	.620	.266	.154	.525	.293	.180	.530	.340	.165	.530	.311	.150	.570	.263	.150	.610	.246
4.0	.180	.690	.261	.195	.560	.348	.205	.580	.353	.175	.560	.313	.138	.580	.224	.185	.660	.280
4.5	.180	.670	.269	.195	.560	.348	.200	.570	.351	.195	.560	.348	.175	.590	.297	?	?	?
5.0	.190	.780	.244	.170	.560	.304	.160	.560	.286	.175	.540	.324	.155	.580	.267	?	?	?
5.5	.145	.660	.220	.195	.570	.342	.180	.570	.316	*			.160	.550	.291	?	?	?
3.0	.160	.660	.242	.140	.590	.237	.150	.620	.242	.155	.590	.263	.150	.630	.238	.145	.640	.227
3.5	.155	.680	.228	.175	.590	.297	.180	.650	.277	.160	.610	.262	.170	.650	.262	.140	.650	.215
4.0	.180	.780	.231	.185	.560	.330	.175	.550	.318	.155	.540	.287	.160	.590	.271	.165	.600	.275
4.5	.160	.680	.235	.180	.580	.310	.160	.550	.291	.150	.530	.283	.165	.590	.280	.163	.580	.281
5.0	.150	.650	.231	.175	.550	.318	.160	.545	.294	*			.150	.590	.254	.140	.610	.230

* : PLL ended run.

APPENDIX L (cont'd)

Centrifuge experiment 3:
α, T, and α/T values (sec) for increasing +Gz load obtained before, during, and after ROR profiles. Values are averages of five waveforms per time period. Timing is measured with respect to the beginning of the +Gz plateau.
Subject S11

Gz	Prestress			Plateau									Post Stress					
				0-5 sec			5-10 sec			10-15 sec			20-25 sec			30-35 sec		
	α	T	α/T	α	T	α/T	α	T	α/T	α	T	α/T	α	T	α/T	α	T	α/T
3.0	.175	.638	.274	.175	.520	.337	.180	.520	.346	.190	.500	.380	.155	.500	.310	.150	.500	.273
3.5	.175	.594	.295	.185	.540	.343	.165	.510	.324	.185	.495	.374	.160	.490	.327	.140	.520	.269
4.0	.165	.560	.295	.185	.525	.352	.170	.500	.340	.175	.500	.350	.160	.520	.308	.155	.630	.246
4.5	.190	.660	.288	.180	.575	.313	.170	.530	.321	.175	.530	.330	.185	.530	.349	.175	.680	.257
5.0	.180	.675	.267	.200	.570	.351	.170	.520	.327	.180	.495	.364	.170	.540	.315	.165	.630	.262
5.5	.185	.620	.298	.175	.510	.343	.172	.480	.358	*			.160	.520	.308	.165	.66	.250
3.0	.135	.610	.221	.195	.710	.275	.165	.590	.280	.150	.610	.246	.170	.650	.262	.170	.710	.239
3.5	.163	.750	.217	.160	.630	.254	.150	.570	.263	.195	.620	.315	.165	.620	.266	.160	.695	.230
4.0	.138	.690	.200	.180	.630	.286	.165	.550	.300	.155	.530	.292	.160	.570	.281	.160	.610	.262
4.5	.163	.660	.247	.170	.570	.298	.160	.520	.308	.185	.520	.356	.160	.660	.242	.155	.630	.246
5.0	.167	.650	.257	.170	.560	.304	.160	.520	.308	*			.150	.530	.283	.155	.580	.267

* : PLL ended run.